CHARACTERIZATION OF REAL POWER CABLE DEFECTS BY DIAGNOSTIC MEASUREMENTS

A Thesis
Presented to
The Academic Faculty

by

Jean Carlos Hernández Mejía

In Partial Fulfillment
of the Requirements for the Degree
Doctor of Philosophy in the
School of Electrical and Computer Engineering

Georgia Institute of Technology
December 2008

CHARACTERIZATION OF REAL POWER CABLE DEFECTS BY DIAGNOSTIC MEASUREMENTS

Approved by:

Dr. Ronald Harley, Advisor
School of Electrical and Computer Engineering
Georgia Institute of Technology

Dr. John Buck
School of Electrical and Computer Engineering
Georgia Institute of Technology

Dr. Miroslav Begovic
School of Electrical and Computer Engineering
Georgia Institute of Technology

Dr. J. Rhett Mayor
School of Mechanical Engineering
Georgia Institute of Technology

Dr. Nigel Hampton
School of Electrical and Computer Engineering
Georgia Institute of Technology

Date Approved: October 21, 2008

To my loving mother, Dulce, my father, Argenis, my sister, Johanna, and my "little" brother Jesus Argenis.

ACKNOWLEDGEMENTS

This thesis is the end of my journey for obtaining my Ph.D. degree in Electrical and Computer Engineering at Georgia Tech. I have not traveled in a vacuum during this journey. There are some very special individuals who made this journey easier and possible with words of encouragement and more intellectually satisfying by offering different places to look to expand my theories and ideas.

First, a very special thank you to Professor Ronald G. Harley. Professor Harley gave me the confidence and support to begin my M.Sc. and Ph.D. programs. Dr. Harley challenged me to set my benchmark even higher and to look for solutions to problems rather than get stuck on them. I learned from him to believe in my future, my work, and myself. Thank you Professor.

This thesis would not have been possible without the priceless advice and guidance of Dr. Nigel Hampton from The National Electric Energy Testing Research and Applications Center (NEETRAC), who patiently took the time to respond to my countless queries and whose help, stimulating suggestions, and encouragement, gave me the willingness to continue working during all the time of the research and writing of this thesis. These words are certainly not enough to thank him for his invaluable help.

It is difficult to overstate my appreciation for Mr. Rick Hartlein, who gave me the opportunity to be part of the Cable Diagnostic Focus Initiative (CDFI) project. He first brought me into the world of power cable systems. Not only a great mentor and manager, he has also been a cornerstone in my professional development. Rick, thank you does not seem sufficient but it is said with appreciation and respect.

I would like to thank Professor Miroslav Begovic for his support, motivation, and valuable advice. I would also like to thank Professor John Buck and Professor J. Rhett Mayor for taking some time of their busy schedule to serve on my Ph.D. thesis defense committee.

Moreover, I would like to acknowledge NEETRAC, the School of Electrical and Computer Engineering (ECE), the Universidad de Los Andes (ULA), and the Organization of American States (OAS) for providing the financial support for my M.Sc. and Ph.D. graduate studies. Specially, I would like to thank Mr. Thomas Parker and Mr. Jorge Altamirano (NEETRAC) who were always available and willing to help with the laboratory and field experimental setups. I would also like to thank Deborah King (ECE) and Gail Reeves (NEETRAC) for patiently putting up with my purchase requests and travel accommodations.

More importantly, I was fortunate to have many exceptional peers and colleagues in my research environment that eventually became my friends and putative family in Atlanta. Among them, I wish to especially thank “my brothers” Joshua Perkel, Harjeet Johal, Jorge Altamirano, Satish Rajagopalan, “my sister” Yamille del Valle, and “my niece” and goddaughter Elizabeth Perkel who came towards the end to give us the “last push.” Thank you for their love, support, help, invaluable input, and countless enlightening conversations.

I cannot end without thanking my family, on whose constant love and encouragement I have relied throughout my time at Georgia Tech. I am deeply grateful to the life example set by my mother, Dulce María Mejía de Hernández, and my father, Argenis Urbano Hernández Valladares. Their unflinching courage and conviction will always inspire me, and I hope to continue, in my own small way, the noble mission to which they have given their lives. It is to them, my sister, Johanna Carolina Hernández Mejía, and my “little” brother, Jesús Argenis Hernández Mejía, that I dedicate this thesis. Thank you all!

TABLE OF CONTENTS

LIST OF TABLES

LIST OF FIGURES

LIST OF TERMS AND ABBREVIATIONS

AC	Alternating current
AEIC	Association of Edison Illuminating Companies
ANOVA	Analysis of variance
ASTM	American Society of Testing and Materials
AWG	American wire gage
CDFI	Cable Diagnostic Focus Initiative
CEA	Canadian Electricity Association
CSA	Canadian Standards Association
D	Symmetry factor
DC	Direct current
DoE	Department of Energy
EPR	Ethylene propylene rubber
EV	Partial discharge extinction voltage
FDDF	Frequency domain dissipation factor
HDPE	High density polyethylene
HMWPE	High molecular weight polyethylene
ICEA	Insulated Cable Engineers Association
IEC	International Electrotechnical Commission
IEEE	Institute of Electrical and Electronics Engineers
IPL	Inverse power law
IQR	Interquartile range

IV	Partial discharge inception voltage
LDPE	Low density polyethylene
LLDPE	Linear low density polyethylene
LMWPE	Low molecular weight polyethylene
MCM	Thousands of circular mils
MDPE	Medium density polyethylene
MV	Medium voltage
NEETRAC	National Electric Energy Testing Research and Applications Center
Nw	Average number of partial discharge pulses per cycle
OAS	Organization of American States
OW	Oscillating wave
p.p.m.	Parts per million
PE	Polyethylene
PILC	Paper insulated lead covered
PVC	Polyvinylchloride
Q1	First quartile
Q3	Third quartile
RFE	Recursive feature elimination
RMS	Root mean squared
Std.	Standard
Stdv.	Standard deviation
SVM	Support vector machine
Tan δ	Dissipation factor

TDR	Time domain reflectometry
TECK cable	Metal clad cable
Tip-Up	Changes in Tan δ with increasing test voltage
TRXLPE	Tree retardant cross-linked polyethylene
ULA	Universidad de Los Andes
U_0	Rated or operating phase-to-ground voltage
URD	Underground residential distribution
VLF	Very low frequency
WTRXLPE	Water tree retardant cross-linked polyethylene
XLPE	Cross-linked polyethylene

SUMMARY

The increased need for electric power combined with an aging underground cable infrastructure in a deregulated market environment have forced utilities to refocus their attention on reliability while at the same time reducing maintenance costs as much as possible. This has created a significant need for diagnostic methods and technologies to assess the condition of the underground cable systems. However, while several cable diagnostic technologies are available, they have not all yet been fully accepted in the United States. This is because the different technologies lead to different conclusions for the same cable system, and thus utilities do not completely trust the conclusions. A better understanding of the diagnostic technologies and their correct application is therefore required.

The most widely used diagnostic technologies in the United States include dissipation factor (Tan δ) and partial discharge measurements; these tests are therefore, the main focus of this thesis; in particular, when applied to underground extruded cable systems. The purpose of this research is to advance the field of characterization of power cable defects by addressing a number of theoretical and practical diagnostic measurements and their interpretation issues. The discussion is based on data from laboratory experiments and field tests.

This thesis consists of two major parts. The first part (Chapters 3 to 5) is devoted to the characterization by Tan δ measurements in which the major contribution is a new approach for condition assessment using this technology. The second part (Chapters 6 and 7) is devoted to the work on characterization by partial discharge measurements, and the major contribution is a novel approach that is able to analyze, evaluate, and reduce the number of partial discharge diagnostic features.

CHAPTER 1

INTRODUCTION AND OBJECTIVE OF THE RESEARCH

1.1 Background

The increased need for electric power combined with an aging underground cable system infrastructure in a deregulated market environment have forced utilities to refocus their attention on reliability. This has created a significant need for diagnostic methods and technologies to assess the condition of the underground cable systems.

While several cable diagnostic technologies are available, they have not yet been fully employed in the United States. American utilities are conservative entities and there are still many unresolved issues concerning the cable diagnostic methods and technologies. Utilities often report that diagnostic testing results are inconclusive, confusing, and that condition assessments sometimes do not agree with traditional diagnostic evaluation techniques. Many utilities are not convinced that cable diagnostic testing methods and technologies are sufficiently accurate to justify the cost of conducting these tests. This is further complicated by the fact that no one diagnostic technology has proven that is able to reliably and consistently assess the condition of the wide variety of cable systems currently in service. Therefore, in an effort to advance the area of power cable diagnostics, the National Electric Energy Testing Research and Applications Center (NEETRAC) launched the Cable Diagnostics Focus Initiative Project (CDFI) in February 2005.

The intent of the initiative is to provide cable diagnostic technology assessment and development via a series of projects designed by the NEETRAC and Georgia Tech research team, with technical advice from the initiative participants. The CDFI project is designed to bring together utilities, cable diagnostic providers, and other interested parties such as the United States Department of Energy (DoE), for the purpose of

assessing and enhancing technologies used to diagnose the condition of underground medium voltage (MV) power cable systems.

The research presented in this thesis is part of the CDFI project and deals with the characterization of real power cable defects by diagnostic measurements commonly used in the United States.

1.2 Problem Statement

Electrical insulation is one of the more important parts for any high voltage power system component. The quality of the insulation plays an important role in determining the reliability of the component. In the case of power cables, the insulation quality plays the most important role in their reliability. The insulation is designed to contain the electric field inside the cable insulation for safe operation during the service life of the cable. The insulation should be able to perform its function for a variety of different system operating conditions including temperature changes, load cycles, mechanical stresses, water ingress, and others. However, even if the insulation fulfills all required tests before installation and use, it may not maintain the same operation characteristics during the many expected years of service. There may be built-in manufacturing imperfections and/or workmanship errors that were not detected during commissioning tests. Furthermore, as in any other system, the insulation will experience aging and, eventually, degradation that could be quite dissimilar between different service conditions. All these could cause premature and unexpected failures; thus, affecting the reliability and maintenance costs.

In the United States, electric power distribution relies on a vast network of underground medium voltage cables. The distribution network has a finite life span, and at some point utility engineers must decide when to replace these components in order to avoid as much as possible unexpected cable failures and the associated costumer outages. In the past, corrective maintenance was normally applied, *i.e.* components were replaced

after failure. However nowadays, the deregularization of the electric energy market has forced utilities to refocus on the reliability of the aging power distribution cable system infrastructure, while at the same time reducing maintenance costs as much as possible. Matters are further complicated by the ever increasing need for electrical energy, thus leading to higher and higher demands on the existing cable system.

Consequently, utilities are interested in accurately determining the condition of the cable system components, and ultimately their expected remaining life span, before initiating permanent maintenance and replacement test programs. The proper application of condition based maintenance strategies can avoid unexpected outages and ultimately result in substantial savings for utilities. This requires the use of dependable cable diagnostic technologies. Nevertheless, while several cable diagnostic technologies are available, they have not yet been fully employed across the United States because utilities do not completely trust their assessments. This is not a simple problem to overcome since it requires a complete understanding of the diagnostic technologies as well as how to best apply them.

1.3 Objective

The objective of the research is to advance the field of characterization of power cable defects by addressing a number of theoretical and practical diagnostic measurements and their interpretation issues. The most widely used diagnostics technologies in the United States are dissipation factor (Tan δ) and partial discharge measurements; therefore, they are the main focus of this research. The discussion is based on data from laboratory experiments and field tests of underground distribution medium voltage power cable systems.

1.4 Thesis Outline

A brief introduction and the objective of this research are described in this

Chapter. The rest of the thesis is presented in seven more Chapters in which technical discussions, simulation, and experimental results are presented. The final Chapter summarizes and concludes the research work, and suggests directions for future research work. Each of the following Chapters is briefly described in the following paragraphs.

Chapter 2 provides the basic concepts of power cable systems and their diagnostics. The basic structure and accessories of a power cable system are explained. In addition, aging, degradation, and breakdown mechanisms of power cables are presented.

Chapter 3 presents the basic concepts, means of diagnosis, limitations of Tan δ measurements, and a comprehensive literature review on the "state of the art" on characterization of power cable defects by Tan δ measurements. More importantly, Chapter 3 discusses a number of issues that arise when using Tan δ measurements at very low frequency (VLF) to characterize the insulation of non-aged and field-aged MV cable systems using data from laboratory experiments and field tests.

Chapter 4 describes a laboratory test program conducted to investigate the correlation between Tan δ diagnostic features and the VLF breakdown performance for MV cross-linked polyethylene (XLPE) cables. The Chapter introduces the use of a new diagnostic feature that takes into account the scatter in the Tan δ measurements.

Chapter 5 introduces the basics of low voltage time domain reflectometry (TDR) test on power cable systems. The Chapter also presents the Tan δ versus length models. Particularly, the most common situations of non-uniform degradation and neutral issues are modeled and demonstrated through both theory and experiments. Finally, the Chapter discusses a new approach for condition assessment of MV polyethylene (PE) based power cable systems using combined diagnostics. The new approach is executed by an evaluation procedure that uses diagnostic features management with feature categorization and decision organization.

Chapter 6 provides the basic concepts, means of diagnosis, and limitations of

partial discharge measurements. Brief descriptions of the available types of partial discharge data, feature extraction, and classification tools, are also provided. A comprehensive literature review of the "state of the art" on characterization of power cable defects by partial discharge measurements is presented. Moreover, the Chapter describes and briefly analyzes laboratory and field partial discharge data that are the basis for the analysis and evaluation process of partial discharge diagnostic features presented in Chapter 7.

Chapter 7 presents a process for analysis and evaluation of partial discharge diagnostic features. The process allows for the selection of the most relevant diagnostic features when the partial discharge data is considered into groups of cable and accessory. The process is divided into two portions, *i.e.* an initial analysis and a final evaluation.

Conclusions, contributions, and recommendations for future work are discussed in Chapter 8.

CHAPTER 2

BASIS OF POWER CABLE SYSTEMS AND DIAGNOSTICS

2.1 Introduction

This Chapter introduces the basic concepts of power cable systems and their diagnostics. The fundamental structure and accessories of power cables are explained. In addition, aging, degradation, and breakdown mechanisms are presented. The Chapter finishes with an overview of power cable diagnostics technologies.

2.2 Basis of Underground Distribution Cable Systems

Underground distribution cable systems represent a significant investment and are a vital part of the power delivery distribution network. In an increasingly competitive and deregulated environment, it is essential that utilities maximize the profitability of their assets. This requires utilities to have knowledge of power cable systems and their diagnostics to make the right decisions about what cable system equipment to purchase and to have a general idea of how well it will perform in service, how it ages, degrades, and fails, and how it should be diagnosed for repair or replacement. The next sections give a brief description of the basics of underground distribution cable systems.

2.2.1 Distribution Power Cable

A distribution power cable is designed to carry electric current and withstand a certain operating voltage, which together allow it to deliver electric power. In some cases, it is simply defined as “a conductor with insulation” [1-2]. The use of distribution power cables encompasses a wide variety of applications that mainly include underground, underwater, overhead distribution, and electrical machines applications [3]. Generally, distribution power cables are described by their type of insulation material, voltage class, conductor material, conductor type, conductor size, and sheathing materials.

2.2.2 Distribution Power Cable Structure and Types

In the United States, the cable design that is mostly used in distribution systems is the single-conductor medium voltage cable. Its basic design has not changed over the last 100 years, but the improvement in the old and discovery of new materials and manufacturing processes have created a variety of types for the different applications. The voltage range for distribution power cables is from 6 to 36 kV [3].

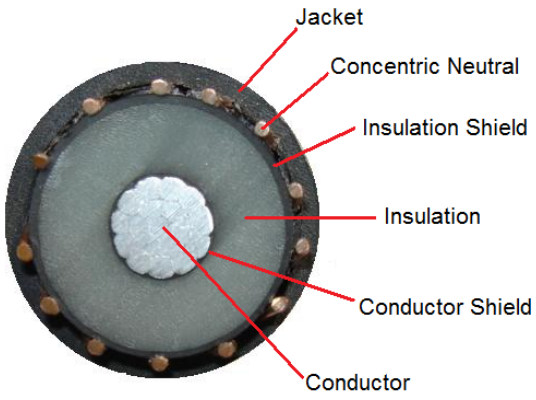

Figure 2.1. Cross section of a modern distribution power cable.

Figure 2.1 and Figure 2.2 show the cross and longitudinal sections of a modern distribution power cable, respectively. Starting from the center of the cable, the cable structure is composed of the conductor, conductor shield, insulation, insulation shield, concentric neutral, and the jacket.

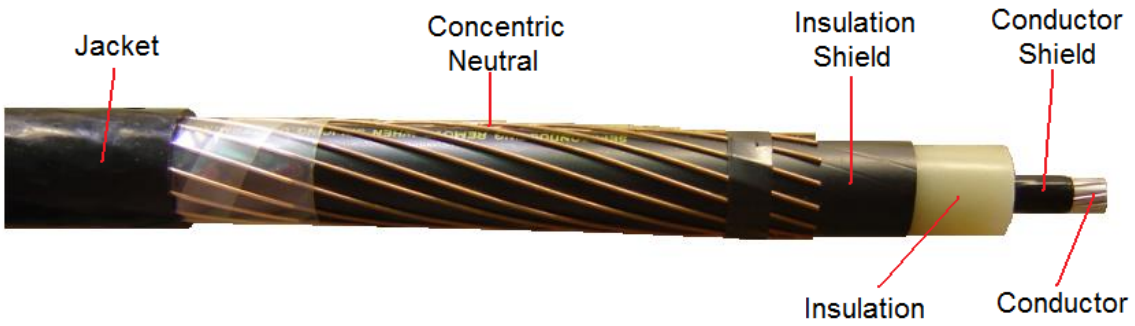

Figure 2.2. Longitudinal section of a modern distribution power cable.

2.2.2.1 Conductor

The main function of the conductor is to carry the electric current. Typically, it is made of copper or aluminum alloys and can be solid or stranded. A stranded conductor has more flexibility compared to a solid conductor; the wire strands may be filled with a resin to prevent water ingress and then it is called a "filled" conductor. Unfilled conductors, on the other hand, simply do not contain resin. It will be seen later that water plays an important role in cable degradation and failure mechanisms.

Copper alloys are about three times denser than aluminum alloys. Therefore, copper conductors are three times heavier than aluminum conductors. Lighter cables are preferable for installation. Nevertheless, because of the electrical conductivity of both materials and for a given current specification, a copper conductor can be two sizes smaller than an aluminum conductor. Thus, sizing and material selection of the conductor are not easy tasks since the criteria also depend on voltage drop along the cable, characteristics of the insulation material, flexibility, cable design, installation method, weight, and cost.

In some situations, the conductor is concentric round, but in other situations the conductor is compressed with the idea of providing an even smoother interface at the outer surface of the conductor, see Figure 2.3.

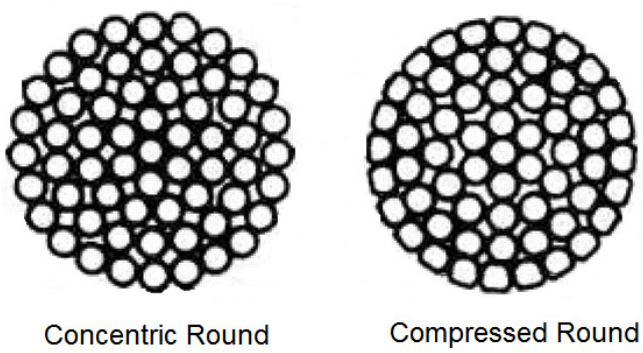

Figure 2.3. Concentric round and compressed round conductors.

The conductor size is given by the conductor cross sectional area. In the United States, the conductor size is defined by the American Wire Gage (AWG), known also as the Brown and Sharpe Gage [4]. The gauge is formed by a geometric progression between two consecutive diameters. The largest AWG size is 0000, commonly known as 4/0, and the smallest is 36, which is approximately 0.0050 in. in diameter. When the conductor size is greater than 4/0 AWG, it is given by the cross sectional area in thousands of circular mils (MCM), or kcmils. In some situations, MCM is used instead of kcmils. One circular mil (cmil) is defined as the area of a solid conductor having a diameter of one mil (one thousand of an inch) [1]. In addition, solid conductor types are found only up to 1/0 AWG size.

2.2.2.2 Conductor Shield

The main function of the conductor shield, or conductor screen, is to provide for a smooth interface between the conductor and the insulation. The smooth interface between the conductor shield and insulation avoids the presence of sharp points (known as protrusions) that could impose high-voltage stress to the insulation. The conductor shield and the insulation are chemically bonded. If the conductor shield is not present, electric field lines are more concentrated in the sharper edges around the outside perimeter of the conductor. As a result, high-voltage stress areas are created between the conductor and

the insulation interface. This decreases the life of the cable, as its eventual failure will likely be caused by this increased voltage stress.

The conductor shield is made of a semiconductive material. The semiconductive material is specially designed with about 30% to 40% carbon black to meet the required conductivity [3] such that the conductor shield and the conductor are at the same potential when the cable is energized.

2.2.2.3 Insulation

The insulation is capable of withstanding the operating voltage at the operating rated temperature, typically from 75° C to 90° C [3, 5]. The insulation can be classified as laminated or extruded insulation. The insulation should be clean there should be smooth interfaces with the conductor shield and insulation shield to avoid high electrical stresses that could cause early insulation failure.

The first insulation type, laminated insulation, is represented exclusively by Paper Insulated Lead Covered (PILC) cables. Layers of impregnated paper are placed on top of one another to create the cable insulation. Impregnated paper is the oldest and the most widely used material. Generally, the paper is impregnated with oil or gel that has dielectric properties suitable for insulation applications. As the impregnator needs to be contained within the insulation, the cable typically has a lead sheath. This type of cable has been used for over a 100 years and has seen extensive mature testing and evaluation procedures developed. Even with these procedures in place, the manufacturing and installing of paper cable still requires significant skill.

The use of PILC cables is declining. This situation is mainly due to environmental concerns with the lead cover and the impregnators [3]. In addition, paper cables have higher insulation losses and installation and maintenance costs than extruded insulation cables [5]. In fact, there has been a closure of paper impregnated manufacturing plants in

the last few decades, which in some situations makes PILC cable even difficult to find for new installations, maintenance, or repairs [3].

The second insulation type, extruded insulation, can be classified as thermoplastic or thermoset insulation. A thermoplastic melts at a certain temperature and freezes to a brittle and glassy state when the temperature is decreased sufficiently. Thermoplastic insulation includes polyethylene (PE), which is divided into Low Molecular Weight PE (LMWPE) also known as Low Density PE (LDPE), and High Molecular Weight PE (HMWPE) also known as High Density (HDPE). On the other hand, a thermoset is a polymer that cures to a more durable form because of curing. The curing converts the resin into a plastic or rubber using a cross-linking process into a rigid three-dimensional molecular structure. The cross-linking process creates a molecule with a larger molecular weight, resulting in a material with a higher melting point. In general, a thermoset is stronger than thermoplastic because of the three-dimensional molecular structure. Thermoset materials can withstand higher temperatures and are not recyclable as are thermoplastics [3]. Thermoset insulation includes Cross-linked PE (XLPE), Water Tree Retardant XLPE (WTRXLPE) also known as Tree Retardant XLPE (TRXLPE), and Ethylene Propylene Rubber (EPR). These are the insulations in popular use today.

2.2.2.4 Insulation Shield

The insulation shield, or insulation screen, serves the same function as the conductor shield and provides a smooth interface between the insulation and the concentric neutral. If the insulation shield is not present, electric field lines will appear around outside the cable insulation. The insulation shield assures that the voltage outside the cable is at ground potential. In the United States, the insulation shield and the insulation are not chemically bonded; in this case, the insulation shield is called a strippable shield. Strippable shields facilitate the cutback for terminating and splicing the cable [3].

The group of the conductor, conductor shield, insulation, and insulation shield is known as the cable core. The cable core is designed to keep the electric field inside the cable insulation and carry the electric current while dissipating the heat generated by the conductor during the useful life of the cable [3].

2.2.2.5 Concentric Neutral

The concentric neutral is placed over the insulation shield to keep the outer part of the cable core at ground potential, thus providing protection against accidental contact. It is also designed to carry fault currents, stray currents, charging currents, and imbalanced currents. The concentric neutral can be replaced by a metallic sheath to accomplish the same function. In this situation, the cable is said to be completely shielded. Generally, the concentric neutral or metallic sheath have been made of lead, aluminum, or copper in a variety of designs that include thin tapes, round wires, and solid or corrugated extruded tubes [3].

Corrosion is a problem for concentric neutrals and metallic sheaths and may occur at the interface between the metal and its surroundings. The corrosion is accelerated by the presence of water and the related pH of the soil [2].

The concentric neutral or the metallic sheath must be continuous along the cable length and have good contact with the insulation shield to guarantee that the outer area of the cable core is at ground potential. The lack of sufficient contact can generate a voltage gradient between the insulation shield and concentric neutral or metallic sheath. In this situation, electrical discharges could be generated and cause erosion of the insulation screen and subsequently the insulation. Eventually, this will lead to a cable failure [3].

2.2.2.6 Jacket

The jacket, also known as the over-sheath, is a protective covering that may also provide additional insulation. The protection could be against mechanical, thermal, or chemical stresses. Therefore, it reduces the concentric neutral or metallic sheath corrosion as well as the moisture ingress to the cable. It could also be designed to hold a metallic armor, wires, or tapes [2-3], enhancing even more the level of protection. Typical materials include Polyvinylchloride (PVC), chlorosulfonated PE, PE, LDPE, Linear Low Density PE (LLDPE), Medium Density PE (MDPE), HDPE, and nylon [2-3].

Variations on the designs previously described are available and are shown in Figure 2.4. They include concentric neutral without a jacket, metal clad cable (TECK cable) mainly used in mining and industrial applications, shielded cables with copper tape shields, and PILC cable [4].

Figure 2.4. Different cable types.

2.2.3 Distribution Power Cable and Accessories

Generally, a single length of cable is not long enough to cover the distance between points to which it is desired to distribute the electric power and therefore multiple cable lengths are cascade connected. The cable lengths are connected by joints or splices. At both ends of the cable lengths, a termination is used to make the transition from the underground to the overhead part of the distribution system or to a distribution transformer. When the transition is between the cable and a transformer the termination is usually known as an elbow termination or, simply, elbow. The joints and terminations are commonly known as accessories of the power cable system. The group of cable lengths, joints, and terminations are together referred to as a section of the power distribution cable system or simply cable segment.

Cable accessories play an important role in the power cable system insulation performance. As part of the power distribution cable system, they can also lead to failure. Therefore, the quality of cable accessories should be comparable to the quality of the cable itself such that the cable segment experiences uniform performance over time. When a segment contains more than one cable insulation type and one or more type of cable joints and terminations, the segment is said to be a hybrid.

2.2.4 Distribution Power Cable History

Power cables have their origin in the 1880s when the need for power distribution cables became evident after the invention of the incandescent light bulb [3, 5]. As urban areas grew, it became a necessity to replace some overhead lines with underground distribution cables since the number and size of feeders were impossible to accommodate using the overhead approach [5]. Impregnated paper insulated power cables were the first to be commercialized in 1884 by Callender Cables of England [5]. Medium-voltage PILC cables are still in use because of their durability and reliability. For some utilities they still constitute a considerable part of their underground distribution network.

Cable history from the 1800s to the present has been full of technological improvements with the invention of new materials, designs, and manufacturing processes; however, it is more relevant to take a closer look at the last 50 years of cable history because of the invention of polymeric material-based insulation, and since this research deals with some of these old cables.

Before and during the 1950s, the need for cable designs that were flexible and easier to handle for installation, compared to PILC cables, became apparent. Several forms of rubber were utilized to accomplish this goal. However in 1933, PE was discovered and started to gain acceptance for distribution power cable applications. By the 1950s, PE had already gained general acceptance and had replaced almost all previous rubber-based designs as well as a considerable percentage of PILC cables [5]. Initially, plastic cables manufactured in the United States were made of HMWPE. HMWPE has been used since 1951 for distribution voltages up to 35 kV [5] and was first introduced as an insulating material for medium-voltage Underground Residential Distribution (URD) cables in the late 1960s [4]. In 1963 with the invention of XLPE, HMWPE was quickly abandoned since XLPE-insulated conductors could operate at a higher temperature than HMWPE. Thus, utilities were able to use a smaller conductor size for the same current requirement [5].

It soon became apparent that PE-based cables were susceptible to a new failure mechanism when early cables began failing prematurely when the cables were operating in a wet environment, in some cases with less than 10 years of service. Thus, cable manufacturers and utilities were challenged to discover the possible causes and to find solutions that would give them the required confidence to continue their commitment to the underground polymeric insulation cable. It was discovered that these early failures were caused by a water-treeing degradation process starting from protrusions in the conductor and insulation shields, contaminants in the insulation and shields, or voids in the insulation. Water treeing is discussed in more detail in future sections.

In the 1980s remarkable advances were made to control water treeing with the introduction of a dry curing process for thermosets, super smooth and clean conductor and insulation shields, and ultra clean TRXLPE insulation. This new insulation includes tree-retardant technology developed to resolve the water treeing problem. It is based on two approaches; one is the use of additives and the other involves copolymer technology [3-4]. There is no question that tree-retardant technology is an innovation made possible by different compound suppliers. As a result, different TRXLPE technologies can be expected to have different characteristics and performance under identical service conditions [4].

In the 1960s, EPR-insulated cables were introduced to the market for voltages up to 60 kV [5]. EPR cables have better flexibility than PE-based cables, but they are also susceptible to water treeing. Unfortunately, this mechanism is not as well understood in EPR cables as it is for XLPE cables. In addition, the dielectric losses of an EPR cable are much higher than those of an equivalent XLPE or TRXLPE cable so the use of EPR cables above 69 kV for new installations is less desirable [5]. This is also the main reason why EPR cables are not used for transmission applications. It is important to mention that EPR cables are only extensively used in the United States, South America, and Italy [5].

Nowadays, the most popular insulation materials are TRXLPE and EPR, but some XLPE cables are also used. In the United States most utilities have not yet standardized the use of TRXLPE or EPR cables. Nevertheless, it has been shown that for typical URD-type applications, the advantages of low initial costs as well as the lowest total operating costs, such as dielectric losses through the life of the cable, suggest the use of TRXLPE over EPR insulation [6].

2.2.5 Distribution Power Cable Standards

Globally, cable standards are established by several organizations. Specifically in the United States and Canada, there are the Institute of Electrical and Electronics

Engineers (IEEE), the Association of Edison Illuminating Companies (AEIC), the American Society of Testing and Materials (ASTM), the Canadian Standards Association (CSA), the Canadian Electricity Association (CEA), and the Insulated Cable Engineers Association (ICEA). On the international scene, the International Electrotechnical Commission (IEC) is the dominant organization. In addition, many utilities have written their own standards that have gained international recognition [4, 7]. The standards that are available from these organizations cover all cable types, cable designs, cable materials, accessories, installation, operation and cable testing and include some indications for diagnostics.

2.2.6 Distribution Power Cable Aging, Degradation and Breakdown

As any other system, a power cable system ages as time progresses. Aging is responsible for changes in insulation properties because of the electrical, thermal, mechanical, and environmental stresses applied to the components of the cable system with time. An example of aging is the oxidation of the insulating material. In practical cases, there may be one or more aging mechanisms that could be dependent on one another. The exact path in which the cable system ages, degrades, and fails depends on several factors such as voltage, thermal stresses, maintenance, system vintage, cable system technology, and environment [8]. With time, the aging mechanisms contribute to the degradation process and eventually lead the cable system to failure or breakdown. Because the main reason that PILC cables fail is that the outer sheath is cracked or corroded, allowing moisture penetration [3, 9], the discussion on this section is mainly based on the aging, degradation, and breakdown of cables with extruded polymeric insulations. Special attention is given here to XLPE insulation since it represents 35.4% of the total installed cable, making it the most common insulation material [10]. In addition, as mentioned before, the use of PILC cable is declining; the old HMWPE cable is being replaced by new cable, the aging mechanisms of TRXLPE cable are somewhat

similar to XLPE cable, and the aging mechanisms for EPR cables are still not as well understood as those for XLPE cables.

Defects in cables with polymeric insulation that can lead to failure are pictorially described in Figure 2.5. These defects mainly include protrusions, voids, cracks, delaminations, conductor shield interruptions, water trees, and electrical trees [8].

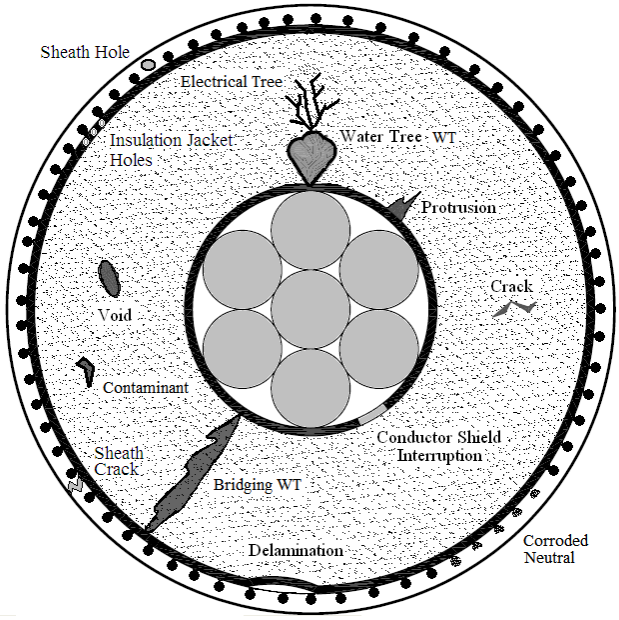

Figure 2.5. Typical defects found in power cables with polymeric insulation [8].

In addition, typical defects that can evolve into failures in a cable joint with extruded insulation are shown in Figure 2.6. Defects including voids, interface discharge or tracking between the interfaces of the cable insulation and the joint insulation, and knife cuts made during the shield cutback operation are all possible. The same types of defects can occur in different joint constructions (taped and pre fabricated) and terminations [8].

The aging mechanisms for a cable system depend on factors that involve the cable, accessories, and operating conditions. Therefore, different cable systems age in

different ways. The aging, degradation, and breakdown mechanisms are statistical in nature [11-12]. Thus, significant variations are expected in how these mechanisms develop and evolve with respect to cables and accessories, and even between cable systems operating under similar operating conditions and environments [8].

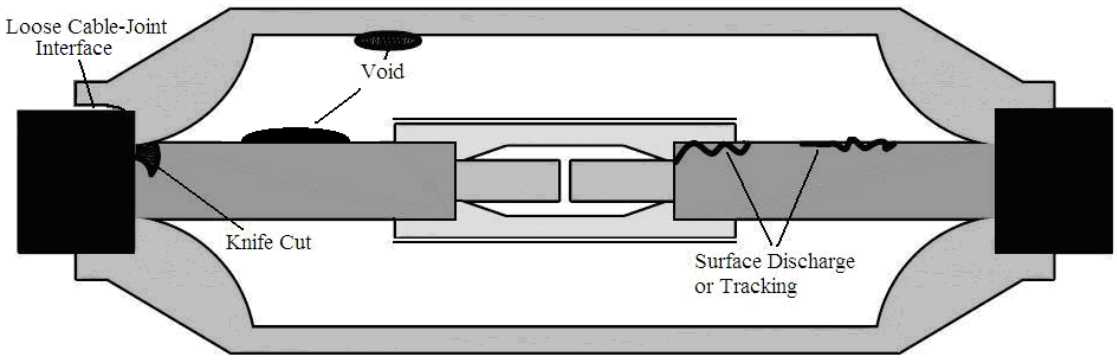

Figure 2.6. Typical defects found in cable joints with extruded insulation [8].

2.2.6.1 Physical and Chemical Aging

In addition to the degradation resulting from the presence of the electric field inside the cable insulation, physical and chemical aging play important roles in the overall cable system life. Physical and chemical aging are important since they may influence the probability of breakdown and may also contribute to electrical aging [12]. Physical aging is related to the physical changes occurring in the insulation material with time. Physical degradation includes, for example, the diffusion of additives or absorption of foreign solvents, causing the cable to swell [12].

Chemical aging is due to the appearance of free radicals inside the polymer. Free radicals are highly reactive. In other words, they are likely to take part in chemical reactions that cause propagating chain scissions or cross-linking network formation in the polymer. In the case of XLPE, the chain scission sequence is random in space with free

radical transfer between chains [12]. Chemical aging can be initiated by thermal, oxidative, ionizing radiation, or mechanical factors [12]. Among these, chemical aging resulting from oxidative factors is one of the more important forms of chemical degradation, particularly the oxidation caused by heat or thermal oxidation. Oxidation can increase the electrical stress and reduce the breakdown strength. Therefore, the breakdown statistics may be skewed to the disadvantage of the insulation material. This can be prevented by selecting the proper insulation material morphology or through the use of chemicals such as antioxidants [12].

2.2.6.2 Electrical Aging

Electrical aging requires the presence of an electric field. The most common processes are water tree degradation, electrical tree degradation, and partial discharge degradation [12]. Because of the relevance of these degradation processes, they are discussed in detail in the next sections.

2.2.6.3 Water Tree Degradation

The degradation that can occur inside the bulk polymeric insulation of a distribution power cable when it is exposed to moisture and electrical stress is known as water treeing. Small tree-shaped defects appear inside the insulation and grow in the direction of the electric field. The presence of water trees inside the insulation causes the reduction of the electrical breakdown strength of the cable insulation system. Water trees are diffused and blurry and give the impression of disappearing upon drying, unlike the electrical trees that have distinct hollow channels [13-14]. Figure 2.7 shows two water tress that have grown from the insulation shield toward the conductor shield as well as trees inside the bulk insulation for an XLPE cable. Note that both water trees have different shapes and sizes; the longest water tree is almost bridging the insulation.

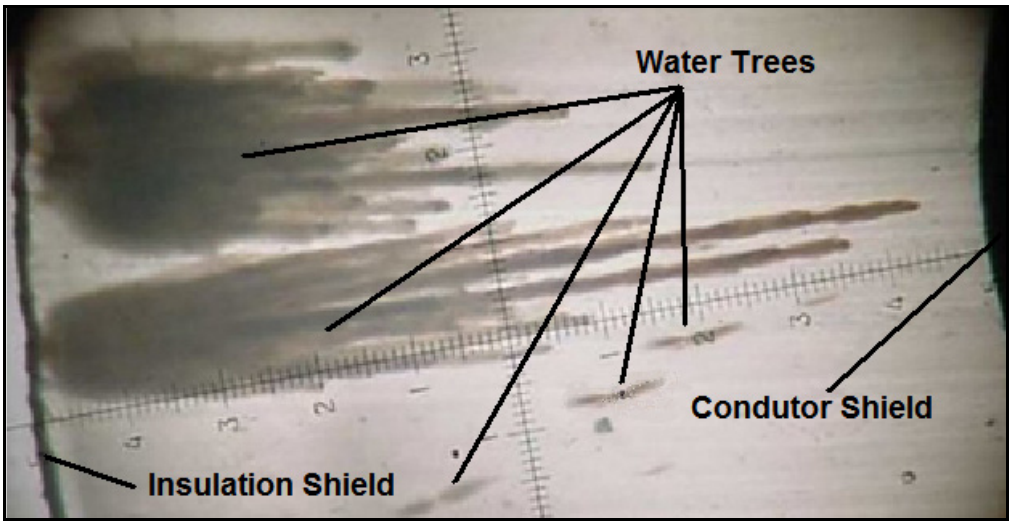

Figure 2.7. Water trees for a XLPE cable [15].

Water trees are classified as follows:

Bow-tie Water Trees: This type of water tree grows from a specific location inside the bulk insulation; the location is typically a void, water soluble contaminant, or other defect type. Generally, they grow up to several hundred microns [5, 16] and have a symmetrical shape that resembles a bow-tie from which they derive their name. In most cases, bow-tie water trees do not result in failure. Nevertheless, they have a significant role in the reduction of the breakdown strength compared to vented water trees [12].

Vented Water Tress: This type of water tree grows from the interfaces between the semiconductive shields and the insulation. Vented water trees are considered as the primary cause of failure in water treed samples [12-13]. The critical vented trees are those that grow from the conductor shield. These trees may be confined to only a small portion of the total cable length. However, they can grow quite long, depending on the cable design and service conditions.

Figure 2.8 shows bow-tie and vented water tress for an XLPE cable. Note the difference in size and shape between them. In general, bow-tie trees stop after initial rapid growth, while vented trees continue to grow [12].

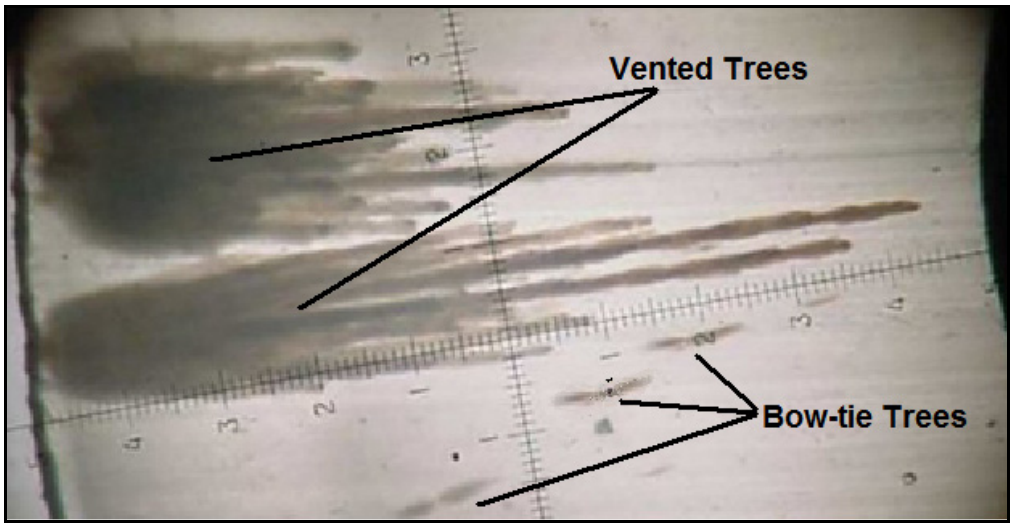

Figure 2.8. Bow-tie and vented water trees [15].

2.2.6.4 Water Tree Modeling

There is no well-established model for water trees, but generally water tree initiation is assumed to be due to mechanical overstressing and the formation of micro-cracks around water droplets inside the insulation [17]. In general, water treed insulation is considered to be formed by water droplets forming a string of pearls interconnected by narrow channels of crazed insulation. This is illustrated in Figure 2.9.

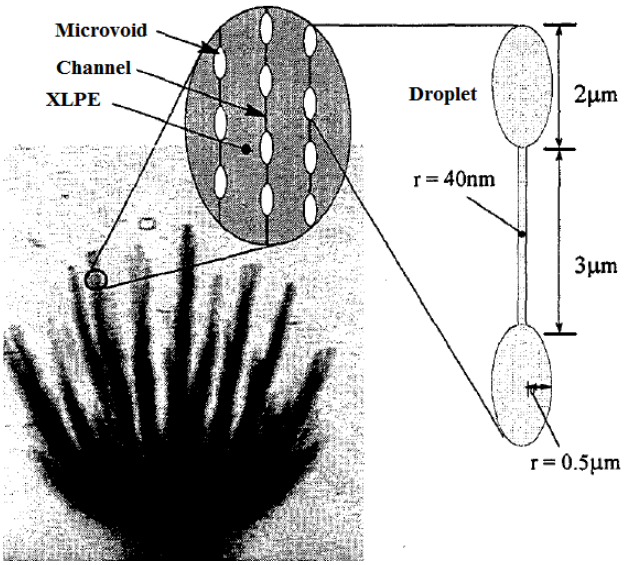

Figure 2.9. Model of a water tree structure showing ellipsoid shaped microvoids forming a string of pearls interconnected by small channels [17].

In a new cable, the formation of water filled voids will probably be a slow process. It is therefore likely that newly formed water tree regions close to the tips of the water trees will have a lower density of water filled voids and, consequently, lower water content than the main body of the tree structure. Therefore, as water decreases the conductivity of the polymer, these regions will be less conductive [17].

In general, it is accepted that the degradation of the cable insulation resulting from water trees has three main stages: the initiation of the water tree, the growth of the water tree, and the final breakdown process. Although the initiation and growth of water trees have been intensively studied, some of their true physical mechanisms still remain unknown [18]. Dissado *et al.* [19] have shown that the water trees grow more rapidly in early aging stages and then more slowly later on. By comparison, the propagation rate of an electrical tree is at least 1000 times faster than the water tree rate. This is the main reason Dissado *et al.* [12] split the water-tree degradation process into before and after the presence of electrical tress in the insulation. When an electrical tree is initiated from a

water tree, breakdown follows within some hours even under normal operating stresses of (2 kV/mm) [18].

The breakdown stage starts with the transition of the water tree into an electrical tree. Generally, this transition occurs at the tip of the water tree since at this particular location the electric field gradient has its maximum. This situation is shown in Figure 2.10. Some recent literature has reported the growing of electrical trees not from the tips of the water trees but from the base [20], see Figure 2.11. This is considered to be uncommon because the electrical tree often, but not always, confines itself to the volume of the water tree [18]. Eventually, the electrical tree propagates through the insulation and ultimately bridges the electrodes and causes a failure.

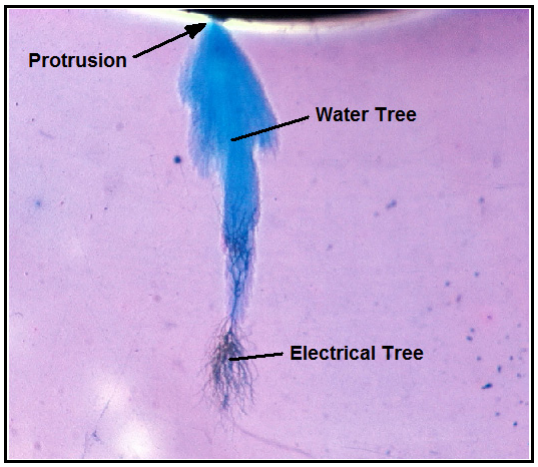

Figure 2.10. Electrical tree growing from the tip of a water tree [15].

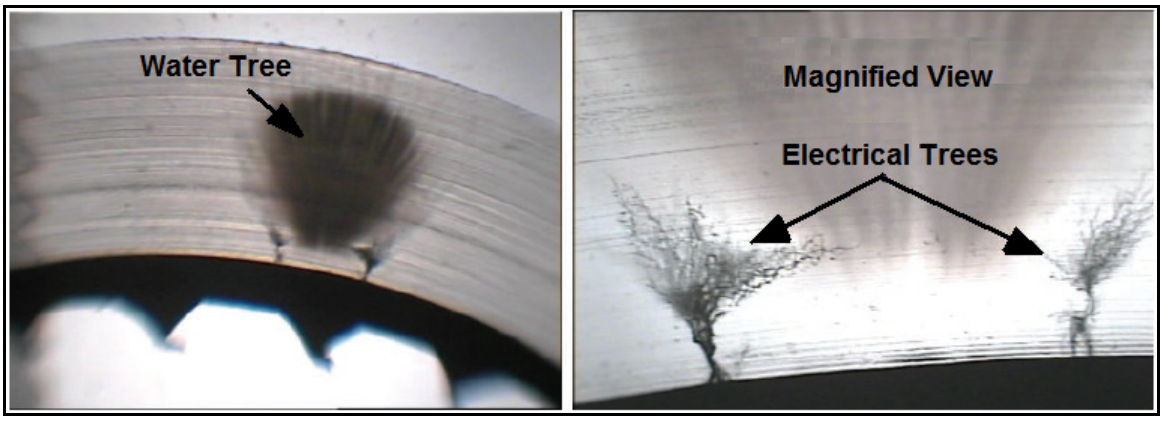

Figure 2.11. Electrical trees growing from the base of a water tree [20].

The transition of a water tree to an electrical tree depends on various factors that include the voltage magnitude, voltage transients, cable design, and the oxidation within the insulation [14]. Bulinski *et al.* [18] have shown that the transition of a water tree to an electrical tree for field-aged cables and modeled specimens of XLPE occurs approximately when the length of the vented water tree has reached the insulation shield or within 200 μm from it. As mentioned before, the water trees consist of miniature paths and microvoids along which water penetrates because of the electric field. When the voltage and the water are removed, the water trees seem to disappear. After the reappearance of water and reapplication of voltage stress, the water trees regenerate [13-14]. It has been also shown that the temperature influences the transition of a water tree into an electrical tree. As the temperature increases, the time required to initiate an electrical tree decreases; this could be due to the increased oxidation inside the insulation as a result of the increase in temperature [14]. In addition, no particular contaminant type or contaminant concentration as presented by [14] has shown any correlation with the transition of a water tree into an electrical tree.

A water tree can also generate an electrical tree as a consequence of the application of a transient overvoltage. The shorter the duration of the overvoltage, the higher the magnitude needed to initiate an electrical tree [5].

When water trees change from dry to wet, then their dielectric properties also change. Wet water trees have different and nonlinear dielectric properties, while it is generally found that dry water trees have the same dielectric properties compared to the surrounding dry polymeric insulation material [21]. Wet water trees are often found to have a relative dielectric permittivity of 2.3 to 3.6 [21]. In addition, Notingher *et al.* [22] have computed a relative dielectric permittivity of 9.2 at the tip of a wet water tree growing from a needle, assuming an average permittivity of 4.8. The conductivity of a wet water tree is much larger compared to the surrounding polymeric material [12]. Therefore, it is generally assumed that wet water treed areas will exhibit higher permittivity as well as conductivity.

Under conditions of very low frequency (VLF), or power frequency of 60 Hz, or high frequency electric fields (because of transient overvoltages), the voltage distribution within the cable insulation is mainly determined by the capacitive coupling, which in turn is governed by the permittivity. Wet water treed areas have relatively higher capacitance. Therefore, they take a smaller proportion of the total voltage difference between the conductor shield and insulation shield, while the surrounding dry areas of polymeric insulation become overstressed. This situation is shown in Figure 2.12 by the equipotential lines that identify four enhanced stress areas around the vented and bow-tie water trees. As the water trees grow larger, so does the stress in these areas, which increases the likelihood that the water tree will transition to an electrical tree.

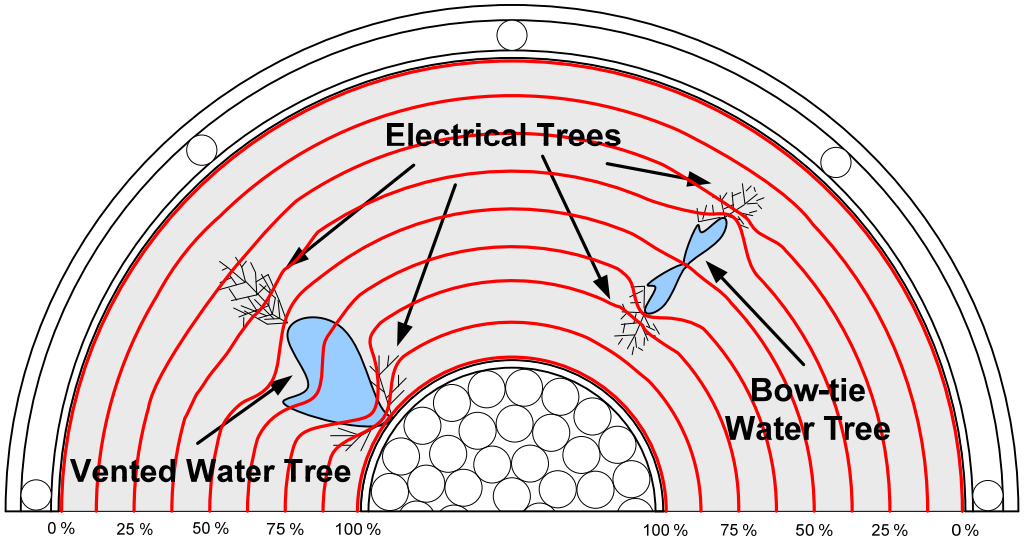

Figure 2.12. Stress enhancement sites of possible creation of electrical trees by water trees.

The time taken for a vented water tree to grow right through the entire insulation during the cable service life has been found to vary considerably, from around 5 years and up [12-13]. This time depends on cable design, cable quality, manufacturing process, maintenance, and service conditions.

2.2.6.5 Electrical Tree Degradation

Electrical treeing was the first degradation mechanism observed in polymeric insulated power cables [23]. An electrical tree is a network structure formed by fine channels that grow relatively quickly through the insulation and eventually cause insulation breakdown [24]. The channel walls are normally only partly carbonized. Therefore, some electrical trees can bridge the entire insulation layer without breakdown [12-13]. Like water trees, electrical trees can be divided into vented trees initiated from an electrode, and bow-tie trees generated inside the bulk insulation. Figure 2.13 shows an electrical tree growing from the tip of a needle.

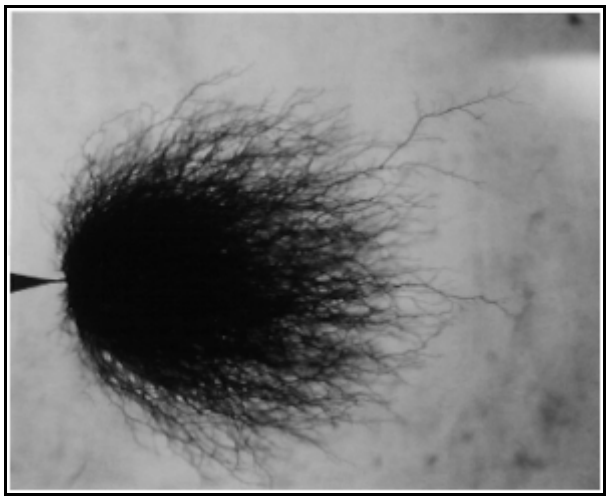

Figure 2.13. An electrical tree growing from the tip of a needle [15].

An electrical tree is usually initiated from a defect, such as a conductive contaminant or a needle tip. The defect can cause local field enhancements up to several hundreds of kV/mm [13]. In addition, electrical trees can also initiate from eroded surfaces in a void, water trees, or any other stress enhancement without a void [24].

The local field enhancement may give rise to electrons with energies of several electron-volts. With this energy, electrons are able to break polymer bonds directly or even excite polymer molecules. In the latter case, the excited molecule emits photons when returning to a neutral level. The photon emissions can then break new bonds or excite new molecules. As time progresses, especially in combination with oxidation, bond breakage could lead to void formations or electrical tree initiation [12].

The growth of an electrical tree can be divided into inception stage, propagation stage, and runaway stage [12], illustrated in Figure 2.14. The propagation stage is further divided into two periods. After inception, the electrical tree will undergo a fast growth period followed by a period of slow fractal propagation. A more accurate representation of the growth of an electrical tree includes intermittent growth with bursts of growth decaying to a standstill and followed by further growth activity [12, 25]. After inception, electrical trees can keep growing even at voltages lower than the inception voltage [12].

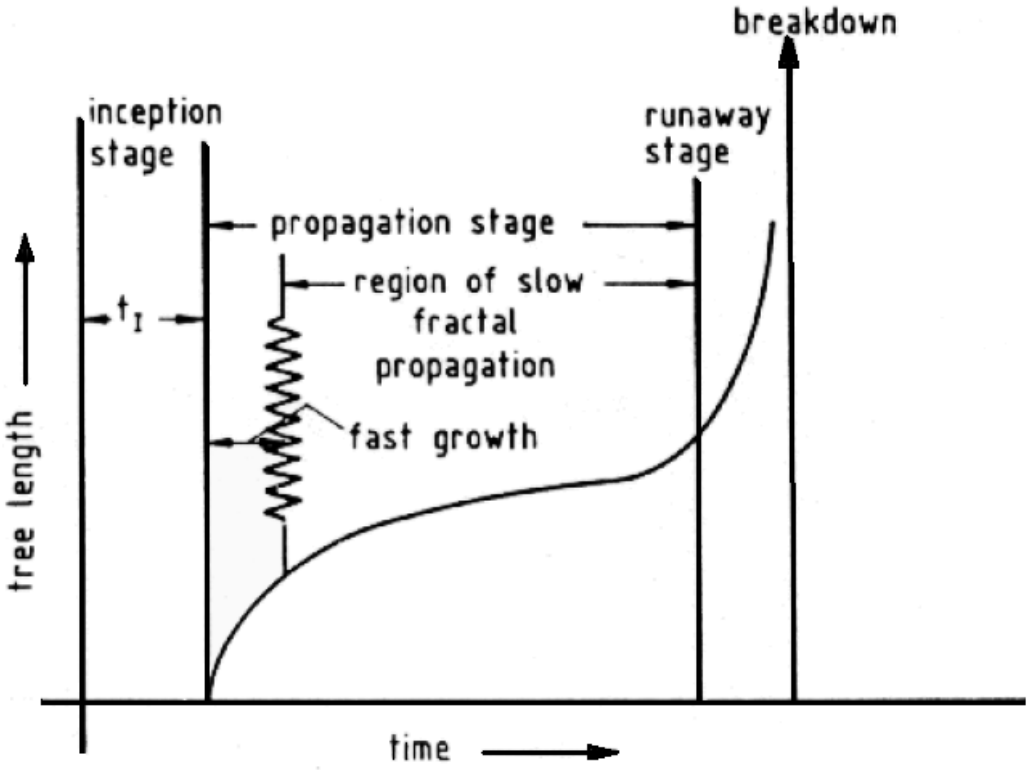

Figure 2.14. Schematic representation of electrical tree growth [12].

To reduce electrical tree inception, smooth insulation shield interfaces and clean insulation material are of paramount importance. The growth of electrical trees is dependent on voltage level, voltage waveform, voltage frequency, and insulation material.

2.2.6.6 Partial Discharge Degradation

Partial discharge is defined as "an electrical discharge that only partially bridges the insulation between conductors, and may or may not occur adjacent to a conductor" [1]. Partial discharges occur when the local electric field intensity exceeds the dielectric strength of the dielectric involved, resulting in local ionization and breakdown. Partial discharges can be generated from electrical trees, voids, cuts, cracks, protrusions, delaminations, and contaminants with poor adhesion to the polymeric insulation material

[24]. Prolonged partial discharge activity causes erosion of the insulation material by weakening and breaking chemical bonds, which leads to the formation of scissions [12]. As time progresses, scissions get deeper. When the chemical bonds are broken, the physical and electrical properties of the insulation material change. In addition, the momentary discharge results in a contained, hot, and ionized plasma. This plasma can be sufficiently hot to carbonize the surrounding insulation material. The resulting carbonized material is highly conductive and concentrates the electrical stress at the ends of the scission that align with the electrical field. Consequently, the changing electrical stress pattern allows the process to continue. Since part of the insulation is now electrically shorted out, the remaining intact insulation must now withstand an increasing level of electrical stress. Eventually, this leads to the formation of an electrical tree and consequently electrical tree degradation. These trees will grow and complete the route to breakdown.

2.2.6.7 Breakdown Mechanisms

The breakdown mechanisms of extruded insulation can be divided into electric, thermal, electromechanical, and partial discharge mechanisms [2, 12].

Electric Breakdown

Electric breakdown can occur at very high electric field strength. In this case, a free electron is forced by the electric field to initiate an electron avalanche, thus causing the breakdown. In practical situations, the very high electric field never appears. Nevertheless, the breakdown level is determined by imperfections or defects that reduce the field strength in a localized area of the insulation.

Thermal Breakdown

This type of breakdown occurs when a localized area of the insulation cannot dissipate the heat losses to the surrounding media, resulting in an increase of temperature

in the particular location. The temperature increment causes an increment of the insulation material conductivity that as a consequence increases the dissipation current and therefore the losses. The increment in the losses causes an increment in the temperature and the process is repeated. This is like a domino effect. The temperature will increase to a point where the insulation material melts, thereby resulting in thermal breakdown or runaway breakdown.

Electromechanical Breakdown

This breakdown is caused by the forces induced by the electrostatic field in the cable. The conductor and neutral attract each other; this reduces the insulation thickness and therefore the required breakdown stress. This situation is more likely to occur when the insulation material is at a temperature at which the material is in a softening condition. However, this is unlikely to occur since in practical situations the cables are operating well below the softening point.

Mechanical Breakdown

This type of breakdown occurs when some mechanical damage is done to the cable. Digging constitutes a good example. This situation is random and is not related to cable system degradation.

Partial Discharge Breakdown

The presence of partial discharge inside the bulk insulation of a cable system implies the presence of electrical trees. Because of the partial discharge, the electrical trees will increase their size and continue propagating through the insulation. This reduces the breakdown strength, leading eventually to an electric breakdown.

Breakdown in polymeric cable insulation is always a catastrophic event. In other words, the event is irreversible and destructive. It generally results in a narrow breakdown channel between the electrodes. All breakdown processes in polymers are

power driven and ultimately thermal in the sense that the discharge channel involves at least the melting and probably the carbonization and vaporization of the material [12]. Dissado *et al.* [12] have presented the relationship between low-level degradation mechanisms such as water trees and electrical trees and the breakdown processes in a graphical manner. This is shown in Figure 2.15. However, the distinction between the degradation and breakdown stages is not clear. As mentioned before, the breakdown mechanism is assumed to have started only after the presence of partial discharges. Figure 2.15 also shows that there is an overlap between the electrical and thermal breakdown mechanisms; because of in some situations, a bridging water tree could cause a thermal breakdown without the presence of partial discharges. Nevertheless, this situation is quite uncommon and it is generally accepted that more than 90 % of cable polymeric insulation failures follow to some extent the degradation and breakdown processes shown in Figure 2.15.

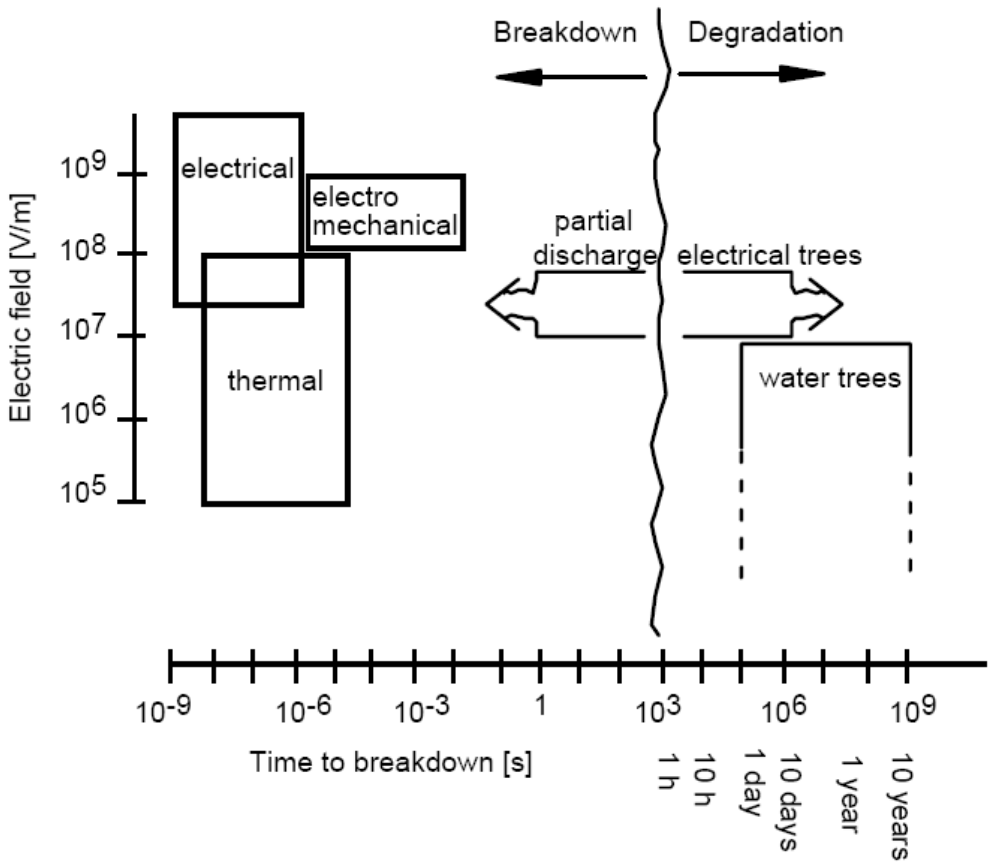

Figure 2.15. Time and electric fields at which various electrical breakdown mechanisms are operative [12].

2.3 Overview of Power Cable Diagnostic Technologies

Power cable diagnostic technologies can be used in two ways: to verify that a new or repaired cable segment has no problems or to assess that an aged cable segment system will soon experience failures. In most cases, the proper application of the technologies, together with corrective action, results in a reduction of cable system failure rates, which increases the system reliability [12, 26]. This section discusses the basic principles of the various diagnostic technologies.

The main cable diagnostic testing technologies used to assess cable circuit conditions are as follows:

- Partial discharge at 60 Hz elevated voltage, Very Low Frequency (VLF) of 0.1 Hz elevated voltage, or Oscillating Wave (OW) elevated voltage.
- Dissipation factor (Tan δ) at 60 Hz, VLF (0.1 Hz) or various frequencies and voltages.
- Withstand voltage tests at elevated VLF, 60 Hz, AC, or DC voltages.
- DC leakage current.
- Polarization/depolarization current and recovery voltage.

2.3.1 Partial Discharge

A large amount of research has been published over the past decade regarding the characterization and classification of partial discharge sources in power cable systems. Nevertheless, the study of partial discharge in cables for practical applications is still empirical in nature. This is due to the complexity of the partial discharge phenomenon itself [27-29]. The partial discharge diagnostic test is typically used to find localized defects in cable systems. The technology can be applied to all cable types. The test equipment detects transient electrical or acoustic signals generated at the discharge site. These signals travel from the discharge site through the cable system to the test equipment.

Multiple methods exist for detecting partial discharge signals. The sensors used for detection can be either electrical or acoustic in nature. For electrical detection, partial discharge sites generate microvolt and microampere signals, which may be detected either with potential or current transformers. Potential transformers in the form of capacitive dividers must be connected to the cable at one or both ends of the segment under test, while current transformers may be installed wherever there is access to the cable. Acoustic detection is done with a sensitive microphone that is positioned as close as possible to the partial discharge site. When a partial discharge occurs, it produces an

immediate release of energy that results in a mechanical wave that propagates through the material of the device in which it occurs [30-31]. Therefore, the partial discharge site acts as an acoustic wave source. Partial discharge testing can be performed both online and offline [32]. Most offline techniques apply 1.5 to 2.5 U_0, where U_0 is the rated phase to ground RMS voltage.

Partial discharge testing is not a simple test, as it requires specialized equipment and trained operators. The partial discharge is a stochastic process and therefore difficult to interpret. In addition, partial discharge measurements strongly depend on the type and location of defects, operating and testing voltage magnitude and frequency, circuit operating conditions, type of insulation material, and ambient noise [33].

2.3.2 Dissipation Factor (Tan δ) and Dielectric Spectroscopy

Dissipation factor (Tan δ) is a measure of the degree of real-power dissipation in a dielectric material and therefore its losses. In the case of underground cables, this test measures the bulk losses rather than the losses resulting from a specific defect. The dissipation factor can be applied to all cable types; however, test results must be considered with respect to the specific cable insulation material and accessory type. The dissipation factor is measured by applying an AC voltage and measuring the phase difference between the voltage waveform and the resulting current waveform. This phase angle is used to resolve the total current into its charging and loss components. The dissipation factor is the ratio of the loss current to the charging current. The term "Tan δ" is often used interchangeably with dissipation factor and arises from the fact that the dissipation factor is simply the ratio of orthogonal current components. The angle δ is the angle between the total current and the charging current when they are represented as phasors [34].

The cable segment under test is disconnected from the grid and energized from a separate power supply. The segment is typically energized using a voltage level of U_0 and

2 U_0. Measurements are then compared to known Tan δ values for the specific type of dielectric [35]. As this test requires a separate power supply, it is important to understand the differences between 60 Hz AC and VLF (0.1 Hz) power supplies used for Tan δ measurements. There are two current components that correspond to Tan δ, the loss current and charging current. The latter depends on the capacitance of the cable and thus inversely on the frequency. The benefits of using a low test frequency are that (a) the power supply must supply a lower total current, which dramatically reduces the power supply size and (b) increased sensitivity to the loss current. For example, the charging current at 60 Hz is 600 times larger than at 0.1 Hz.

It is important to mention that some factors could influence the dissipation factor, such as accessories that employ stress relief materials with nonlinear loss characteristics. They can cause the measurement to indicate a condition that is not the true condition of the cable insulation. This can be overcome by performing periodic testing at the same voltage levels while observing the general trend in dissipation factor values [34]. Additional factors not so easily controllable include temperature, moisture content, non-uniform degradation, and corrosion of the neutral wires.

Additional information on the condition of the insulation may be obtained by repeating dissipation factor measurements at frequencies in the range of 0.01 to 100 Hz [13, 36]; this is known as dielectric spectroscopy.

2.3.3 Withstand

Withstand tests are the application of an elevated voltage for a finite duration and can be applied to all types of cables and accessories. When elevated voltage with respect to the normal operating voltage is applied, the intent is to cause weak points in the cable segment to fail during the test.

This technique is conducted offline. The applied voltage could be DC, VLF, or 60 Hz AC. Typical testing voltages range from 1.5 U_0 to 3.0 U_0 or even more. DC voltages

are not advised for aged polyethylene cables, as the DC voltages may cause space charge accumulation in the bulk insulation, thus causing the cable to fail prematurely [37]. In general if a failure occurs during testing, the failure is repaired and the segment is retested. If additional failures occur, then the entire segment should be replaced. Withstand tests are intentionally destructive and therefore should not be performed without proper planning in segments that are considered critical to system operation.

2.3.4 DC Leakage Current

The DC leakage current test is based on the application of DC voltage together with the measurement of the leakage current. It is primarily intended to measure the global condition of the cable insulation, but it can also be useful for measuring tracking currents at insulation interfaces and terminations. This technique can be applied to all cable segment types except those with aged PE-based insulation materials [37]. The test voltage is increased stepwise; each step usually takes 30 seconds. The duration of the test is about 10 minutes. The maximum step voltage is typically about twice the peak value of the cable operating voltage. Following the voltage application, the cable must then be grounded for a period of at least four times the duration of the test before retesting or being returned to service [38].

2.3.5 Depolarization Current and Recovery Voltage

These two techniques are conducted offline and are able to give a global insulation condition. They are sensitive to the level of water tree degradation in the insulation [39]. Both techniques can be applied to cable segments with one type of insulation material with conventional or nonlinear stress relief accessories. The testing procedure is as follows: the cable segment is energized using a DC voltage. Typical voltages range from 0.5 U_0 up to 2 U_0. The energizing time is usually 15 minutes. After energizing, the segment is discharged for 2 to 5 seconds through a ground resistor. Then,

the open circuit voltage (recovery voltage) or short circuit current (depolarization current) is measured for 15 to 30 minutes [8].

By using the short circuit current, the depolarization current technique measures the time constants of the trapped charge within the insulation. Time constants carry the information on the cable insulation condition. An aging factor that uses the time constants can be defined [40], but its values are only applicable to assess cable segments with similar designs.

The recovery voltage technique uses the maximum value of the open circuit voltage. Non-aged cables exhibit a well-established proportionality between the maximum value and the energizing voltage, while aged cables do not. The proportionality is used as the indicator for diagnostics. Although this proportionality is considered to be a good indicator, an erroneous assessment can be obtained when using only the maximum value of the recovery voltage. Thus, overlooking the time dependency of the recovery voltage could lead to an incomplete diagnosis [8]. In addition, the indicator is only applicable to cable segments with similar designs.

2.3.6 Discussion

Various diagnostic testing technologies are capable of assessing different specific characteristics of a cable system. In most situations, more than one technology should be utilized to establish a better picture of the cable system condition. Then, it may be convenient to combine diagnostic tests that identify bulk or global degradation with those that identify local defects. Combining one test from each of these groups will also aid in deciding whether a segment should be repaired (*i.e.* local defect) or replaced (*i.e.* global degradation).

It is also a good practice to perform periodic testing. This is because any accepted criteria are valid only for specific cable segment configurations. For example, criteria for cable segments that have multiple insulation types are not available. Therefore, the best

approach is to observe trends in the measurements over time. Changes in the data will clearly indicate whether or not further degradation has occurred. Nearly all diagnostic tests may be used in this fashion, with the exception of withstand, as it only provides pass/fail indications. In the United States, the main diagnostic technologies used are dissipation factor, withstand, and partial discharge [8].

2.4 Summary and Conclusions

This Chapter has introduced the basic concepts, structure, and accessories of power cable systems and their diagnostics required for understanding the upcoming Chapters of this theses. In addition, aging, degradation, and breakdown mechanisms have also been presented together with an overview of power cable diagnostics technologies.

CHAPTER 3

CHARACTERIZATION BY TAN δ MEASUREMENTS

3.1 Introduction

Medium voltage distribution cables and their accessories form a critical part of power delivery systems. The systems employ insulation materials that have a low permittivity and loss. The permittivity and the loss are dielectric properties of the insulation material. As the systems age, these dielectric properties change such that they may provide a convenient way to monitor the insulation degradation. Generally, the dielectric loss is monitored because it can increase several orders of magnitude during the service life of the systems. This approach correlates well with the known mechanisms of degradation, namely the ingress of water and the subsequent growth of water trees as discussed in Chapter 2.

During the last decade, VLF testing for extruded distribution cables has gained interest among the North American utilities. The increasing interest is evidenced by recent publications as [41] and [10] and discussions inside the expert community in which standards are being proposed and continuously discussed [42].

In practice, it is convenient to measure the dielectric properties at a VLF of 0.1 Hz. This both reduces the size and power requirements of the energizing source and increases the resolution. While it seems there is a general consensus as to the interpretation of the dielectric properties for diagnosis, many issues regarding the definition of more accurate means of system evaluation still need further study.

Consequently, this Chapter discusses a number of the practical issues that arise when making these measurements at VLF on field-aged and non-aged cables, particularly Tan δ measurements. The goal is to show that the interpretation of Tan δ measurements is not as simple as it appears to be and that Tan δ is a feature rich diagnostic tool when the

data are obtained and interpreted appropriately. The discussion is based on data obtained from laboratory experiments and field tests performed on actual cable systems in operation.

3.2 Basis of Tan δ Measurements

Tan δ measurement constitutes a cable diagnostic technique that assesses the general condition of the cable system insulation, which can be represented by an equivalent circuit that consists of two elements; a resistor and a capacitor [37]. When voltage is applied to the system, the total current is the result of the contributions from the capacitor current and the resistor current. Generally, the measurements are carried out offline with an energizing source that could be of 0.1 Hz or 60 Hz. The equivalent circuit and the correspondent phasor diagram are shown in Figure 3.1.

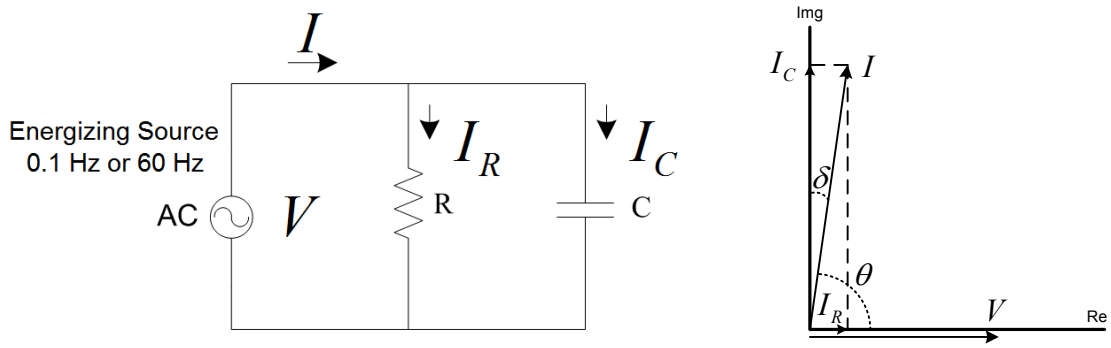

Figure 3.1. Equivalent circuit for Tan δ measurements and phasor diagram.

The equivalent circuit parameters of Figure 3.1 are as follows:

R: Equivalent resistance representing the insulation losses in Ω,

C: Equivalent capacitance in F,

V: Applied voltage phasor in V,

I: Leakage current in A,

I_R: Loss current in A,

I_C: Charging current in A,

δ : Phase angle between I_C and I in degrees.

The dissipation factor as function of the equivalent circuit parameters is given by,

$$DF = Tan\ \delta = \frac{I_R}{I_C} = \frac{V/R}{V/(1/\omega C)} = \frac{1}{\omega RC}, \tag{3.1}$$

where,

DF: Dissipation factor commonly named Tan δ,

ω : Angular frequency in rad/s.

The power P in watts, that is absorbed by the circuit, is given by,

$$P = V^2 \cdot \omega \cdot C \cdot Tan\,\delta, \tag{3.2}$$

where,

V: RMS voltage in V,

There is a relationship between the parameters describing the equivalent electrical circuit and the dielectric parameters describing the cable insulation material. In some cases, it is convenient to describe Tan δ as a function of dielectric parameters rather than the equivalent circuit parameters since it has more physical meaning. Therefore, the concept of complex permittivity is introduced in order to express the insulation losses. The complex permittivity is defined by equation (3.3),

$$\varepsilon = \varepsilon' - j\varepsilon'', \tag{3.3}$$

where,

ε : Complex permittivity in F/m,

ε' : Real part of the complex permittivity in F/m,

j : Imaginary unit $\sqrt{-1}$,

ε'': Imaginary part of the complex permittivity in F/m.

The real part of the complex permittivity, ε', is the value of the complex permittivity that characterizes the cable insulation material while the imaginary part of the complex permittivity, ε'', is closely related to the insulation losses. There is a relation between ε'', the conductivity of the insulation material, and the frequency [5]. This relation is shown in equation (3.4),

$$\sigma = \omega \cdot \varepsilon'', \tag{3.4}$$

where,

σ: Conductivity of the material in S/m,

ω: Angular frequency in rad/s.

The Tan δ value can be expressed as a function of the complex permittivity as follows,

$$Tan\,\delta = \frac{\varepsilon''}{\varepsilon'}. \tag{3.5}$$

By substituting equation (3.4) into equation (3.5), the Tan δ value can also be expressed as a function of the conductivity and electric permittivity of the dielectric material as shown by equation (3.6),

$$Tan\,\delta = \frac{\sigma}{\omega\varepsilon'}. \tag{3.6}$$

The conductivity, σ, of the dielectric is a parameter that represents the losses due to conduction that takes place inside the dielectric because of the presence of the electric field. The dielectric losses will heat up the insulation material.

There are two main processes by which a dielectric material can increase its temperature under the presence of an electric field, namely electrical conduction and dipole rotation. In electrical conduction the current flow due to the electric field causes the material to absorb energy as heat. In dipole rotation, dielectric molecules are

polarized due to the presence of the electric field [5]. The polarized molecules have an electrical dipole moment. Thus, if the electric field alternates, the polarized molecules rotate aligning themselves with the direction of the alternating electric field. Successive rotations produce heat through friction at the molecular level, thus increasing the dielectric temperature. The dipole rotation process is commonly known as dielectric heating since it is related to the natural polarization of the dielectric material [5].

Consequently, higher Tan δ values represent higher losses and therefore an increase in the dielectric material temperature. When the increment in losses is localized and because the extruded insulation materials are fairly good thermal insulators, the localized losses can lead to a hot spot inside the cable insulation. As the temperature increases, the insulation material conductivity and therefore the power losses increase causing a further increment in temperature. The process repeats itself like a chain reaction leading to "thermal runaway" breakdown [12]. This thermal breakdown process is also called "thermal instability" [12].

From a practical point of view, the significance of Tan δ is that it represents the ratio of the dissipated energy inside the dielectric per radian of the test voltage to the energy stored at maximum polarization [43]. It has been shown that the real and imaginary parts of the complex permittivity are frequency dependent [13, 43]. Thus, the Tan δ value is the ratio of two frequency dependent quantities. While the changes in the real component are marginal, the changes in the imaginary component are significant during the cable insulation system life [43]. However, the Tan δ value does not provide as much information as the simultaneous evaluation of the complex permittivity components; a more exhaustive evaluation process would consider the changes with frequency of these components separately [13]. This evaluation technique is commonly known as dielectric spectroscopy [36].

One of the major practical advantages of the Tan δ measurement is that it is

independent of the cable insulation geometry. As seen before, it is the ratio of two parameters that are both affected by the same geometry factors [5]. Therefore, in situations in which the cable insulation geometry is not known, the Tan δ test is the only tool that can be used to assess the cable insulation condition by dielectric measurements [43].

3.3 Tan δ Measurements as a Tool for Diagnosis

Under ideal conditions, the cable insulation system should behave as a pure capacitance. In this case, the angle (δ) between the leakage current and the charging current would be zero and therefore so would the Tan δ value. As mentioned before, the insulation system has inherent losses which are represented in the model as a resistor in parallel to the capacitor representing the insulation under ideal conditions. It is well known that for a new XLPE cable, the Tan δ value is quite small, typically less than 0.0001 [5]; however, during its life the Tan δ value will increase due to the natural aging process.

As the density and size of water trees inside the cable insulation increase, the insulation loss and therefore the Tan δ value also increases. In addition, a nonlinear behavior with changes in voltage is also observed [13]. It has been shown that the increase in the dielectric losses is due mainly to the current flowing inside water tree structures [17], which is an indication that the dielectric losses depend on the electrical conductivity and the density of water trees while the degree of non linearity is mostly assumed to depend on the length of the water trees [17]. This latter case has also been reported in [44] in which the cable sample with the longest water trees has more significant nonlinear behavior and with losses significantly higher than what is typically measured for a cable with resistive field grading splices. Thus, the nonlinear behavior of water tree degraded XLPE insulation as a function of voltage has been proposed by researchers as an important additional diagnostic criterion [13]. It has also been

experimentally shown that in the case of long water trees the dielectric response is highly nonlinear as a function of the increasing test voltage above a certain level [13].

Nevertheless, from a single measurement of the Tan δ value, only an average degree of the insulation system degradation can be obtained as it may be used to provide a qualitative assessment of water tree formation. Unfortunately depending on the cable section length, higher density regions of water trees do not have a significant effect on the measured value. The overall Tan δ value will be lower than the value at the high water tree density region [45].

A progressive increase in the Tan δ value over time does indicate the presence of growing water trees. Therefore, historical records must be maintained over a period of time. Until now, there is no analytical relationship between the Tan δ value and the number and length of water trees in the cable insulation. Thus, it is necessary to rely on changes over time in the Tan δ value rather than on one specific measurement [34].

In conclusion, higher insulation losses and nonlinearities as a function of the voltage are indicators that the cable insulation system may be approaching failure. Therefore, the Tan δ value can be used as an indicator of the severity of water treeing in underground distribution cables.

3.4 Measuring the Tan δ Value

In field testing applications, the measurement is performed as an offline test in which the cable segment under test is disconnected from the grid at both ends and energized from a separate power supply with a fixed AC frequency typically of 60 or 0.1 Hz [37]. The frequency could also be in the range of 0.01 to 100 Hz [17]. The segment is typically energized using voltage levels of 1.0 U_0 and 2.0 U_0, where U_0 is the operating phase to ground system voltage [37].

In laboratory testing applications, for the research presented here, the samples under test are in a restricted environment that includes the control of the temperature and

the humidity.

3.5 Tan δ Measurements Diagnostic Criteria

Nowadays, two different criteria are applied for diagnosing a cable insulation system using the Tan δ value. One criterion uses the magnitude of the Tan δ value as a tool for diagnostics while the other uses the difference in Tan δ values for particular electrical stresses or voltage levels. The latter is commonly known as the "Tip-Up" of the Tan δ value. The results for both criteria are often interpreted using recommendations given in the standards. The standards provide a hierarchical level that evaluates the cable insulation system.

Unfortunately, there are no unified criteria for Tan δ measurements for different insulation materials and frequencies. This can be seen in Table 3.1 that shows the pass and fail indications for Tan δ measurements considering the Tan δ magnitude and the Tip-Up criteria. Establishing unified criteria is complicated by the fact that the Tan δ values depend not only on the cable system quality but also on the cable and accessory technologies. Nevertheless, a general procedure can be implemented in order to assess a particular case.

Table 3.1. Pass and fail indications for Tan δ measurements considering the Tan δ magnitude and the Tip-Up criteria [8].

Insulation Material	Frequency [Hz]	Pass Indication	Fail Indication
XLPE	0.1	See Table 3.2	See Table 3.2
	60	No unified criteria	No unified criteria
HMWPE TRXLPE	0.1		
	60		
EPR	0.1		
	60		
PILC	0.1		
	60		

The criteria established in the United States are given by the IEEE Std. 400 [37]. But, only Tan δ values for a 0.1 Hz sinusoidal voltage source are reported. Table 3.2 shows the Tan δ values and the cable system condition assessments in the IEEE Std. 400 [37]. Figure 3.2 shows the same information as in Table 3.2 but regarding the Tan δ magnitudes only.

Table 3.2. Tan δ and cable condition assessments in the IEEE Std. 400 [37].

Assessment	**Tan δ [1e-3]**		**Tip-Up [1e-3]**
	U_0	**2 U_0**	**U_0 to 2 U_0**
	Clause 8.4		
Good†	-	Less than 1.2	Less than 0.6
Aged	-	Between [1.2, 2.2]	Between [0.6, 1.0]
Highly Degraded	-	More than 2.2	More than 1.0
	Clause 9.7		
OK†	Less than 4.0	-	-
Replace Eventually	More than 4.0	-	-
†: The cable system is not degraded, *i.e.* no maintenance action is required.			

Even though these values are widely used to assess the cable insulation condition, a complete understanding of the standard recommendations is unclear. Care is needed in the direct application of these values as the cable systems and operating conditions are different from those in different countries; yet the values serve to show how an assessment protocol might be constructed. It is also important to recognize that data at 60 Hz cannot be compared with those at 0.1 Hz since the time constants for the polarization of the dipoles inside the dielectric are different.

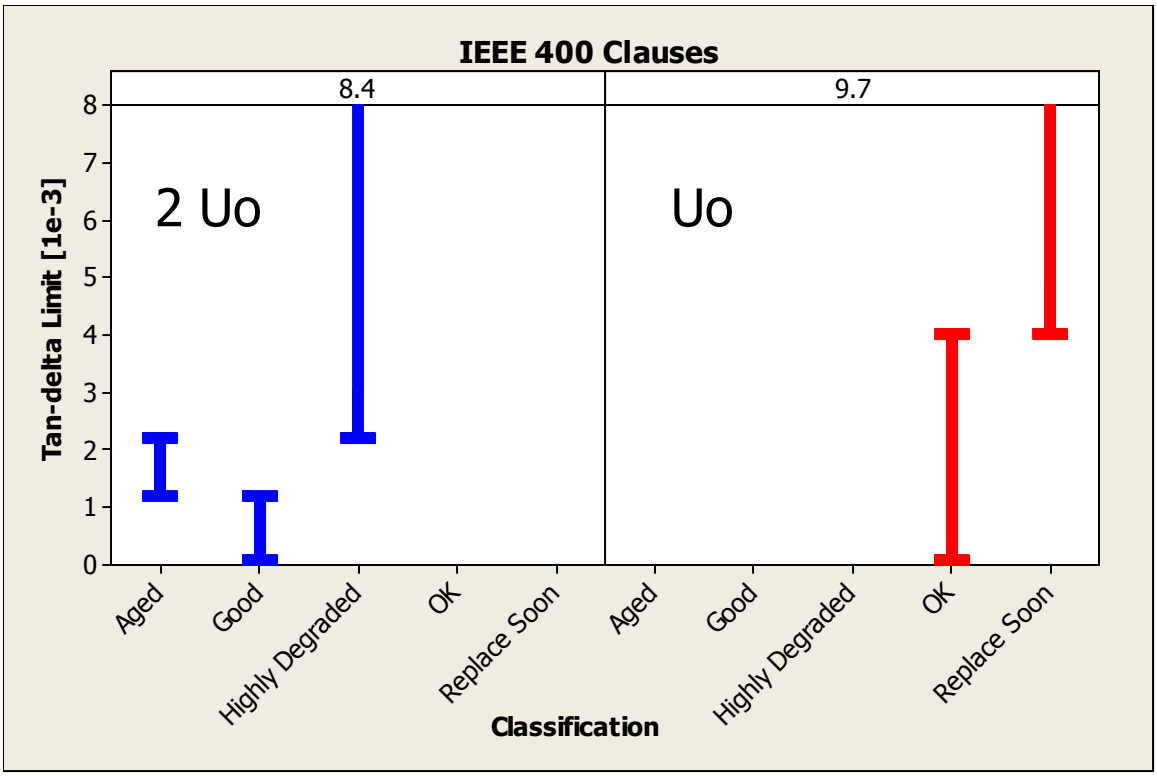

Figure 3.2. Tan δ magnitudes and cable condition assessments in IEEE Std. 400 [37].

One important point shown in Table 3.2 (Clause 8.4) is that the Tan δ should only vary slightly between different voltage levels. However, an increase in Tan δ with increasing voltage could be due to the presence of partial discharge. Meanwhile, a decrease in Tan δ with voltage and time mainly indicates humidity problems in accessories [8]. The values presented in Table 3.2 should be taken as approximate guidelines only.

The values of the IEEE Std. 400-Clause 8.4 [37] come from practical measurement results of numerous field data, 2400 km of XLPE insulated cables, and cross correlation with data from research centers of several European universities [37, 47]. The values given in Clause 9.7 of the IEEE Std. 400 [37] come from statistical analyses of more than 1500 onsite Tan δ measurements on service aged XLPE insulated cables. Nevertheless, the sensitivity of the commercial measurement system was limited

between 0.001 and 0.002 and the scatter was quite high [48]. Therefore, it was not possible to distinguish between new or non-aged cables and moderately field-aged cables. In both clauses, the values correspond to cables of a German design [48].

Moreover, the standard does not provide information on the timing, criteria for voltages different from U_0 and 2 U_0, voltage sequence, or failure risk during test. The recommended actions are also confusing. Therefore, a reevaluation of standard values and recommendations taking account American cable designs, would enhance the cable diagnostics testing by Tan δ measurements in the United States.

3.6 Limitations of Tan δ Measurements

Tan δ can be considered as a measure of the average condition of a cable system, and so unfortunately, if higher density regions of water trees exist only in part of the cable segment length; then their effect on Tan δ would not be reflected in the overall measurement. In other words, the overall Tan δ value may be lower than the value that corresponds to the high density regions of water trees [45], which means that an incorrect condition assessment could be formed. Therefore, the usefulness of Tan δ is limited by its inability to give more specific information than the average condition of the insulation of the complete cable system.

Nevertheless, a progressive increase of Tan δ value over time does indicate the presence of gradually growing water trees and therefore degradation. Thus in order to recognize this trend, records must be maintained over a period of time, typically several years. In this case, when the Tan δ measurements exceed historically established thresholds of its magnitude and Tip-Up for a particular insulation type, cable design, and voltage levels, the cable may be evaluated to have degraded and therefore it could be scheduled for replacement. On the other hand, if the Tan δ is below the thresholds then additional tests could be performed to determine whether the cable insulation is defective or not. Specifically, IEEE Std. 400 [37] suggests the application of a VLF withstand test.

Cable accessories such as splices and terminations could have a significant effect on the measured Tan δ values. The accessories themselves could dominate the measurement, and this is generally observed for two cases: (a) the insulation losses for a certain type of accessory (*e.g.* resistive field grading accessories) are higher than the cable insulation losses and (b) traditional accessory types that have reached highly degraded condition and thus their insulation losses are higher than the cable insulation losses [49-50]. Therefore, when performing Tan δ measurements if possible, the number of accessories, types, and conditions must be considered in order to evaluate their effects on the Tan δ value of the cable.

Another limitation is that VLF Tan δ has been mainly applied in the United States to polyethylene based insulation, *i.e.* HMWPE and XLPE. This polyethylene focus is due mostly to the availability of basic diagnostic interpretation information contained in IEEE Std. 400 [37]. However, one issue that remains unanswered is how to interpret data for the rest of the cable system population composed of TRXLPE, EPR, and PILC cable systems. A survey conducted by NEETRAC among United States utilities reveals that 60 % of underground cable insulation material is HMWPE, XLPE, or TRXLPE [10]. The survey also shows that approximately 25 % of the underground insulation material is EPR. However, there are no unified success criteria for Tan δ measurements when considering the different insulation materials, cable designs, cable system quality, and accessory technologies. This constitutes a problem when doing the diagnosis since every case should be treated separately considering all the related issues.

3.7 Previous Work on Characterization by Tan δ Measurements

Several researchers have tried to address the issues surrounding the characterization of power cable insulation using Tan δ measurements. In particular, in the method for characterization presented in [45], the degree of insulation deterioration has been estimated using Tan δ measurements together with the DC leakage current for an

online test system for XLPE cables. The evaluation of insulation condition has used Tan δ values at power frequency. The final assessment has been divided into three groups that have been specified as (a) un-deteriorated, (b) signs of insulation deterioration, and (c) deteriorated insulation. Results have indicated that the diagnostic accuracy is high for deteriorated cables. The authors have also reported a correlation between Tan δ values and the AC breakdown voltage.

Kuschel *et al.* [48] have reported Tan δ values for new MV power cables with different insulation materials and observed that different materials have different Tan δ values. This has been true in particular for different compounds of XLPE. The measurements have been done at frequencies of 0.1 Hz and 50 Hz. The classification of XLPE compounds has shown to be more efficient at 0.1 Hz as compared to 50 Hz because the differences in the values are greater at the lower frequency. It has also been observed that for some XLPE compounds, there is a slight increase in Tan δ with voltage while for other compounds there is no change at all. Moreover, the paper has also reported on the analyses of more than 1500 onsite 0.1 Hz Tan δ measurements on field-aged 20 kV XLPE cables manufactured in Germany. Typical Tan δ measurement results for field-aged and non-aged cables are shown in Figure 3.3. From these measurements, diagnostic criteria have been established. The criteria has determined that cables with a Tan δ value higher than 0.004 are considered to be highly water tree degraded and expected to have a low AC breakdown voltage. Unfortunately, the sensitivity of the measurement system used has been limited between 0.001 and 0.002 and the scatter has been quite high. Therefore, it has not been possible to distinguish between new, non-aged, and moderately aged cables. The authors have also mentioned the importance of using the change in Tan δ value with voltage as an additional diagnostic criterion, *i.e.* the Tip-Up value.

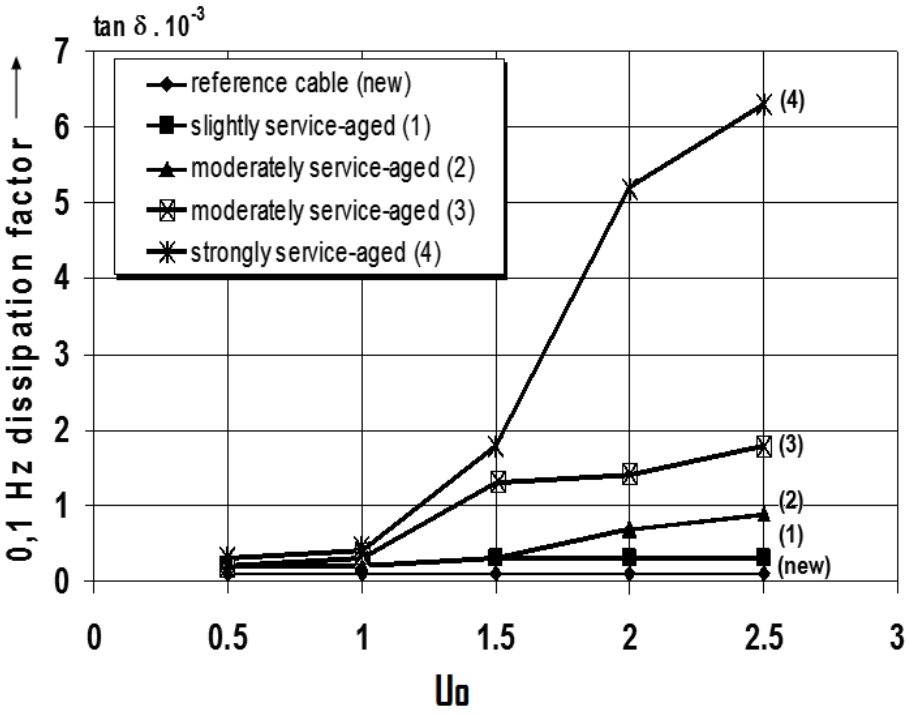

Figure 3.3. Voltage dependence of 0.1 Hz Tan δ of non-aged and field-aged XLPE-insulated medium voltage cables [48].

In the work by Hvidsten *et al.* [46], the authors have described the methodology for experiments performed on laboratory-aged 12 kV and field-aged 24 kV XLPE cable samples. The methodology has included Tan δ measurements at VLF, AC breakdown test, and water-tree examination. Measurements have been conducted using a 0.1 Hz source at voltages starting from 0.1 to 0.5 times the phase-to-ground operating voltage of samples. Results have indicated that there is a correlation between the Tan δ measurements at 0.1 Hz and the AC breakdown voltage. The authors have also shown that a reduction of the AC breakdown strength is related to the length of the longest vented water tree rather than to the tree density. Additionally, it has also been shown that the degree of nonlinearity in Tan δ measurements with respect to voltage may be used as a valuable parameter for assessment even at test voltages lower than the operating voltage.

Baur and Blank [47] have introduced the concept of frequency domain dissipation factor (FDDF). This concept is also known as dielectric spectroscopy. Their method has been based on Tan δ measurements at different frequencies using a sinusoidal power source with a variable frequency range from 0.01 Hz to 1 Hz. Their work has shown that changes in values with frequency may be used as an additional evaluation criterion. They have also shown that after 1000 hours and 90 ºC of aging, the characteristics of TRXLPE and XLPE, as observed using the FDDF method, have been similar to one another. But more importantly, the paper has also introduced a method for assessment of XLPE cable insulation based on practical measurement results from numerous field measurements. The data have been compared with cross validation tests from high voltage research centers of several European Universities. The method has used Tan δ measurements at two voltage levels of 1.0 and 2.0 times the phase-to-ground operating voltage at 0.1 Hz. Values of Tan δ have been used to assess the condition of a cable system by considering the Tan δ values and the change in Tan δ with voltage (Tip-Up). Actually, this method has been the base for the current assessment criteria found in the IEEE Std. 400 [37].The authors have also pointed out that these criteria may be used for TRXLPE cable, but that care must be taken because values for this type of insulation material only stabilize one or two years after commissioning and normal system operation.

The concept of change in Tan δ with frequency as a means of diagnosis has been further advanced by Werelius [13] who has developed a method that uses dielectric spectroscopy for diagnosis of medium voltage XLPE cables. He has reported that Tan δ measurements are independent of voltage level, voltage class, and humidity for non-aged cables. However, he has observed that for cables with considerable water-tree degradation, the Tan δ values are higher when a sequence of voltage is applied more than once. In other words, Tan δ values in the second sequence are higher than those in the first sequence when the two sequences are identical. This is akin to a hysteretic effect. In some cases, he has found that the response is not reproducible. This behavior is explained

by changes inside the structure of water trees. He has also observed the change in Tan δ value with time for a particular voltage level. In particular, he has shown that these changes occur more rapidly at the beginning of the test than after applying the voltage for some time. The effect is even more pronounced for a cable that has not been energized for a long period of time.

Pedersen *et al.* [41] have also shown the application of dielectric spectroscopy for the detection of water trees in XLPE cables, which has supported the applicability of the method developed by Werelius [13]. The authors have shown that the fundamentals of high voltage testing are not directly applicable at low voltages since the nonlinearity of the Tan δ measurements has not been as noticeable at the lower test voltages. They have also shown that for high voltage testing, the hysteretic effects are significant and could be useful in condition assessment.

Most recently, Skjolberg *et al.* [44] have shown the application of trend analysis for Tan δ measurements on field-aged MV XLPE cables. They have found that the Tan δ increases in the range of 0.0001 to 0.001 per year for the cables that have been tested. They have also found that the cable sample with the longest water tree has the most nonlinear behavior with losses that are significant higher than what is typically measured for a cable with resistive field grading splices.

In summary, research efforts have shown that Tan δ is a useful diagnostic tool for cable system insulation condition assessment. Nevertheless, there are still questions that need to be answered. Additional work is required for a better understanding of the measurement regarding different insulation materials, additional features that could be used for diagnosis, influence of test voltage sequence, test voltage levels, and risk of failure during testing.

3.8 Laboratory Tan δ Measurements

In order to address some of the VLF Tan δ issues previously discussed, laboratory measurements are performed and described in this section. Field Tan δ measurements are described in Section 3.9.

The laboratory experiments on distribution MV cable samples are designed to contribute in understanding time, voltage, and discharge time dependence of Tan δ diagnostic measurements at VLF of 0.1 Hz. The results assist in clarifying issues that arise when characterizing MV cable insulation by Tan δ diagnostic measurements. The issues include: (a) time-on-test, (b) voltage level as a diagnostic tool, (c) diagnostic features, and (d) reproducibility and repeatability of the measurements.

3.8.1. Cable Sample Description

The cable samples used in this experiment are composed of field-aged and non-aged MV cables. The field-aged samples have been provided by one of the utility participants of the CDFI project and the non-aged samples have been provided by NEETRAC. A description of the samples is presented in Table 3.3.

Table 3.3. Cable samples description.

Sample ID	Condition	Length	Year	Voltage Class [kV]	Insulation
S-1	Field-aged	80 ft (25 m)	1968	15	XLPE
S-2					
S-3					
S-4					
S-5					
S-6					
X-1	Non-aged		1999		
TR-1			1997		TRXLPE
E-1			2006		EPR
N-1	New		2005	25	TRXLPE
TR-2	Non-aged	200 ft (61 m)	1997	15	

The field-aged cable samples are a uniform set of the same 15 kV, XLPE, unjacketed cable, provided by the same utility, and coming from the same service area. Thus, it can be assumed that the aging conditions to which these cables have been exposed during their service life are similar. This is important since this group then constitutes a uniform group in which comparisons can be made without regard to cable design and aging conditions. Prior to measurements, the field-aged samples were permanently stored in a water tank to keep moisture in the insulation (see Figure 3.4). The field-aged samples are unjacketed; thus during testing the sample is moved to a different water tank to have a good contact between the insulation shield and neutral wires, as shown in Figure 3.5.

In contrast, the non-aged samples are a diverse set of 15 kV and 25 kV TRXLPE and 25 kV EPR jacketed cables. Sample N-1 is a new cable with void defects inside the bulk insulation. The EPR sample is included since it is well known that it has a higher Tan δ value than the equivalent non-aged XLPE or TRXLPE sample [5]. All the samples are terminated using stress relief cones.

Figure 3.4. Water tank in which field-aged cable samples are permanently stored.

Figure 3.5. Water tank in which the field-aged cable samples are tested.

3.8.2 Testing Protocols and Equipment

This section focuses on understanding: (1) how the Tan δ value varies with time for a particular voltage level when measurements are taken for a relatively long period of time, (2) how the Tan δ value varies with test voltage level when different voltage sequences are applied, and (3) how the Tan δ value varies when the sample under test is left resting, connected to ground, for different periods of time. Understanding these issues would add knowledge resulting in a better diagnosis since the understanding could help clarifying such issues as time-on-test, voltage level as a diagnostic tool, additional diagnostic features, and reproducibility and repeatability of measurements.

Thus, three testing protocols are designed to test the cable samples in a laboratory environment controlled in terms of humidity and temperature. The humidity is kept bellow 80 % non-condensing and the temperature is maintained at around 18º C with changes limited to ±3º C. The testing protocols, shown in Table 3.4, include three test types: a time dependence test, a voltage dependence test, and a discharge time dependence test.

Table 3.4. Protocol description.

Protocol	**Test Type**						**Sample Set Size (#)**	**Samples Tested**
	Time Dependence		**Voltage Dependence**		**Discharge Time Dependence**			
Freq. [Hz]	**0.1**	**60**	**0.1**	**60**	**0.1**	**60**		
I	√		√		√		Small (4)	S-4, S-5, S-6, and X-1
II	√		√				Medium (7)	S-1, S-2, S-3, TR-1, E-1, N-1, and TR-2
III				√			Full (11)	All

Protocols I and II are at VLF (0.1 Hz) and both include time dependence and voltage dependence. Protocol I is the only one to consider discharge time dependence. Protocol III only considers voltage dependence at 60 Hz. Not all the samples are tested in all protocols; the sample set size is reduced for protocols I and II. An explanation of each test now follows:

- **Time Dependence:** changes in Tan δ with time are studied when the cable sample is energized with the rated phase to ground voltage (U_0). The changes in values are measured for a period of 10 minutes and 5 repetitions are conducted. Between repetitions, the cable samples are left de-energized and resting, shorted to ground, for 10 minutes. Before the first voltage application, all cable samples are de-energized for at least 24 hours.
- **Voltage Dependence:** the voltage magnitude applied to the sample is changed in steps of 0.5 U_0 with a maximum applied voltage of 1.5 U_0. The voltage magnitude applied to the samples can be represented as a sequence of voltage steps, each of which lasts for 1 minute. The test sequence is designed to assess the effect of the repeated voltages in the reproducibility of Tan δ values when more than one increasing voltage sequence (classical approach) is considered.
- **Discharge Time Dependence:** changes in Tan δ with discharge time are observed. Samples are left de-energized, and shorted to ground resting, for a period of time considered here as the discharge time. This time is increased from 1 minute to 60 minutes. A total of seven voltage applications for Tan δ measurements are conducted. Each voltage application lasts 1 minute and the magnitude of the applied voltage is U_0.

All tests are carried out in the specified order. A resting time of 60 minutes between tests is allowed to minimize the influence of previous tests. During this time samples are left de-energized and shorted to ground. Figure 3.6 and Figure 3.7 show the

voltage magnitude as a function of the voltage application number for both protocols I and II respectively.

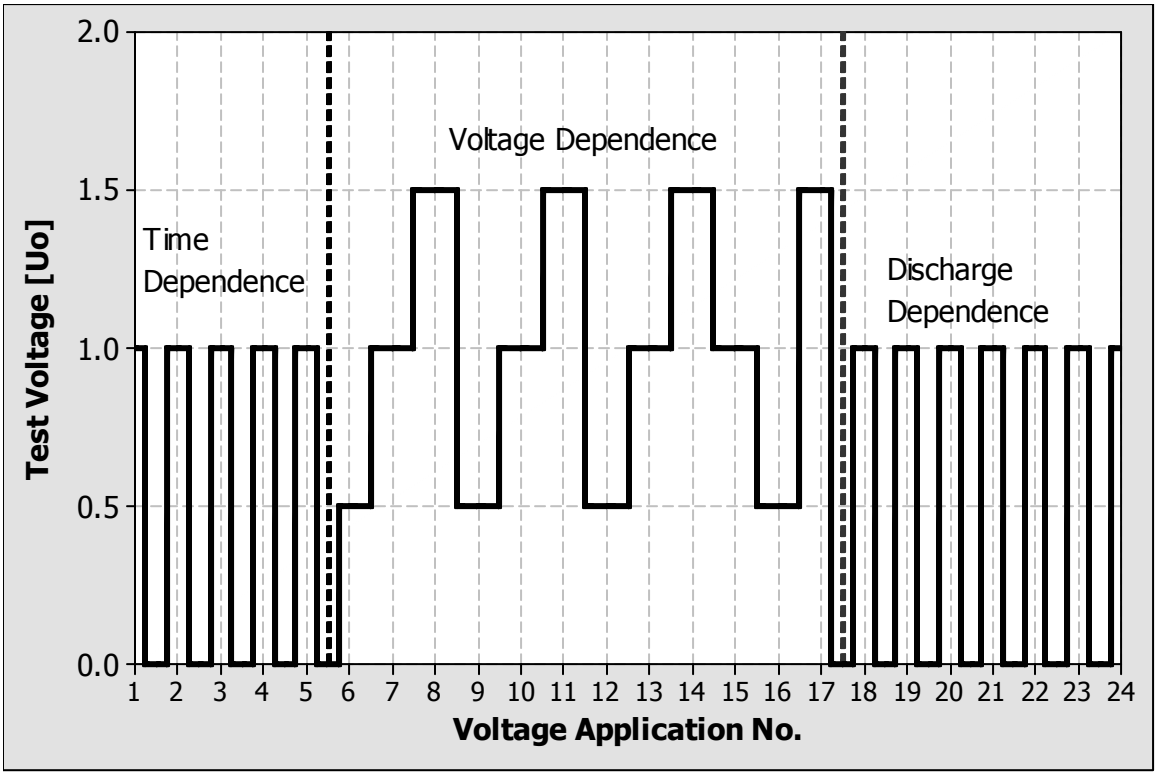

Figure 3.6. Voltage sequence - protocol I (0.1 Hz).

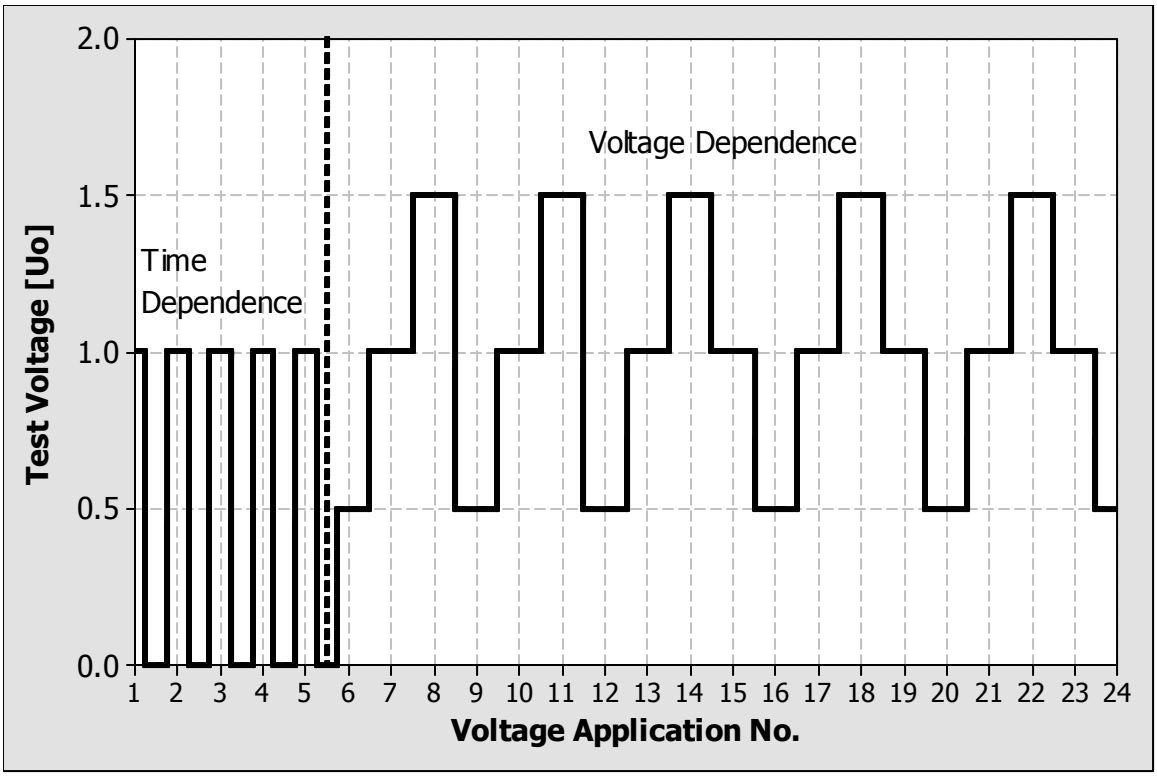

Figure 3.7. Voltage sequence - protocol II (0.1 Hz).

Protocol III is at the power frequency of 60 Hz. Only a voltage dependence test is conducted; specifically, the voltage magnitude is changed in steps of 0.5 U_0 from 0.5 U_0 to 2.0 U_0 and only one reading is taken at each voltage level. The voltage sequence includes two sweeps of increasing voltage from 0.5 U_0 to 2.0 U_0 as illustrated in Figure 3.8.

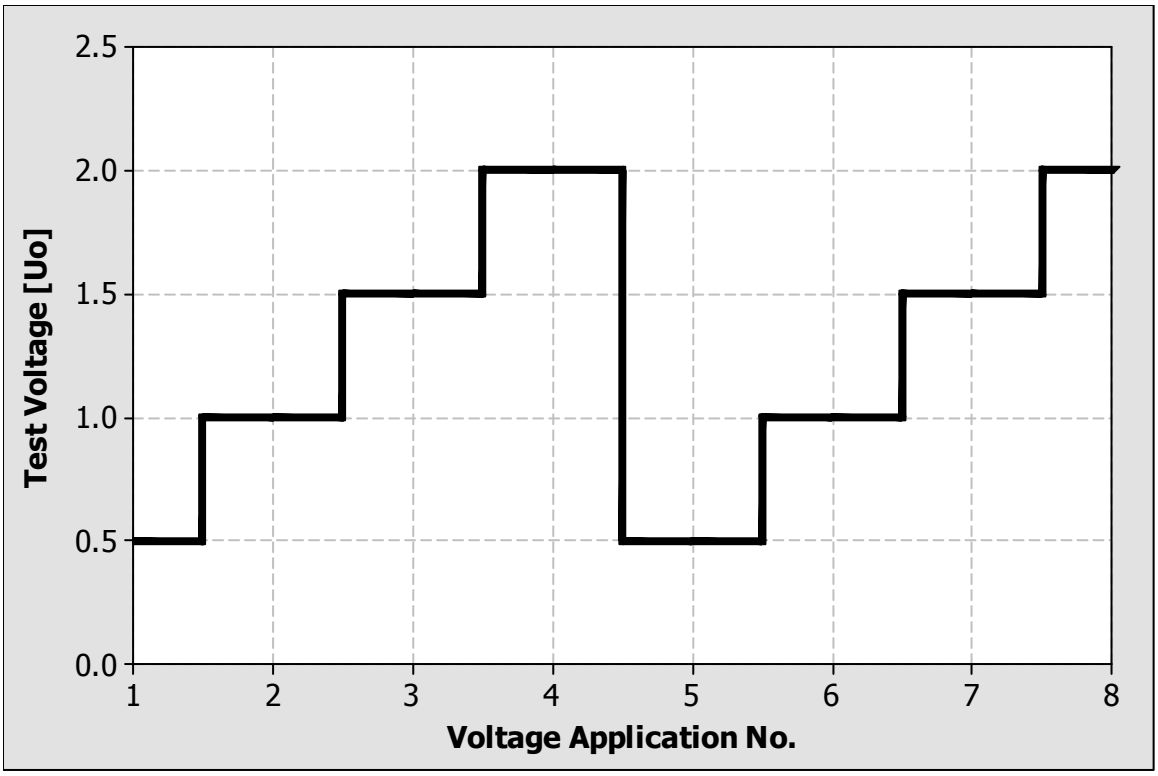

Figure 3.8. Voltage sequence - protocol III (60 Hz).

Different measurement equipments are used for each protocol and they are described below.

For protocol I, the equipment is the Baur® PHD-TD/PD 80 (see Figure 3.9), its technical details appear in Table 3.5 and the test setup is shown in Figure 3.10.

Table 3.5. Description of Tan δ equipment used for protocol I measurements.

Voltage Range	1.0 to 57.0 kV (RMS)
Zero Error	0.1×10^{-3}
Resolution	0.01×10^{-3}
Accuracy	± 1% of measured value ± 0.1×10^{-3}

Figure 3.9. Baur PHD – TD/PD 80 equipment.

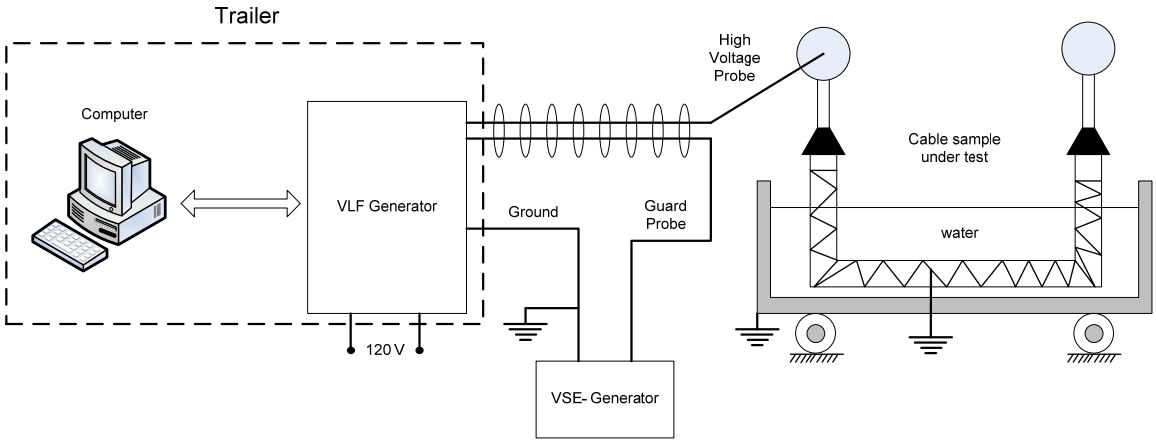

Figure 3.10. Schematic of test setup for Tan δ protocol I measurements.

For protocol II, the measurement equipment is the HV Diagnostics® TD-30 (see Figure 3.11), its technical details appear in Table 3.6 and the test setup is shown in Figure 3.12.

Table 3.6. Description of Tan δ equipment used for protocol II measurements.

Voltage Range	0.0 to 23.0 kV (RMS)
Zero Error	0.2×10^{-3}
Resolution	0.1×10^{-3}
Accuracy	$\pm 0.2\times10^{-3}$

Figure 3.11. TD 30 equipment.

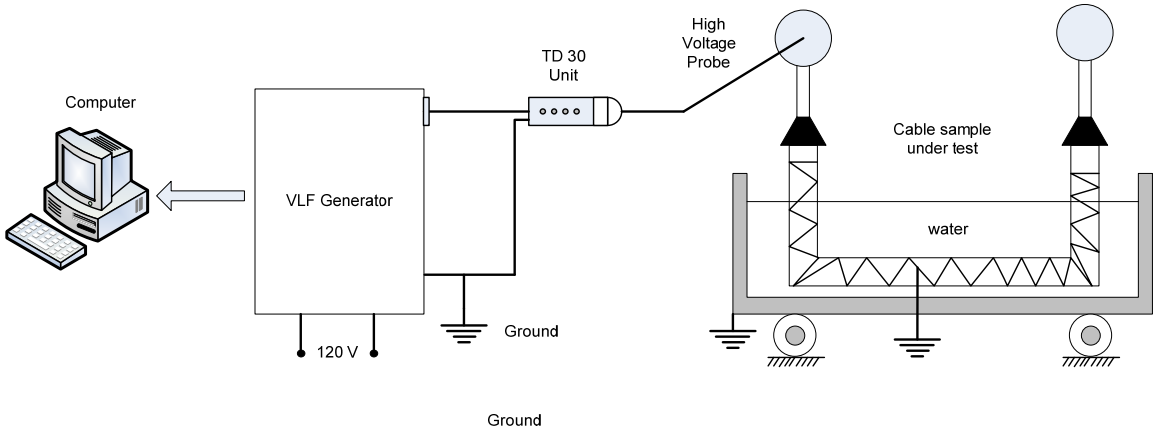

Figure 3.12. Schematic of test setup for Tan δ protocol II measurements.

For protocol III, the measurement equipment is the AVO/Biddle/Megger® Tan δ Bridge CB-605 (see Figure 3.13), its technical details appear in Table 3.7 and the test setup is shown in Figure 3.14.

Table 3.7. Description of Tan δ equipment used for protocol III measurements.

Voltage Range	0.0 to 100 kV (RMS)
Zero Error	0.02×10^{-3} on the 10^{-6} range 2 digits on all other ranges
Resolution	0.1 of the selected range
Accuracy	±2% of reading ±0.02×10^{-3} on the 10^{-6} range ±2% of reading + 2 digits on all other ranges

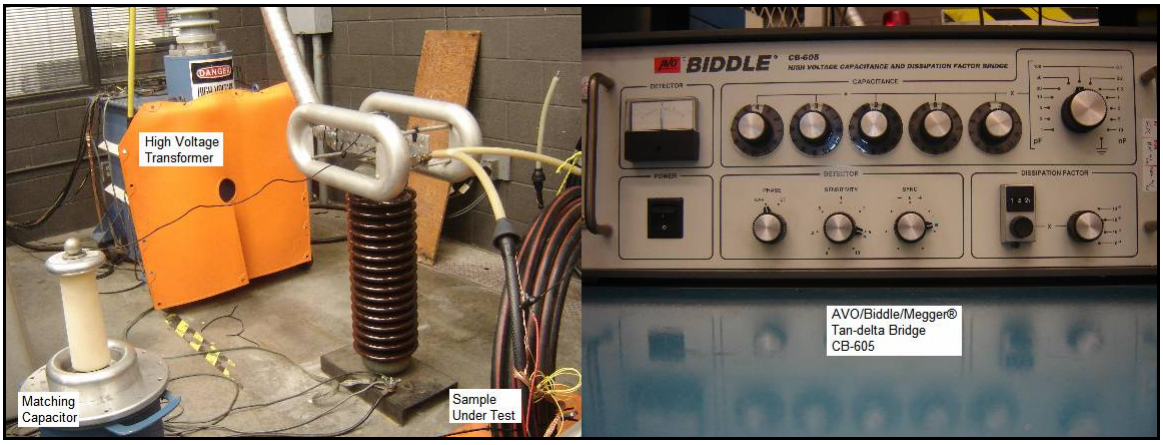

Figure 3.13. AVO/Biddle/Megger Tan δ Bridge CB-605 equipment.

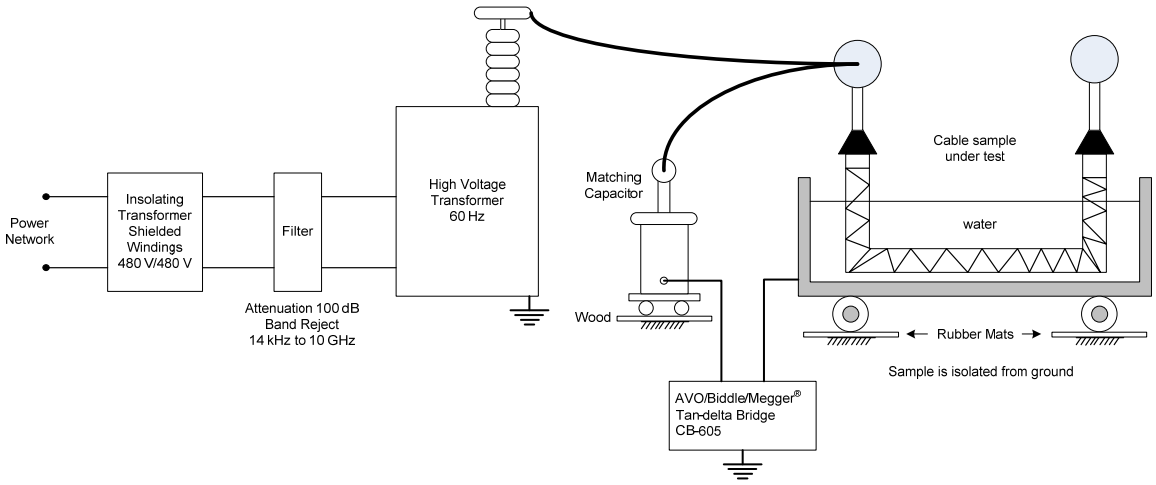

Figure 3.14. Schematic of test setup for Tan δ protocol III measurements.

3.8.3 Laboratory Experimental Results

The experimental results are classified by time dependence test, voltage dependence test, and discharge time dependence test.

3.8.3.1 Time Dependence Test Results

No change of Tan δ with time is observed for the non-aged cable samples. This is expected since their insulation should be free of water-tree degradation. In contrast, different time dependences are observed for the field-aged cables. Samples S-2, S-4, S-5, and S-6 show a time dependence while samples S-1 and S-3 do not. The difference in responses can be an indication of the level of water-tree deterioration in these cables; in fact, the responses can be a consequence of transient activity inside the water tree structure. As illustration, Figure 3.15 shows the time dependence test response for sample S-4. Similar results are observed for the other field-aged samples that show the largest variation during the first voltage application after the cable sample is de-energized for a long period of time. During subsequent voltage applications, the Tan δ shows some variation but, in general and for practical applications, it can be assumed that the value is

stable.

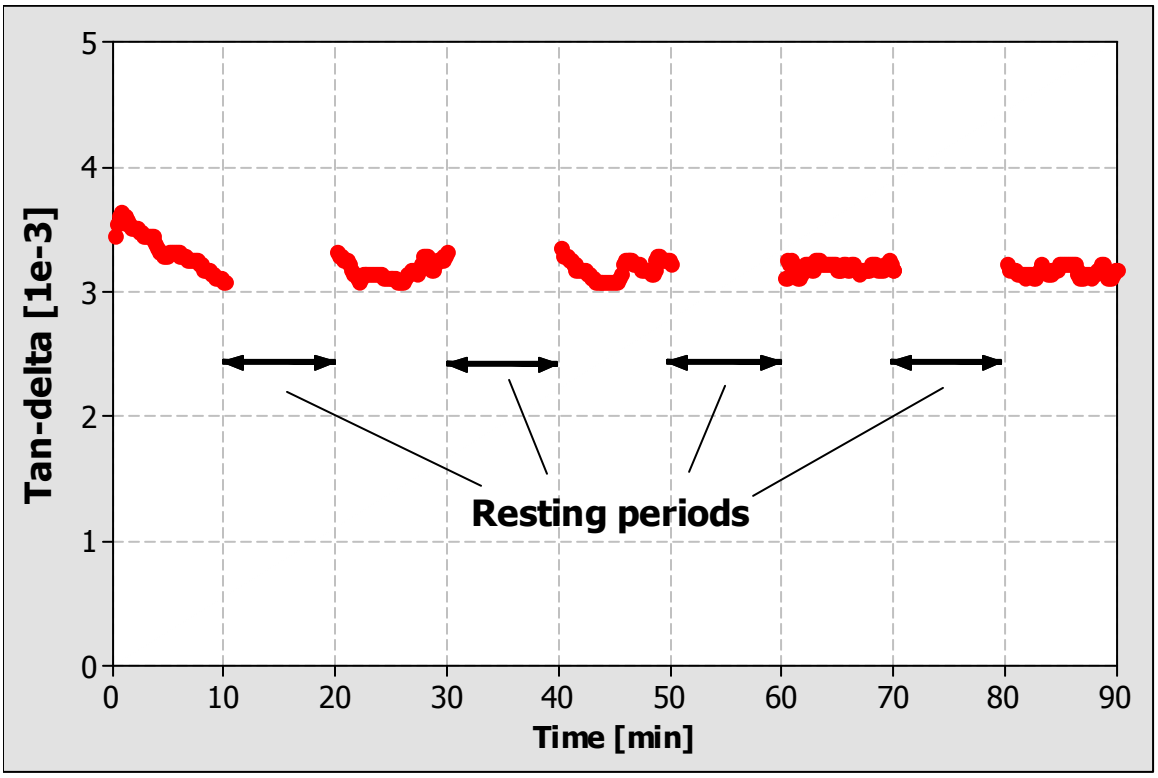

Figure 3.15. Tan δ time dependence test response of sample S-4.

3.8.3.2 Voltage Dependence Test Results

Overall Results

Tables 3.8 to 3.10 show the overall results for protocol I, protocol II, and protocol III respectively. The mean Tan δ value and its associated standard deviation values are presented for protocols I and II while only Tan δ values are presented for protocol III. Samples S-2 and S-4 failed under protocol III testing.

The mean and standard deviation for protocols I and II have been computed for all the Tan δ data at the particular test voltage level in the voltage sequence of the voltage

dependence test, *e.g.* the values of mean Tan δ and standard deviation in protocol I are calculated considering the four voltage applications at each test voltage level of 0.5, 1.0, and 1.5 U_0. See Figure 3.6.

Table 3.8. Voltage dependence test protocol I (0.1 Hz) results.

Sample ID	**Mean Tan δ [1e-3], {Stdv.† [1e-3]}**		
	Voltage [U_0]		
	0.5	**1.0**	**1.5**
S-4	2.53, {0.60}	8.36, {3.14}	19.42, {4.63}
S-5	0.58, {0.02}	0.80, {0.07}	1.75, {0.70}
S-6	1.13, {0.08}	2.60, {0.29}	5.61, {0.40}
X-1	0.20, {< 0.01}	0.20, {< 0.01}	0.20, {< 0.01}
†: Standard deviation			

Table 3.9. Voltage dependence test protocol II (0.1 Hz) results.

Sample ID	**Mean Tan δ [1e-3], {Stdv.† [1e-3]}**		
	Voltage [U_0]		
	0.5	**1.0**	**1.5**
S-1	0.6, {< 0.1}	0.6, {< 0.1}	0.6, {< 0.1}
S-2	1.7, {0.4}	2.3, {0.4}	3.5, {0.3}
S-3	0.6, {< 0.1}	0.6, {< 0.1}	0.6, {< 0.1}
TR-1	0.2, {< 0.1}	0.2, {< 0.1}	0.2, {< 0.1}
E-1	3.7, {< 0.1}	3.7, {< 0.1}	3.7, {< 0.1}
N-1	1.9, {0.2}	2.2, {0.2}	2.0, {< 0.1}
TR-2	0.2, {< 0.1}	0.2, {< 0.1}	0.2, {< 0.1}
†: Standard deviation			

Table 3.10. Voltage dependence test protocol III (60 Hz) results.

Sample ID	Mean Tan δ [1e-3]			
	Voltage [U_0]			
	0.5	**1.0**	**1.5**	**2.0**
S-1	0.32	0.50	0.67	0.83
S-2	0.50	0.86	1.07	1.19
S-3	0.33	0.5	0.63	0.76
S-4	0.71	1.47	-	-
S-5	0.67	1.39	1.83	2.10
S-6	0.60	1.13	1.62	1.97
X-1	0.10	0.11	0.11	0.11
TR-1	0.17	0.17	0.17	0.17
E-1	0.15	0.15	0.15	0.15
N-1	1.50	1.75	1.57	1.35
TR-2	0.17	0.17	0.17	0.17

Results from Tables 3.8 to 3.10 indicate that, similarly to the time dependence test, no change of Tan δ with voltage is observed for the non-aged cables. The Tan δ values remain unchanged for all test voltage levels. This means that the insulation of these cables has a linear behavior without the presence of water trees. In other words, the measurements of Tan δ are reproducible; the repeated measurements give the same results within the ability of the measuring equipment to maintain reproducibility at constant humidity and temperature.

Nevertheless, different voltage dependent responses are observed in Tables 3.8 to 3.10 for the field-aged cables. Samples S-2, S-4, S-5, and S-6 show a voltage dependence while samples S-1 and S-3 do not. For those samples that show voltage dependence, a nonlinear behavior and changes in the values with time, for the particular test voltage level are also observed. The Tan δ increased with voltage while the changes with time represent the scatter in the measurements. The scatter is quantified in terms of a standard deviation. In addition, the values also depend on the voltage sequence; in particular, hysteresis is observed. This phenomenon is explained in more detail later in the Chapter.

The increment in the dielectric loss with voltage for the field-aged samples in

Tables 3.8 to 3.10 can be explained by the current flowing inside the water tree structures, since it mainly depends on the water tree electrical conductivity and their density. The degree of nonlinearity is probably due to the length of the water trees. This phenomenon has also been reported in [44] in which the cable sample with the longest water tree has the larger nonlinear behavior with losses significantly higher than what is typically measured for a cable with resistive field grading splices.

Tan δ and Partial Discharges

It is also observed during the voltage dependence test that there is an effect of partial discharges on the measurements of Tan δ at VLF. This happens for at least two cases: corona at the terminations and partial discharges from large voids within the cable insulation. The first case may perturb the measurement in that the corona discharge current adds to the measured leakage current. Thus this may not really be considered as adding to the cable loss. Nevertheless, it does indicate the importance of ensuring discharge-free terminations when conducting any sort of measurement in the field.

The second case is particularly observed for sample N-1. The presence of internal partial discharges for this sample is checked (using a partial discharge prescreening test) before Tan δ testing. Figure 3.16 shows the Tan δ as a function of voltage for sample N-1 and compares it with the Tan δ as a function of voltage for sample TR-2, which did not have partial discharge activity. It can be observed that the presence of internal partial discharge increases the measured Tan δ value for new TRXLPE cables by an order of magnitude. If tested lengths of cable were to contain partial discharges, which often comes from accessories, then this effect will likely complicate the diagnosis.

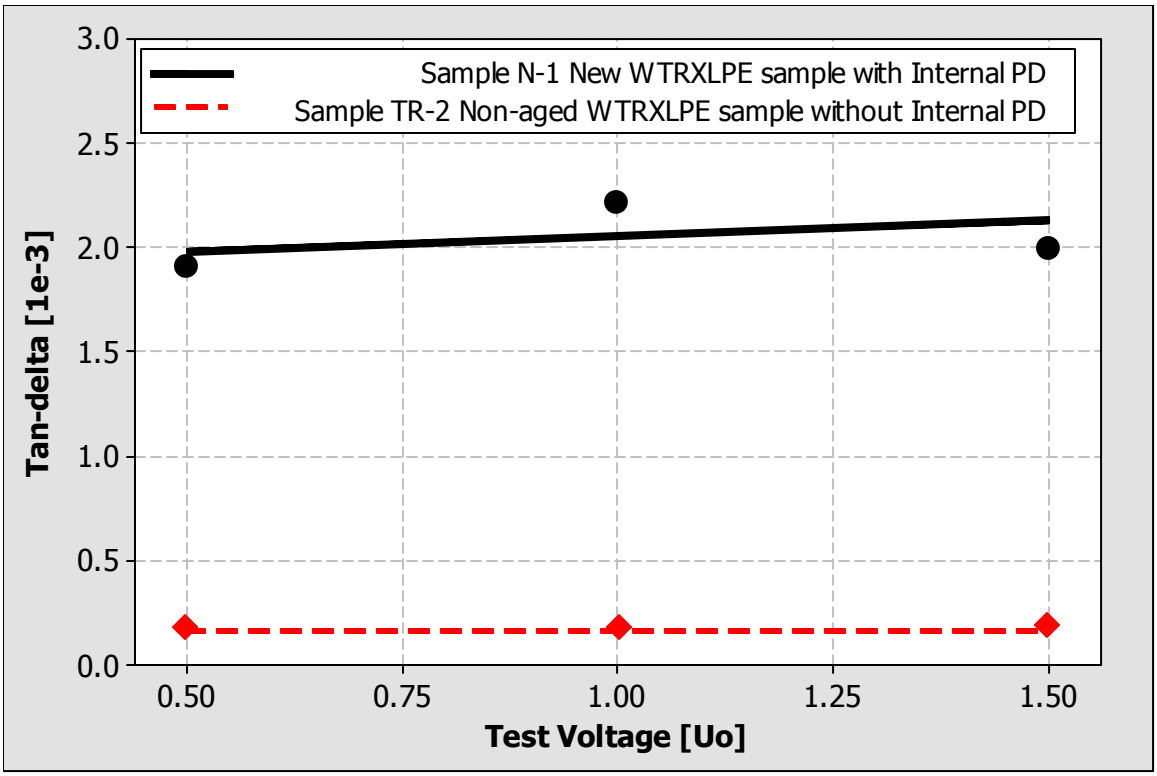

Figure 3.16. Effect of internal cable partial discharges on Tan δ measurements for new TRXLPE MV cables.

VLF Results in Perspective

In order to put the laboratory data at 0.1 Hz into perspective, a comparison is performed in Figure 3.17 between the Tan δ results and data reported in recent literature from Sweden [13], Canada [41], and Norway [44] for similar cable designs and laboratory tests similar to those considered in this thesis. The comparison uses only XLPE cable and testing voltages up to 2.0 U_0. These results show that the Tan δ values measured in this project are in the same range as the values reported from the different countries.

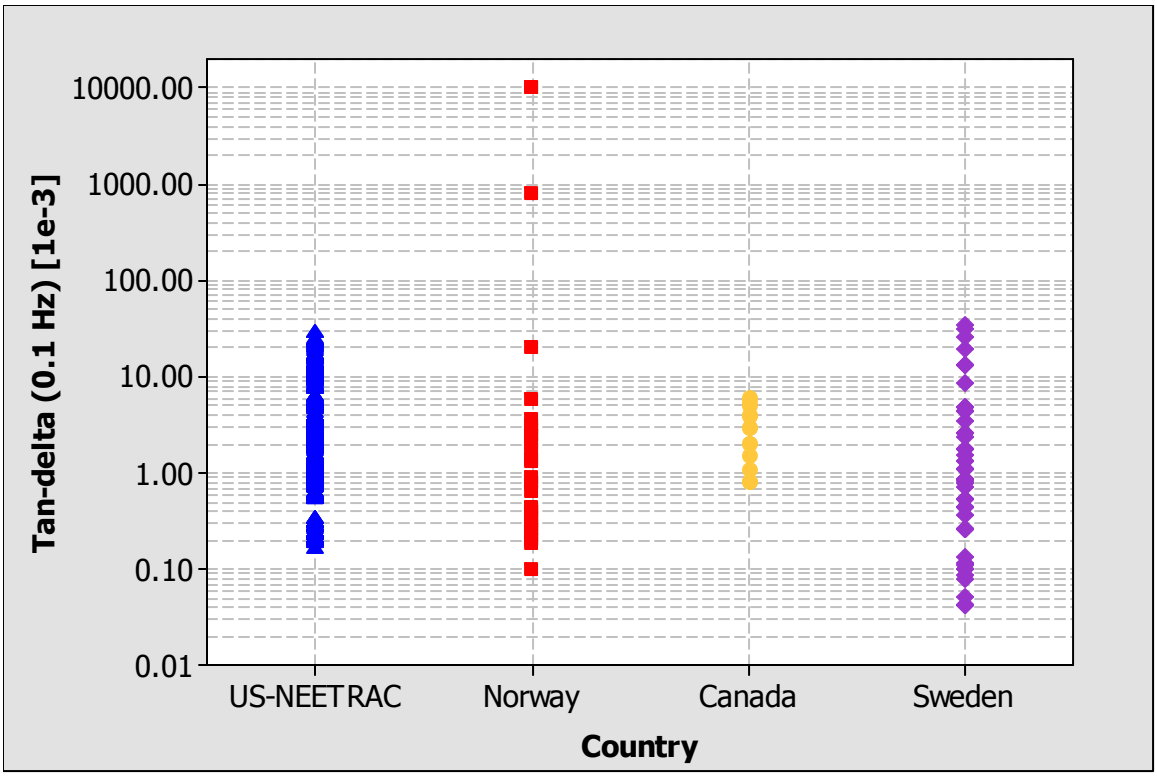

Figure 3.17. Comparison of Tan δ values from different countries, non-aged and field-aged XLPE MV cables tested in the laboratory.

Tan δ at VLF and Power Frequency

The overall results for the voltage dependence test also allow for establishing the correlation between Tan δ values at the frequencies of 0.1 Hz and 60 Hz by sample and test voltage level. This correlation in Figure 3.18 shows that there is not a perfect 1:1 correlation represented by the black dashed line. Nevertheless, there is some correlation that could be useful in translating diagnostic criteria from one frequency to the other. Moreover, the test voltage level seems not to have a major effect in the correlation. In addition, Tan δ values at 0.1 Hz are generally larger than those at 60 Hz because of the better sensitivity of 0.1 Hz Tan δ measurements as compared to 60 Hz.

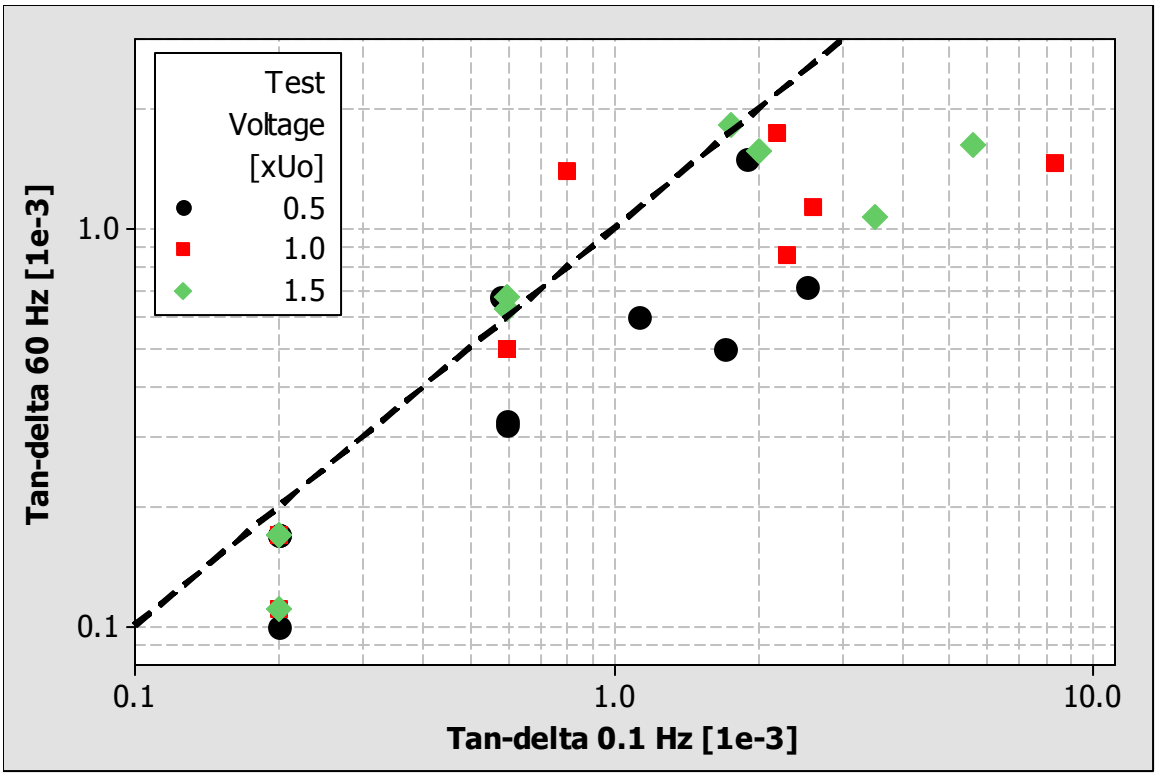

Figure 3.18. Correlation between laboratory Tan δ measurements at different frequencies.

3.8.3.3 Discharge Time Dependence Test Results

Analysis of variance (ANOVA) is performed to quantify the significance of the discharge time on the variation of Tan δ values. ANOVA is similar to regression in that it is used to investigate and model the relationship between a response variable and one or more independent variables called factors. However, analysis of variance differs from regression in two ways: the independent variables are qualitative (categorical), and no assumption is made about the nature of the relationship. Table 3.11 shows the ANOVA results for protocol I. In this particular case, the response variable is the Tan δ value during the discharge time test for all the samples, and the factors are the sample ID and the discharge time.

Table 3.11. Analysis of variance (ANOVA) for discharge time dependence test.

Source	DF[1]	SS[2]	Adj SS[3]	Adj MS[4]	F-value	P-value
Sample ID	3	6144.40	6076.85	2025.62	2384.15	<0.001
Discharge Time	5	15.55	15.55	3.11	3.66	0.003
Error	315	267.63	267.63	0.85		
Total	323	6427.58				

1: Degrees of freedom, 2: Sums of squares, 3: Adjusted sums of squares, and 4: Adjusted mean squares.

Results for P-values in Table 3.11 indicate that both factors are significant. The sample ID factor is more significant than the discharge time factor, *i.e.* P-values of less than 0.001 and 0.003 respectively. However, results also indicate (F-value) that the magnitude of Tan δ is more influenced by the sample ID factor and that only a marginal increase in Tan δ values is observed as the discharge time factor increases. This situation is illustrated in Figure 3.19 which shows the main effects plot of the ANOVA analysis of protocol I. This is the main reason why the discharge time dependence test has only been considered in protocol I. The main effects plot is a graph of means at the various levels of each factor and allows for an evaluation of the effect of the factor levels to the Tan δ means.

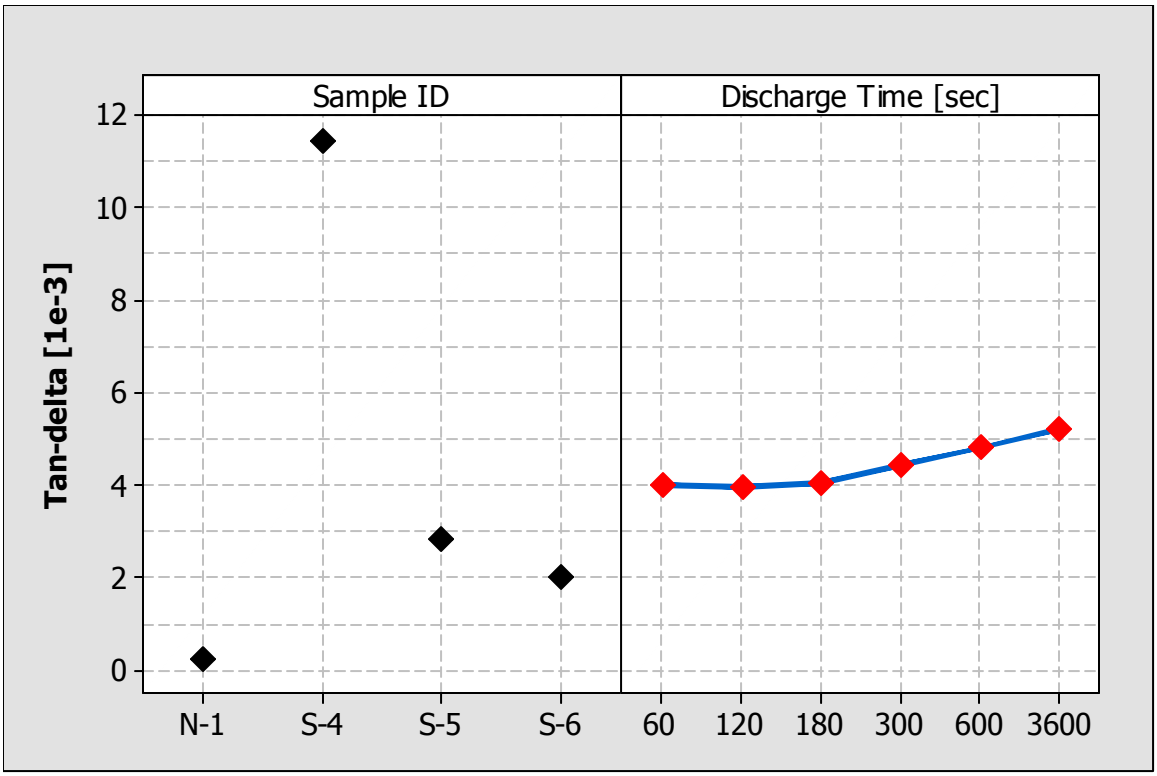

Figure 3.19. Main effects plot of ANOVA analysis of protocol I (means plotted).

3.8.3.4 Tan δ and Measurement Sequence

One of the more important observations made during the experimental work is the effect of voltage sequence in the Tan δ values for the field-aged samples that show a time dependence and a voltage dependence. To illustrate this, results for sample S-4 are shown in Figure 3.20. The figure shows Tan δ values as a function of voltage application number for the time dependence, voltage dependence, and discharge time dependence tests. The Tan δ response has sudden changes after the first application of 1.5 U_0. Considerable variation in the values is present during the test following this first voltage application, *i.e.* compare the values between voltage applications 1-5 and 10, 13, and 15 after voltage application 8. This is an indication that the Tan δ values for 0.5 U_0 and U_0 suffer from hysteresis after the application of the elevated voltage. The voltage level at

which this change occurs could be used as an indication of the severity of water-tree deterioration in the cable insulation. The results are in accordance with the results published by Hvidsten *et al.* [51] in which similar findings are reported. Nevertheless, more research work is required to support this conclusion.

Another consequence of Figure 3.20 is that the voltage sequence during testing plays an important role; in particular, by properly selecting the voltage sequence, more information can be obtained about the behavior of Tan δ with voltage and even with time for a particular test voltage level. Information about this behavior could be used to enhance the diagnosis.

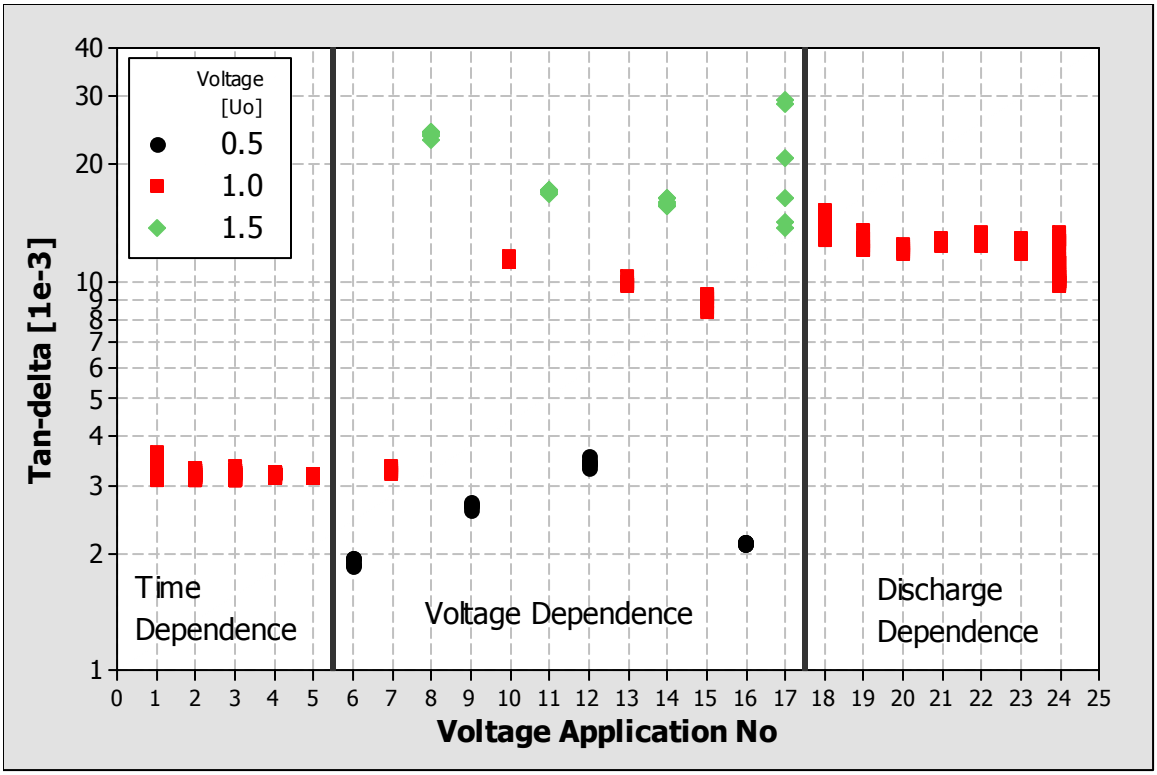

Figure 3.20. Tan δ as a function of voltage sequence for sample S-4.

3.8.3.5 Tan δ Diagnostic Features

When results from the laboratory experiments are considered as a whole, it is evident that there are a set of diagnostic features that can be used in order to characterize each cable sample from Tan δ measurements. The most attractive ones are as follows:

- The Tan δ value as a function of voltage; particularly, the Tan δ value at each voltage level and changes from one voltage level to another (Tip-Up). In fact, this is the classical approach described in the IEEE Std. 400 [37].
- Another feature that could be potentially used is the variation over time for a particular voltage level. This variation can be quantified by the scatter in the measurements for the particular test voltage level. For instance, as it has been done in this thesis, the scatter can be quantified by using the standard deviation. Nevertheless, another measure of scatter could be used; *e.g.* interquartile range. This feature seems to have potential in enhancing the diagnostics. In fact additional work, reported in Chapter 4 and [52], shows that there is a clear correlation between this feature and the VLF breakdown performance of the field-aged cable samples.
- Another potential feature that could be used is the test voltage level that causes the Tan δ value to suffer a sudden hysteretic effect.
- The comparison between similar cables could also be useful for characterization. In particular, the field-aged cable samples showed different Tan δ behaviors even though they had been subjected to similar aging conditions during their service life.

3.8.3.6 Time on Test and Preconditioning

Regarding the time-on-test at each voltage level during the voltage dependence test, it has been found that 1 minute is enough time to capture most of the variation. This

is because most of the variation occurs at the beginning of each voltage change. If more variation is required, 2 minutes is a good choice; nevertheless, more than 5 minutes seems to be excessive unless the interest is on Tan δ time dependence rather than voltage, *i.e.* a Tan δ stability test.

Furthermore, preconditioning of the cable sample before any voltage dependence test is recommended since this would minimize the effect of the sample being de-energized for a long period of time. Particularly, results from the discharge time dependence test indicate that preconditioning for at least 10 minutes seems to be a good choice.

3.9 Field Tan δ Measurements

In this case, Tan δ measurements carried out in the field are considered. The testing is performed at one of the utilities participating in the CDFI project. Its name is not revealed here because of the confidential nature of the data. The utility decided to conduct Tan δ measurements on 25 kV, XLPE, jacketed, and direct buried cable system that initially operated at 15 kV and was upgraded to 25 kV in 2006. A considerable number of failures occurred after the upgrading and the utility seriously considered total replacement of the affected system.

Approximately, 30,000 ft of cable is tested. Tan δ measurements are conducted at 0.5, 1.0, 1.5 and 2.0 U_0 of the new operating phase to ground voltage. Figure 3.21 shows the cumulative distribution functions of the Tan δ field data for all test voltages.

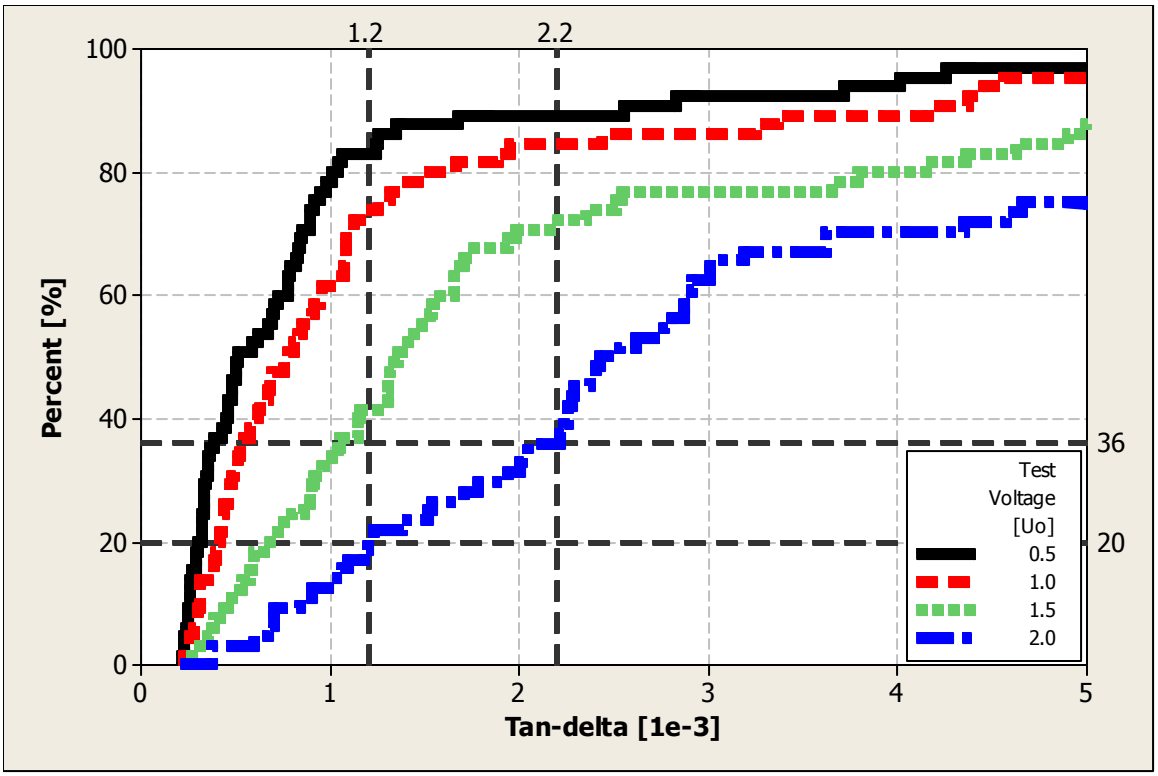

Figure 3.21. Tan δ field data cumulative distribution function.

The results of Figure 3.21 show that if the values given by the IEEE Std. 400 (Clause 8.4) [37] are considered for assessment, 64% of the cables are considered to be highly degraded, 16% to be aged, and only 20% is considered to be in good condition. These proportions seem to be extreme in the sense that a follow-up record of onsite failures after testing has been kept and to date no more failures have occurred. Similar results are obtained when evaluating the data using the Tip-Up criteria. This is an indication that the values as given for the standard are too conservative or that more diagnostic features are needed for an improved evaluation.

3.10 Modified Tan δ Diagnostic Criteria

The field data has revealed a way in which Tan δ values may be collected and compared to data collected using lower testing voltages. The conditioning and

comparison methods enable existing success criteria used at the higher voltages to be mapped or modified to lower levels, thereby providing the same level of previous discrimination, but delivering this at a lower test voltage. This significantly reduces the risk of failure under the test. The level of risk reduction may conveniently be estimated from an appropriately parameterized version of the well known Weibull equation [12].

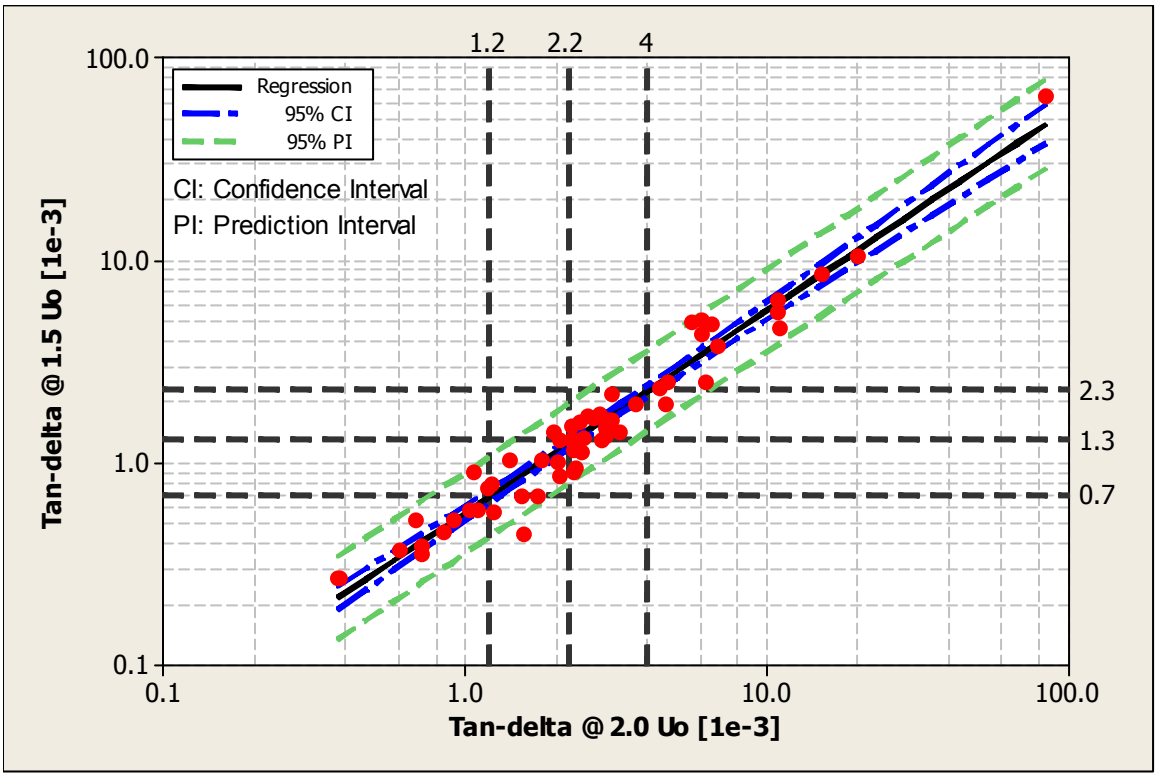

Figure 3.22. Correlation between Tan δ measurements from field testing at 2.0 U_0 and 1.5 U_0 for modified diagnostic criteria.

Figure 3.22 shows the correlation between Tan δ measurements from field testing at 2.0 U_0 and 1.5 U_0 for modified diagnostic criteria. The voltage of 1.5 U_0 represents a lower risk of failure during testing to the cable system. The plot in Figure 3.22 shows a relationship between the data collected at the different voltages. The clarity of the plot is improved by adopting logarithmic scales which further facilitate the identification of the

relationship. In this case, the relationship is linear in logarithmic terms, but this need not be so. It is sufficient that the relationship is clear.

The vertical lines represent the already established success criteria from the IEEE Std. 400 [37]. In the absence of the relationship, an engineer wishing to utilize the experience set out in IEEE Std. 400 [37] is constrained to test at 2.0 U_0 This forces the engineer to accept a higher level of risk than he may be comfortable with. With the relationship, it is a straightforward procedure for the engineer to translate the success criteria from the higher voltage (1.2, 2.2, and 4 Tan δ values on the upper *x*-axis for 2.0 U_0) to a lower voltage (0.7, 1.3, and 2.3 Tan δ values on the right *y*-axis for 1.5 U_0) thus reducing the risk. The same procedure can be followed using the Tip-Up values since the same relation have been observed, see Figure 3.23.

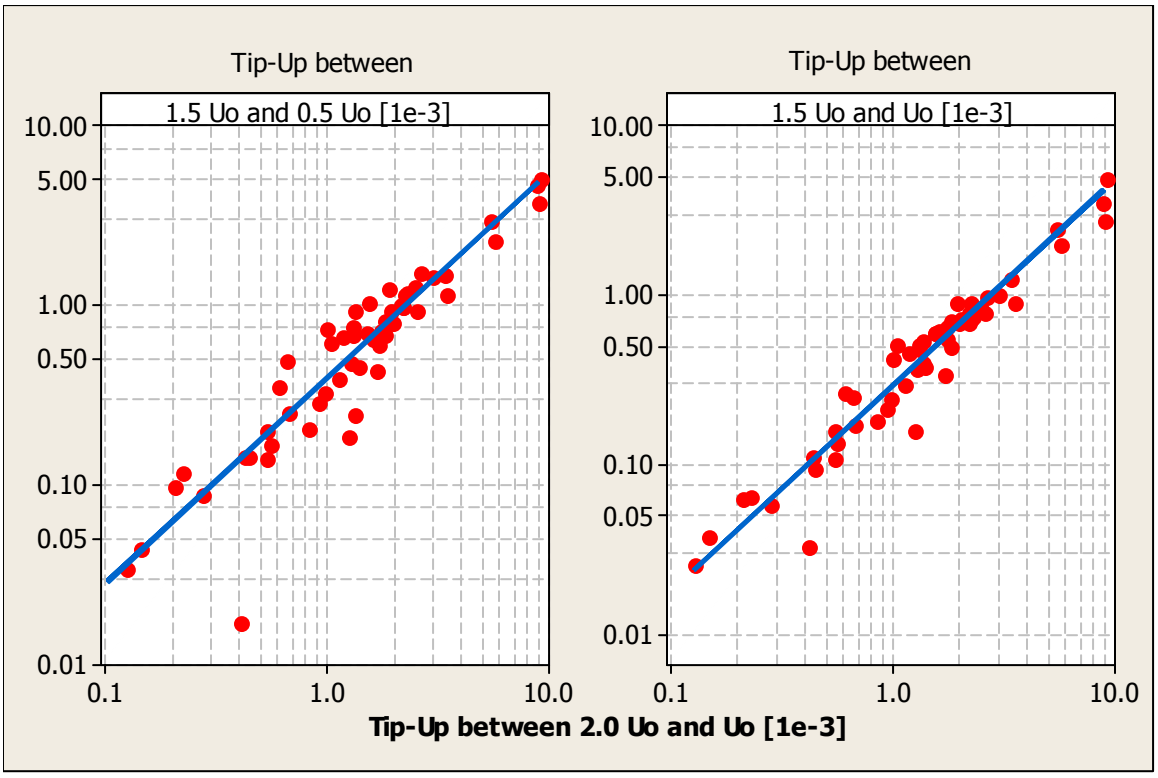

Figure 3.23. Correlation between Tip-Up for modified diagnostic criteria.

3.11 Summary and Conclusions

This Chapter has discussed a number of issues that arise when using Tan δ measurements at VLF to characterize the insulation of non-aged and field-aged MV cables. The discussion has been based on data from laboratory experiments that consider time dependence, voltage dependence, and discharge time dependence tests for different test protocols.

Results have indicated that there are a number of useful diagnostic features that can be used to characterize each sample. The features include Tan δ values, Tip-Ups, hysteresis, and most importantly, the scatter in the measurements for a particular test voltage level. The scatter has been quantified by using the standard deviation in the measurements. Nevertheless, other scatter metrics, such as interquartile ranges could also be used.

The correlation between Tan δ values at different frequencies of 0.1 Hz and 60 Hz has also been presented. Results have shown that there is not a perfect 1:1 correlation. Nevertheless, there is some correlation that could be useful in translating diagnostic criteria from one frequency to the other. Moreover, Tan δ values at 0.1 Hz are generally larger than those at 60 Hz because of the better sensitivity of 0.1 Hz Tan δ measurements as compared to 60 Hz.

In addition, the significance of the discharge time on the variation of Tan δ values has been quantified by performing ANOVA. Results have indicated that the discharge time is significant but the magnitude is insignificant when comparing samples.

Regarding the time-on-test, it has been found that 1 minute is enough time to capture most of the Tan δ time variation for changes in test voltage level. If more variation is required to be captured, 2 minutes is a good choice. More than five 5 minutes seems to be excessive unless the interest is on Tan δ time dependence (*i.e.* Tan δ stability) rather than voltage dependence.

It has also been observed in the voltage dependence test that there is an effect of partial discharges on the measurements of Tan δ at VLF for at least two cases, corona at the terminations and partial discharges from large voids within the cable insulation. Particularly, the presence of internal partial discharges in new TRXLPE with voids inside the bulk insulation causes an increase in the measured Tan δ of an order of magnitude when compared to a new cable without internal defects. If tested lengths of cable were to contain partial discharges, this effect could complicate the diagnosis.

Field Tan δ testing has also been conducted and the resulting data allows for reevaluation of diagnostic criteria in two ways. Firstly, this data indicate that existing values for diagnostic criteria are probably too conservative for the American cable designs. Secondly, the data also show that it is possible to map diagnostics criteria to lower test voltages, thereby reducing the risk of failure under test while maintaining the accuracy of assessment.

Finally, the Chapter has shown that higher insulation losses, nonlinearities with voltage, hysteresis, and variation in voltage and time of Tan δ diagnostic measurements at VLF, are indicators that could be used to properly characterize the insulation and enhance the diagnosis. But most importantly, Tan δ can be considered a feature rich diagnostic tool when testing is performed in an appropriate way and data are analyzed correctly.

The next Chapter shows how the Tan δ diagnostic features are correlated with the VLF breakdown performance.

CHAPTER 4

CORRELATION BETWEEN TAN δ DIAGNOSTIC MEASUREMENTS AND VLF BREAKDOWN PERFORMANCE

4.1 Introduction

In many practical situations only a portion of a cable may be degraded. In such situations, a method for localization of this degraded portion is desirable. One typical approach is to conduct an elevated voltage withstand test in order to fail, localize, and repair, the weakest portion of the cable, thus resulting in a more reliable future service performance. Therefore, the correlation between the dielectric response, measured here by Tan δ at VLF of 0.1 Hz and the future service performance is of paramount importance when improving existing or developing new diagnostic criteria. The correlation can be used as an evaluation parameter for Tan δ diagnostic measurements in the sense that cables with the poorest Tan δ behavior are expected to fail first.

Establishing the correlation is not a simple task. On the one hand for field applications, determining the service performance requires a follow-up of service failures after returning each cable to service after testing. On the other hand, an alternative is to evaluate the service performance in the laboratory using a withstand test and assuming that the first cable to fail the withstand test would have been the first cable to fail after returning to service. This needs the suspect cable to be removed from service and taken to the laboratory. Therefore, establishing the correlation requires time and effort by the utility that translate to spent dollars. In addition, after the dielectric response and the service performance are known, there is no direct quantitative means of evaluating the correlation.

Therefore, the work presented in this Chapter describes a laboratory test program conducted to establish the correlation between Tan δ diagnostic measurements at 0.1 Hz

and the VLF breakdown performance for MV cable samples. The samples are a uniform set of 15 kV, XLPE, service aged, unjacketed cables, and removed from the same service area. These samples therefore experienced similar operating conditions throughout their forty year service life. The samples are the same set of field-aged samples presented in Chapter 3. The test program includes Tan δ measurements at different voltage levels and a subsequent VLF withstand test to establish breakdown performance. This allows for the evaluation of risk-of-failure determined during VLF Tan δ testing. It is important to recognize the importance of the cable system as a whole. This includes cable, terminations, and joints; however, the work presented here limits itself to cable insulation only.

4.2 Previous Work

Several researchers have tried to correlate insulation dielectric measurements with the service performance of tested cable samples. On the one hand, the dielectric measurements have included Tan δ at 0.1 Hz or power frequency, polarization or depolarization currents, and recovery voltage. On the other hand, the service performance has been characterized by performing a withstand test typically at power frequency and impulse test voltages. The literature review presented in this section only focuses on the use of Tan δ as insulation dielectric measurement. The more relevant efforts in correlating Tan δ measurements with power frequency or impulse breakdown voltages are shown in the next paragraphs.

Yamaguchi *et al.* [45] have developed a new type of insulation diagnostic system for XLPE MV power cables that makes automatic measurements of the Tan δ at power frequency and the DC leakage current. More importantly, the authors have also presented the correlation between the measured Tan δ and the AC breakdown performance for aged 6 kV XLPE cables. Their results have shown that the breakdown voltage of these cables decreases with increasing Tan δ. In addition, the authors have also demonstrated that the

Tan δ magnitude increases with increasing maximum water tree length. Similar findings have also been reported by Ohata *et al.* [53] for a 22 kV XLPE cable.

The area of VLF withstand testing has been further advanced by Eager *et al.* [54]. They have described a methodology that is used to establish the voltage magnitude and duration of 0.1 Hz withstand field tests for MV XLPE cables. Results have shown that the breakdown voltage of laboratory-aged XLPE cable samples at 0.1 Hz is approximately equal to that at 60 Hz. In addition, the authors indicate that the VLF withstand test causes little damage to the cable insulation as compared to DC testing in the sense that only the weakest portion of the cable under test is damaged during the test. The paper has presented preliminary values of voltage magnitude and time duration that have been taken into account in the present IEEE Std. 400.2 [34]. However, the investigation has not considered the correlation between the breakdown performance and any diagnostic measurement.

In addition, Kuschel and Kalner [55] have presented dielectric response measurements that have included Tan δ at 0.1 Hz, depolarization current, and recovery voltage for different aged and non-aged MV XLPE cables. The dielectric response measurements have been compared with results of an AC (60 Hz) extended-step withstand test. Even though the comparison is presented, no clear correlation has been observed neither quantified. However, the correlation has been graphically established here. Figure 4.1 shows the correlation between Tan δ magnitude at U_0 and the AC breakdown voltage for 12 kV-XLPE cables. As seen in the figure, in general cables with higher Tan δ magnitudes have shown poorer breakdown performance.

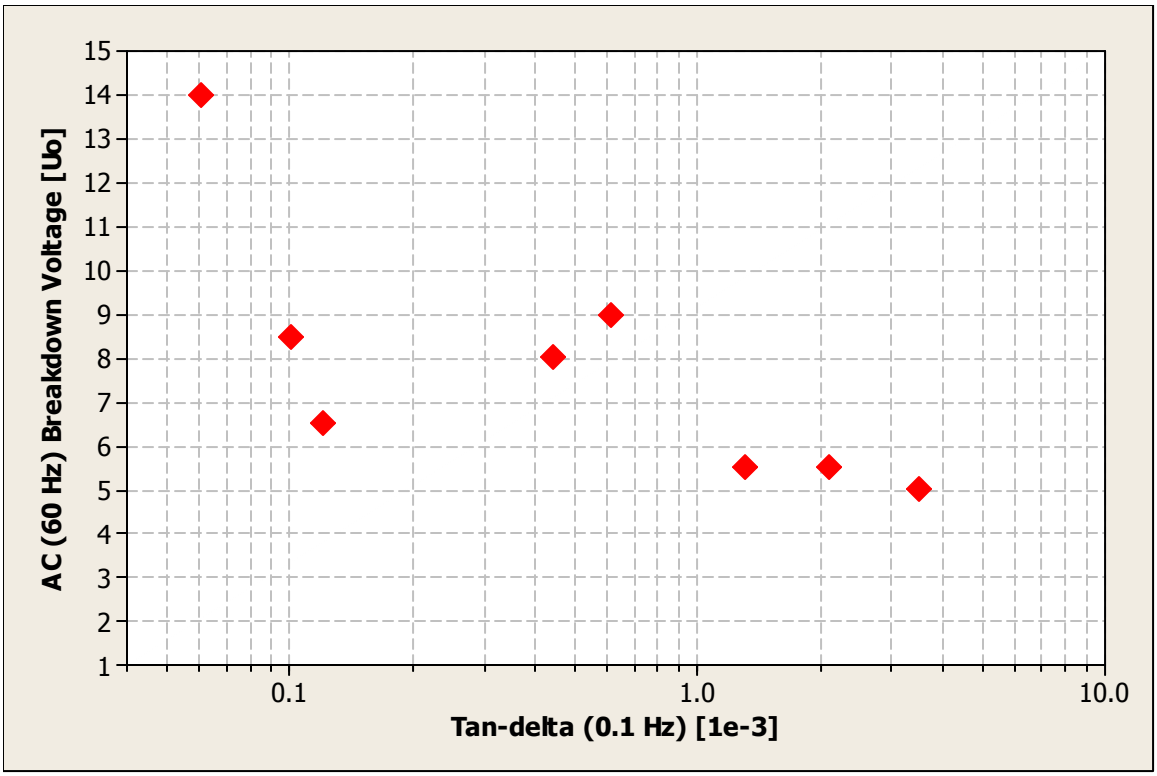

Figure 4.1. Correlation between Tan δ (U_0) and AC (60 Hz) breakdown voltage [55].

The work by Hvidsten *et al.* [46, 51, 56-57] has clearly shown that there is a correlation between the Tan δ in the frequency range of 0.01 Hz to 10 Hz and the AC breakdown performance for MV XLPE cables. In particular, in [51] the authors have shown that cables having a breakdown performance of 4 U_0 or greater, where U_0 is the phase-to-ground rated voltage, do not show any signs of insulation deterioration. However, cables with a breakdown performance of 3 U_0 or lower are distinguished by the Tan δ measurements. In addition, the paper has indicated that cables with water trees bridging the insulation have breakdown voltages ranging from U_0 to about 3 U_0.

Moreover, the correlation between the breakdown voltage for lightning impulse test and Tan δ at 0.1 Hz for MV XLPE cables has been reported by Werelius [13]. In particular, Figure 4.2 shows the correlation between Tan δ magnitudes at 0.5 U_0 and the impulse breakdown voltage for 6 kV-XLPE cables. As seen in Figure 4.2, Werelius has

shown that higher Tan δ values are correlated with lower impulse breakdown voltages.

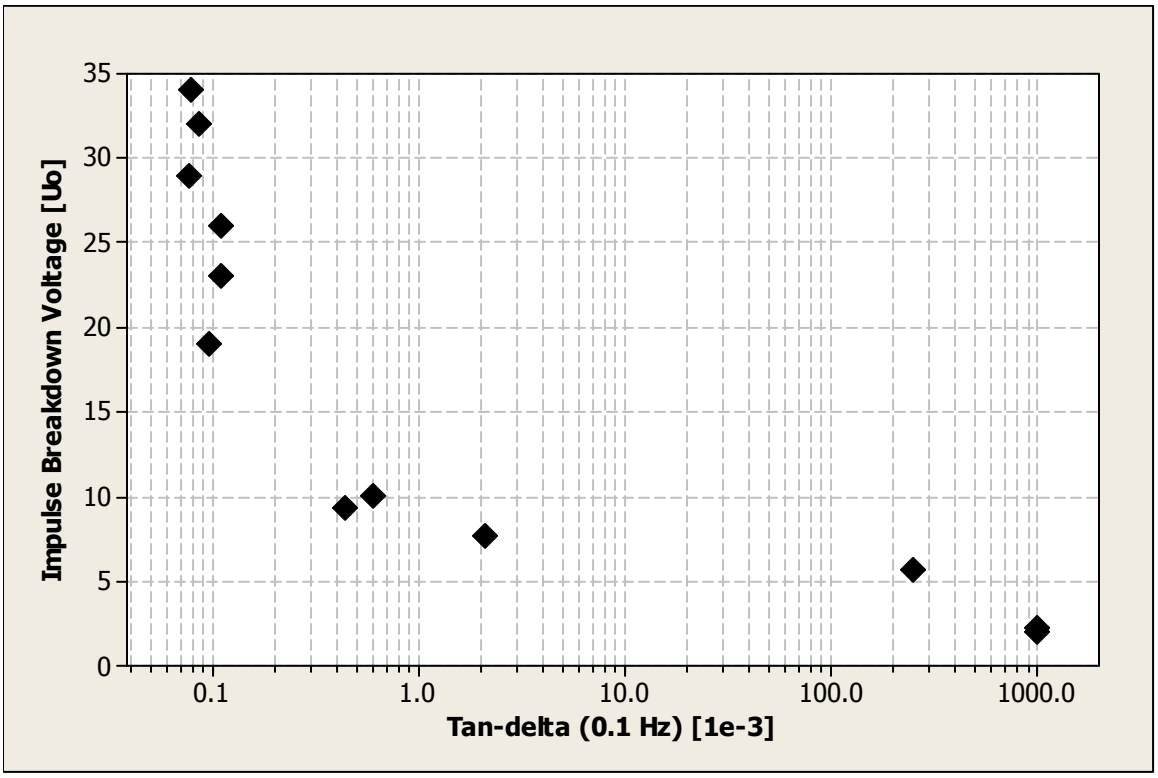

Figure 4.2. Correlation between Tan δ (0.5 U_0) and impulse breakdown voltage [13].

Additionally, at the present time there is no clear correlation between changes in Tan δ with voltage (*i.e.* Tip-Up) and the breakdown performance. It is clear that an understanding of this correlation could enhance the diagnosis.

In summary, research efforts by others have shown that there is a correlation between Tan δ measurements at different frequencies and the breakdown performance at power frequency and impulse test voltages. However, no work has been reported considering VLF breakdown voltages. In addition, the efforts have been mainly focused on PE based insulation and Tan δ magnitude. There is currently no research effort reporting on a correlation between other Tan δ diagnostic features such as Tip-Up or scatter with any breakdown voltage type. It is evident that additional work is required for

a better understanding and quantification of the correlation, different insulation materials, and additional diagnostic features.

4.3 Tan δ Measurements at VLF

The Tan δ measurements considered here are the measurements performed for the field-aged samples that are presented in Chapter 3. From Chapter 3, testing protocols I and II are considered, the protocols use 0.1 Hz and only the voltage dependence test for voltages of 0.5, 1.0, and 1.5 U_0 is considered. All samples are tested in a controlled environment in terms of humidity and temperature. The humidity is kept below 80 % non-condensing and the temperature is maintained at around 18º C with changes allowed only up to ±3º C. The voltage magnitude applied to the samples during the voltage dependence test consists of a sequence of voltage steps, each with 1 minute duration. The sequences are designed in order to assess the effect of the repeated voltages in the reproducibility of Tan δ measurements, as shown in Figures 3.6 and 3.7 for protocols I and II respectively.

Table 4.1. Tan δ and standard deviation (Stdv.) measurements results.

Sample ID	**Mean Tan δ [1e-3], {Stdv. [1e-3]}**			**Voltage Dependence Test Protocol**
	Test Voltage Level [U_0]			
	0.5	**1.0**	**1.5**	
S-1	0.6, {< 0.1}	0.6, {< 0.1}	0.6, {< 0.1}	II
S-2	1.7, {0.4}	2.3, {0.4}	3.5, {0.3}	
S-3	0.6, {< 0.1}	0.6, {< 0.1}	0.6, {< 0.1}	
S-4	2.5, {0.6}	8.4, {3.1}	19.4, {4.6}	I
S-5	0.6, {<0.1}	0.8, {<0.1}	1.8, {0.7}	
S-6	1.1, {<0.1}	2.6, {0.3}	5.6, {0.4}	

Table 4.1 shows the overall results of the voltage dependence test of the two protocols. The mean Tan δ magnitude and its standard deviation (Stdv.), at the particular test voltage level, are presented. They are computed considering all Tan δ data at the

particular test voltage level, *e.g.* they are calculated considering the four voltage applications at each test voltage level of 0.5, 1.0 and 1.5 U_0 for protocol I (see Figure 3.6). For convenience, all the values are rounded to one decimal digit.

Table 4.1 shows the different voltage dependent responses of the samples tested in both protocols. Samples S-2, S-4, S-5, and S-6 show voltage dependence while samples S-1 and S-3 do not. Those samples that show voltage dependence also display nonlinear behavior with changes in voltage and time variability.

From Table 4.1, there are several features that can be used to characterize each sample by its Tan δ diagnostic measurements. The most attractive features are the Tan δ magnitude as a function of voltage, Tip-Up, and scatter in the measurements for a particular test voltage level. Here the scatter is quantified by the standard deviation; however, another scatter metric such as range or interquartile ranges could also be used. In addition, the comparison between similar cables could also be useful for feature characterization since the samples have different Tan δ behaviors even though they have been subjected to similar aging conditions during their service life.

4.4 Breakdown Performance and Correlation with Tan δ Results

4.4.1 VLF Extended-step Withstand Test

This part of the study is conducted in two stages. First, an assessment of the breakdown strength under VLF conditions at voltage levels up to 3 U_0 is conducted and, second, a post-mortem examination of the cables for water treeing, electrical treeing, and other defects is performed. The VLF extended-step withstand test is selected as no evidence is found in the literature about the application of this test in conditions similar to the ones described here. In addition, the test allows for the evaluation of failure risk during testing for the particular cable population under study. Four of the samples in Table 4.1 are subjected to this test and failed at various voltages and times as shown in

Figure 4.3.

Samples S-2 and S-4 failed under the 60 Hz Tan δ testing; therefore, their breakdown performance is assumed to be the voltage level during testing at which they failed. This assumption is supported by the literature which shows that the breakdown value of XLPE field-aged MV cables at 0.1 Hz is approximately equal to the breakdown value at 60 Hz [54].

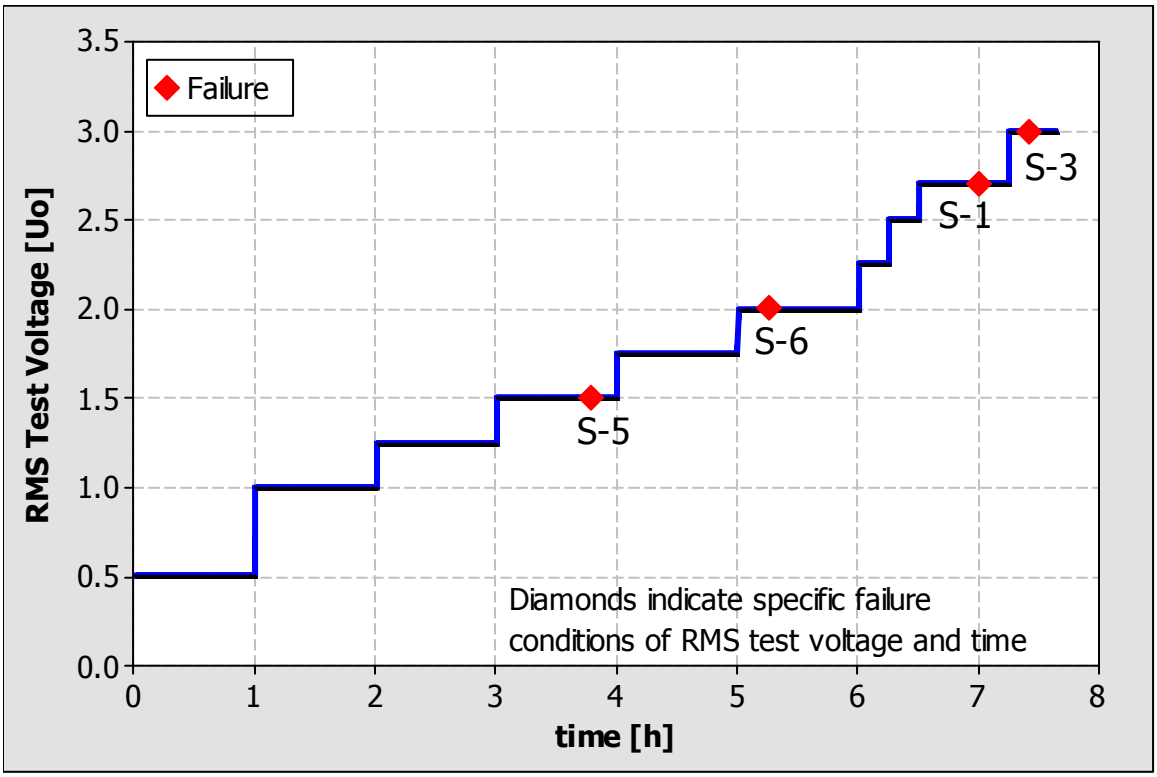

Figure 4.3. VLF withstand breakdown performance.

Figure 4.4 shows the failures for sample S-3 during the VLF extended-step withstand test and illustrates the smoke and waves in the water surface that are generated just after the failure has occurred.

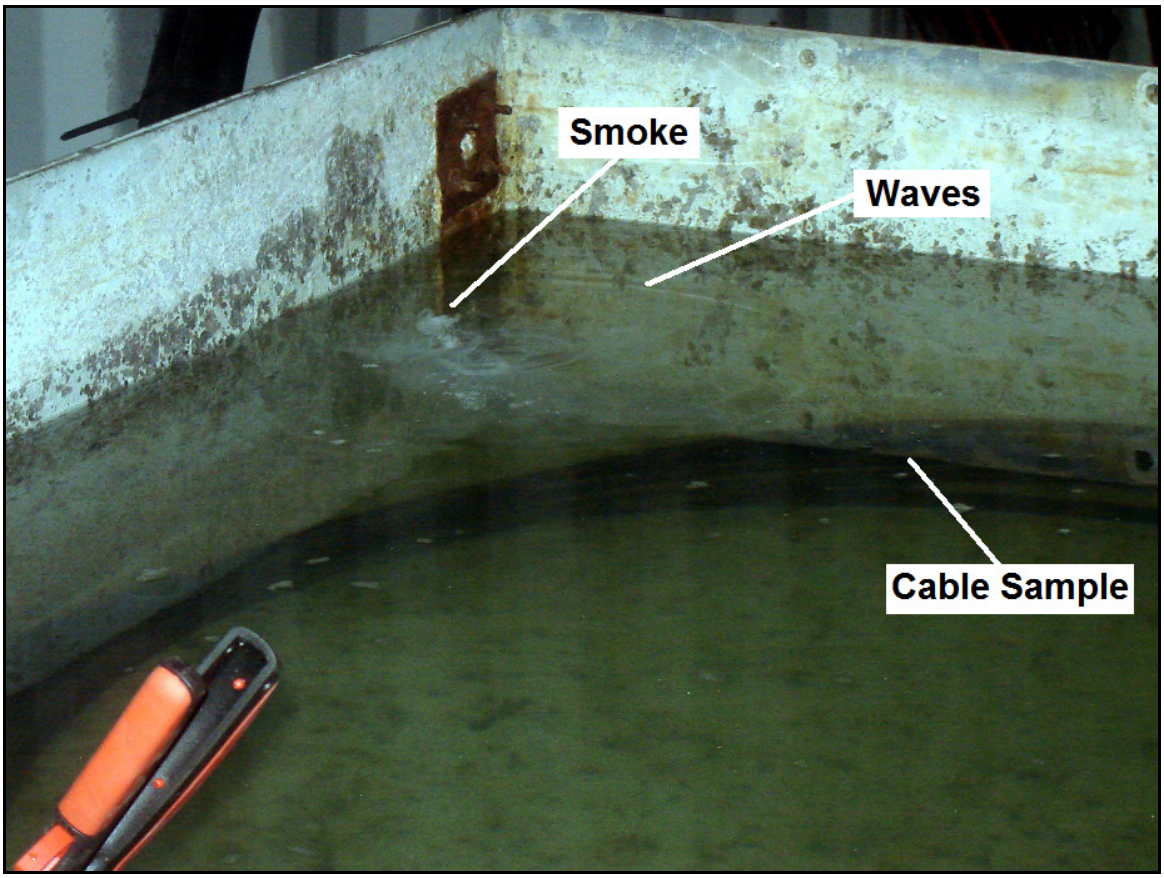

Figure 4.4. VLF extended-step withstand test – failure of sample S-3.

Analysis of the breakdown voltage indicates that it follows a standard Weibull model. The probability plot of the Weibull model fitting is shown in Figure 4.5. Specifically, Figure 4.5 shows the probability of failure in percent for the VLF extended-step withstand test as a function of the breakdown voltage. As seen in the figure, the failure data lie on a single straight line. This indicates that the breakdown is driven by a single failure mechanism [12]. Thus it is possible to conclude that if any highly degrading mechanism operates, it will do so at stresses higher than those used here, *i.e.* more than 3 U_0. This is of practical interest as the IEEE Std. 400.2 [34] gives a voltage range (VLF) for maintenance tests of 1.6-2.4 U_0 respectively for 5-35 kV cable systems.

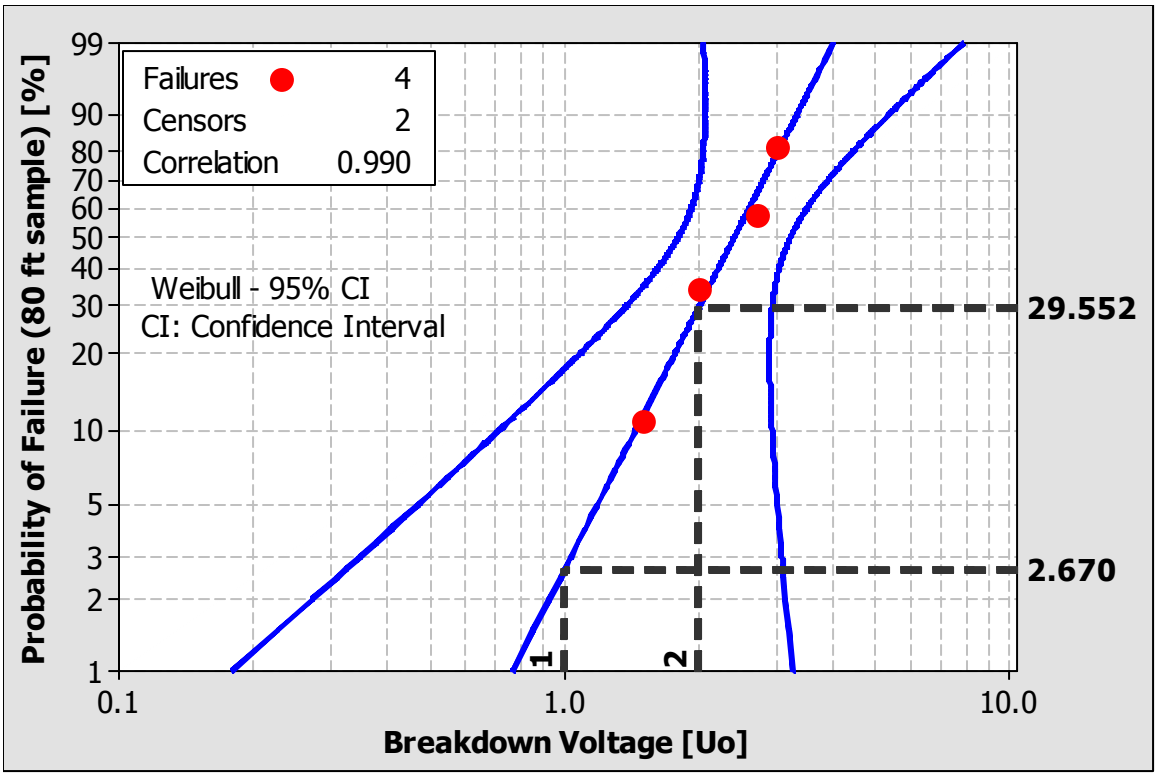

Figure 4.5. VLF breakdown performance of field-aged cable samples.

The analysis of Figure 4.5 makes it possible to determine the risk of failure during any application of elevated VLF (0.1 Hz) voltage. This is important since it has been shown by Moh [58] that the risk of failure, during the application of elevated VLF voltage for XLPE-33 kV cables, is around 10 % for a 60 minutes constant stress withstand test. Moreover, Mho [58] has also shown that approximately 70 % of the failures during test occur in the first 12 minutes of testing. Therefore, for any Tan δ test that considers the application of an elevated VLF voltage, the risk of failure during testing is an important variable that have to be taken into account. This is due to the fact that in the ideal case, the Tan δ test should be performed without posing any risk of failure to the cable under test.

In Figure 4.5, when comparing the probability of failure at 2 U_0 to that at U_0 it is observed that there is a significant reduction in the risk of failure. In fact, this reduction is

one order of magnitude (from 29.55 % at 2 U_0 to around 2.67 % at U_0) for this particular cable population. The two cable samples that failed under 60 Hz Tan δ testing (S-2 and S-4) are included in this analysis as censored data. Here the assumption is that these two samples would have failed at a voltage level lower than the minimum observed VLF breakdown voltage for sample S-5, if they had been exposed to this test.

4.4.2 Progressive Stress Test

The probability of failure in Figure 4.5 can also be considered as the result of a progressive-stress test in which a linear rate of VLF withstand voltage rise is applied to the cable samples. The voltage applied to the samples is not linear, but it can be approximated to a ramp using the least-squares linear regression fit and forcing the ramp line to go through zero at the beginning of the test. Figure 4.6 is the same as Figure 4.3 but Figure 4.6 shows the linear approximation that is represented by the dashed black line. The approximation gives a rate of increase of 0.4 U_0 per hour. In other words, it will take approximately five hours at this rate to increase the RMS test voltage from zero up to about 2 U_0.

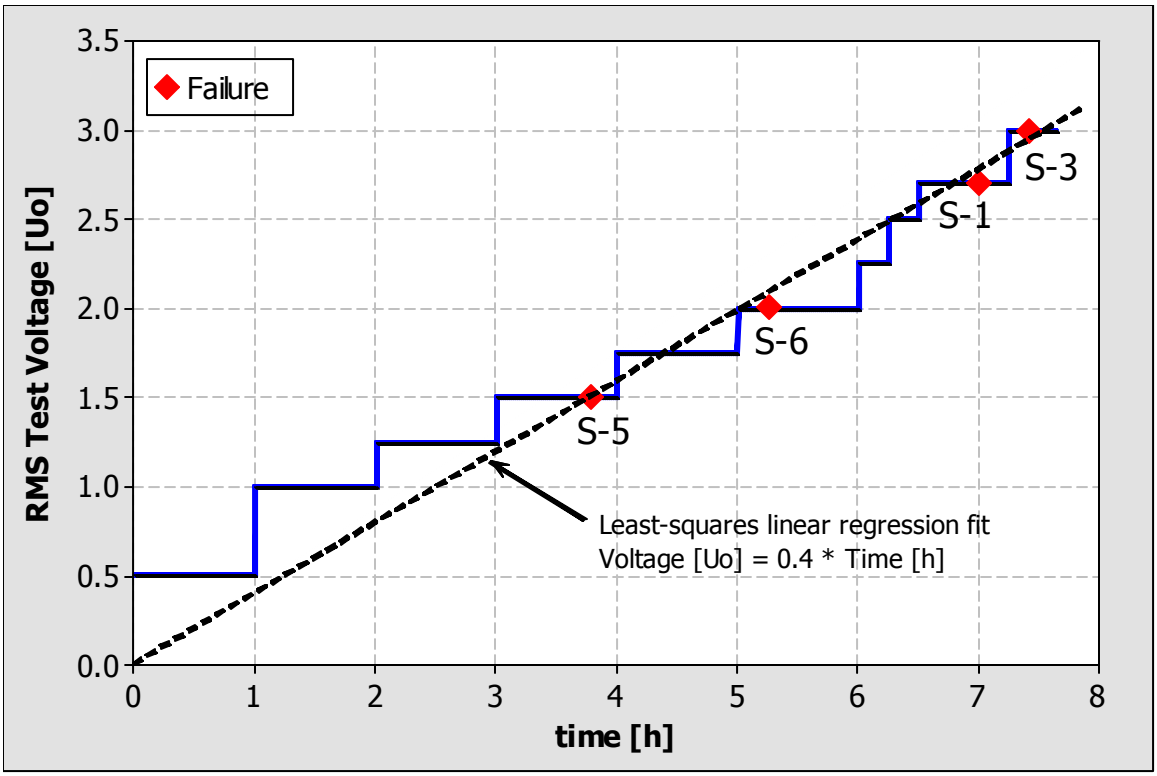

Figure 4.6. Linear ramp approximation of the VLF extended-step withstand test.

The probability of failure under a progressive-stress test can be equated to the probability of failure under a constant-stress condition. This is important because by equating the probabilities, an estimation of the breakdown performance can be made of the cable population under consideration at constant-stress. The estimate gives an indication of how long the samples would withstand a constant-stress test. If the breakdown threshold voltage is assumed as zero, the breakdown time under constant-stress can be estimated as follows [12],

$$t \approx \sqrt[a]{\frac{a}{a+b}\frac{1}{\dot{V}^{a}}V_{B}^{\,a+b}\frac{1}{V^{b}}}, \tag{4.1}$$

where,

t : Estimated breakdown time under constant-stress test in hours,

a : Shape parameter of the Weibull model breakdown time,

b : Shape parameter of the Weibull model breakdown voltage,

$\dot{V}$: Voltage rate change from progressive-stress test in U_0/hour,

V_B: Characteristic breakdown voltage chosen from initial progressive-stress voltage Weibull analysis in U_0,

V : Equivalent voltage at constant-stress voltage test in U_0.

Values of the a and b parameters have been deduced from the literature [12] for polyethylene-based insulation and water-tree degradation. In this case, the a parameter is 1.7, the value of b is between 3 and 7. These parameters are related to the common inverse power law (IPL) exponent ($n = b/a$) [12]. The IPL exponent is strongly related to the electrical aging field. The values of a and b used here for the degraded portion of the tested cable samples relate to the n exponent in the range of 2 and 4. The exponent of the un-degraded portions of the tested cable samples is expected to be higher and could approach a value of n=10 [12].

To compute the estimated breakdown time during a constant-stress test, monte-carlo simulations have been performed by considering that the b parameter is uniformly distributed between the above limits (3 and 7). Another parameter that contains uncertainty is the characteristic breakdown voltage chosen from the initial progressive-stress voltage. For this parameter, the upper and lower limits are determined using a 95 % confidence interval during the initial test.

Figure 4.7 shows the mean estimated breakdown time at constant-stress for different percentages (10, 50, and 95) of failed samples from the simulations. The level of 1.84 U_0 corresponds to the suggested VLF withstand test voltage magnitude in IEEE Std. 400.2 [34] for 15 kV cable systems.

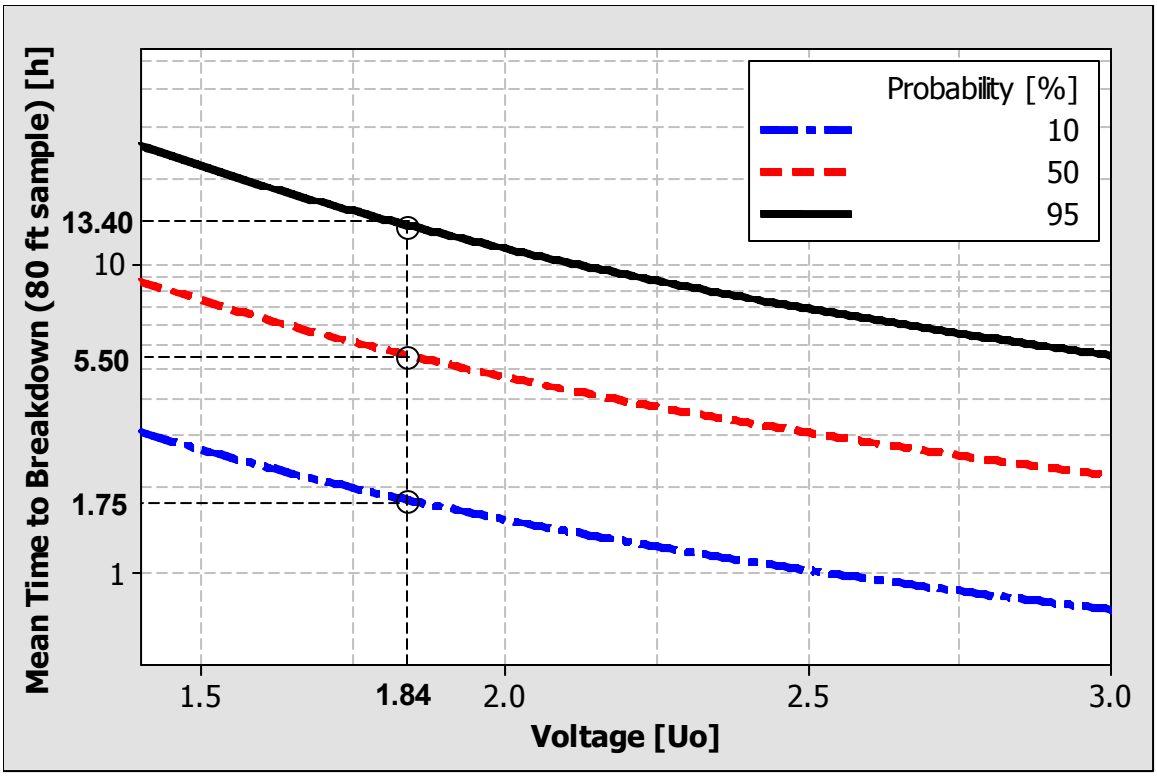

Figure 4.7. Estimated mean time to breakdown for constant-stress withstand test.

As seen in Figure 4.7, at least 13.40 hours are required to have 95 % of expected failures, 5.50 hours are required to have 50 % of expected failures, and 1.75 hours are required to have 10 % of expected failures for this particular population. The usefulness of the time-voltage analysis is that it allows for an estimate of the time-to-breakdown at constant-stress and percentage of failures. Thus, for this particular cable population, the utility may select a 2 hour test at 3 U_0 with an expectation of 50 % of failures during the test.

4.4.3 Correlation with Breakdown

This study also considers the correlation between Tan δ diagnostic features and VLF breakdown performance. The Tan δ measurements, used here to establish the correlation, are the values from the voltage dependence test as shown in Table 4.1.

Figure 4.8 shows the correlation between the mean Tan δ magnitude at 1.5 U_0 and the VLF breakdown performance. The Tan δ at 1.5 U_0 is selected to establish the correlation since the differences in Tan δ magnitude between cable samples for this particular test voltage level are maximum. In Figure 4.8, the dots correspond to the field-aged samples that failed during the VLF extended-step withstand test while the squares correspond to the samples that failed during the 60 Hz Tan δ test. This also holds for Figure 4.9 and Figure 4.10.

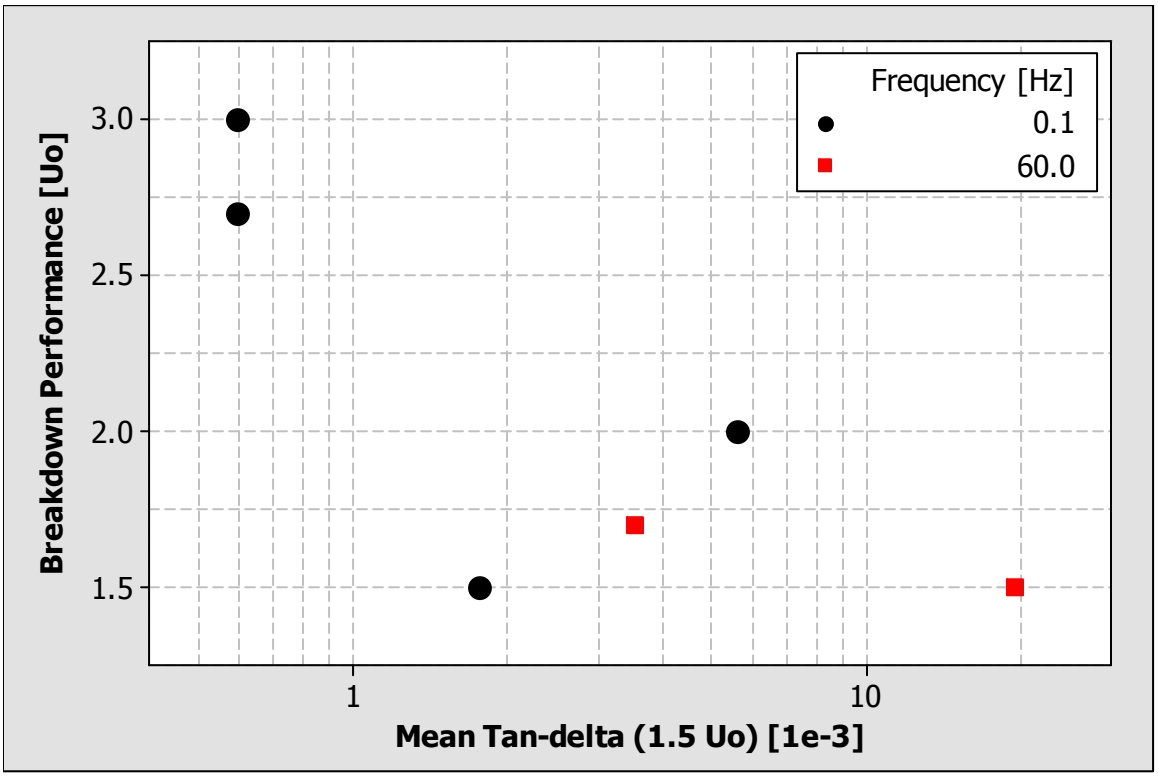

Figure 4.8. Correlation between Tan δ at 1.5 U_0 and VLF breakdown performance.

Figure 4.9 shows the correlation between the mean Tan δ Tip-Ups for 0.5 U_0 and the VLF breakdown performance. The Tip-Ups have been quantified as the mean values of the Tan δ changes with voltage from 0.5 U_0 to U_0 and from U_0 to 2.0 U_0 (see Table 4.1).

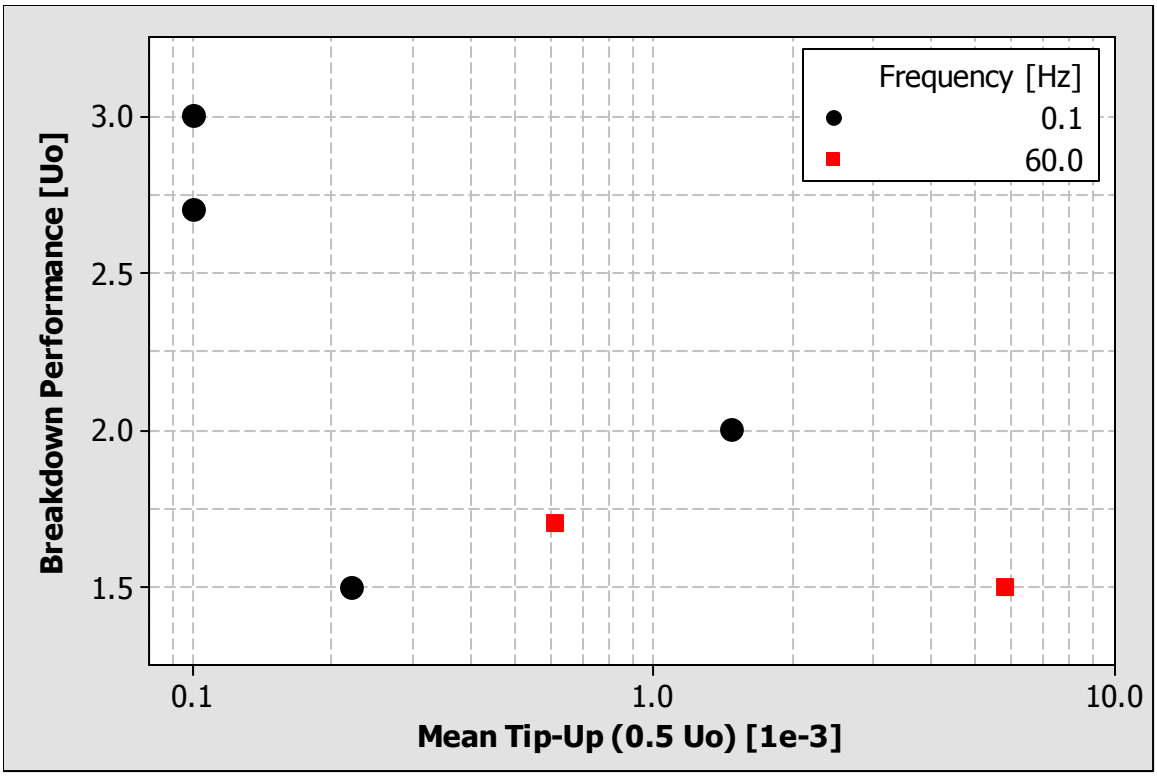

Figure 4.9. Correlation between Tip-Up of 0.5 U_0 and VLF breakdown performance.

Figure 4.10 shows the correlation between the scatter of Tan δ measurements at 1.5 U_0 and the VLF breakdown performance. The scatter has been quantified here by the standard deviation of the measurements for the particular test voltage level. Nevertheless, other scatter metrics such as interquartile ranges could also be used. In addition, it is important to mention that no attention has been given to the scatter direction. The scatter direction involves how the Tan δ values change in time, *i.e.* whether the values increase, decrease, or both, for the time period under consideration.

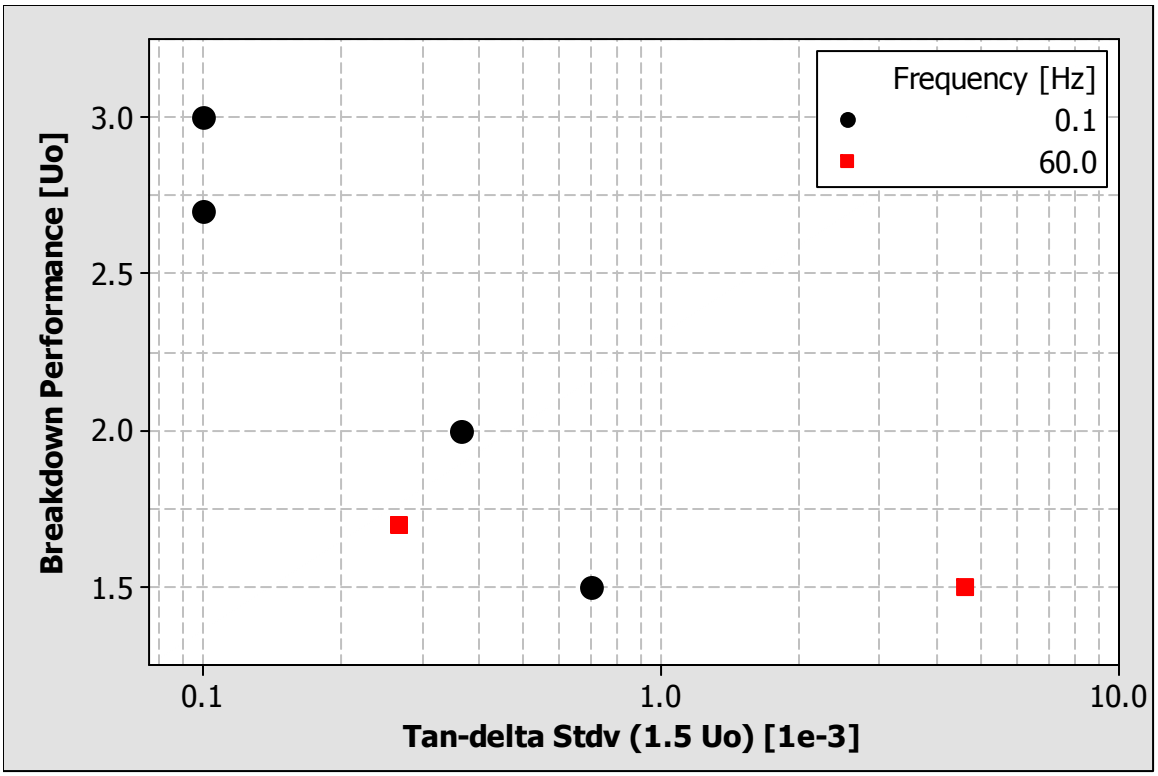

Figure 4.10. Correlation Tan δ scatter at 1.5 U_0 and VLF breakdown performance.

Results from Figure 4.8 to Figure 4.10 show that there is a correlation between Tan δ measurements and the VLF breakdown performance. Inspection of the figures suggests that the Tan δ magnitude and Tip-Up show similar results in the correlation while the scatter of the measurements gives a better correlation. The good correlation between the scatter and the breakdown performance reveals yet more evidence that this additional parameter could be used to characterize and enhance the diagnosis of cable insulation by Tan δ measurements. In addition, results also show that the cable samples with a breakdown voltage of 2.7 U_0 or more do not show any insulation deterioration from the Tan δ measurements. However, cables with a breakdown level lower than 2 U_0 can be characterized by Tan δ diagnostic measurements.

In addition, Figure 4.11 shows the comparison between correlations for the different breakdown voltage types; in particular, the correlations for impulse and AC (60

Hz) breakdown voltages correspond to the data presented in Section 4.2 as previous work while the correlation for VLF (0.1 Hz) considers the Tan δ magnitude at U_0 and breakdown performance as shown in Table 4.1 and Table 4.2 respectively.

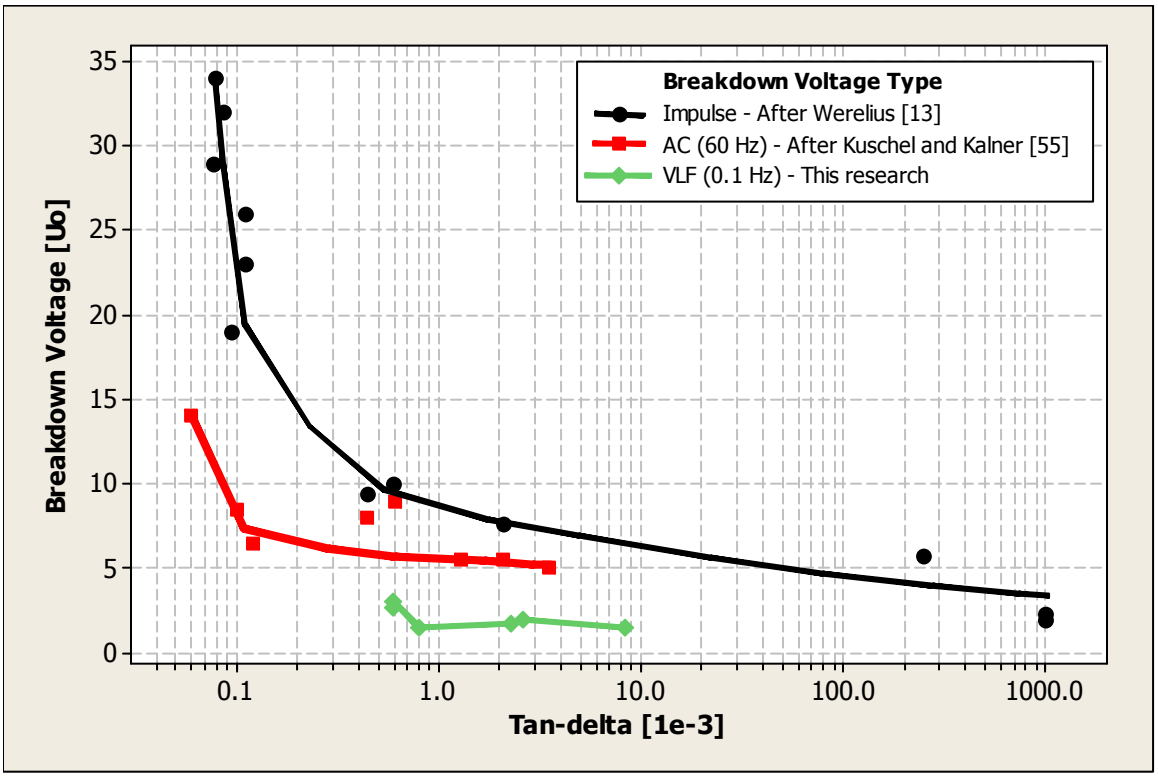

Figure 4.11. Comparison between correlations of Tan δ and breakdown performance for different breakdown voltage types.

As seen in Figure 4.11 for all breakdown voltage types, cables with higher Tan δ show a poorer breakdown performance. In general, it can also be observed that the breakdown voltages are the highest for impulse breakdown, the lowest for VLF (0.1 Hz) breakdown, and in between for AC (60 Hz) breakdown. This may be due to the frequency components of the breakdown voltage type. Consequently, the higher the frequency of the breakdown voltage the lesser time the cable at its weakest location is able to dissipate heat coming from insulation losses; thus the "thermal instability" process is more likely

to occur. The relationship between the decrease in breakdown voltage and an increase in frequency is termed frequency acceleration. Previous work has shown that frequency accelerated tests exhibit a good inverse power law fit over twelve orders of magnitude of effective frequency-accelerated lifetimes [12].

4.4.4 Performance Ranking of Tan δ Diagnostic Measurements

The previous section showed that there is a correlation between features of Tan δ data and the VLF breakdown performance. However, a question that can be raised is which one of the Tan δ features, *i.e.* Tan δ magnitude, Tip-Up, or scatter (standard deviation), has the best correlation with the VLF breakdown performance. In other words, which of the features relate in the best way possible to the breakdown performance. Thus, the correlation has to be evaluated. Before explaining in details the performance ranking technique, the issue of modeling of thermal breakdown processes is presented in the next paragraphs.

All breakdown processes in solid dielectrics are ultimately thermal breakdown processes in nature in the sense that the creation of the breakdown channel involves the melting and vaporization of the dielectric. It is well established that aged or un-aged XLPE shows increasing electrical conductivity and decreasing thermal conductivity as the temperature increases [12]. The increase in temperature is related to the amount of power absorbed by the dielectric. From Equation 3.2, this power absorption is directly proportional to the Tan δ magnitude. Consequently, higher Tan δ represent higher power absorption and increase in temperature. The increase in temperature causes and increase in the Tan δ and the process repeats itself leading to "thermal instability" as described in Section 3.1.

Therefore, it is expected that cables having higher Tan δ magnitudes would exhibit poorer breakdown performances, since the "thermal instability" is more likely to happen at the weakest location of the cable [12]. In fact in a deterministic and simplistic

modeling, the relationship between the Tan δ magnitude and the breakdown performance can be established by assuming that the breakdown performance is inversely proportional to the Tan δ magnitude [12]. The correlation would be completely established if the model is known. Nevertheless, models currently available are not completely developed and the failure statistics are not sufficient to estimate the level of degradation and the remaining life because the models do not take into account the temperature, stress, aging, ambient conditions, and mechanical stress variables during the cable service life; and even if the model would have considered these variables, in most cases they are unknown anyway. Therefore, establishing and evaluating the correlation between the Tan δ diagnostic features and the VLF breakdown performance without knowing all relevant variables is not feasible.

However, the establishment and evaluation of the correlation can be accomplished using the performance ranking technique [59-60]. This technique has been developed by the CDFI as a means of evaluating the effectiveness of diagnostic testing by comparing diagnostic data with real world performance; *i.e.* situations in which the relevant variables are unknowns. In this work, the effectiveness of the diagnostic is represented by the different features of Tan δ data, and the real world performance is represented by the VLF breakdown performance. The technique provides a quantitative measure of the correlation and level of significance for the feature under evaluation.

Table 4.2 shows features of Tan δ data, breakdown level, and frequency of the breakdown voltage used for the performance ranking procedure.

In Table 4.2, diagnostic ranks have to be assigned to the features of mean Tan δ magnitude at 1.5 U_0, Tip-Up for 0.5 U_0, and standard deviation of the Tan δ at 1.5 U_0. In addition, performance ranks have to be assigned that take into account the breakdown performance.

Table 4.2. Breakdown performance and Tan δ diagnostics features.

Sample ID	Breakdown [U_0] (Hz)	Mean Tan δ (1.5 U_0) [1e-3]	Tip-Up (0.5 U_0) [1e-3]	Tan δ Stdv. (1.5 U_0) [1e-3]
S-1	2.7 (0.1)	0.6	<0.1	<0.1
S-2	1.7 (60)	3.5	0.6	0.3
S-3	3.0 (0.1)	0.6	<0.1	<0.1
S-4	1.5 (60)	19.4	5.8	4.6
S-5	1.5 (0.1)	1.8	0.2	0.7
S-6	2.0 (0.1)	5.6	1.5	0.4

The diagnostic ranks are simply assigned by considering the value of the feature under consideration. For example, if the mean magnitude of Tan δ at 1.5 U_0 is considered; then, the cable sample that has the highest value (S-4) is selected as the poorest performer. Thus, it is assigned the rank of one. The procedure continues until the best performer is identified and this one is assigned a rank of six. The same procedure is repeated for the other diagnostic features.

Unfortunately, in some cases there is not enough information to differentiate between samples. For instance, samples S-1 and S-3 are tied even after considering additional cable and test information. Therefore, the tie cannot be broken. This unbreakable tie generates two cases: case 1 considers S-3 as the best performer and case 2 considers S-1 as the best performer.

The performance rank is determined by considering the breakdown level in the same way as for the diagnostic ranks, *i.e.* the sample with the lowest breakdown level is considered to be the poorest performer; thus, it gets assigned rank of one. Similarly, the sample with the highest breakdown performance is considered as the best performer and is assigned a rank of six. In this case, as can be observed in Table 4.2, two samples (S-4 and S-5) share the lowest breakdown level. This tie is broken by considering additional test information such as time and sequence to failure. Subsequently, sample S-4 is the

poorest performer since, as mentioned previously, it failed during 60 Hz Tan δ testing, which was conducted prior to the VLF withstand test.

Table 4.3. Performance and diagnostic ranks.

Sample ID	**Rank**							
	Breakdown	**Mean Tan δ (1.5 U_0)**		**Tip-Up (0.5 U_0)**		**Tan δ Stdv. (1.5 U_0)**	
		case 1	**case 2**	**case 1**	**case 2**	**case 1**	**case 2**
S-1	5	5	6	5	6	5	6
S-2	3	3	3	3	3	4	4
S-3	6	6	5	6	5	6	5
S-4	1	1	1	1	1	1	1
S-5	2	4	4	4	4	2	2
S-6	4	2	2	2	2	3	3

The diagnostic and performance ranks are shown in Table 4.3 for both case 1 and case 2. After the ranks have been established, they may be analyzed either graphically (qualitatively) or statistically (quantitatively).

In the qualitative analysis, a plot of the diagnostic rank versus the performance rank is generated. For example, Figure 4.12 shows the resulting performance ranking plot for the Tan δ standard deviation (at 1.5 U_0) diagnostic rank and the breakdown performance rank for case 1. The accuracy of the diagnostic test feature is directly related to how far from the dashed line the dots are in Figure 4.12.

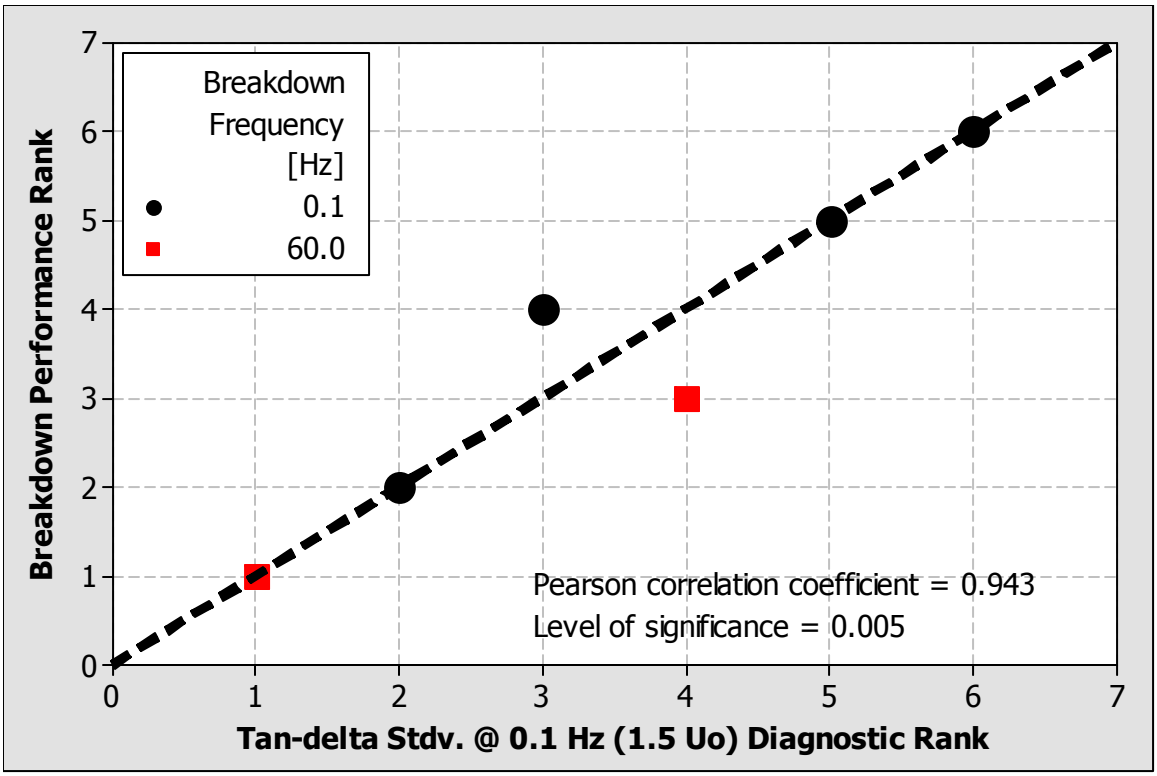

Figure 4.12. Performance ranking plot for Tan δ Stdv. rank and breakdown performance rank – case 1.

Figure 4.12 is to be interpreted as follows: the samples in the lower left corner are the worse performers, *i.e.* they have lower breakdown levels and diagnostic features that indicate a worse condition when compared to the other cable samples in the group. In contrast, the upper right corner in Figure 4.12 contains the better performers, *i.e.* the ones that have higher breakdown and diagnostic features that indicate a better condition when compared to the other cable samples in the group. The dashed line can be thought of as the perfect correlation between the performance and diagnostic ranks. In other words, if the diagnostic feature under analysis is able to rank the samples in the same way as the performance rank; then, all the dots in Figure 4.12 would be exactly on the dashed line. Therefore, the most suitable statistical approach to quantitatively evaluate the correlation is to examine the Pearson correlation coefficient between the Tan δ diagnostic feature

ranks and the breakdown performance ranks [60].

In the quantitative evaluation, the Pearson correlation coefficient and level of significance between all the diagnostics ranks and all the performance ranks are computed, and results are shown in Table 4.4. For example, if the Tan δ standard deviation at 1.5 U_0 diagnostic rank is considered for case 1, the Pearson correlation coefficient is 0.943 which is significant at the 0.005 level. Therefore, these results would only occur randomly with a probability of less than 0.5%.

Table 4.4. Performance ranking results.

Tan δ Diagnostic Feature	**case 1**		**case 2**	
	Correlation Coefficient	**Level of Significance**	**Correlation Coefficient**	**Level of Significance**
Mean Tan δ (1.5 U_0)	0.771	0.072	0.714	0.111
Tip-Up (0.5 U_0)	0.771	0.072	0.714	0.111
Tan δ Stdv. (1.5 U_0)	0.943	0.005	0.886	0.019

A further analysis of Table 4.4 reveals that the Tan δ standard deviation diagnostic feature has the highest correlation with the breakdown performance, and it is also the most significant. These results again show the importance of considering this new feature in the diagnosis of XLPE cable insulation by Tan δ at VLF.

Finally, it is important to note that another possible way of obtaining the performance rank is to consider the time-to-failure rather than the breakdown voltage level. The ideal situation would consider these two parameters at the same time in order to obtain a combined performance rank. This could be especially useful for breaking ties in the case of a large number of samples under evaluation. For example, if two or more samples fail during the withstand test at the same voltage level then the time-to-

breakdown could be used to break the tie caused by determining the rank by only considering the breakdown voltage level.

4.5 Postmortem Examination

After the VLF withstand test is performed, the failure sites are located and cut out of the samples. Six cuts are analyzed. Each cut is approximately 0.91 m (3 ft) long with the failure site located at the center of the sample length. All the cuts for the samples that failed during the VLF withstand test are shown in Figure 4.13. For each cut, the failure site is located in the middle of the green-tape marks.

The cuts are subjected to two tests. First, a failure site examination test is conducted in which insulation wafers of the failure site are examined for the cause of failure. Second, a hot-oil examination test is conducted in which the remainder of the cut is simmered in hot-oil until the insulation becomes translucent. Then, the insulation is visually examined for large water tress, electrical tress, and contaminants.

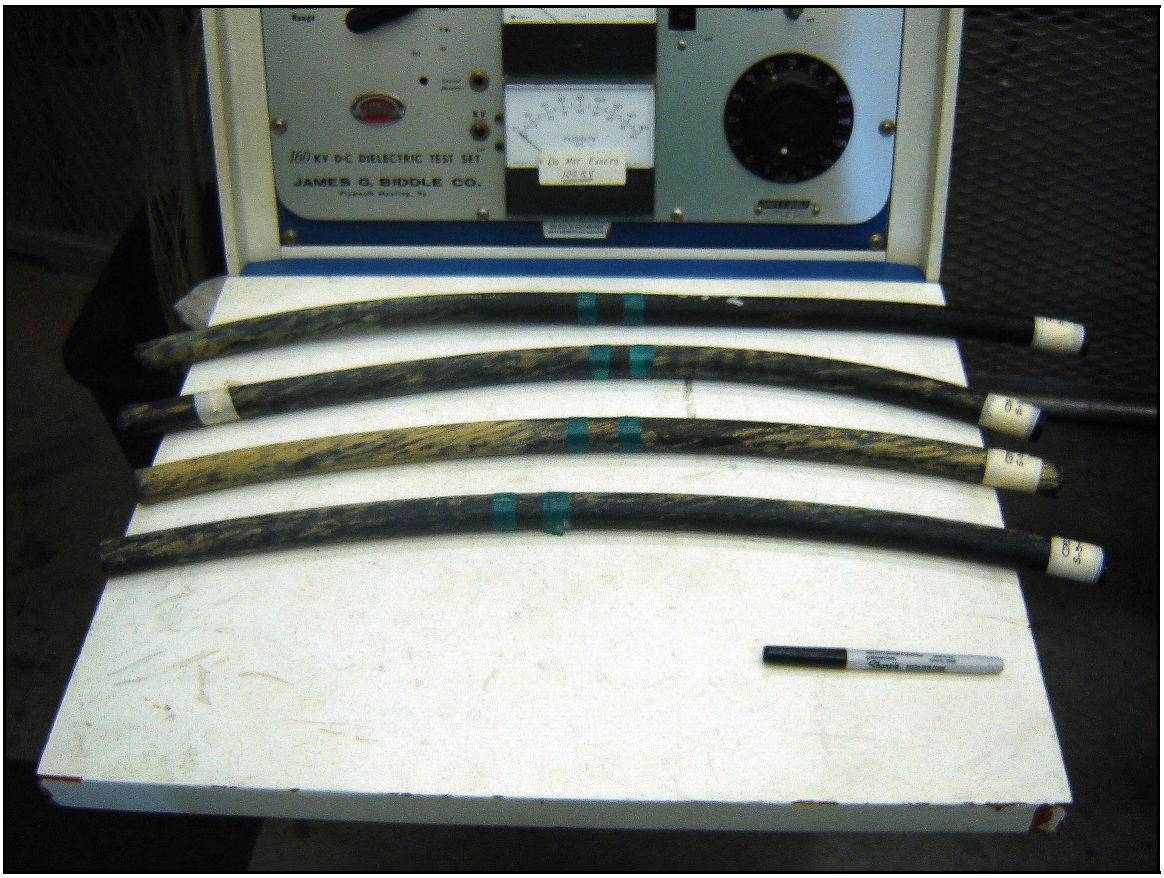

Figure 4.13. Failure site cuts for the samples that failed during the VLF withstand test.

The failure site examination test did not reveal the cause of failure for any of the samples. However, the hot-oil examination test showed that most of the samples exhibited water-tree sites or other irregularities. Therefore, the cause of failure is more likely a water-tree related failure mechanism. In addition, it should be noted that for the two samples that did not show signs of degradation (S-1 and S-3), the failure channel is narrow, thus causing little damage to the insulation. In fact, sample S-3 was defect-free according to the hot-oil examination. On the other hand, for the remaining samples that showed signs of degradation, the insulation damage is extensive. This could be an indication that for the latter case the failures are due to much larger water trees, *i.e.* the thermal "run-away" process is more extensive.

Figure 4.14 shows defects found in the analysis of failure sites. Figure 4.14 (a) shows a 2.74 mm (108 mil) bow-tie water tree growing from a 0.25 mm (10 mil) contaminant for sample S-4; Figure 4.14 (b) shows a 0.56 mm (22 mil) contaminant at a visual water-tree site location for sample S-4; and Figure 4.14 (c) shows a typical water-tree site as viewed in the hot-oil examination test for sample S-6. Sizing of the trees is performed with a LEICA® MZ9.5 stereo zoom microscope. A LEICA® MZ16 stereo zoom microscope and a POLAROID® DMC digital camera are used to capture images of the water trees.

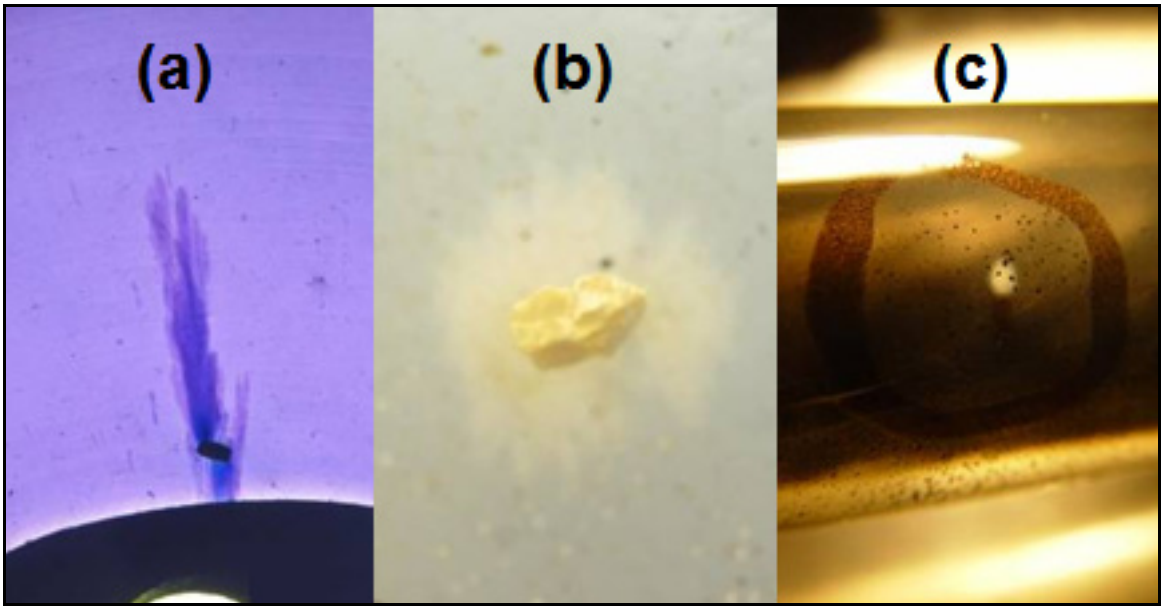

(a) A 2.74 mm (108 mil) bow-tie water tree growing from a 0.25 mm (10 mil) contaminant (sample S-4).
(b) A 0.56 mm (22 mil) contaminant at a visual water tree site location (sample S-1).
(c) A typical water tree site as viewed in the hot-oil examination test (sample S-6).

Figure 4.14. Analysis of failure sites results.

4.6 Summary and Conclusions

This Chapter has described a laboratory test program conducted to investigate the correlation between Tan δ diagnostic features and the VLF breakdown strength for MV XLPE cables. The Tan δ diagnostic features include the mean Tan δ magnitude, the Tip-Up, and the scatter in the Tan δ measurements for a particular test voltage level. The sample set is a uniform group of service aged 15 kV, XLPE, unjacketed cables, removed from the same utility service area, and having experienced similar operating conditions for almost four decades. This is important in the sense that comparisons between these samples can be made without regard to cable design and aging conditions. The test program has included Tan δ measurements at different voltage levels and subsequent VLF extended-step withstand test to breakdown.

It has been found that there is a correlation between the Tan δ diagnostics features and the VLF breakdown performance. This is important in the sense that the correlation between the Tan δ diagnostic features and the breakdown performance has only been previously established for impulse and AC breakdown voltages and mainly considering the Tan δ magnitude as diagnostic feature. Results have shown that in general the VLF (0.1 Hz) breakdown performance is the lowest when compared to impulse and AC (60 Hz).

More importantly, the Chapter has introduced the use of a new diagnostic feature that takes into account the scatter in the Tan δ measurements for a particular test voltage level. The scatter has been quantified using the standard deviation. It has been shown that the cable insulation condition can be assessed using this new feature since more scatter in the measurements implies a lower breakdown voltage.

The Chapter has also introduced the application of a new method called performance ranking. This method has been able to quantitatively evaluate the correlation between each diagnostic feature and the breakdown performance. Results indicate that

the scatter in the measurements is the feature that is most correlated with the breakdown performance for the cable population under study.

Further investigations such as Weibull breakdown performance and time-voltage analysis have also been presented. The Weibull breakdown performance results have also allowed for evaluation of the risk of failure during testing. A considerable reduction of one order of magnitude in the risk of failure has been observed when the testing voltage is reduced from 2 U_0 to U_0. Therefore, it is clear that testing at lower voltages is desirable.

Time-voltage analysis under constant-stress has been estimated from breakdown results of the progressive-stress test. The estimation has been done using Monte Carlo simulations considering typical Weibull models parameters found in the literature for water-tree degradation regarding time and voltage to breakdown. The usefulness of the time-voltage analysis is that it enables the estimation of the time to breakdown at constant-stress and percentage of failures.

Finally, failure site and hot-oil examinations have also been performed. The failure site examination test has not revealed the cause of failure for any of the samples. Nevertheless, the hot-oil examination has shown that most of the samples have water-tree sites and other irregularities. Therefore, the possible cause of failure is more likely to be a water-tree related failure mechanism.

The Tan δ versus cable segment length models and the deployment of Tan δ diagnostic features are next addressed in Chapter 5.

CHAPTER 5

ANALYSIS AND DEPLOYMENT OF TAN δ DIAGNOSTIC FEATURES

5.1 Introduction

It has been shown in Chapter 4 that for Tan δ measurements, the cable system insulation can be modeled by an approximate or basic equivalent circuit that consists of two elements connected in parallel; a resistor and a capacitor. Unfortunately, this model does not consider real situations such as non-uniform degradation or neutral issues, all of which can lead to an incorrect assessment if their effects are not considered in the modeling.

Therefore, this Chapter explores the importance of modified equivalent circuits that are able to consider the non-uniform degradation and neutral issues for Tan δ measurements in order to study and identify useful diagnostic features and indicators that may lead to an enhanced diagnosis.

More importantly, the Chapter introduces a new approach for condition assessment of MV power cables using combined diagnostic technologies. This combination includes time domain reflectometry (TDR), VLF Tan δ measurements, and VLF-Tan δ monitored withstand. The approach considers the deployment of Tan δ diagnostic features in field testing applications of PE-based MV cable systems of 15 and 25 kV which include HMWPE, XLPE, and TRXLPE insulation materials. The condition assessment is accomplished by performing an evaluation process that uses diagnostic feature management with feature categorization and decision organization.

5.2 Time Domain Reflectometry (TDR)

Because of its ease of use, cost, and simplicity in identifying cable segment configuration and basic problems, the usefulness of TDR in the work presented here is that the TDR is used and proposed as one of the initial steps for any cable condition assessment in the field using Tan δ at VLF (0.1 Hz) measurements. Specifically, the greatest value of TDR lies in its ability to identify neutral issues such as loss of neutral or poor contact between the insulation shield and neutral wires. This is important since the identification of these issues combined with other tools such as visual inspection of the cable segment, cable segment history, and Tan δ versus length models, aids in improving the cable condition assessment as illustrated later in the Chapter.

The basic low voltage TDR system works essentially like a radar system. It mainly consists of a fast rise-time pulse generator and a high speed recording oscilloscope as shown in Figure 5.1.

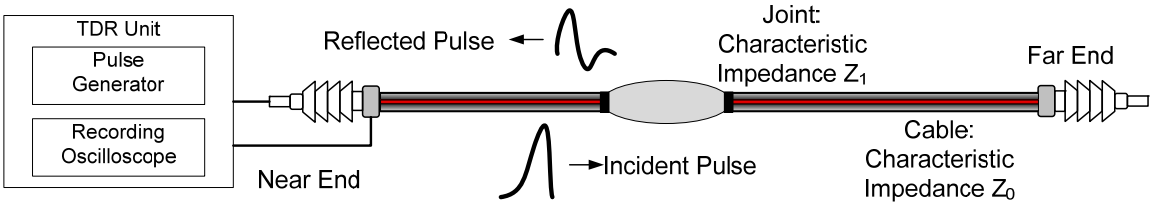

Figure 5.1. Basics of a low voltage TDR test.

In Figure 5.1, the pulse that is sent by the fast rise-time pulse generator, or incident pulse, travels through the cable that has a characteristic impedance Z_0. If at some point along the cable length there is a joint with characteristic impedance Z_1, a portion of the travelling pulse is reflected back to the TDR unit where it is recorded by the oscilloscope. The sent pulse keeps travelling to the far end of the cable segment where a portion of the pulse is reflected back to the near end because of any other impedance

mismatch along the cable segment. The reflected pulse components are positive or negative depending on whether the impedance is more or less than the characteristic impedance (Z_0) of the cable.

Subsequently, the sent pulse and its reflections are plotted against time on the display of the instrument. Since calibrations can be performed to determine the speed of the pulse in the cable, the distance to the far end of the segment can be determined. The location of the impedance mismatches can be determined in the same way as the far end of the cable segment. In this case, shapes of reflected pulses help to determine the type of impedance mismatch.

The magnitude of the reflection at an impedance mismatch can be calculated using the reflection coefficient (ρ), which is calculated as follows [5],

$$\rho = \frac{Z_d - Z_0}{Z_d + Z_0}, \tag{5.1}$$

where,
Z_0: Characteristic impedance of the cable,

Z_d: Impedance of a discontinuity.

The reflection coefficient value ranges from 1 (open circuit) to -1 (short circuit). A reflection coefficient of zero indicates that there is no change in the cable characteristic impedance; therefore, no reflected pulses are observed.

Regarding the test goal, TDR is used to locate and characterize when possible changes in impedance of a cable segment. These changes in impedance can be caused by:

- Faults (short circuits).
- Joints (splices).
- Open connections.
- Neutral issues.

- Water ingress into cable insulation or joints.

TDR results, both location and identification of impedance mismatches, require an experienced interpreter of TDR signals. Interpretation of TDR results could be a challenging task; nevertheless, the basic configuration and problems can be identified by typical waveforms. Their meanings are shown in Table 5.1.

Table 5.1. Usual cable segment conditions distinguishable using TDR.

Condition	TDR
Uniform cable segment with no joints.	
Uniform cable segment with no joints and shorted conductor at distance L from Near End.	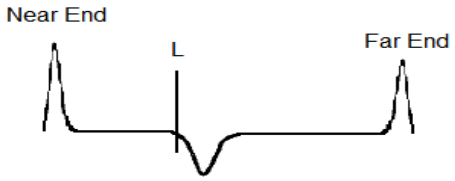
Cable segment with a joint at a distance L from Near End.	
Cable segment with a wet joint at a distance L from Near End.	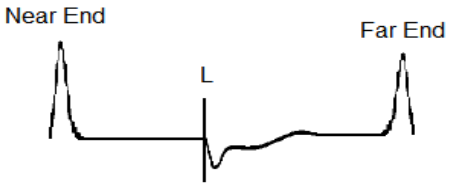
Uniform cable segment with water ingress at a distance L from Near End.	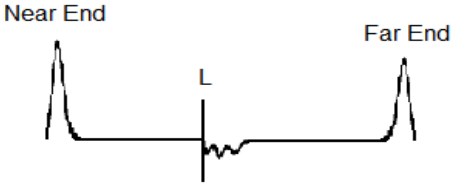

5.3 Tan δ Length Models

This section is built on the Tan δ basis presented in Chapter 3 and explores the importance of the modified equivalent circuits that consider, to some extent, the non-uniform degradation and neutral issues for Tan δ measurements. The main goal is to introduce modifications to the basic equivalent circuit to study and identify their usefulness as diagnostic indicators.

5.3.1 Non-uniform Degradation

As explained in Chapter 3, Tan δ is a measure of the average condition of a cable segment and it may be therefore only used to provide a qualitative assessment of the overall degradation of the cable segment insulation. Unfortunately, if a highly aged portion only exists in a short length of the cable segment; its effect on Tan δ of the entire segment would be small, perhaps even insignificant. For example, a highly aged portion could be a short length of cable insulation with a high density of water trees, or a highly degraded accessory, or a localized corroded neutral. The assumption here is that the highly aged portion just by itself would show a much higher Tan δ magnitude as compared to the healthy, or un-aged, portion of the cable segment. As a consequence, it is generally accepted that the usefulness of Tan δ is limited by its inability to give localized information. Additional diagnostic tests may be required to account for this situation.

Figure 5.2 shows two cases for a cable segment with non-uniform degradation. Particularly, Case 1 represents a situation in which the highly aged portion is located inside the cable segment length and Case 2 represents a situation in which the highly aged portion is located at one of the extremes of the cable segment. Both situations can be modeled by making certain modifications to the basic equivalent circuit presented in Chapter 3. A similar case would arise for a highly degraded accessory installed with a healthy length of cable or a localized corroded neutral.

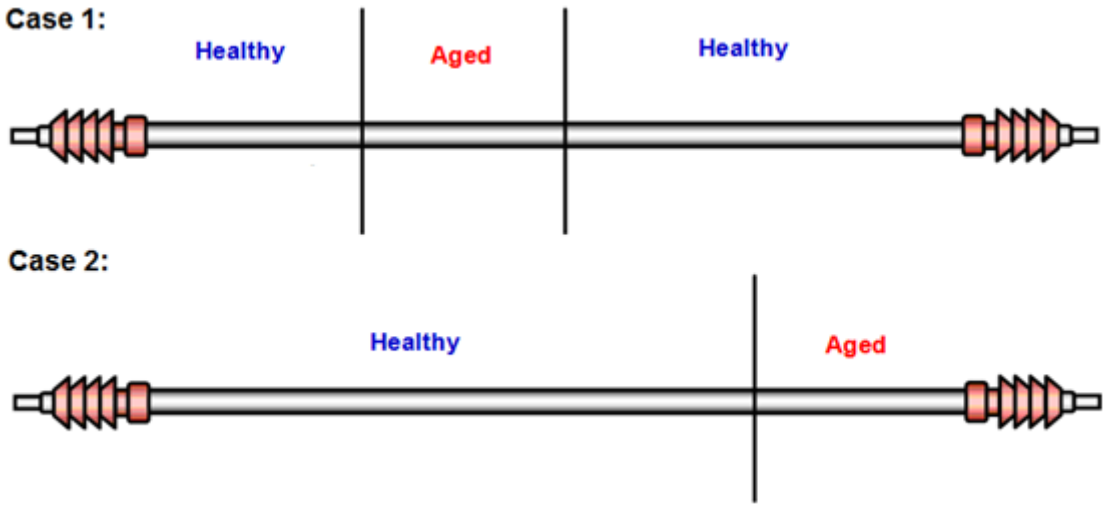

Figure 5.2. Some possible cases for a cable segment with non-uniform degradation.

5.3.1.1 Non-uniform Degradation Modeling

The non-uniform degradation can be modeled by considering two separate sections of the cable segment, one section representing the healthy portion and the other representing the aged portion. Each portion has an appropriate set of parameters in its equivalent circuit to represent its Tan δ value. Thus, considering the two portions together, a set of four parameters are considered in the model, *i.e.* the resistance and capacitance of the healthy portion (R_1 and C_1) and the resistance and capacitance of the aged portion (R_2 and C_2), as shown in Figure 5.3.

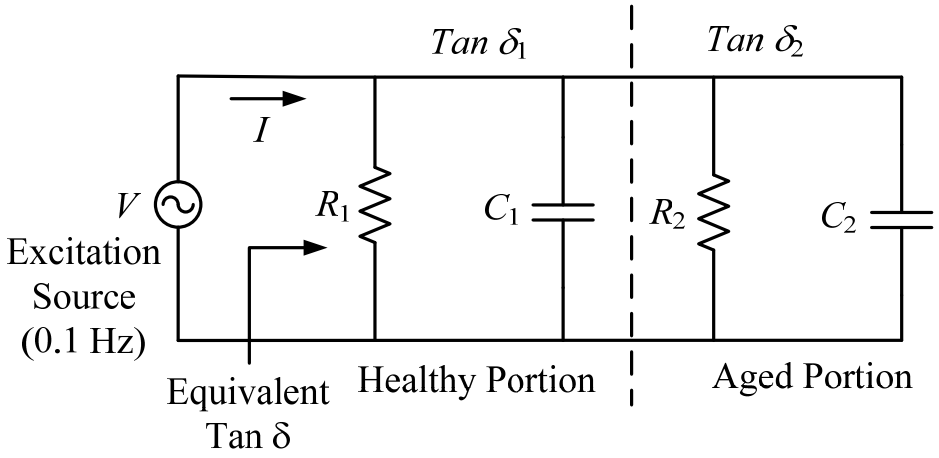

Figure 5.3. Non-uniform degradation modeling.

Tan δ_1 and *Tan* δ_2 are defined as follows as the Tan δ magnitudes of the healthy and aged portions of the cable segment respectively,

$$Tan\,\delta_1 = \frac{1}{\omega R_1 C_1} \quad \text{(a)},$$
$$Tan\,\delta_2 = \frac{1}{\omega R_2 C_2} \quad \text{(b)}, \tag{5.2}$$

where,

Tan δ_1: Tan δ of the healthy portion of the cable segment,

ω: Angular frequency in rad/s,

R_1: Insulation resistance of the healthy portion of the cable segment in Ω,

C_1: Insulation capacitance of the healthy portion of the cable segment in F,

Tan δ_2: Tan δ of the aged portion of the cable segment,

R_2: Insulation resistance of the aged portion of the cable segment in Ω,

C_2: Insulation capacitance of the aged portion of the cable segment in F,

Tan δ: Equivalent or combined Tan δ for both healthy and aged portions of the

cable segment.

The modeling objective is to find a mathematical relation between the equivalent Tan δ (as it would be "seen" by measurement equipment) and the values of $Tan\ \delta_1$, and $Tan\ \delta_2$ and portion lengths. The relationship is developed in detail in Appendix A where it is shown that the equivalent Tan δ is given by,

$$Tan\ \delta = \frac{(1 + R_2 / R_1)\, Tan\ \delta_1\, Tan\ \delta_2}{Tan\ \delta_1 + (R_2 / R_1) Tan\ \delta_2}. \tag{5.3}$$

Taking into account the healthy and aged portion lengths, L_1 and L_2 respectively, and considering per-unit length parameters instead of lumped parameters for the equivalent circuit, the equivalent Tan δ is given by equation (5.4),

$$\Gamma = \frac{L_1}{L_2} \quad \text{(a)},$$

$$Tan\ \delta = \frac{1 + (r_2 / r_1)\Gamma}{(Tan\ \delta_1 / Tan\ \delta_2) + (r_2 / r_1)\Gamma} Tan\ \delta_1, \text{ in terms of } Tan\ \delta_1 \quad \text{(b)}, \tag{5.4}$$

$$Tan\ \delta = \frac{1 + (r_2 / r_1)\Gamma}{1 + (r_2 / r_1)(Tan\ \delta_2 / Tan\ \delta_1)\Gamma} Tan\ \delta_2, \text{ in terms of } Tan\ \delta_2 \quad \text{(c)},$$

where,

Γ: Length ratio between L_1 and L_2,

L_1: Length of the healthy portion of the cable segment in ft,

L_2: Length of the aged portion of the cable segment in ft,

r_1: Insulation resistance per-unit length of the healthy portion of the cable segment in Ω-ft,

r_2 : Insulation resistance per-unit length of the aged portion of the cable segment in Ω-ft.

Subsequently, if the cable insulation geometry and electrical permittivity between

the healthy and aged portions of the cable segment are assumed equal; then, the ratio between the insulation resistance per-unit length of the aged portion of the cable segment (r_2) and the insulation resistance per-unit length of the healthy portion of the cable segment (r_1), can be simply expressed as the ratio between $Tan\ \delta_1$ and $Tan\ \delta_2$. This is shown in equation (5.5). The electrical permittivity between the healthy and aged portions of the cable segment can be assumed to be equal since it has been shown for water-tree degradation [13] that this intrinsic parameter of insulation material only changes marginally between the healthy and the aged portions of the cable segment.

$$\frac{Tan\ \delta_1}{Tan\ \delta_2} = \frac{r_2}{r_1}. \tag{5.5}$$

Substituting equation (5.5) into equation (5.4)(b) or (5.4)(c), the equivalent Tan δ as a function of $Tan\ \delta_1$, $Tan\ \delta_2$, and the length ratio (Γ) yields,

$$Tan\ \delta = \frac{Tan\ \delta_2 + Tan\ \delta_1 \Gamma}{1+\Gamma}. \tag{5.6}$$

From equation (5.6), if Γ is zero; then, the equivalent Tan δ is $Tan\ \delta_2$, *i.e.* there is not any healthy portion in the cable segment. In contrast, if Γ tends to infinity; then, the equivalent Tan δ tends asymptotically to $Tan\ \delta_1$, *i.e.* as the length of the healthy portion of the cable segment increases compared to the aged portion, the effect of the aged portion on the equivalent Tan δ decreases and eventually the equivalent Tan δ is $Tan\ \delta_1$. The equivalent Tan δ as a function of $Tan\ \delta_1$, $Tan\ \delta_2$, and the length ratio (Γ) is studied quantitatively in detail in the following section by simulations and laboratory experiments.

Another important point is that if the equivalent Tan δ is much larger than $Tan\ \delta_1$, *i.e.* if $Tan\ \delta >> Tan\ \delta_1$, then the equivalent Tan δ follows a linear model in length when it is plotted in a log-log scale. This is important since it will be shown later that this behavior can be used as an additional diagnostic indicator for Tan δ measurements. The

derivation is also shown in Appendix A.

5.3.1.2 Simulation and Laboratory Experimentation

Figure 5.4 shows the simulation results using equation (5.6) for the equivalent Tan δ as it would be measured. The simulation considers four cases; it takes into account four different values for the Tan δ of the aged portion of the cable segment (*Tan* δ_2) while the Tan δ of the healthy portion of the cable segment (*Tan* δ_1) is constant and equal to 0.2×10^{-3}. The four cases consider values for *Tan* δ_2 of 1.2×10^{-3}, 2.2×10^{-3}, 4.0×10^{-3}, and 100×10^{-3}. The first three values for *Tan* δ_2 are selected because they are used for diagnosis in the present IEEE Std. 400 [37]; however, the last value for *Tan* δ_2 is selected to represent the case of a high Tan δ magnitude for the aged portion of the cable segment. The value for *Tan* δ_1 is selected on the basis that the Tan δ magnitude for an un-aged XLPE cable is approximately 0.2×10^{-3} as shown in Chapter 3.

In Figure 5.4 the *x*-axis is the length ratio (Γ) between the lengths of the healthy portion (L_1) and aged portion (L_2) of the cable segment and the *y*-axis is the equivalent Tan δ magnitude as calculated from equation (5.6). From Figure 5.4, if the length ratio is 0.01; then, the equivalent Tan δ is *Tan* δ_2 for all cases, *i.e.* there is a small portion of healthy cable in the segment as compared to the aged portion. In contrast, if the length ratio is 1000; then, the equivalent Tan δ tends asymptotically to *Tan* δ_1 for all cases, *i.e.* as the length of the healthy portion of the cable segment increases compared to the aged portion, the effect of the aged portion on the equivalent Tan δ decreases and eventually the equivalent Tan δ simply becomes *Tan* δ_1. Particularly, consider points A and B in Figure 5.4, where the length ratio is equal to 10, *i.e.* 10 % of the cable segment is aged relative to the healthy portion of the cable segment. The equivalent Tan δ for points A and B are approximately 9×10^{-3} and 0.5×10^{-3} respectively. This represents a difference of about one order of magnitude between the Tan δ of the aged portion of the cable segment

($Tan\ \delta_2$) and the equivalent Tan δ for both points.

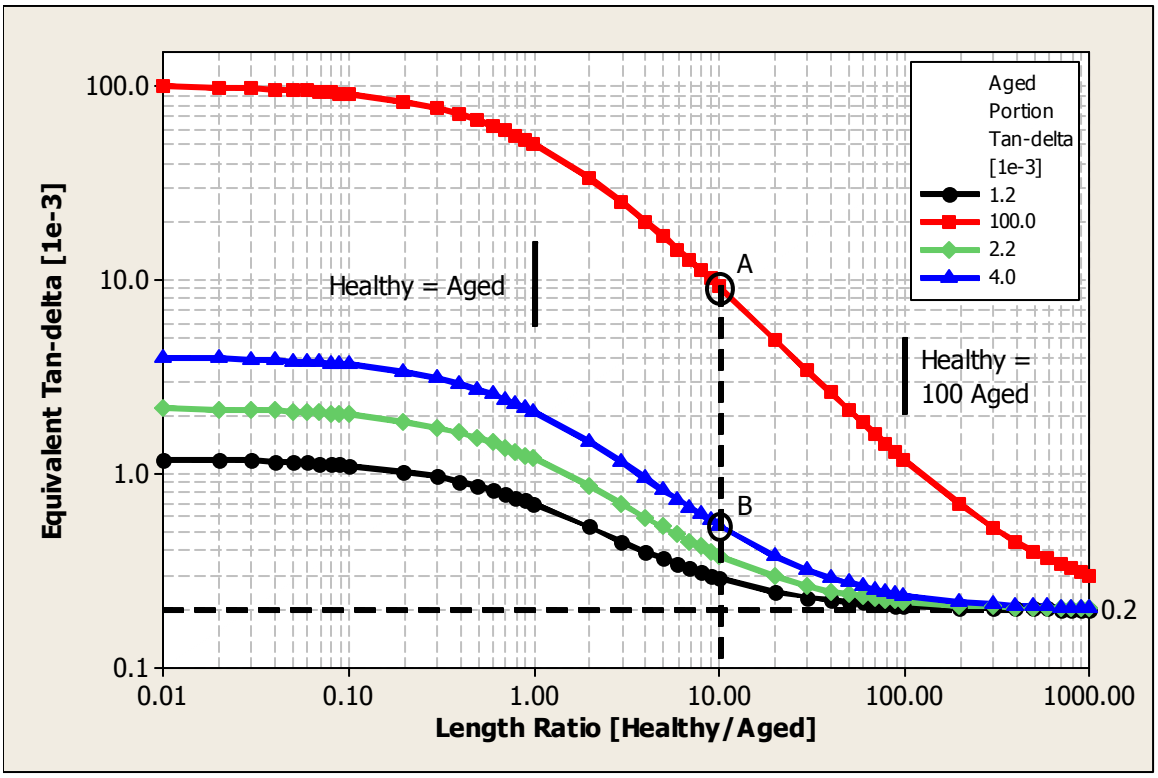

Figure 5.4. Simulation for non-uniform degradation modeling.

The model presented in equation (5.6) is validated though laboratory measurements as shown in Figure 5.5. In this case the approach consists of using two cable samples with known Tan δ characteristics and connecting them in cascade to emulate the non-uniform degradation situation. One of the samples, the sample with the highest Tan δ magnitude, represents the aged portion of the cable segment while the sample with the lowest Tan δ magnitude, represents the healthy portion of the cable segment. In Particular, the aged portion is represented by an un-aged EPR-15 kV cable sample with a Tan δ of 3.7×10^{-3} and the healthy portion of the cable segment is represented by an un-aged XLPE-15 kV sample with a Tan δ of 0.2×10^{-3}. The length of

the aged portion (L_2) is kept constant at 80 ft and the length of the healthy portion (L_1) is changed from 0 to 2400 ft as seen in Figure 5.5.

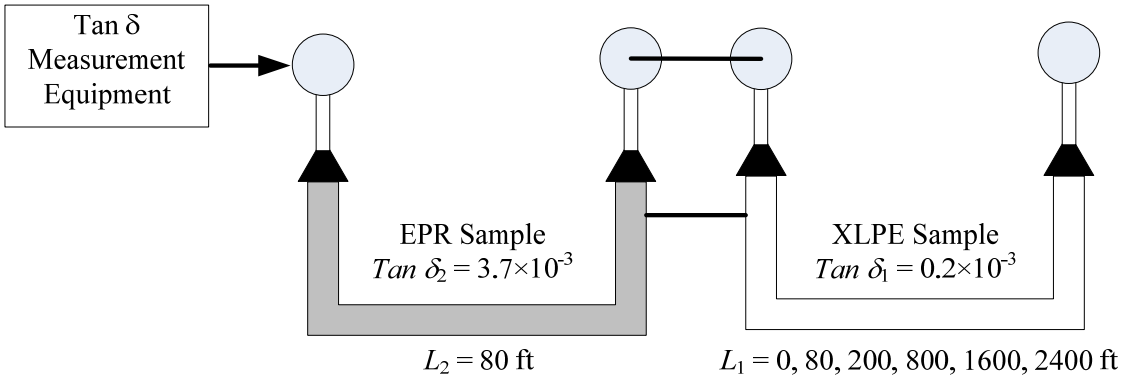

Figure 5.5. Laboratory experiment for non-uniform degradation.

The results of the laboratory measurements taken in Figure 5.5 are compared in Table 5.2 with the computed equivalent Tan δ using equation (5.6) and Figure 5.6 illustrates this graphically.

Table 5.2. Results of the laboratory experiment for non-uniform degradation.

Healthy Portion length (L_1) [ft]	**Aged Portion length (L_2) [ft]**	**Length Ratio (Γ)**	**Computed Equivalent Tan δ [1e-3]**	**Measured Equivalent Tan δ [1e-3]**
0	80	0.0	3.7	3.7
80		1.0	2.0	1.6
200		2.5	1.2	1.2
800		10.0	0.5	0.4
1600		20.0	0.4	0.2
2400		30.0	0.3	0.2
Tan δ healthy portion ($Tan\ \delta_1$) = 0.2×10^{-3} and Tan δ aged portion ($Tan\ \delta_2$) [1e-3] = 3.7×10^{-3}				

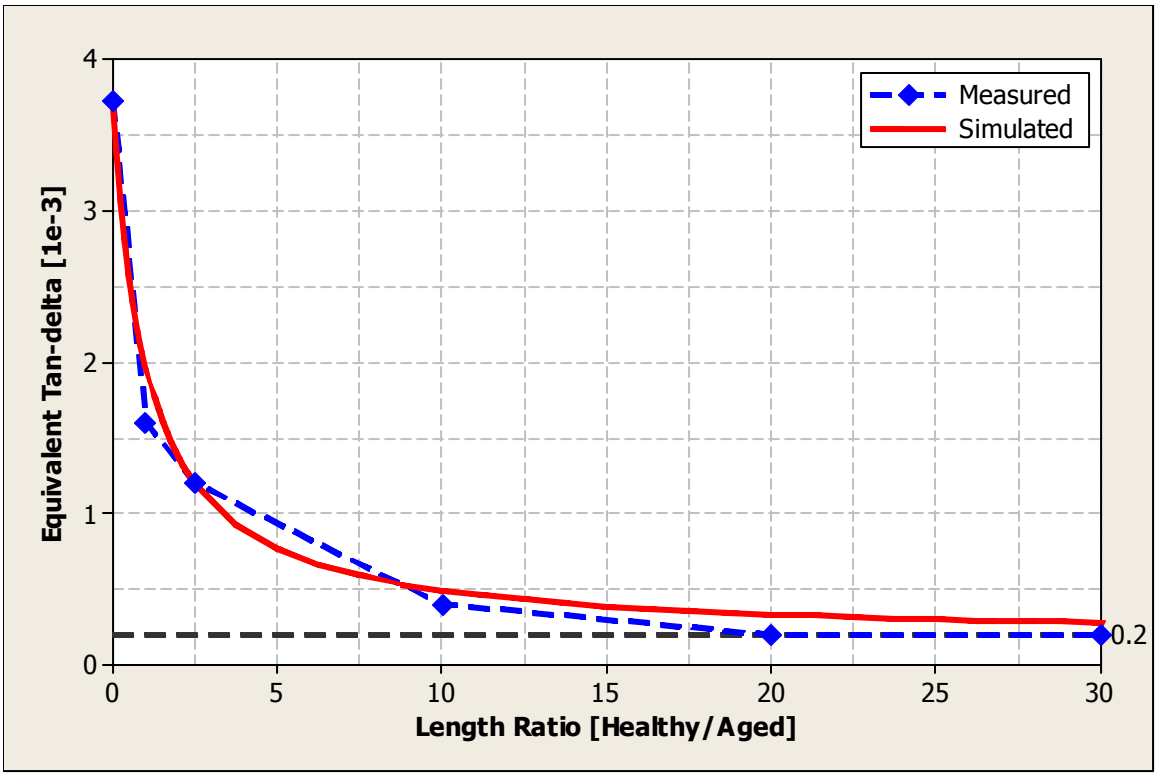

Figure 5.6. Comparison between computed and measured equivalent Tan δ values for the non-uniform degradation laboratory experiment.

Figure 5.6 shows that there is a good match between the computed and measured equivalent Tan δ values. In other words, the modified equivalent circuit model is able to predict how the equivalent Tan δ would change as the healthy portion of the cable segment increases in length.

In addition, the model presented in equation (5.6) is also used to estimate the Tan δ of an aged portion of a cable segment that fails in the field during VLF Tan δ testing. The cable segment under test is XLPE-25 kV, 13.8 kV operating voltage (U_0), jacketed, and installed in the early 1980's. The testing is performed on the Duke Energy system; specifically, the Hampton Leas Subdivision in Charlotte, North Carolina. The testing site is shown in Figure 5.7.

Figure 5.7. Field testing site at the Hampton Leas subdivision in Charlotte – North Carolina.

The cable segment under consideration fails during VLF Tan δ testing at a voltage level of 1.7 U_0. Therefore, the Tan δ values during initial testing are the values before failure. Subsequently, the failure site is located and is determined that the failure occurred in the cable. No joints are present in the cable segment. A 4 ft portion of cable is removed and the cable segment is repaired using a new joint. After repair, the cable segment is retested at the same voltage levels before failure and Tan δ values after failure are registered. The segment configuration is shown in Figure 5.8. The aged portion is 4 ft long and the healthy portion is 411 ft long. Therefore, the length ratio (Γ) between the lengths of the healthy and aged portions is approximately 103.

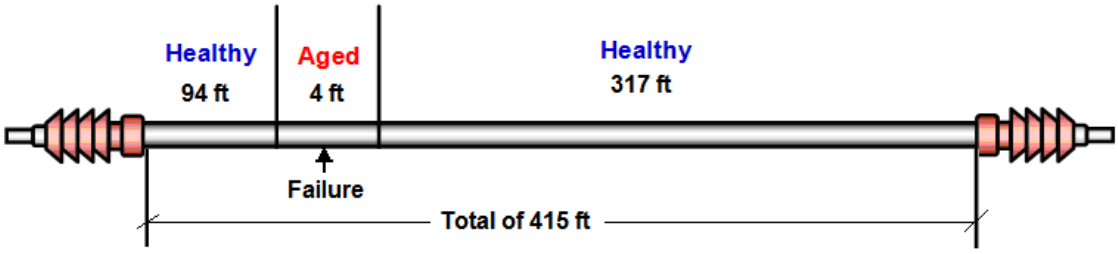

Figure 5.8. Segment configuration for field testing cable failure.

Using the Tan δ magnitudes before and after failure, the model presented in equation (5.6) can therefore be used to estimate the Tan δ magnitude of the aged portion of cable that failed. The estimated values are the values just before failure happens. The importance of estimating the Tan δ magnitude for the aged portion of cable that failed is that the estimation provides reference values for Tan δ of a short piece of cable just before failure, and this can be used as a benchmark.

The Tan δ of the healthy portion of the cable segment is assumed to be equal to the equivalent Tan δ after the repair since a new joint, because of its low losses, has no effect on the measurements. Therefore, from equation (5.6), the Tan δ of the aged portion just before failure can be estimated from equation (5.7) as,

$$Tan\ \delta_2 = (1+\Gamma)Tan\ \delta - \Gamma Tan\ \delta_1\ , \tag{5.7}$$

where,

$Tan\ \delta_2$: Tan δ of the aged portion before failure,

Γ: Length ratio, approximately equal to 103 (see Figure 5.8),

$Tan\ \delta$: Equivalent Tan δ before failure,

$Tan\ \delta_1$: Equivalent Tan δ after repair.

The comparison between the estimated Tan δ magnitude of the aged portion of

the cable segment, the equivalent Tan δ magnitude measured before failure, and the equivalent Tan δ magnitude measured after repair, is shown in Figure 5.9. Note the considerable difference of more than one order of magnitude between the Tan δ magnitude of the aged portion and the equivalent Tan δ magnitudes before failure and after repair. The usefulness of the estimated values for the Tan δ magnitude of the aged portion of the cable segment is that those values correspond to Tan δ values of a short cable just before failure. Therefore, the values could be used as a reference when developing diagnostic criteria thresholds. Particularly, the cable failure occurred between Tan δ magnitudes of 100×10^{-3} and 200×10^{-3} at a voltage level of 1.7 U_0. If diagnostic criteria is to be designed for the type of cable under consideration, a value between the Tan δ magnitudes of 100×10^{-3} and 200×10^{-3} maybe a good choice to consider the cable as severely aged.

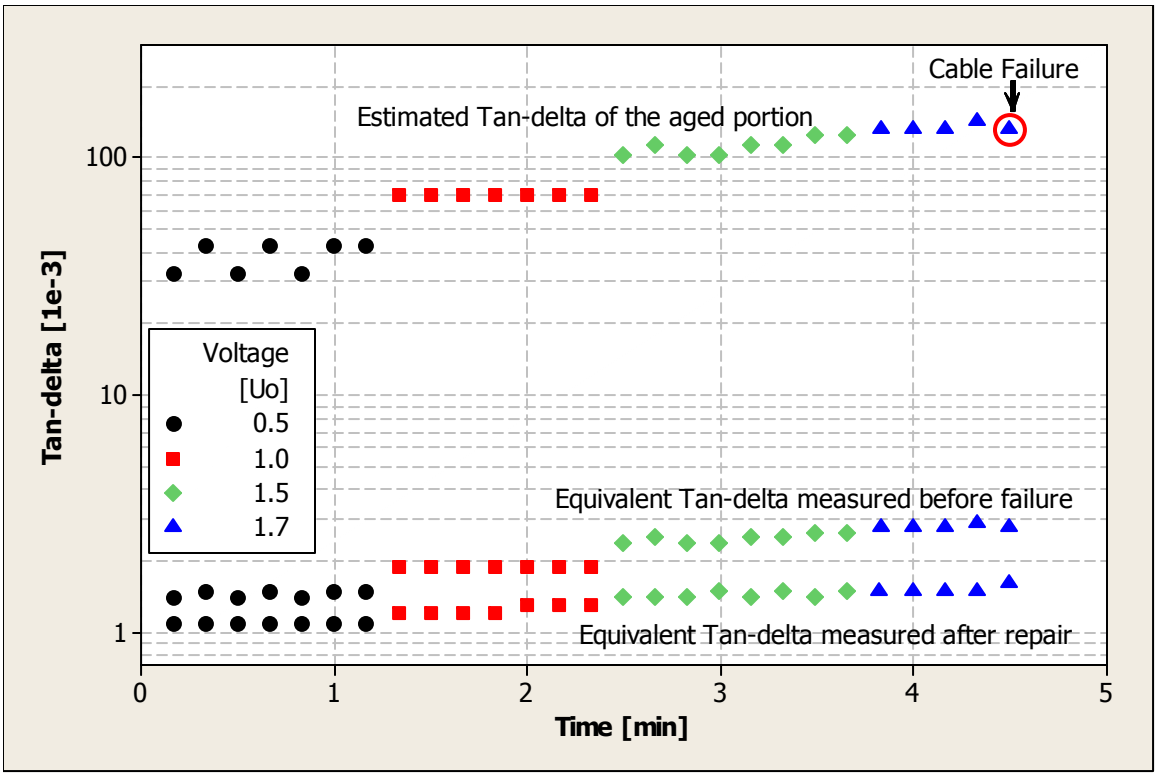

Figure 5.9. Comparison between Tan δ of the aged portion of the cable segment and equivalent Tan δ before failure and after repair.

5.3.1.3 Non-uniform Degradation Diagnostic Indicators

The non-uniform degradation modeling has permitted the identification of two new levels for the diagnostic indicators that may be used to enhance the diagnostic process of the insulation of power cable systems using VLF Tan δ measurements. The first diagnostic indicator level considers Tan δ values available during testing for each cable segment. The second diagnostic indicator level considers the collection and comparison of Tan δ magnitudes as a function of length after a number of tests have been performed. Each diagnostic indicator level is explained in detailed in the next paragraphs.

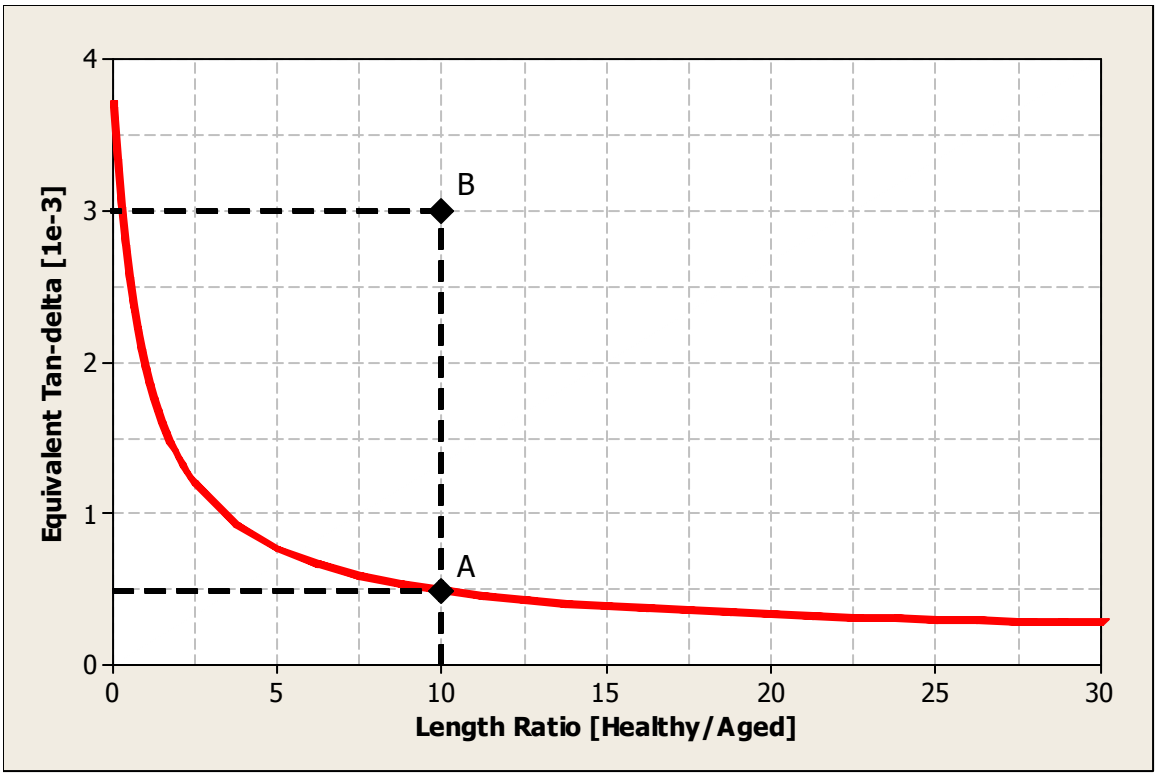

Figure 5.10. First level of non-uniform diagnostic feature.

To explain the first level, Figure 5.10 is used, which is the same as Figure 5.6 but considering only the simulated equivalent Tan δ and additional points A and B. Point A represents a length ratio between the healthy and aged portions of the cable segment of 10 and an equivalent Tan δ of 0.5×10^{-3} as "seen" by the measurement equipment, while point B represents the same length ratio as point A but the equivalent Tan δ of 3×10^{-3} as "seen" by the measurement equipment. Considering a value of 0.2×10^{-3} as the Tan δ magnitude of the healthy portion of the cable segment and the information provided by points A and B in Figure 5.10, the Tan δ magnitude of the aged portion of the cable segment can be estimated by using equation (5.7). In this case, the estimation yields to the values of 3.7×10^{-3} and 31×10^{-3} for points A and B respectively. The comparison between the Tan δ magnitudes of the aged portions corresponding to points A and B shows that the higher the equivalent Tan δ magnitude (as "seen" by the measurement

equipment), the higher would be the Tan δ magnitude of the aged portion of the cable segment if a non-uniform degradation situation were present.

In real field situations, it is not possible to know the length ratio or Tan δ magnitudes of the healthy and aged portions of the cable segment separately. Thus, the only available information would be the equivalent Tan δ magnitude as "seen" by the measuring equipment and maybe some information from cable segment and subdivision (in which the cable segment is located) failure history regarding localized cable or accessory problems or localized or distributed neutral issues. The question then is how the equivalent Tan δ magnitude can be interpreted just by itself if a non-uniform degradation situation is present.

If a non-uniform degradation situation is present in cable segment, a high value of equivalent Tan δ truly carries information about the cable segment condition. A high value means that the cable segment is generally aged or in a bad condition and some action on the segment needs to be taken. However, a low equivalent Tan δ does not necessarily mean that the cable segment is in a good condition. Other tests may be required to account for this situation, *e.g.* a follow-up VLF withstand test after performing a Tan δ test in order to fail the aged portion. If the segment survives the withstand test, then it can be concluded with some degree of confidence that the cable segment is in good condition.

The second diagnostic indicator level consists of a comparison of Tan δ magnitudes as a function of cable segment length. The comparison is made between cable segments of the same design and located in the same subdivision. The assumption here is that those cable segments have seen relatively similar operating and aging conditions which allows for the comparison.

If a non-uniform degradation situation is present in a subdivision; then, it is expected to see a general trend of equivalent Tan δ magnitudes decreasing with cable

segment length. In other words, the effect of the aged portions on the equivalent Tan δ decreases as more healthy cable length is present in the cable segment. This situation is shown in Appendix A; specifically, if the equivalent Tan δ is much larger than the Tan δ of the healthy portion, then the equivalent Tan δ, when plotted on a log-log scale, follows a linear model in length.

In real field situations, what is important is the fact that for non-uniform degradation, the equivalent Tan δ magnitude generally decreases in length. Knowing that the degradation is localized has a great value as a diagnostic indicator in the sense that repairing a bad segment with localized problems is less expensive than an overall cable segment replacement. Therefore, it is worth repairing the segment. This is particularly the case for direct buried systems in which the major cost is due to landscaping.

Figure 5.11 shows a real example, using data obtained in field testing, of the non-uniform degradation second level diagnostic indicator. Particularly, Figure 5.11 shows the equivalent Tan δ magnitude at U_0 (13.8 kV) as a function of length for a subdivision with non-uniform degradation problems. The subdivision is an underground residential distribution (URD) network, XLPE-25 kV, jacketed, and direct buried cable system without neutral corrosion problems. As seen in Figure 5.11, the equivalent Tan δ magnitude has a general trend going downwards as the cable segment length increases. The trend is represented by the blue line that is the linear regression of the data.

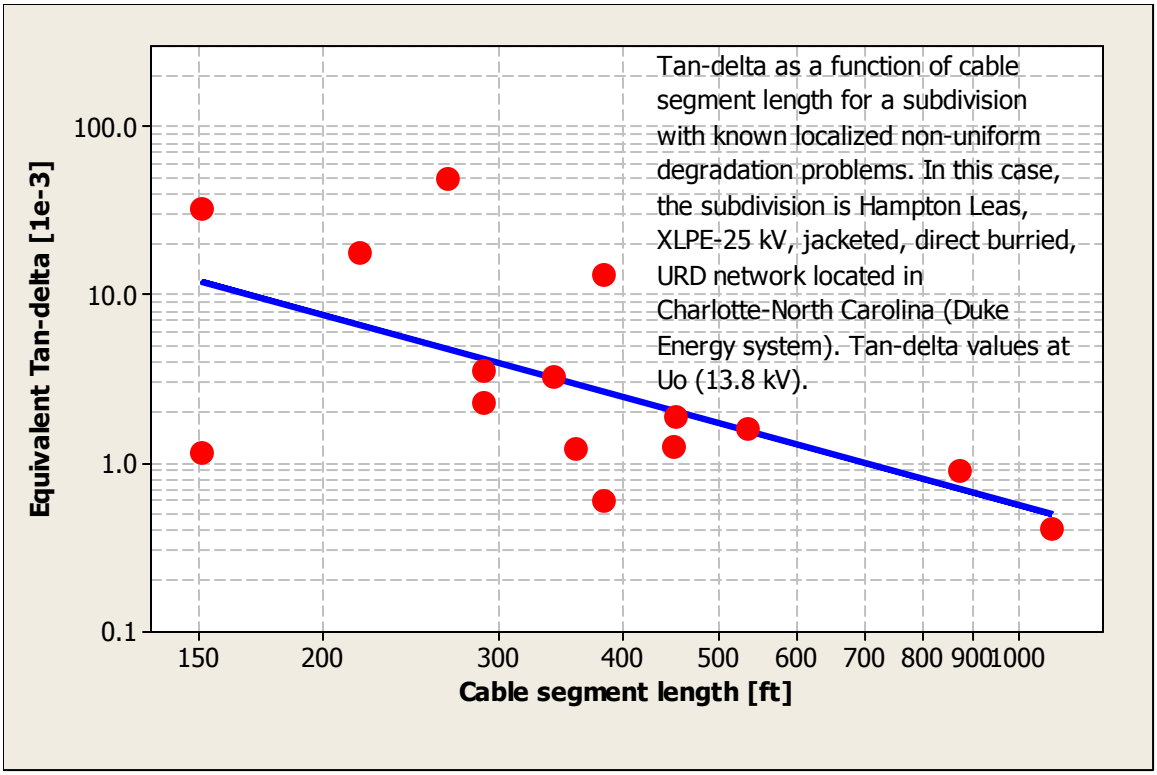

Figure 5.11. Second level of non-uniform diagnostic indicator.

In summary, the non-uniform degradation length model has been useful for discovering and understanding two levels of diagnostic indicators for VLF Tan δ measurements. The diagnostic indicators are as follows:

- A high equivalent Tan δ value truly carries information about the cable segment condition. A high value means that the cable segment is generally aged. However, a low equivalent Tan δ does not necessarily mean that the cable segment is in good condition. Other tests may be required to account for this situation.
- If the equivalent Tan δ generally decreases with cable segment length in a subdivision; then, the subdivision most likely has localized non-uniform degradation problems.

5.3.2 Neutral Issues

The development of power cable diagnostic techniques that are able to assess the condition of in-service power cable systems have been mainly focused on detecting changes in electrical properties of the cable system insulation, *i.e.* insulation defects or water treeing. This is due to the fact of the general belief, by the cable community, that the failure modes are mainly due to aging and degradation of the cable system insulation alone. However, research work reported here and by others [61-63] show that there are other failure modes related to neutral wires issues; particularly, neutral wires corrosion or simply neutral corrosion and mineralization of neutral wires. These issues are termed as neutral issues in this thesis. Neutral issues lead to breaks in the neutral wires and poor contact between the neutral wires and insulation shield. Neutral issues are important since they can cause arcing damage to the insulation shield leading to an eventual failure. Figure 5.12 shows the two neutral issues previously mentioned; particularly, the broken neutral wire in Figure 5.12(a) caused by corrosion, then it caused arcing damage to the insulation shield. Figure 5.12(b) shows a cable with neutral wires embedded into ridges in the insulation shield as result of mineralization of the neutral wires. The mineralization of the neutral wires causes a poor contact between the neutral wires and the insulation shield. In addition, neutral issues also influence diagnostic measurements such as Tan δ and partial discharge.

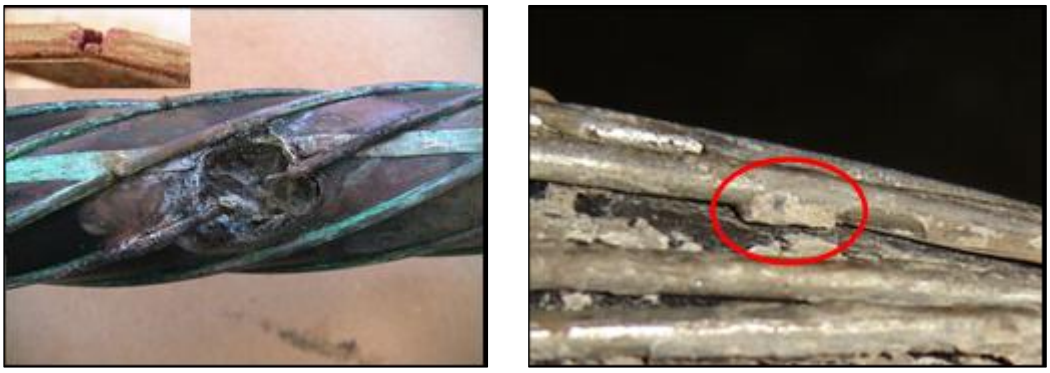

(a) Broken neutral wire.

(b) Poor contact between neutral wires and insulation shield.

Figure 5.12. Illustration of neutral issues.

A classification of the degree of corrosion of neutral wires has been performed by Hanck and Nekoksa [63], and it is based on field tests conducted at 36 excavations in California, Oklahoma, and North Carolina. No corrosion was found in 8 (22.2 %) excavations, minor to severe corrosion was found in 20 (55.6 %) excavations, and very severe corrosion was found in 8 (22.2 %) excavations. The classification is shown in Table 5.3.

Table 5.3. Neutral wires corrosion classification [63].

Index	Type of Corrosion	Description	Pitting
0	None	No green color	None
1	Minor	Spots of light green	Slight
2	Moderate	Spots of green color	Shallow
3	Severe	Heavy buildup of corrosion products (thinning of wires evident)	Deep
4	Very Severe	One or more missing wires	-

Figure 5.13. Minor to moderate neutral wires corrosion.

An example of minor to moderate corrosion found during the field testing is shown in Figure 5.13. Note the spots of green color and the slight pitting of the neutral wires.

Good contact between the neutral wires and the insulation shield is needed to contain the cable core at ground potential, *i.e.* to contain the electric field inside the cable insulation. This function can be affected by mechanical damage, high volume resistivity of the insulation shield, corrosion of the neutral wires, and poor contact between the insulation shield and neutral wires. As mention before, a loss of the function of the neutral wires and insulation shield together would result in arcing damage and eventual failure. To illustrate this situation, a finite element computation of the electric field is

performed in a planar two-dimensions cable geometry with the insulation shield modeled as floating with a dielectric constant of 100 and volume resistivity of 500 Ω-m (typical values for highly degraded insulation shield). The cable geometry is for a XLPE-15 kV unjacketed cable with 8 neutral wires and insulation thickness of 175 mils (approximately 4.4 mm). The conductor size is in this case 1/0. In the simulation, the neutral wires are separated slightly (40 mils or 1mm) from the insulation shield. This cable geometry is typical of 15 kV class cable. The applied voltage to perform the simulation is 8.7 kV which corresponds to the phase-to-ground rated voltage. The simulation results for the electric field are shown in Figure 5.14.

In Figure 5.14 under ideal conditions, *i.e.* when there is a good connection between the insulation shield and neutral wires and the insulation shield has a low volume resistivity, all the electric field would be contained inside the cable insulation. The maximum electric field in this ideal case is located in the conductor and would be equal to 2.6×10^6 V/m. However, in the situation presented in Figure 5.14, when the insulation shield is floating, the maximum electric field is located at the neutral wires and is equal to 3.6×10^6 V/m which is 1.4 times the maximum electric field under ideal conditions. This value is sufficient to produce arcing and cause erosion and degradation of the insulation shield and insulation leading to an eventual failure.

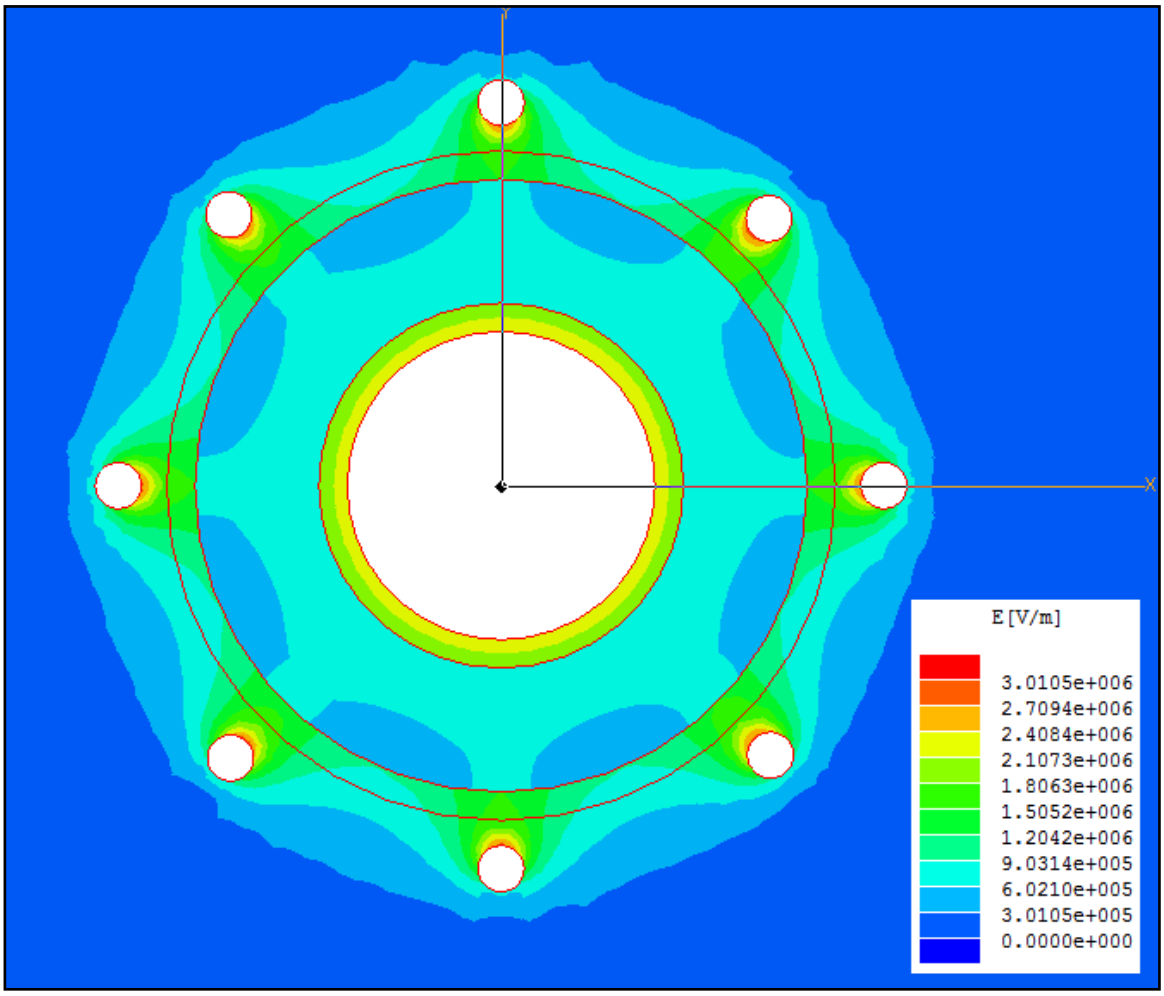

Figure 5.14. Finite element simulation for a typical XLPE-15 kV cable with floating insulation shield.

There is no question that knowing that the neutral issues are present in a cable segment adds a great value since the cable segment then has to be eventually replaced. Thus, this part of the research focuses on understanding how the neutral issues can influence VLF Tan δ measurements by again considering modifications of the basic equivalent circuit presented in Chapter 3. The modified model is validated below by simulations, laboratory experiments, and data from field tests. This identifies useful diagnostic indicators that enhance the diagnostic process.

5.3.2.1 Neutral Issues Modeling

When there is significant corrosion of the neutral wires or a poor contact between the insulation shield and neutral wires, the equivalent Tan δ value has a contribution from the equivalent model series resistance. The series resistance as shown in Figure 5.15 consists of the equivalent of the conductor shield resistance (R_{CS}), insulation shield resistance (R_{IS}), and the contact resistance between the insulation shield and the neutral wires and resistance of the neutral wires themselves (R_N). In addition, R_I and C_I represent the resistance and capacitance of the insulation respectively.

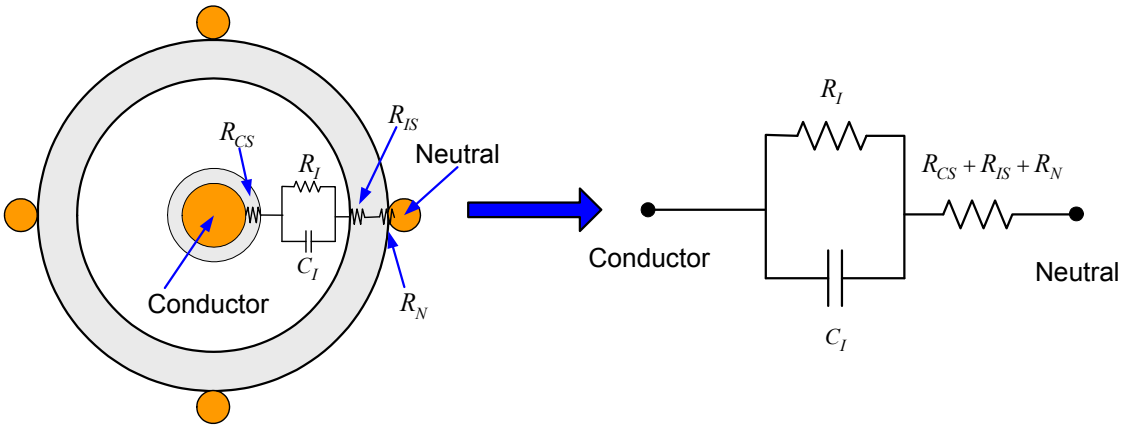

Figure 5.15. Equivalent circuit for neutral issues.

Under normal conditions, *i.e.* without neutral issues, the series equivalent resistance is very small as compared to the insulation parameters and can be neglected. In contrast, when neutral issues are present, a considerable increment in the value of R_N is expected because of mineralization and corrosion of the neutral wires, as illustrated in Figure 5.16. The increment in the value of R_N can be significant compared to the insulation parameters and therefore the equivalent Tan δ value is affected.

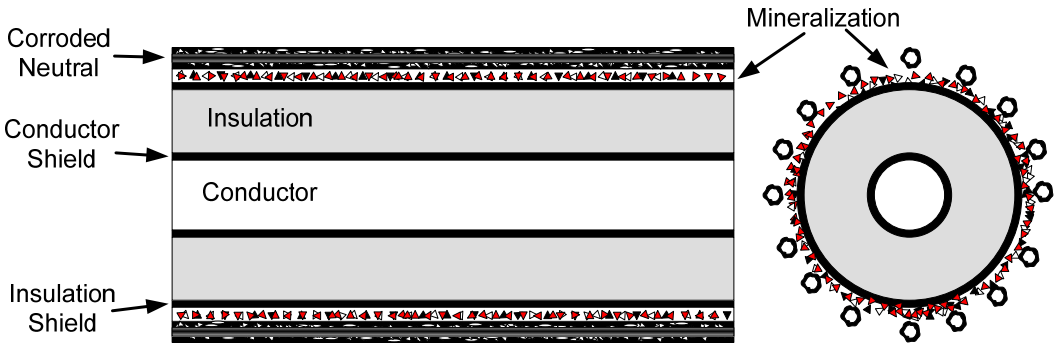

Figure 5.16. Longitudinal and transversal section of an unjacketed power cable with mineralization and corrosion of neutral wires.

To model the neutral issues, a quadrupole (or two-port network) model per-unit length is used. The equations for the model, considering one and several quadrupoles, are developed in Appendix B. The basic quadrupole model is shown in Figure 5.17.

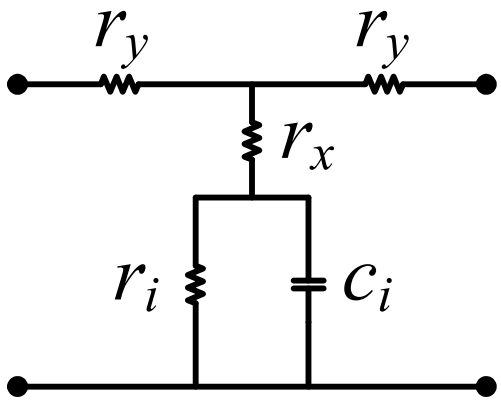

Figure 5.17. Quadrupole model per-unit length for neutral issues.

In Figure 5.17, r_i and c_i represent the per-unit length insulation parameters, which are the same as the ones presented in Chapter 3 when there are not any neutral issues. In addition, r_x represents the contact resistance per-unit length between the insulation shield and neutral wires and r_y represents the resistance of the neutral wires themselves. In some

cases, a capacitance between the insulation shield and neutral wires could be considered [61, 62]. However, it has been found in this research that this parameter has no major influence and thus it is not considered any further.

The parameters shown in Figure 5.17 are in per-unit length; thus, as the length of the cable segment increases, the effect of the parameters r_x and r_y also increases. Recall from Chapter 3 that the length and geometry effect for the insulation parameters cancel each other. Therefore, it is expected that there would be an increment in the equivalent Tan δ magnitude that is a function of cable segment length when the neutral issues are present. In other words, the total power loss will be the result of the contribution of the bulk insulation losses (parameter r_i) and the length dependent series resistance losses (parameters r_x and r_y). This leads to a situation similar to the one for non-uniform degradation but with different diagnostic indicators.

The neutral issues can be localized or distributed. Localized neutral issues mean that only portions of the cable segment present the problem. Distributed neutral issues mean that the neutral issues are present all over the cable segment length. Figure 5.18 shows the case for a cable segment with localized neutral issues while Figure 5.19 shows the case of a cable segment with distributed neutral issues.

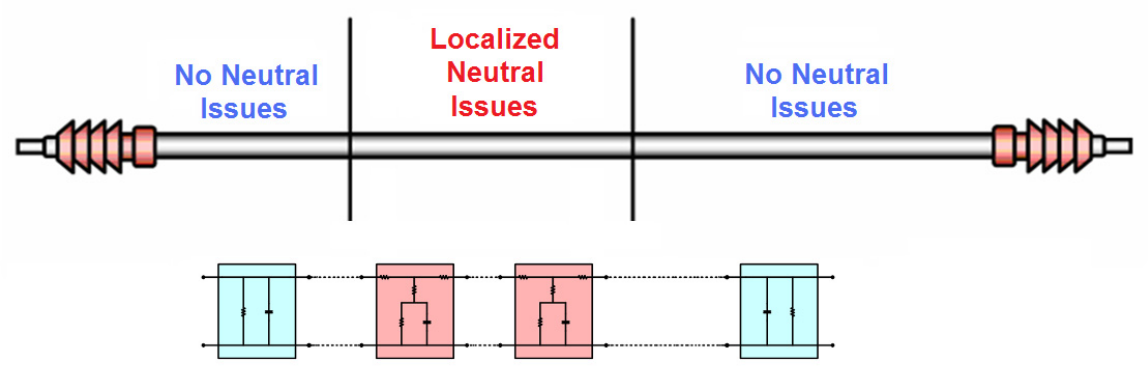

Figure 5.18. Localized neutral issues.

As seen in Figure 5.18, to model a localized neutral issue situation, two types of quadrupoles are used. The blue quadrupoles represent the portions of the cable segment without neutral issues; therefore, the parameters r_x and r_y are not considered. This leads to a situation in which the portions without neutral issues can be modeled by one single quadrupole considering only the lumped insulation parameters (r_i and c_i) of their respective portion. The portion of the cable segment with neutral issues is modeled by the red quadrupoles in which the parameters r_x and r_y are considered. To find the equivalent Tan δ in the quadrupole configuration shown in Figure 5.18, the inverse of the overall transfer function matrix is computed and the equivalent Tan δ is computed as shown in equations (B.12) and (B.13) of Appendix B.

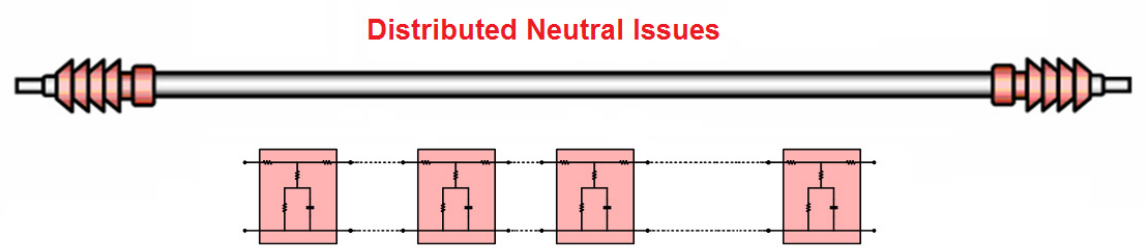

Figure 5.19. Distributed neutral issues.

A distributed neutral issue is less complex to model compared to a localized neutral issue situation. In this case only one type of quadrupole is used as shown in Figure 5.19. The equivalent Tan δ is computed using the same procedure previously described for the localized neutral issue situation.

5.3.2.2 Simulation and Laboratory Experimentation

Figure 5.20 shows the simulation results of equivalent Tan δ magnitude as a function of length for distributed neutral issues. The cable geometry used in the simulation is the same geometry of a typical XLPE-15 kV cable for the finite element

simulation of Figure 5.14. The Tan δ magnitude of the cable insulation is 0.2×10^{-3}. Using the cable geometry and the insulation Tan δ magnitude, the insulation parameters (r_i and c_i) per-unit length can be computed. Three cases for the parameter r_x are considered; specifically, 0.1, 1.0, and 2.0 parts per million (p.p.m) of the insulation resistance. The parameter r_y is 2000 Ω/ft and represents a very severe corrosion of the neutral wires.

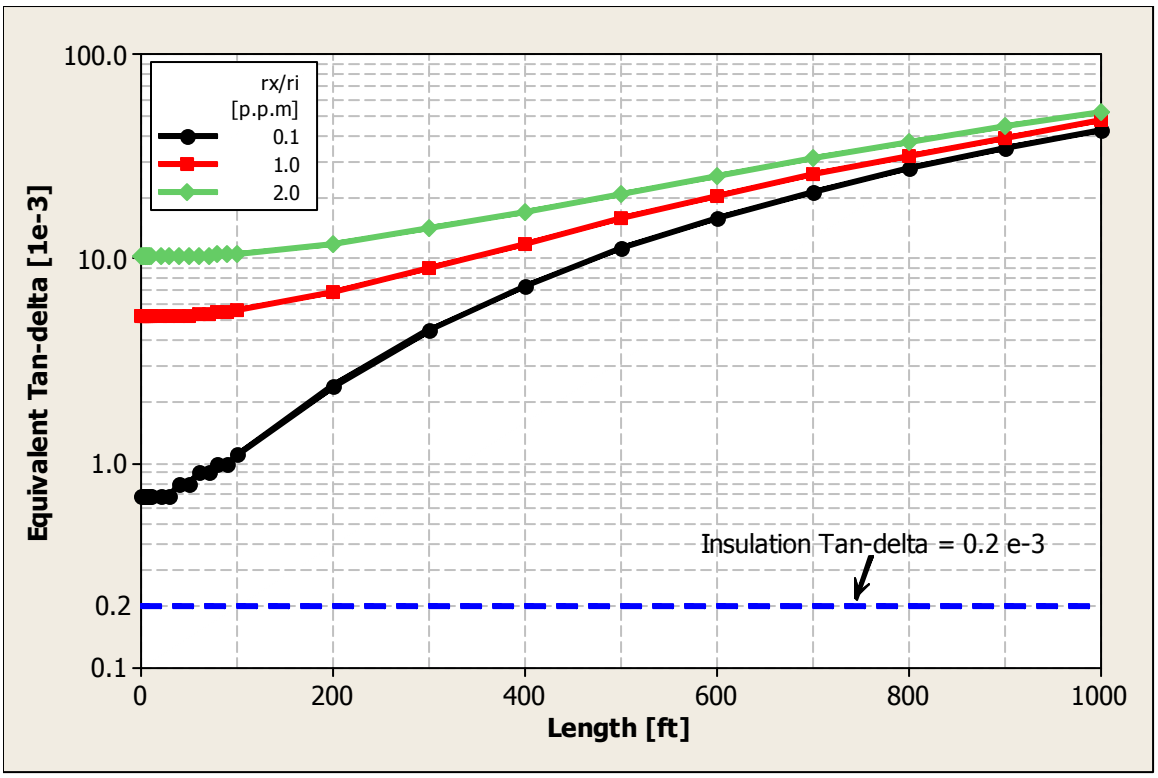

Figure 5.20. Simulation of distributed neutral issues.

Figure 5.20 compares the insulation Tan δ magnitude of 0.2×10^{-3} (blue-dashed line) with the simulation results for the equivalent Tan δ magnitudes for the 0.1 p.p.m (black line), 1.0 p.p.m (red line), and 2.0 p.p.m (green line) cases, and shows that when the neutral issues are present, the equivalent Tan δ is considerably higher than the Tan δ of the insulation. The effect is amplified as the contact resistance between the insulation

shield and neutral wires increases. In addition, it is also observed that for all the cases the equivalent Tan δ increases with length. Therefore, it can be concluded that when there is a significant corrosion of the neutral wires and a poor contact between the insulation shield and neutral wires distributed along the cable segment, the equivalent Tan δ value has a contribution from the equivalent model series resistances (r_x and r_y) and increases in length.

However, to gain a better appreciation of what happens if neutral issues are present in a cable segment, two laboratory experiments are conducted. These experiments consider two cases; specifically, case 1 considers the localized neutral issues and case 2 considers the distributed neutral issues. In both cases, an 80 ft EPR-15 kV jacketed cable is used. It is determined in the laboratory that the cable has a Tan δ magnitude of 3.4×10^{-3} that is independent of the test voltage level. The transversal section of the cable is shown in Figure 5.21.

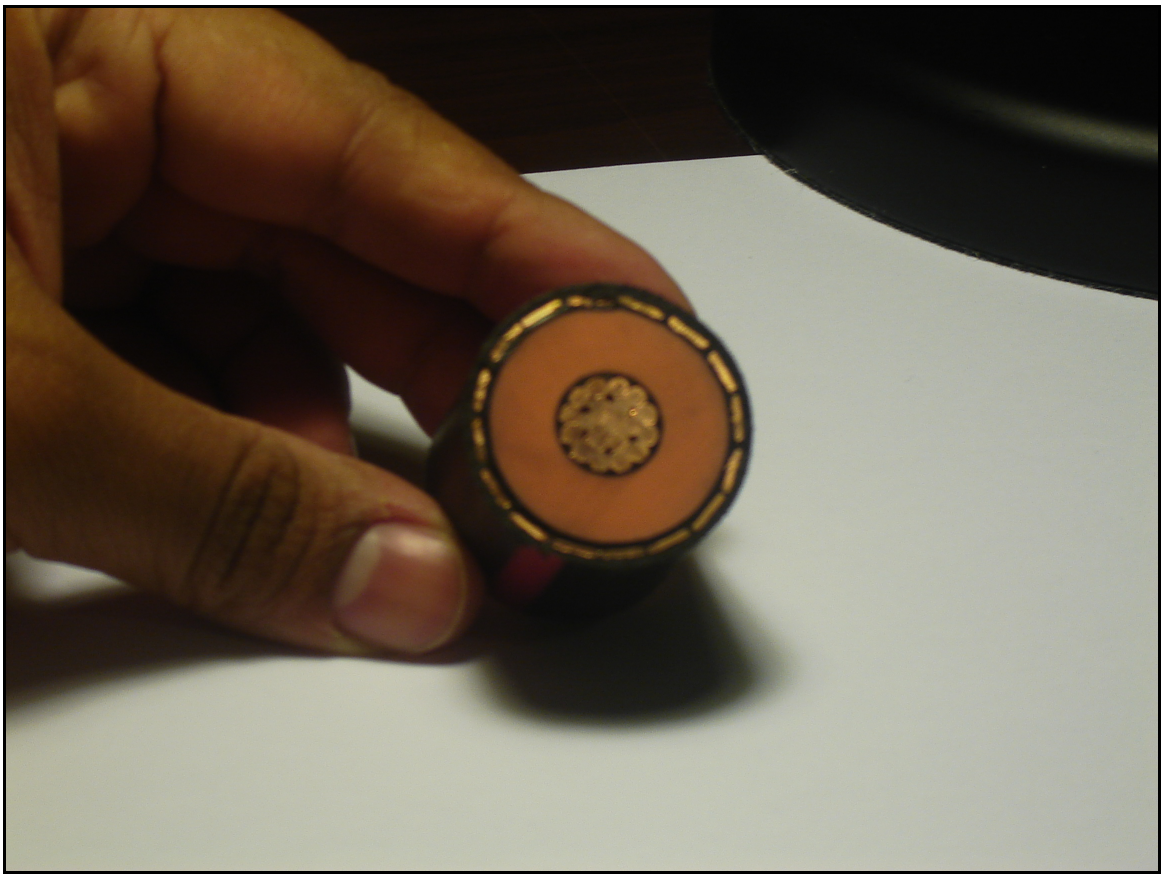

Figure 5.21. Transversal section of the 80 ft EPR-15 kV jacketed cable used for neutral issues laboratory experiments.

Case 1: Loss of Neutral Wires.

The localized neutral issues are reproduced in the laboratory by introducing an artificial break in the neutral wires of the 80 ft EPR-15 kV jacketed sample as shown in Figure 5.22. The artificial break is introduced at 40 ft from the testing end and it exposes a distance *d* of the cable insulation shield.

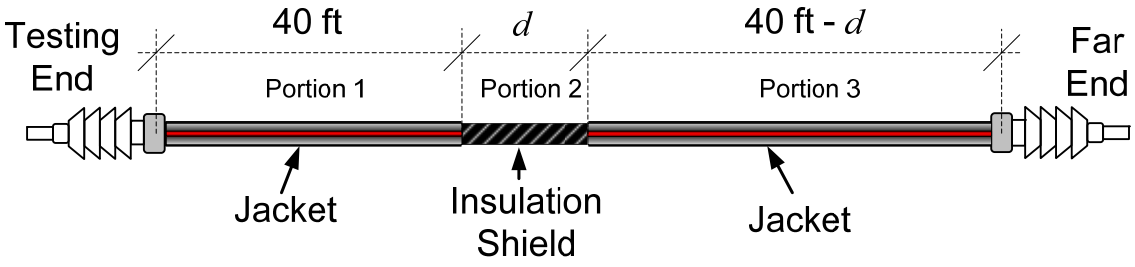

Figure 5.22. Illustration of cable sample used for loss of neutral wires laboratory experiment.

Figure 5.23 shows the case of the artificial break for a distance *d* of 1 ft. Particularly, Figure 5.23(a) shows the actual break of the neutral wires and Figure 5.23(b) shows the TDR results. The TDR results in are characterized by a strong reflection peak from the localized artificial neutral wires break and attenuated reflection from the far end of the cable sample.

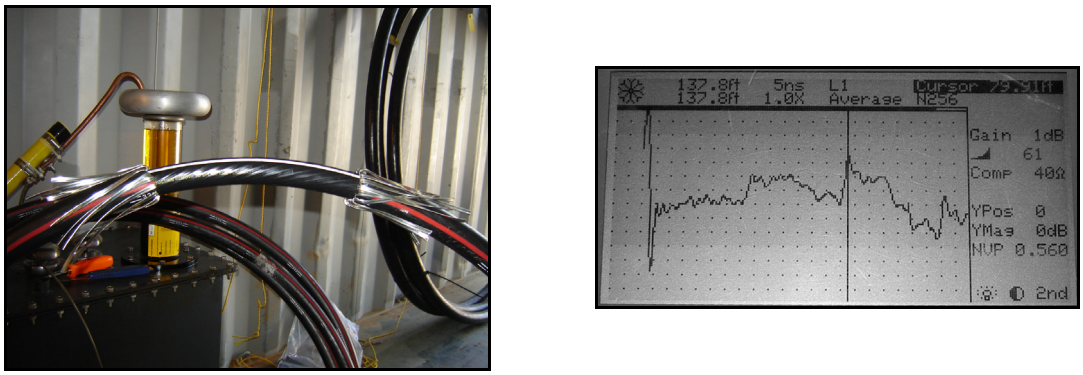

(a) Neutral wires artificial break of 1 ft. (b) TDR results.

Figure 5.23. Neutral wires artificial break and TDR results.

In Figure 5.22, a break in the neutral wires can also be seen as a loss of neutral wires for a distance *d*. When the neutral is lost, the cable segment is divided into three portions. Portions 1 and 3 have no neutral issues while portion 2 has lost the neutral. The

neutral wires of portions 1 and 3 are connected thought the cable insulation shield of portion 2; therefore, the cable segment can be modeled by considering the series resistance artificially added by the insulation shield of portion 2 between the neutral wires of portions 1 and 3. In particular, quadrupole model of portion 2 only considers the parameter r_y. The parameters r_y is estimated from measuring the resistance of 1 ft of the cable sample insulation shield using a conventional multimeter, the measurement yields a value of 90 kΩ/ft, which corresponds to a volume resistivity of 19 Ω-m.

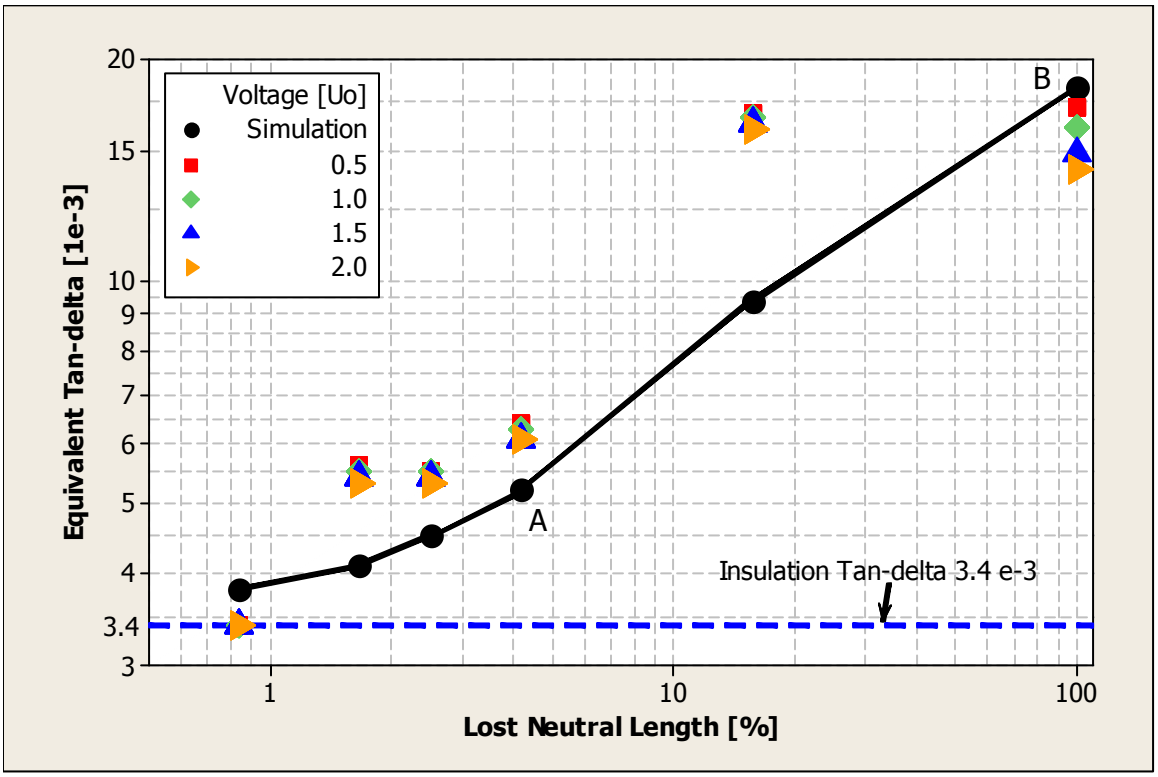

Figure 5.24. Loss of neutral wires laboratory experiment – comparison between simulated and measured values.

Figure 5.24 shows the comparison between the equivalent Tan δ magnitudes from the simulation results and the laboratory experiment. The *x*-axis represents the amount of lost neutral in percent and the *y*-axis the equivalent Tan δ magnitude. The lost neutral in

percent is the ratio between the distance *d* as shown in Figure 5.24 and the total length of the cable sample (80 ft) in percent; for instance, a lost neutral of approximately 5%, point A on Figure 5.24, means that a distance *d* of 5% of 80 ft (*i.e.* $d = 4$ ft) of neutral wires has been lost while a lost neutral of 100 %, point B on Figure 5.24, means that all the neutral wires (*i.e.* $d = 80$ ft) have been lost.

The simulation results in Figure 5.24 are independent of the test voltage level because as mentioned before, the initial insulation Tan δ of the cable sample is independent of the test voltage level and no changes in the volume resistivity of the insulation shield are taken into account. However, voltage dependence is observed on the measured Tan δ when the lost neutral is greater than 1 %. This voltage dependence is the most pronounced for 100 % of lost neutral. In addition, a tip-down in Tan δ is observed. Since the Tan δ of the insulation is independent of the test voltage level, the only plausible explanation for the tip-down is that the volume resistivity of the cable insulation shield is changing. Particularly, the volume resistivity is decreasing with the test voltage level. The decrease in the volume resistivity causes the equivalent Tan δ magnitude to decrease. This behavior is expected since as the insulation shield is a semiconducting material, its volume resistivity decreases with the circulating current that increases with the test voltage level. The differences between the simulated and measured values in Figure 5.24 may also be due to the changes in the volume resistivity of the cable insulation shield. However, the most important fact shown in Figure 5.24 is that the simulated and measured values have the same trend which validates the model for localized and distributed neutral issues.

Case 2: Poor Contact between Insulation Shield and Neutral Wires.

In this case, the neutral wires are basically insulated from the cable insulation shield. As mentioned before, this situation can be caused in the field by a layer of corrosion or mineralization of the neutral wires. The poor contact between the cable

insulation shield and neutral wires is reproduced in the laboratory by using the 80 ft EPR-15 kV cable sample left from the loss of neutral experiment in case 1. What is left from the lost of neutral experiment is the cable core only; therefore, to build the sample and reproduce the poor contact between the insulation shield and neutral wires, cotton pads and a neutral strap are used. The cotton pads are wrapped around the left over cable core and then the neutral strap is wound over the cotton pads as shown in Figure 5.25 and Figure 5.26. The neutral strap plays the same function as the neutral wires and is considered to play the role of the neutral wires in the experiment.

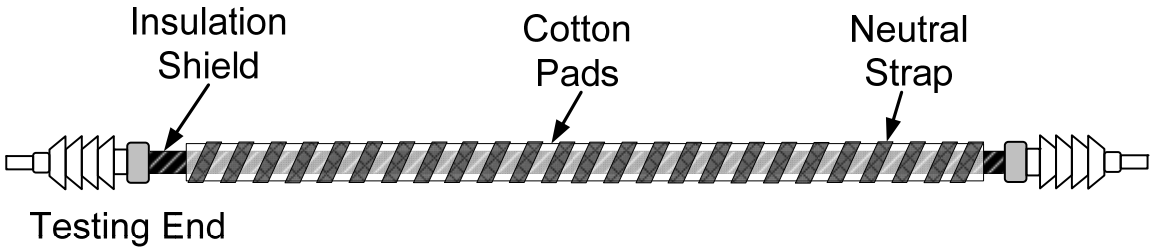

Figure 5.25. Illustration of cable sample used for poor contact between insulation shield and neutral wires laboratory experiment.

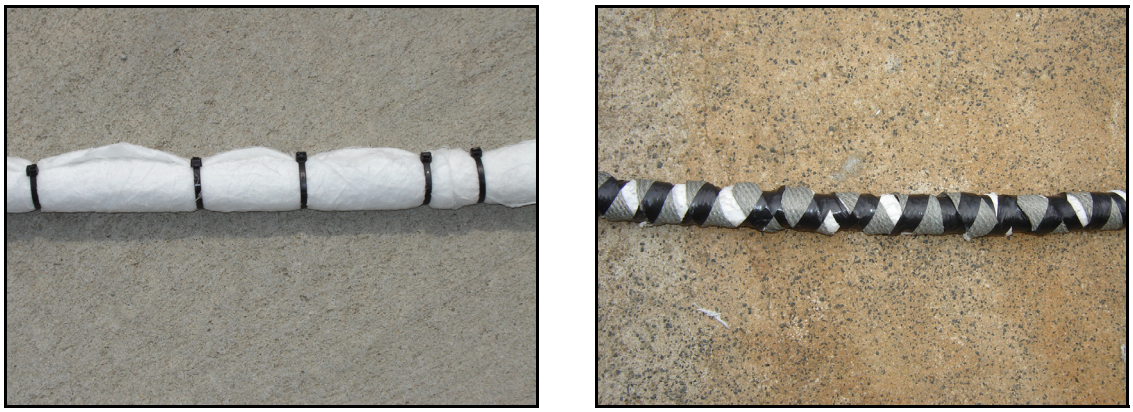

(a) Cotton pads wrapped around cable core. (b) Neutral strap winded above cotton pads.

Figure 5.26. Actual cable sample for poor contact between insulation shield and neutral wires laboratory experiment.

In Figure 5.25, when the cotton pads are dry, they introduce a poor contact between the cable insulation shield and the neutral strap; therefore, the cotton pads dry condition represents the situation in which there is a poor contact between the cable insulation shield and neutral wires. In contrast, if the cotton pads are wet, *e.g.* the cable sample is submerged in tap water, then there is a good contact between the cable insulation shield and neutral strap; therefore, the cotton pads wet condition represents the situation in which there is a good contact between the cable insulation shield and neutral wires. The cotton pads wet condition is shown in Figure 5.27.

Figure 5.27. Cotton pads wet condition.

Figure 5.28 contains the results for the poor contact between the cable insulation

shield and neutral wires laboratory experiment. Particularly and shows the equivalent Tan δ magnitude as a function of drying time in days for test voltage levels of 0.5, 1.0, 1.5, and 2.0 U_0. Three conditions are indicated in Figure 5.28. The initial dry condition shows the equivalent Tan δ as function of the test voltage level when the cotton pads are dry. The wet condition shows the equivalent Tan δ as a function of the test voltage level when the cotton pads are wet, *i.e.* the cable sample is submerged in water as shown in Figure 5.27. After the wet condition Tan δ test is performed, the cable sample is taken out of the water tank and left to dry out for a week; and Tan δ measurements are then performed after 1, 3, 4, and 7 days. After 7 days the cotton pads have completely dried thus going back to the dry condition, and this represents the final dry conditions shown in Figure 5.28.

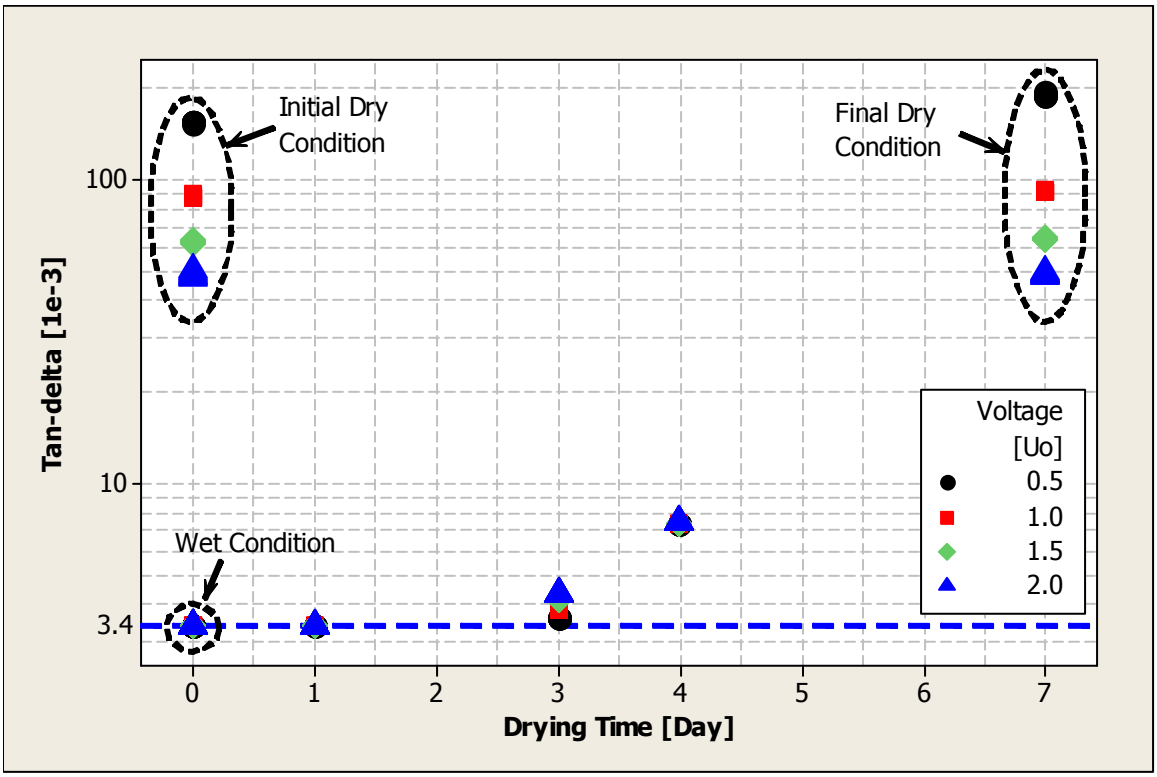

Figure 5.28. Results for poor contact between insulation shield and neutral wires laboratory experiment.

Figure 5.28 shows the similarity between the initial and final dry conditions and the difference between these two dry conditions and the wet condition. The similarity suggests that the poor contact between the cable insulation shield and neutral strap for these two conditions is similar; in other words for the final dry condition, the cotton pads have returned to similar dry conditions after being wet; moreover, for both these conditions there is a tip-down in the equivalent Tan δ magnitude as the test voltage increases. The tip-down may also be due to changes in the insulation shield volume resistivity in a similar way as it has been previously explained in the lost of neutral wires case.

Furthermore, comparing Tan δ magnitudes between days 1, 3, 4, and 7 in Figure 5.28 shows that as the cotton pads dry out, the equivalent Tan δ progressively increases, *i.e.* an indication that the contact resistance between the cable insulation shield and neutral strap also increases.

However, the most important result in Figure 5.28 is the difference of more than one order of magnitude between the equivalent Tan δ magnitudes of dry and wet conditions. The equivalent Tan δ magnitudes for the wet condition are independent of the test voltage level and correspond to the initial Tan δ magnitudes of the cable sample before any laboratory experimentation. Thus, it has been shown that a cable segment with distributed neutral issues regarding a poor contact between the cable insulation shield and neutral wires would show high Tan δ magnitude.

5.3.2.3 Distributed Neutral Issues Diagnostic Indicators

The distributed neutral issues modeling, simulation, and laboratory experimentation have identified a new level of diagnostic indicator that may be used to enhance the diagnosis process of cable systems insulation using VLF Tan δ measurements. The new diagnostic indicator considers the collection and comparison of

Tan δ magnitudes after a number of tests have been performed. The comparison is made between cable segments of the same design and located in the same subdivision. Therefore, the assumption here is that those cable segments have seen similar operating and aging conditions which allows for the comparison.

In particular, if a distributed neutral issue is presented in a subdivision; then, it is expected to see a general trend of the equivalent Tan δ magnitudes increasing with cable segment length. In other words, the effect of the poor contact between the cable insulation shield and neutral wires and resistance of the neutral wires increases as the cable segment length increases. This is an important finding for real field situations in the sense that knowing that the neutral issues are distributed is useful as a diagnostic indicator. Specifically, the cable segments in the subdivision have to be replaced.

Figure 5.29 shows a real example, using data obtained in field testing, of the distributed neutral issues diagnostic indicator. Specifically, Figure 5.29 shows the equivalent Tan δ magnitude at U_0 (7.2 kV) as a function of length for two subdivisions with distributed neutral issues. The two subdivisions have the same cable design and are located in the same geographical area. The subdivisions are URD networks, XLPE-15 kV, jacketed, direct buried cable system. As seen in Figure 5.29, the equivalent Tan δ magnitude has a general increasing trend as the cable segment length increases. The trend is represented by the blue solid line which is the linear regression of the data. The most important conclusion drawn from the results shown in Figure 5.29 is that if the equivalent Tan δ generally increases with the cable segment length in a subdivision; then, the subdivision most likely has distributed neutral issues.

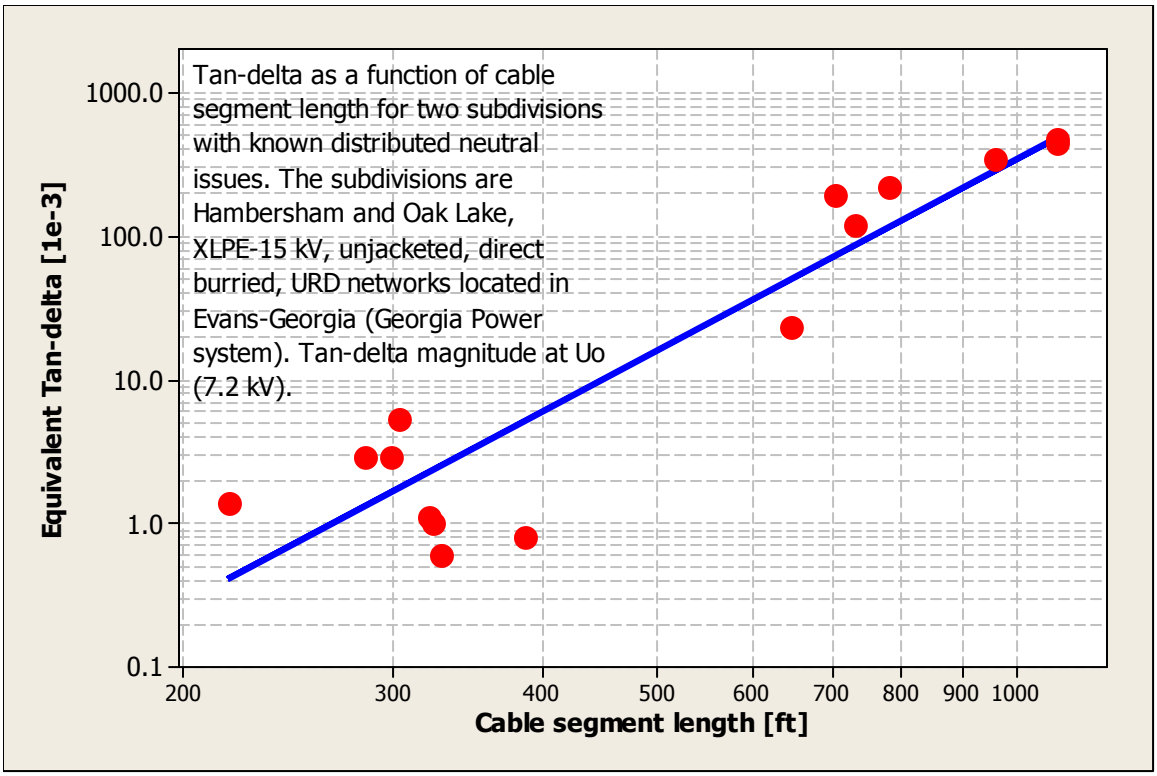

Figure 5.29. Distributed neutral issues diagnostic indicator.

5.4 Deployment of Tan δ Diagnostic Features with Combined Diagnostics in Field Testing Applications.

It has been shown in Chapter 4 and earlier sections of this Chapter that Tan δ measurements at VLF deliver a wide range of valuable diagnostic features and indicators that could be used for diagnosis. These demonstrations have led to the work that is reported within this section. Specifically, this section focuses on the deployment or use in practice of Tan δ diagnostic features in field testing applications in the MV cable systems arena; specially, PE-based cable systems of 15 and 25 kV which include HMWPE, XLPE, and TRXLPE insulation materials.

In the deployment of Tan δ features, the major issues are evaluated in a process with the use of feature management. The feature management used here has two essential

parts: feature categorization and decision organization. Feature categorization and decision organization are explained in detail in the next subsections.

5.4.1 Feature Categorization

The feature categorization approach shows that there are two main levels of categorization. The two levels are as follows:

Primary level categorization: it includes information immediately available at the site and time of the test; for example, cable segment length, failure history, TDR results, Tan δ magnitude and its behavior as functions of voltage and time.

Secondary level categorization: it considers information that becomes available through comparison and collation of data from a number of tests. This includes the presently acknowledged approach of comparing adjacent cables segments and phases. These features include the behavior of Tan δ with the cable segment length as well. These features have been shown to be particularly effective when faced with situations such as non-uniform degradation and neutral issues. Traditionally these situations have been considered as limitations rather than the powerful diagnostic indicators that they are.

5.4.2 Decision Organization

Decision organization is particularly relevant to categorized diagnostic features in MV cable systems as more features require a structure for the test and action decision paths. The need for a proper feature interpretation and organization can be accomplished either through the use of pre-established criteria (such as those described in IEEE Std. 400 [37]) or by the use of evaluation procedures. The evaluation procedure approach offers the widest flexibility since no pre-established criteria are defined and thus it can be adapted for a particular case under study.

Table 5.4 shows a comparison between perspectives for assessment of the IEEE Std. 400 [37] and this research using VLF (0.1 Hz) Tan δ measurements. As seen in the

table, the research perspective presented in this thesis considers a wider range of diagnostic features as well as testing at different voltage levels.

Table 5.4. Comparison between the IEEE Std. 400 [37] and this thesis perspective assessment criteria for VLF (0.1 Hz) Tan δ measurements.

IEEE Std. 400 [37]	**This Thesis**
• Tan δ magnitude (2 U_0). • Tan δ vs. voltage (U_0 and 2 U_0). • VLF withstand. • Comparison between phases and segments.	• Cable segment specification and history. • TDR and visual inspection. • Tan δ magnitude (U_0). • Tan δ vs. voltage (0.5 U_0 and 1.5 U_0) • Tan δ time variability. • Tan δ length models indicators. • VLF-Tan δ monitored withstand.

More importantly is the fact that the research perspective considers the combination of different diagnostic technologies to enhance the condition assessment evaluation process. For instance, the combination of TDR, Tan δ versus voltage, and VLF-Tan δ monitored withstand tests is used here. Table 5.5 shows the fundamentals of the feature deployment in the condition assessment evaluation process.

In Table 5.5, the feature deployment is divided into features that are deployed during the test and features that are deployed after the test. The features that are deployed during test are features from the primary level of categorization and the features that are deployed after the test are features from the secondary level of categorization. The feature deployment can be non-conditional or conditional; the non-conditional feature deployment implies that the primary level diagnostic features can be deployed without taking into account any preexistent conditions; *i.e.* the non-conditional feature deployment is a priori test from which the initial information is obtained to support the decision making process for the conditional feature deployment or derived condition assessments. Therefore, the conditional feature deployments, both during and after test,

depend on the priori test results.

Table 5.5. Fundamentals of the feature deployment in the condition assessment evaluation process.

<table>
<tr><th rowspan="4">Condition Assessment</th><th colspan="4">Feature Deployment</th></tr>
<tr><th colspan="3">During Test</th><th>After Test</th></tr>
<tr><th colspan="3">Primary Level Categorization</th><th>Secondary Level Categorization</th></tr>
<tr><th>Non-conditional</th><th colspan="2">Conditional</th><th>Conditional</th></tr>
<tr><td>Direct</td><td>• TDR and visual inspection.
• Cable segment specification and history.
• Tan δ vs. voltage.</td><td>⇒</td><td>• Tan δ time variability.
• VLF monitored withstand failure on test.
⇓</td><td>-</td></tr>
<tr><td>Derived</td><td>-</td><td></td><td>• Tan δ during VLF monitored withstand.</td><td>⇒ • Tan δ length models indicators.</td></tr>
<tr><td>Time</td><td colspan="3">One hour</td><td>One week</td></tr>
</table>

In addition, the condition assessment can be direct or derived. Only the non-conditional or conditional feature deployment using features from the primary level of categorization during test can generate a direct condition assessment. A derived condition assessment can be generated by a conditional feature deployment using either features from the primary or secondary levels of categorization.

The feature deployment in the condition assessment is an evaluation process. As seen in Table 5.5, the process begins by considering the priori test from non-conditional to conditional feature deployment during test using first level of categorization features and ends by considering conditional feature deployment after test using second level of categorization features.

Table 5.5 also shows that the time to reach a condition assessment varies. Specifically, if the condition assessment is reached by using primary level categorization level diagnostic features; then, the condition assessment can be generally reached non-conditionally or conditionally in one hour. However, if the condition assessment is reached conditionally after test using secondary level categorization diagnostic features, then the time to reach a condition assessment is generally one week as the data have to be collected and analyzed to develop the proper diagnostic indicators.

The evaluation process of Table 5.5 eventually generates two condition assessments. The condition assessments are "No action" and "Action required". The "No action" condition assessment means that the cable segment under evaluation can be returned to service operation, the cable segment may be retested within the following 5 years to observe the trend of the Tan δ magnitude and to determine whether additional degradation has occurred. The "Action required" condition assessment means that the cable has to be replaced or repaired immediately after the test or in the near future. In the evaluation process an intermediate condition assessment termed as "Further study" is also considered. The "Further study" intermediate condition assessment means that additional information is needed to make and assessment. In this case, the additional information comes from the cable segment specifications, failure history, and use of the combined diagnostics. The additional information is used to enhance the evaluation procedure and leads eventually to a condition assessment of "No action" or "Action required".

5.4.3 Evaluation Procedure

The evaluation procedure is presented in detail in Figure 5.30 to Figure 5.33 using flowcharts to represent and organize the decision making process. Figure 5.30 shows the flowchart of the evaluation procedure considering the primary level of Tan δ diagnostic features categorization. In particular, cable segment specifications, failure history, TDR, neutral visual inspection, and Tan δ as a function of the test voltage level are considered.

The Tan δ evaluation process begins by considering the cable segment specifications and failure history. Subsequently, the TDR test and visual inspection of the neutral wires is performed and their results are considered, and if the TDR results and visual inspection indicate broken or highly corroded neutral wires, then no additional tests are required and an action is required on the cable segment under evaluation. The action could be immediate repair or replacement of the cable segment. If the TDR and visual inspection do not provide any signs of broken or extremely corroded neutral wires, then the Tan δ versus voltage test is performed. From the Tan δ versus voltage test, if the Tan δ magnitude at U_0 (U_0 is the cable segment operation voltage) is more than 150×10^{-3} and the tip-up between 0.5 U_0 and 1.5 U_0 is more than 200×10^{-3}, then some action is required on the cable segment. If the Tan δ magnitude at U_0 is less than 6×10^{-3} and the tip-up between 0.5 U_0 and 1.5 U_0 is less than 1×10^{-3}, then no action is required and the cable segment could be returned and left in service. However, if the Tan δ magnitude at U_0 is in the range of 6×10^{-3} and 150×10^{-3} and the tip-up between 0.5 U_0 and 1.5 U_0 is in the range of 1×10^{-3} and 200×10^{-3} a further study action is required. In this case the further study considers the second level categorization diagnostic features to decide if an action is required on the cable segment. The flowchart of the further study process is shown in Figure 5.31.

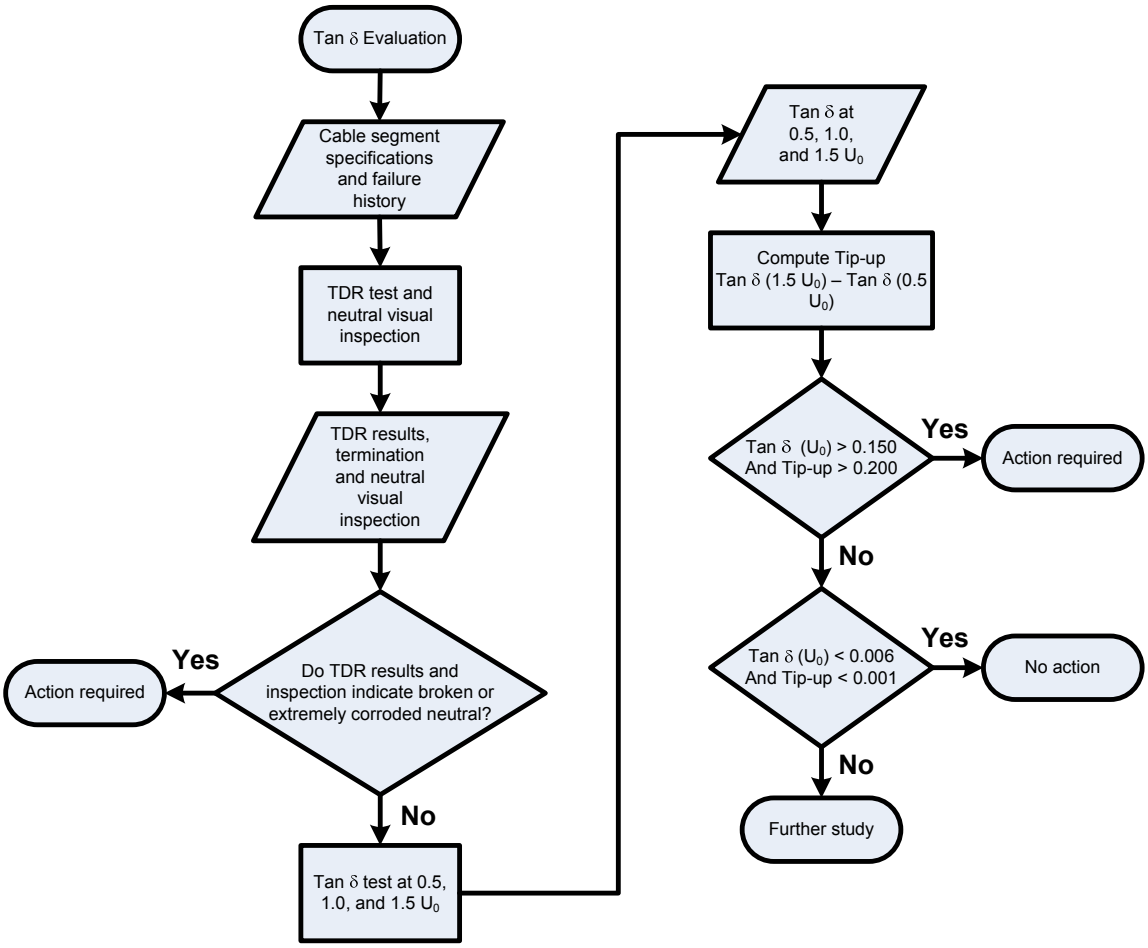

Figure 5.30. Flow chart of the evaluation procedure considering the primary level of Tan δ diagnostic features categorization.

In Figure 5.30, the threshold values for Tan δ magnitude (6×10^{-3} and 150×10^{-3}) and Tip-up (150×10^{-3} and 200×10^{-3}) as a function of the test voltage level have been suggested by the CDFI project [64]. These values represent an effort to revise the thresholds in the current IEEE Std. 400 [37], and are based on statistical analyses of VLF (0.1 Hz) Tan δ data obtained from field tests conducted on cable systems of the utilities participating in the CDFI project. The values are specifically for 15 and 25 kV systems of PE insulated (*i.e.* HMWPE, XLPE, and TRXLPE) cable systems.

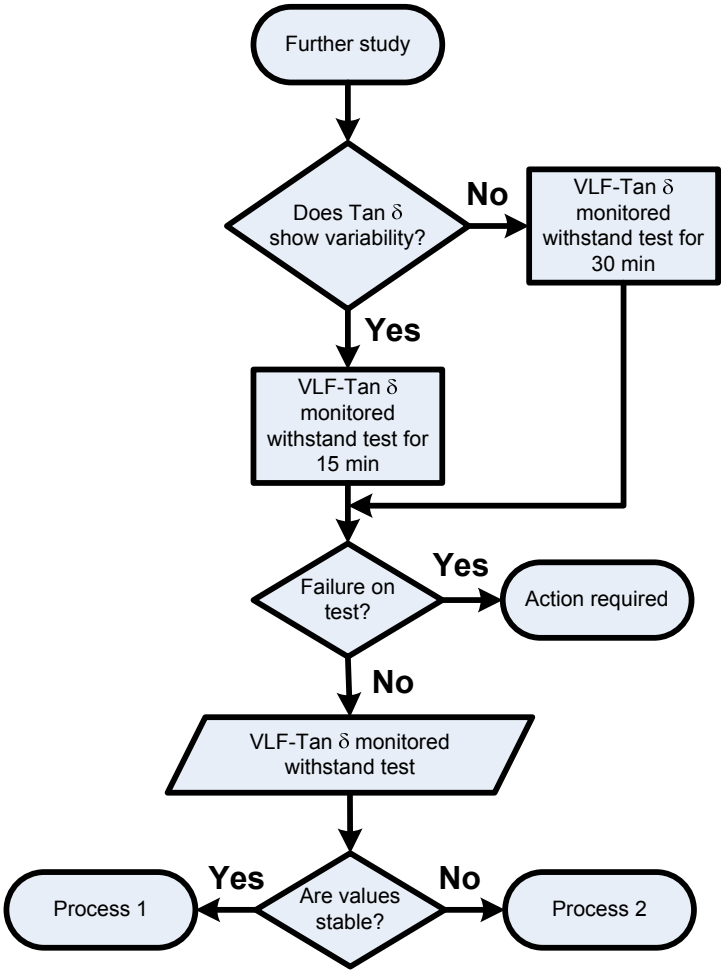

Figure 5.31. Flowchart for the Further Study output of the flowchart of Figure 5.30.

The further study process of Figure 5.31 starts by considering the variability of the Tan δ magnitude as a function of time for each test voltage level of the Tan δ versus voltage test. If the Tan δ magnitude shows variability in time at any voltage level; then a VLF-Tan δ monitored withstand test is performed for 15 minutes. The value of 15 minutes is selected since it is the minimum suggested time for a VLF withstand test in the IEEE Std. 400.2 [34]. On the contrary, if the Tan δ magnitude during the Tan δ versus voltage test does not show any variability; then, the VLF-Tan δ monitored withstand test is performed for 30 minutes. The value of 30 minutes is selected since it is the

recommended time for a VLF withstand test in the IEEE Std. 400.2 [34]. When the Tan δ magnitude shows variability in time during the Tan δ versus voltage test, 15 minutes are selected over 30 minutes to reduce the possibility of having a failure on test, since as it has been shown in Chapter 4, the variability indicates higher risk of failure during testing. Subsequently, if the cable segment under evaluation fails during the VLF-Tan δ monitored withstand test; then, an action is required. However, if the cable segment does not fail during the VLF-Tan δ monitored withstand test; the stability of the Tan δ magnitude during the test is assessed leading to processes 1 and 2.

Processes 1 and 2 consider the secondary categorization level of Tan δ diagnostic features. Specifically, the processes consider the correlation between the Tan δ magnitude at U_0 and the cable segment length. In processes 1 and 2, it is assumed that the previous cable segment failure history is known. Flowcharts of processes 1 and 2 are shown in Figure 5.32 and Figure 5.33 respectively.

Process 1 of Figure 5.32 deals with the case of stable Tan δ during the VLF-Tan δ monitored withstand test. The process starts by studying the correlation between the Tan δ magnitudes with cable segment lengths. If the correlation is positive and significant and the failure history indicates previous neutral wires corrosion problems; then, it can be concluded that most likely the cable segment has distributed neutral corrosion and an action is required. Similarly, if the correlation is positive and significant but the failure history does not indicate neutral corrosion problems; then, no action is required. All the other possible cases are also shown in Figure 5.32.

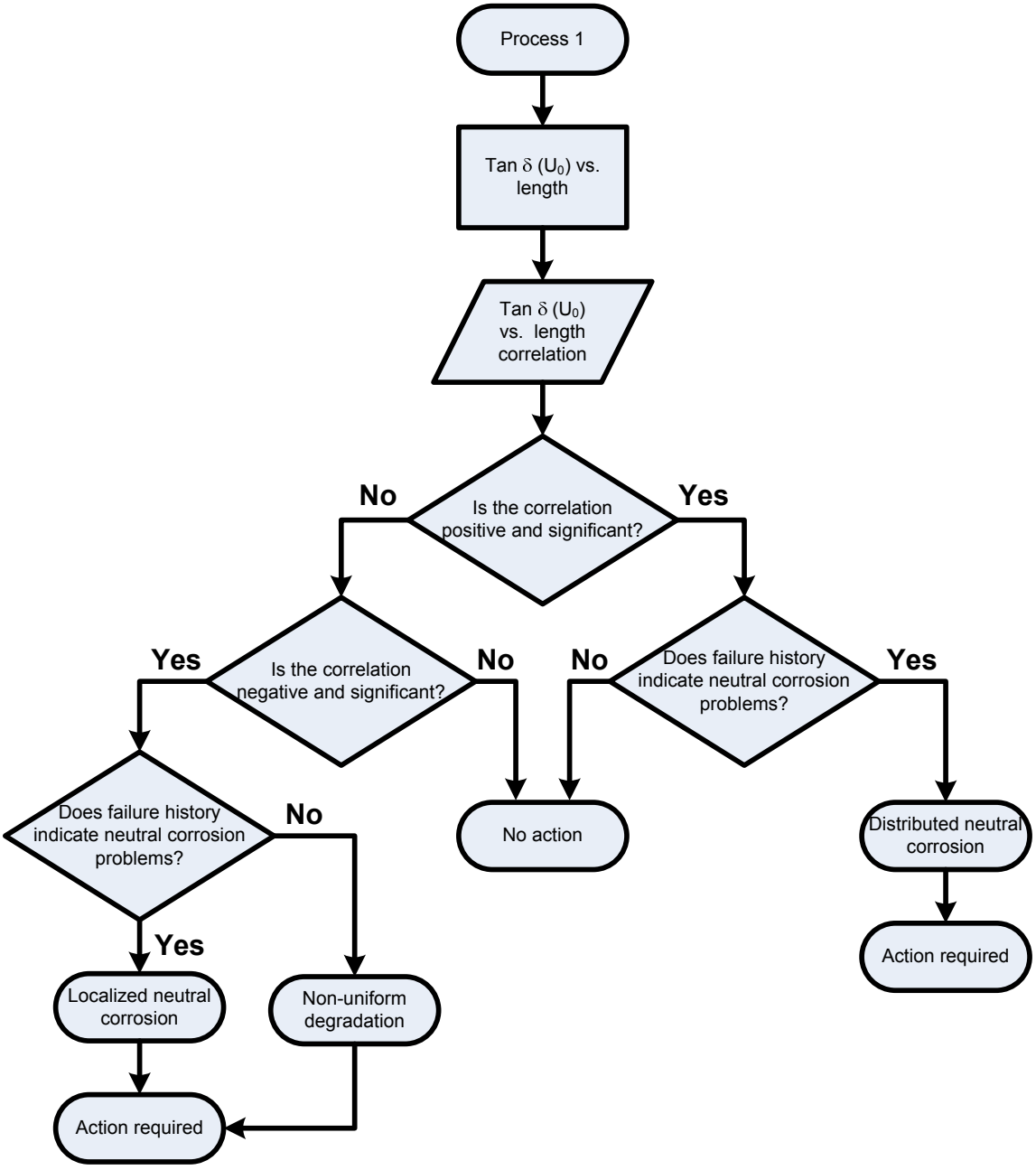

Figure 5.32. Flow chart of Process 1 – output of the flowchart of Figure 5.31 – considering secondary categorization level of Tan δ diagnostic features.

In contrast, process 2 of Figure 5.33 deals with the case of unstable Tan δ during the VLF-Tan δ monitored withstand test. In this case, the process starts by considering the stability of the Tan δ magnitude, increasing values are sufficient to conclude that an

action is required. If the values are decreasing; then, the correlation between Tan δ at U_0 from the Tan δ versus voltage test and the cable segment lengths is used. The previous failure history is also used. For example, if the correlation is negative and significant and the previous failure history indicates no neutral corrosion problems; then, it can be concluded that most likely the cable segment has non-uniform degradation problems and therefore an action is required. All other possible cases are also shown in Figure 5.33.

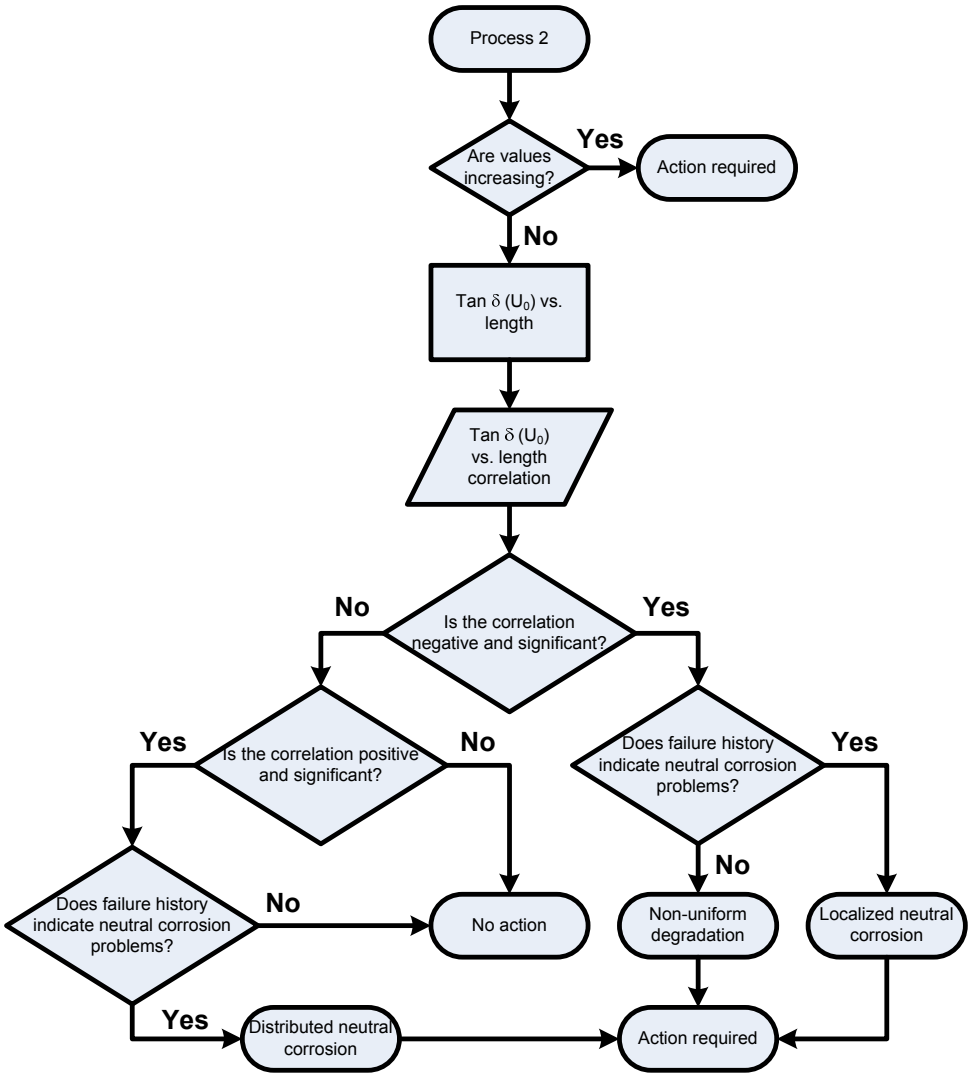

Figure 5.33. Flow chart of Process 2 – output of the flowchart of Figure 5.31 – considering secondary categorization level of Tan δ diagnostic features.

Note that in both processes of Figure 5.32 and Figure 5.33, if there is no significant correlation between the Tan δ magnitudes and cable segment lengths, then both processes lead to no action, which means that the Tan δ versus length diagnostic indicators do not provide the additional information required to assess whether the cable segment under evaluation has non-uniform degradation or neutral wires issues.

5.5 Summary and Conclusions

The Chapter has presented the basics of low voltage TDR test on power cables. Because of its ease of use, cost, and simplicity in indentifying power cable systems configuration and basic problems with neutral wires, the TDR test is proposed and used as one of the initial steps for any cable condition assessment in the field. The use of TDR combined with other diagnostic tests aids in improving the condition assessment of MV power cable systems.

The Chapter has also presented the Tan δ versus length models. The most common situations of non-uniform degradation and neutral issues have been modeled and demonstrated through both theory and experiments. It has been shown that both situations, rather than limitations, provide useful diagnostic indicators that aid for an enhanced condition assessment.

More importantly, the Chapter has introduced a new approach for condition assessment of MV PE-based power cable systems. The approach considers the use of combined diagnostics, which includes the TDR, VLF-Tan δ, and VLF-Tan δ monitored withstand tests. The approach is executed by an evaluation procedure that uses a diagnostic features management technique with feature categorization and decision organization. The evaluation process constitutes a step forward to the currently approach presented in the IEEE Std. 400 [37].

This Chapter finalizes the work on VLF-Tan δ which is one of the major parts of

this thesis. The upcoming Chapters deal with the second major part of the research presented in this thesis, namely partial discharge measurements.

CHAPTER 6

CHARACTERIZATION BY PARTIAL DISCHARGE MEASUREMENTS

6.1 Introduction

The Chapter introduces basic concepts, means of diagnosis, and limitations of partial discharge measurements for MV power cable systems. Brief descriptions of the available partial discharge data, diagnostic feature selection and extraction techniques, and classification tools are also introduced. Furthermore, a comprehensive literature review on the "state of the art" on characterization of power cable defects by partial discharge measurements is also shown.

More importantly, this Chapter describes and briefly analyzes data from partial discharge measurements. The partial discharge data have been collected from laboratory experiments and field tests. No detailed analysis of the partial discharge data is presented in this Chapter; however, the data is further used in Chapter 7 for the analysis and evaluation of partial discharge diagnostic features. The data are based on the phase-resolved partial discharge pattern and are classified into two groups, *i.e.* partial discharge in cable and partial discharge in accessory. The latter group includes joints and terminations. The laboratory partial discharge data have been measured by the author while the data from partial discharge field tests have been provided to the author by one of the utilities participant of the CDFI project.

6.2 Basis of Partial Discharge Measurements

As seen in Chapter 2, partial discharge is defined as "an electrical discharge that only partially bridges the insulation between conductors, and may or may not occur adjacent to a conductor" [1]. Partial discharges occur when the local electric field

intensity exceeds the dielectric strength of the dielectric involved, resulting in local ionization and breakdown. Depending on their intensity, partial discharges are often accompanied by the emission of light, heat, and sound. Partial discharges can be generated from electrical trees, voids, cuts, cracks, protrusions, delaminations, and contaminants with poor adhesion to the polymeric insulation material [24].

Partial discharges may be detected by different methods that mainly include electrical and acoustic detection. The most common form of detection is electrical. In this case, the relative intensity of partial discharge can be observed at the terminals of the sample under test by measuring the apparent charge in pico-coulombs (pC). However, the apparent charge (terminal charge) should not be confused with the actual charge transferred across the discharging defect inside the dielectric material of the sample, which in most cases cannot be ascertained. The partial discharge current in the external circuit is a complex function of the nature of the discharge inducing defect and the geometry of the sample insulation system [65]. To account for this situation a calibration procedure is performed before any partial discharge measurement.

Calibration of partial discharge measurements is a topic on itself and is only treated briefly here. As mentioned before, only the apparent partial discharge magnitude can be measured; in other words, the change in charge on the electrodes of the sample caused by some phenomenon of unknown nature and magnitude within the sample is measured. The transfer function between the internal phenomenon and the change in charge on the electrodes can vary by many orders of magnitude depending on sample and defect geometry [66]. The purpose of calibration is simply to ensure that the apparent partial discharge magnitude is measured accurately by considering, in some way, the transfer function of the sample under test. In general, a known calibration pulse is injected into the sample, and then the testing equipment is adjusted so it measures the known value. The calibration pulse can be injected at the near or far end of the sample under test. In some cases, multiple calibration pulse settings are used to perform a

sensitivity assessment [20].

For a better understanding of the partial discharge process and measurement, different models have been developed to describe the combination between a defect and the surrounding dielectric. For example, in the case of voids, the ABC model is used [66]. The ABC model is a simple capacitive circuit that considers three capacitances of different areas in the insulation named A, B, and C. The defect is represented by the capacitance C, the dielectric in series with the defect is represented by the capacitance B, and the remaining surrounding dielectric is represented by the capacitance A. An example is shown in Figure 6.1 for a void inside the bulk insulation of a cable.

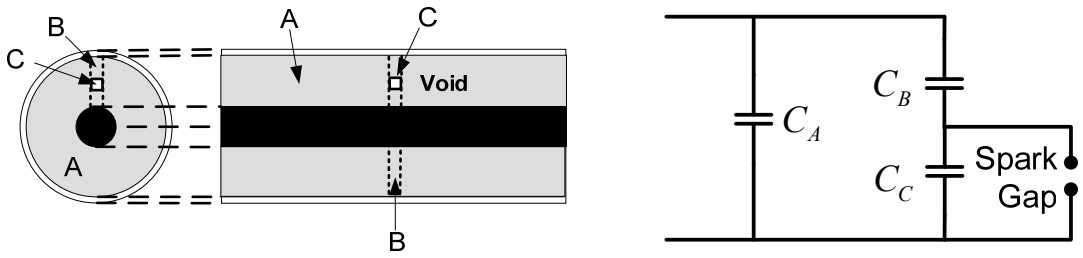

Figure 6.1. ABC model for partial discharges in a cable void.

In the context of power distribution cables, partial discharge can be classified according to the following types [67]:

- **Internal Discharges:** These discharges occur within the insulation or at the interfaces of insulating shield layers.
- **Surface Discharges:** These are discharges that occur along the interface of two dielectric materials.
- **Corona Discharges:** This type of discharge occurs in the gaseous dielectric adjacent to electrodes.
- **Treeing Discharges:** These are discharges that occur within the bulk of the

cable system insulation and are generated from electrical trees.

When a partial discharge event occurs, it produces an electrical pulse that travels along the cable segment. The electrical pulse is detected by the measurement equipment. However, it is important to consider that the pulse received by the detection equipment is not the same as the pulse that is generated by the partial discharge. The cable acts as a low pass filter that attenuates the high frequencies of the pulse, this is true for both paper and extruded cables [68]. This effect causes a reduction in amplitude and dispersion of the partial discharge pulse when it travels along the cable segment. Thus, signals with bandwidths of some tens of MHz can be detected at the cable terminals. For instance, for a typical rise time of a partial discharge pulse of around 1 ns the equivalent bandwidth can go up to some GHz. Therefore, much of the frequency content is lost just in the propagation of the pulse to the detector. This is a fundamental issue for electrical detection of partial discharges. Nowadays, typical bandwidths for partial discharge detection equipment in the field go from several hundreds of KHz up to several tens of MHz [69-70].

6.3 Partial Discharge Means of Diagnosis

Partial discharge measurement is useful for cable diagnosis because it is the only technique that is able to give a localized assessment of the insulation condition. In this case, if partial discharges are present, then there are defects generating the partial discharges. However, care must be taken when interpreting the partial discharge measurements. The diagnosis of insulation degradation using partial discharge measurements is not a simple process because of the wide range of defects that can produce partial discharges and the many different related degradation processes [71]. In addition, partial discharge measurement characteristics also depend on the location of the defect or defects, operating and testing voltage magnitudes, circuit operating conditions, system design, length, and noise. A brief review of the early history of partial discharge

research indicates that effective partial discharge measurement and location technology was developed very quickly. Later progress tended toward incremental improvements through application of new technology, as well as broadening of the range of phenomena covered by the technique [72].

Two general methods are available to detect partial discharge in cable systems. They are offline and online detection methods. Offline testing is normally conducted at higher voltages than to the operating system voltage (U_0) as this method uses a separate power supply to energize the cable after it has been removed from service. Online testing is done during normal operation of the cable system.

Some advantages of the offline method are as follows [73]:

- Partial discharge inception voltage (IV) and partial discharge extinction voltage (EV) can be measured if a variable voltage source is used.
- Partial discharge measurements can be performed at different voltages, which can aid in the diagnosis.

Some advantages of online partial discharge method are as follows [73]:

- Partial discharge measurements can be obtained under different load conditions.
- Measurements can be performed without having to take the cable segment out of service.
- Monitoring may be performed for extended periods of time.

There is a big discussion in the cable community about the benefits of both approaches. The selection of one over the other should be done considering the goals of the testing as well as the particular system conditions. In particular, the duration of the test is important because the electron required to initiate the partial discharge might not be available in a void during the application of the test voltage [24].

6.4 Limitations of Partial Discharge Measurements

Partial discharge measurements alone cannot completely ensure the condition of the insulation of a cable segment, especially if potential defects are marginally present in the insulation. In fact, most industry specifications require an additional test to be performed as a supplement. Some of the most important limitations of partial discharge measurements are discussed briefly in the next paragraphs.

As mentioned before, care must be taken when interpreting partial discharge measurements. The diagnosis of the insulation deterioration using partial discharge measurements is a complicated process [71]. Most defects in polymeric materials that are able to cause partial discharge at normal operating voltage, eventually, generate an electrical tree that will grow and lead to breakdown. In contrast, other types of defects such as protrusions or a conducting contaminant inside the bulk insulation may cause the initiation of an electrical tree without detectable partial discharge prior to the tree initiation. Research efforts on both laboratory experiments and field tests have shown that any relation between the apparent partial discharge magnitude and the deterioration rate or life of the insulation is generally nonlinear [71].

As a general rule, the accuracy in the interpretation of partial discharge measurements when discerning between the conditions of “good” or “very bad” is acceptable. For example, a low IV is an indication of a “very bad” condition while no partial discharge activity at high testing voltages indicates a “good” condition. Unfortunately, the accuracy in interpretation is far less reliable when cable segments are between the “good” and “very bad” conditions. This is probably the reason why some of partial discharge diagnostic providers are now considering partial discharge as a pass/fail test. However, interpretations of partial discharge measurements are available for both extruded and paper cable systems. Different organizations have databases of partial discharge measurements for different defects which have allowed them to create

knowledge-based rules to improve their assessment [26, 73]. For instance, new measurements are compared with the database and knowledge rules to identify the type, location and severity of the defect.

Another important issue that requires mentioning is noise as it is a critical impediment to successfully detecting partial discharge. Magnitudes of the partial discharge pulses as seen by the measuring equipment are in the order of fractions of mV to several tens of mV [67]. In addition, as mentioned before, at the detection point pulses have a bandwidth of several tens of MHz. Unfortunately, this frequency range includes most of the amplitude modulated communication signals and, in some cases, these signals can have a higher magnitude than the partial discharge signals. This depends on several factors including circuit parameters such as length, location, and attenuation, as well as on the particular nature of the partial discharge present in the cable segment. From the perspective of noise, the cable acts as an antenna that picks up the communication signals. Therefore, it is unavoidable for these communication signals to be present in the cable and thus in the detector. Several techniques have been used to reduce the noise. Analog and digital filters are typically applied, but most recently the application of powerful digital signal processing techniques such as wavelet transforms have been used to address this issue [70].

Finally, the stochastic nature of the partial discharge process must be considered. This process creates considerable scattering in the measurements over time and also between identical cable segments operating under similar conditions. Therefore, in most cases partial discharge is described using statistical tools, but the extent to which the statistical information should be analyzed depends on the purpose for which the information is to be used. If it is only desired to have information about the presence of partial discharge, then data based on statistics may become superfluous. In contrast, if a specific defect is to be characterized then statistical tools are required to be able to perform the analysis [74].

In general, the accuracy of the condition assessment may be improved if [73]:

- More data are collected and compared with actual cable system performance.
- Data are compared with information from results of dissections of cable or accessories that were recommended to be replaced.
- Additional testing is carried out on cables and accessories that were recommended to be replaced.
- Periodic measurements are made on the same cable segments. In this case, the general trend can be observed.
- All relevant information about the cable system is known, such as the age, type, and design of the cables and accessories, operating conditions, and others.
- Standardized testing and analysis procedures are developed. This will aid in the comparison of databases of different partial discharge service providers and utilities.

In conclusion, a meaningful evaluation of partial discharge measurements in terms of the rate of degradation or remaining life is not possible in the absence of a microscopic description of the defect.

6.5 Basis of Partial Discharge Data

Partial discharge data can be classified into three types: phased-resolved data, time-resolved data, and partial discharge data without phase or time information. Each of them is briefly explained in the next subsections.

6.5.1 Phase-Resolved Partial Discharge Data

This type of partial discharge data is obtained in relation to the phase of the test voltage, which is assumed to be sinusoidal and constant during the acquisition of the

partial discharge data. The phase of the test voltage is divided into a suitable number of bins. Each bin is characterized by a particular value of the test voltage phase.

For each partial discharge pulse that is detected, the phase value at which it occurs and its partial discharge magnitude are recorded. Therefore, each pulse is described by a phase location and a partial discharge magnitude. By using the phase location, pulses can be assigned to a particular bin. The total number of pulses falling inside a bin is also recorded and this represents the pulse density as a function of the phase.

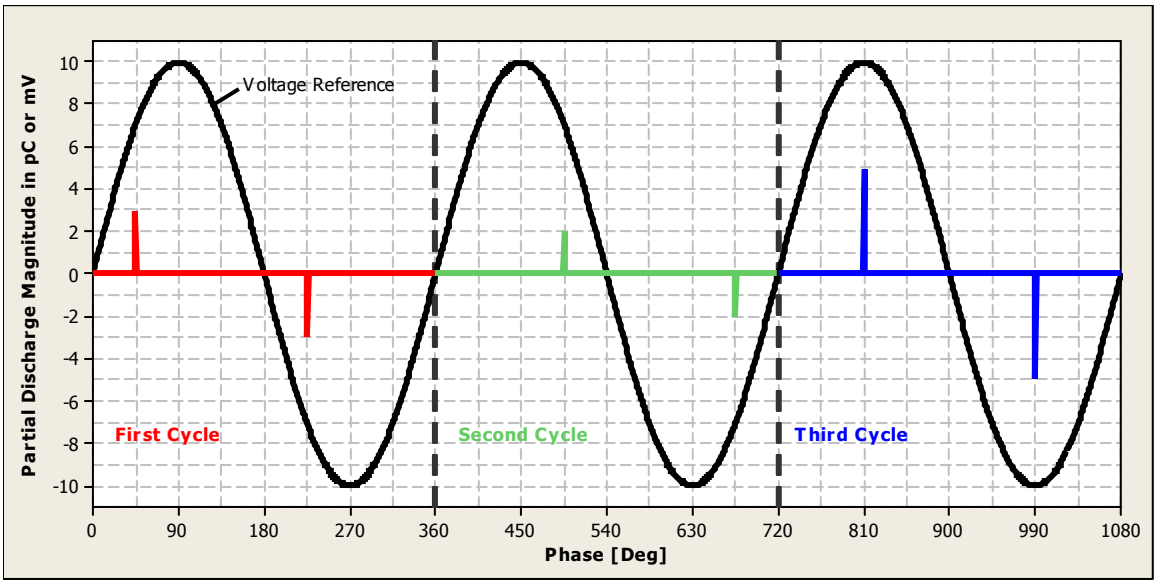

Figure 6.2. Illustrative phase-resolved partial discharge data.

As illustration, Figure 6.2 shows three cycles of the test voltage. The test voltage is represented only as a reference by the black solid line and the partial discharge activity by the colored lines. Different colors have been used for the partial discharge activity to clearly differentiate between cycles. The information contained in the three cycles can be condensed to a single graph in which phases and partial discharge magnitudes are plotted together. As a result, every partial discharge pulse is represented by a dot using the phase and partial discharge magnitude values, see Figure 6.3. This plot is known as the partial

discharge phase-resolved pattern.

As seen from Figure 6.2 and Figure 6.3, the partial discharge magnitude may be in pico-coulomb (pC) or mV. When using mV, the value refers to the maximum amplitude or peak value of the detected partial discharge pulse.

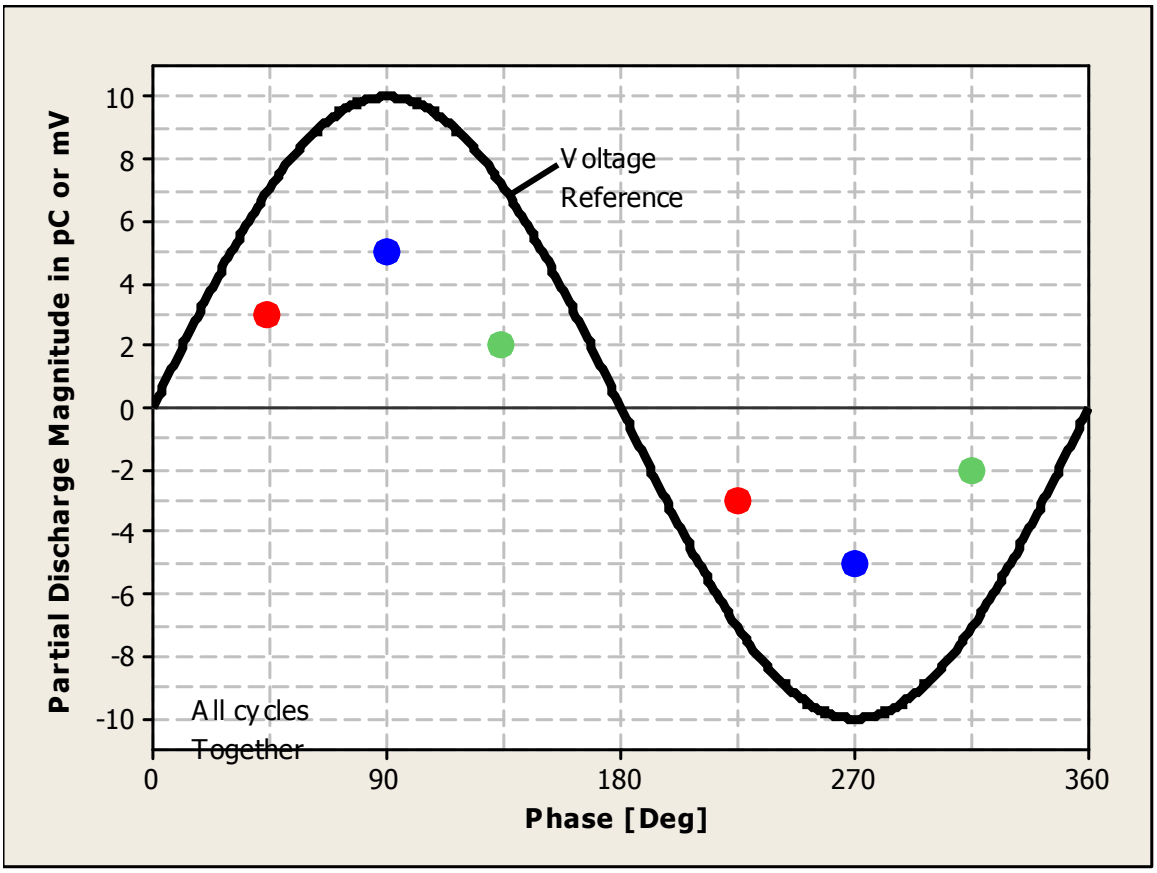

Figure 6.3. Illustrative partial discharge phase-resolved pattern using data from Figure 6.2.

The information from the partial discharge phase-resolved pattern is generally represented as distributions of one variable. The most commonly used distributions are: average magnitude in each bin as a function of phase, maximum magnitude in each bin as a function of phase, and pulse density as a function of phase [28]. Here, it is assumed that sufficient number of pulses have been acquired such that the distributions are statistically

significant.

6.5.2 Time-resolved Partial Discharge Data

This type of data uses the partial discharge pulse waveform as the main diagnostic feature resource. The test voltage is again considered to be sinusoidal and constant during data acquisition. The main advantage of time-resolved partial discharge data is that there is a strong relationship between the shape of the partial discharge pulses and the physics of the defect [28, 69]. Moreover, the measurement equipment requires less expensive instrumentation. It has been shown that partial discharge pulse shapes change considerably during the degradation of insulation materials; therefore, by analyzing their shapes the degradation can be assessed [69].

6.5.3 Partial Discharge Data without Phase or Time Information

Partial discharges also possess valuable information without considering the phase or time. For example, the information can be obtained from the average partial discharge magnitude as a function of the magnitude test voltage, IV, and EV.

6.6 Partial Discharge Data Diagnostic Feature Selection and Extraction

Once the partial discharge data is collected, a considerable number of discriminatory attributes or features may be extracted to characterize the partial discharge data. Depending on the type of data, statistical, time-domain, signal processing, and image processing tools are used to accomplish the goal. These tools are explained in more detail in the next subsections.

6.6.1 Statistical Tools

Statistical tools are mainly used to characterize phase-resolved data patterns. The distributions of one variable are characterized by a set of features that for example may include: mean, variance, skewness, kurtosis, magnitude asymmetry, phase asymmetry,

and cross-correlation factors. In addition, Weibull parameters from the model fitting of the partial discharge magnitude histograms can be used as additional features, As previously mentioned, it is assumed that sufficient number of pulses have been acquired such that the distributions have significant statistical meaning.

6.6.2 Time-Domain Tools

These tools are mainly used to characterize time-resolved partial discharge data. Particularly, the partial discharge pulse waveforms are characterized by a set of parameters that include: rise time, decay time, pulse width, and maximum amplitude. Additional features that can be used here are repetition rate and instantaneous test voltage difference between two consecutive pulses [28].

6.6.3 Signal Processing Tools

Signal processing tools can also be applied for feature selection and extraction of partial discharge data. They mainly include: Fourier transform, wavelet transforms, Haar transforms and Walsh transforms. The signal processing techniques are, for the most part, applied to partial discharge pulse waveform to discover information that cannot easily be seen in the time-domain representation. The features typically include transformation coefficients and some form of their processing.

6.6.4 Image Processing Tools

Image processing tools are used to obtain features from the phase-resolved partial discharge data pattern. In this case, the pattern is treated as an image. This approach has its basis in the fact that different defects produce different phased-resolved data patterns that can be visually discriminated with the naked eye. Three different approaches are used, they include texture analysis algorithms, fractal theory, and wavelet-based image decomposition [28].

6.7 Partial Discharge Feature Classification

The topic of partial discharge feature classification is vast. A considerable number of classifier types are available in the literature that can be used for partial discharge classification. The classifiers are largely based on decision functions, distance functions, likelihood functions, and artificial intelligent techniques such as neural networks and fuzzy logic [28]. At the present, there is no agreement on which type of classifier is the best to use and research efforts continue to address this issue.

6.8 Previous Work on Characterization by Partial Discharge Measurements

A considerable amount of research work has been devoted in the last decade to the characterization and classification of insulation defects by partial discharge measurements. Researchers have made important contributions by characterizing partial discharge in the laboratory using deterministic and stochastic models, but in practical applications, the current approach is still empirical in nature. In some cases, data have been obtained from accelerated aging tests in the laboratory using artificially created defects. But, there is always the question about the validity of the results since the service conditions and factors affecting in-service cable system aging and degradation are quite different compared to laboratory aging. The next paragraphs show the most relevant work in the effort of characterization and classification by partial discharge measurements.

Krivda [75] has shown the application of pattern recognition techniques for the discrimination and classification of partial discharges. Three basic groups of defects are considered: (a) standard defects: these are simple two electrodes models, (b) industrial models: artificial defects are introduced in actual high voltage constructions, and (c) industrial objects: this group comprises naturally occurring defects in actual industrial objects. Only artificially created defects are considered in the case of power cables. The partial discharge features that are analyzed are statistical operators obtained from the phased-resolved data, they include: mean values, skewness, kurtosis, and cross-

correlation factors. This set of features is defined as a fingerprint. The author shows that different defects give different fingerprints and the fingerprints are characterized by typical values of the statistical operators. For discrimination, the group average method has been found to yield good performance, in particular for aging insulation analysis, especially when periodic testing is carried out. Fractal descriptors also show good discrimination performance. The classification is based on the centour score method and on neural networks. In this case, the centour score method has been found to provide good classifications rates while neural networks do not prove to be a valuable tool.

Recognition rate and centour score methods have been also used for classification of partial discharge measurements by Kreuger *et al.* [76]. In this case, a number of simple partial discharge models are considered, they include: surface discharges in air, Sulfur Hexafluoride gas (SF_6), and transformer oil, single and multiple point corona discharges in air and oil, void discharges in dielectrics, and artificial void discharges in cables. Statistical operators are also used as features in this case. Results show that there is a high potential for classification using both methods. In particular, the centour score method gives a better suppression of irrelevant answers because of the percentile rank calculation.

Other research efforts [77-79] have also used statistical operators as features for characterization and classification of partial discharge measurements. In particular, Gulski and Kreuger [79] have considered a series of artificial defects. The classification success rate is found to be acceptable; however, the authors point out that a large number of statistical operators used as features demands a large memory and requires considerable computational effort for the creation and operation of the database used for classification.

Hoff *et al.* [80] uses the external voltage difference between two consecutive pulses as an additional feature for partial discharge characterization. The counter

propagation neural network classifier is used and its performance is compared to the nearest neighbor classifier. Results show that a considerable improvement is accomplished over artificial neural networks based algorithms for the different types of partial discharge defects that are studied.

The Weibull scale and shape parameters from the pulse amplitude histogram have been used by Cacciari *et al.* [81-82] as features. The presence of multiple partial discharge defects is modeled by considering the multiplicative-additive properties of the Weibull parameters. It is shown that Weibull parameters can describe the aging due to partial discharge. But more importantly, the multiplicative-additive properties allow the overlapped partial discharge measurements to be separated and independently analyzed as functions of aging, time, and test voltage.

Digital signal processing techniques have also been used to obtain the feature parameters [83-84]. Particularly, Cotin *et al.* [84] considers the Weibull parameters from the model fitting of the pulse amplitude histogram, statistical operators from the phased-resolved data, and the equivalent time length and the equivalent frequency of the partial discharge pulses. A fuzzy classifier is successfully used in this case. Results show that because of the fuzziness of the classifier, it provides an efficient rejection noise property. Salama and Bartnikas [85] also use a fuzzy logic classifier in the classification of partial discharge measurements.

Partial discharge pulse deterministic parameters such as the pulse maximum amplitude, rise time, decay time, and others, have been used as additional features parameters [86-87]. Mazroua *et al.* [86] use different neural network structures for characterization and classification of artificially created voids of 1.0, 1.5, and 2.0 mm sizes. The different neural network structures classify correctly all void sizes. However, it is also observed that, when classifying between the smaller voids, a Learning Vector Quantization (LVQ) network gives a better performance. In addition, Brosche *et al.* [69]

show that there is a correlation between the parameters that describe the partial discharge pulse waveform and the geometry of the defect.

Most recently, the wavelet transform has also been used for extraction of the feature parameters consisting of different wavelet coefficients in the work reported by Ma *et al.* [87].

The literature review has revealed that the majority of characterization and classification methods used by researchers are based on phase-resolved partial discharge data for recognition of a single partial discharge source. However, a question that remains unaddressed is the evaluation of the relevance of the partial discharge diagnostic features, *i.e.* which features are more important than others for diagnosis. This evaluation could lead to a reduced number of features with more physical meaning and thus to a better understanding of the partial discharge process, this is one of the main motivations for the work presented in Chapter 7.

6.9. Partial Discharge Measurement Data

This section presents the partial discharge measurement data that are the basis for the analysis and evaluation of partial discharge diagnostic features in Chapter 7. The data are based on the phase-resolved partial discharge data pattern obtained from laboratory measurements and field tests. The laboratory measurements have been conducted by the author while the data from field tests have been provided to the author by one of the utilities participants of the CDFI project. Since the data is fully analyzed in Chapter 7, the main goal of this section is only to present a description and a basic analysis of the data.

6.9.1 Laboratory Partial Discharge Data

A description and basic analysis of the laboratory partial discharge data are shown in the next subsections.

6.9.1.1 Laboratory Sample Set Description

The sample set used is composed of field-aged joints (samples J-1 and J-2), a new cable sample with manufacturing defects (sample N-1), field-aged cables (samples C-1 and C-2), and a non-aged cable with artificially created defect (sample A-1). The samples have been provided by the CDFI project participants and by NEETRAC. The sample description is presented in Table 6.1.

Table 6.1. Sample description for laboratory partial discharge measurements.

<table>
<tr><th>Sample</th><th>Condition</th><th>Length [ft]</th><th>Year of Manufacture</th><th>Voltage Class</th><th>Insulation Material</th></tr>
<tr><td>J-1</td><td rowspan="2">Field-aged Joint</td><td rowspan="2">N/A</td><td rowspan="2">Unknown</td><td rowspan="2">15 kV</td><td rowspan="3">TRXLPE</td></tr>
<tr><td>J-2</td></tr>
<tr><td>N-1</td><td>New cable</td><td>77</td><td>2005</td><td>25 kV</td></tr>
<tr><td>C-1</td><td rowspan="2">Field-aged cable</td><td>15</td><td rowspan="2">1968</td><td rowspan="3">15 kV</td><td rowspan="3">XLPE</td></tr>
<tr><td>C-2</td><td>17</td></tr>
<tr><td>A-1</td><td>Artificial defect</td><td>10</td><td>2003</td></tr>
</table>

All the samples have partial discharge activity and partial discharge free terminations, *i.e.* the terminations are properly installed and they do not cause any partial discharge.

6.9.1.2 Laboratory Test Program Description

The test program description is shown in Table 6.2. The test program considers voltage preconditioning and several data captures for each sample. The data captures for each sample are selected randomly. The random selection and number of data captures per sample are considered to account for the variability of partial discharge measurements.

Table 6.2. Laboratory test program description for partial discharge measurements.

<table>
<tr><th>Sample</th><th>Preconditioning time [min]</th><th>No. of partial discharge data captures</th><th>Details for each data capture</th></tr>
<tr><td>J-1</td><td rowspan="6">15</td><td rowspan="2">4</td><td rowspan="6">IV† and EV‡ before and after preconditioning are registered.

Four data acquisitions of partial discharge, two at 1.25 and two at 1.50 the IV after preconditioning.

Each acquisition is for 30 sec or until 5000 pulses are acquired, whichever happens first.</td></tr>
<tr><td>J-1</td></tr>
<tr><td>N-1</td><td rowspan="4">8</td></tr>
<tr><td>C-1</td></tr>
<tr><td>C-2</td></tr>
<tr><td>A-1</td></tr>
<tr><td colspan="4">†: Partial discharge inception voltage, ‡:Partial discharge extinction voltage</td></tr>
</table>

As the samples are stored in a de-energized state, a preconditioning time before each partial discharge data capture is considered. The main goal here is to minimize the variability in the measurements by energizing the sample before the partial discharge data acquisition. The preconditioning time is 15 minutes at a voltage of 1 kV lower than the inception voltage after preconditioning. The inception and extinction voltages are recorded for each sample before and after preconditioning and as it will be seen later in Chapter 7 they are part of the diagnostic features.

Screening partial discharge tests, prior to the laboratory test program, indicate that the variability in the measurements is considerably less for the joints when compared to the cables. Therefore, the number of data captures is smaller for the joints than for the cables.

The test program in Table 6.2 includes partial discharge data acquisition at two test voltage levels. The levels are 1.25 and 1.50 times the inception voltage after preconditioning. During each data acquisition, the following steps are followed in order:

1. The inception and extinction voltage before preconditioning are registered.

2. The sample is preconditioned at 1 kV below the extinction voltage before preconditioning.
3. The inception and extinction voltages are registered after preconditioning.
4. Calibration and sensitivity are performed.
5. Four partial discharge data acquisitions are conducted; specifically, two acquisitions at 1.25 and two acquisitions at 1.50 times the inception voltage after preconditioning.

The schematic of the test set-up is shown in Figure 6.4. In particular, the figure shows the case of testing a field-aged sample. The field-aged samples are unjacketed cables. Thus, in order to guarantee a good electrical connection between the insulation shield and the neutral wires during testing, the sample is tested inside a water tank. This ensures that the tests are free of the confusing partial discharge results due to the poor electrical contact between the insulation shield and neutral wires that may cause arcing as it was seen in Chapter 5.

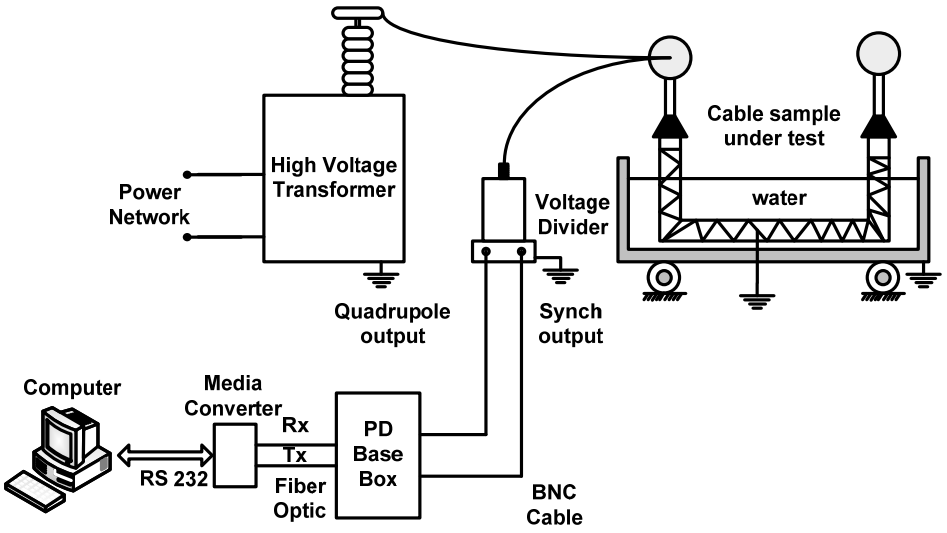

Figure 6.4. Schematic of the test set-up for laboratory partial discharge measurements.

Figure 6.5 shows the actual test set-up. In this case, sample C-1 is under test. The

water tank, the voltage divider and the transformer can be observed in the figure.

Figure 6.5. Actual test set-up for laboratory partial discharge measurements.

6.9.1.3 Laboratory Partial Discharge Acquisition Equipment

The partial discharge acquisition equipment is the PDBase of TECHImp Systems. The PDBase is a diagnostic equipment specially designed for the detection and analysis of partial discharge. The PDBase is largely innovative in the field partial discharge analysis because it is based on analogue to digital converters operating at a sampling frequency of 100 MHz. Thus, it can record the whole wave shape of each individual partial discharge pulse (with a bandwidth of 30 MHz). The system has on-board RAM storage and computing capabilities which allows for extracting a considerable number of

diagnostic features for a large number of partial discharge pulses. In this case, a maximum of 5000 pulses are captured over a maximum capturing time of 30 seconds.

6.9.1.4 Laboratory Partial Discharge Results

As previously mentioned, the laboratory and field partial discharge data considered in this thesis are based on the phase-resolved partial discharge data pattern. Figure 6.6 shows the phase-resolved partial discharge data pattern for one of the data acquisitions of cable sample C-1. The acquisition considers 5000 partial discharge pulses and is conducted at 1.25 the inception voltage after preconditioning. Each partial discharge pulse in Figure 6.6 is represented by two values. For example, the partial discharge pulse A in Figure 6.6 is represented in the phase-resolved data pattern by the phase value (approximately 260 degrees) and the partial discharge magnitude (180 pC or 140 mV), which can be expressed in mV or pC.

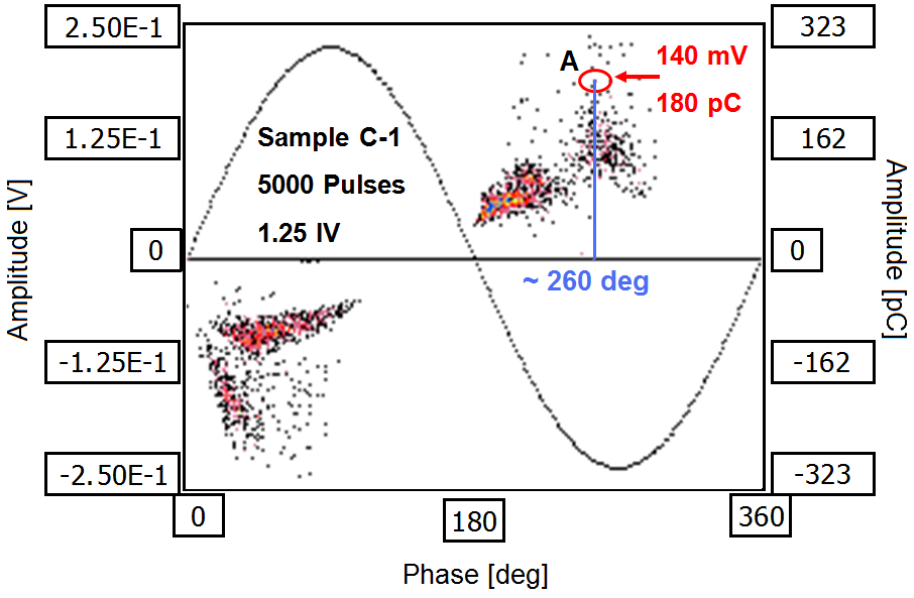

Figure 6.6. One partial discharge data acquisition for cable sample C-1.

Because each data capture, as shown in Table 6.2, has four data acquisitions (two

at 1.25 and two at 1.50 the inception voltage after preconditioning), a total of 32 data acquisitions for each cable sample and 16 data acquisitions for each joint sample are considered. Each data acquisition is represented in the same manner as shown in Figure 6.6.

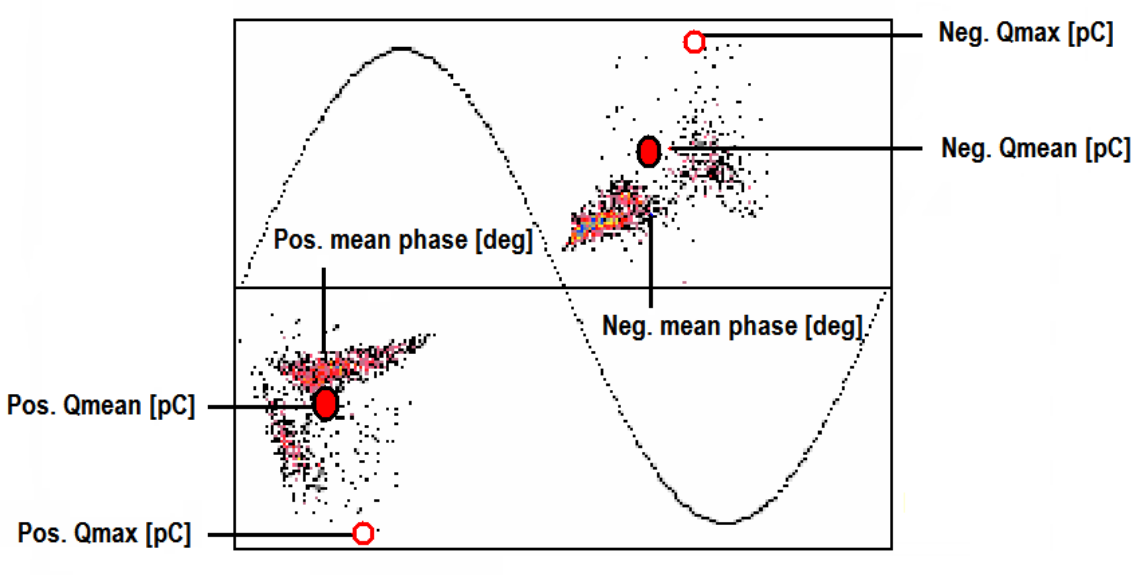

Figure 6.7. Basic partial discharge diagnostic features from phase-resolved data.

There is no question that a considerable number of features can be obtained from each data acquisition using statistical tools. However for illustration and brief analysis, six basic partial discharge features that can be easily obtained from the phase-resolved partial discharge data pattern are shown in Figure 6.7, which is the same as Figure 6.6. The features are as follows:

- **Pos. mean phase**: Mean partial discharge phase for the positive polarity of the test voltage.
- **Pos. Qmean**: Mean partial discharge magnitude for the positive polarity of the test voltage.

- **Pos. Qmax**: Maximum partial discharge magnitude for the positive polarity of the test voltage.
- **Neg. mean phase**: Mean partial discharge phase for the negative polarity of the test voltage.
- **Neg. Qmean**: Mean partial discharge magnitude for the negative polarity of the test voltage.
- **Neg. Qmax**: Maximum partial discharge magnitude for the negative polarity of the test voltage.

As each data acquisition is characterized by a set of six diagnostic features, a total of 32 sets of features for the cable samples and 16 sets for the joint samples are considered. A description of additional features obtained from the phase-resolved partial discharge data pattern is shown in Chapter 7. The additional features in conjunction with the six features previously described are used for the analysis and evaluation processes.

A convenient way to represent and briefly analyze the different features for the different cable and joint samples is the use of box plots. In descriptive statistics, box plots are a method for graphically representing groups of numerical data through their five-number descriptors [88]. The descriptors are the smallest value (0 % of the data), lower quartile (25 % of the data), median (50 % of the data), upper quartile (75 % of the data), and largest value (100 % of the data). Box plots can be useful to display differences between groups without making any assumptions of the underlying statistical distribution. The spacings between the different parts of the box help indicate the degree of dispersion (spread) and skewness in the data.

Figure 6.8 shows the box plot of the laboratory measurements mean partial discharge magnitude by sample and test voltage polarity. In particular, two of the six features previously described are shown in Figure 6.8, they are the Pos. Qmean and the Neg. Qmean.

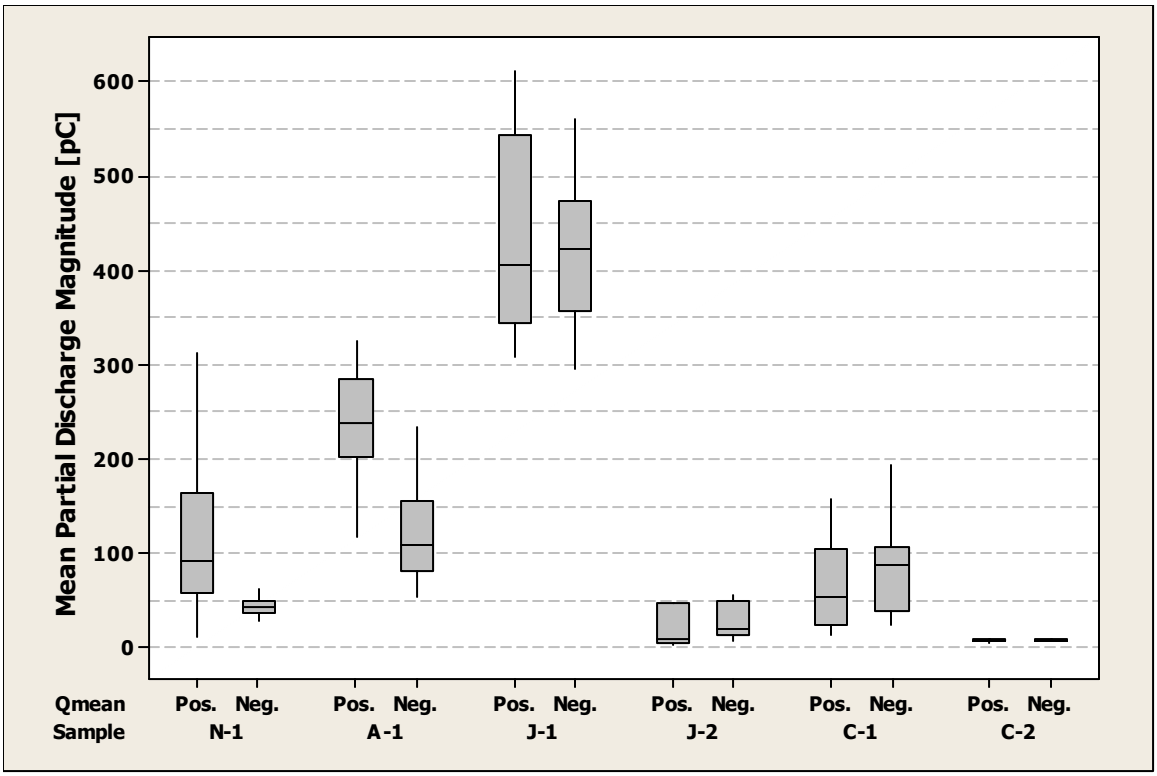

Figure 6.8. Box plot of laboratory measurements mean discharge magnitude by sample and test voltage polarity.

As seen in Figure 6.8, the difference between features for the same sample and between samples is easily observable. For example, the mean partial discharge magnitude for the positive polarity of the test voltage for sample N-1 has much more variability than the mean discharge magnitude for the negative polarity of the test voltage. The variability is related to how the particular feature changes over the 32 data acquisitions for sample N-1. In contrast, it can also be observed in Figure 6.8 that the changes and differences between the features are minimal for sample C-2 as the box plot descriptors are all the same. In Figure 6.8 the two test voltage levels of 1.25 and 1.50 of the inception voltage after preconditioning are considered together.

However, the main goal of the laboratory test program is to study the differences between partial discharge measurements between cable system components, *i.e.* cable

and accessories. Therefore, the laboratory partial discharge data is grouped as partial discharge data from cables and partial discharge data from accessories. In this case, samples C-1, C-2, and N-1 are part of the cable data group and samples J-1, J-2, and A-1 are part of the accessory group. A-1 is considered to be part of the accessory group because the artificial defect is introduced by a joint with metal filing in the middle length of the cable sample.

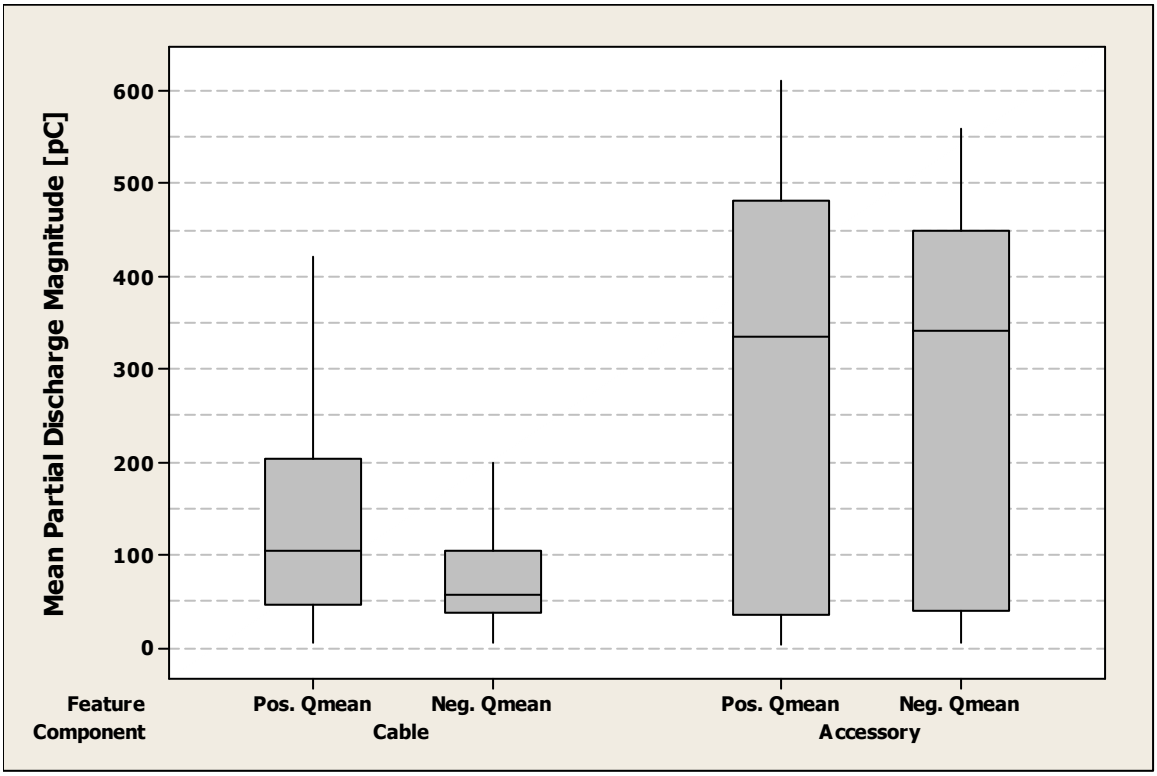

Figure 6.9. Box plot of laboratory measurements mean discharge magnitude by component and test voltage polarity.

Figure 6.9 shows the box plot for the mean partial discharge magnitude by component and test voltage polarity including again all test voltages. As seen in Figure 6.9, when the laboratory data is grouped as cable and accessory, the spread in the mean partial discharge magnitude is the smallest in cable for the negative polarity of the test

voltage. In addition, considerable difference is observed between the mean partial discharge magnitudes for cables by test voltage polarity while no major differences are observed between the mean discharge magnitudes for accessories by test voltage polarity. In addition, it is also observed that the median mean partial discharge magnitude is the biggest for accessories; however, the accessories also demonstrate the greatest variability or spread in their data.

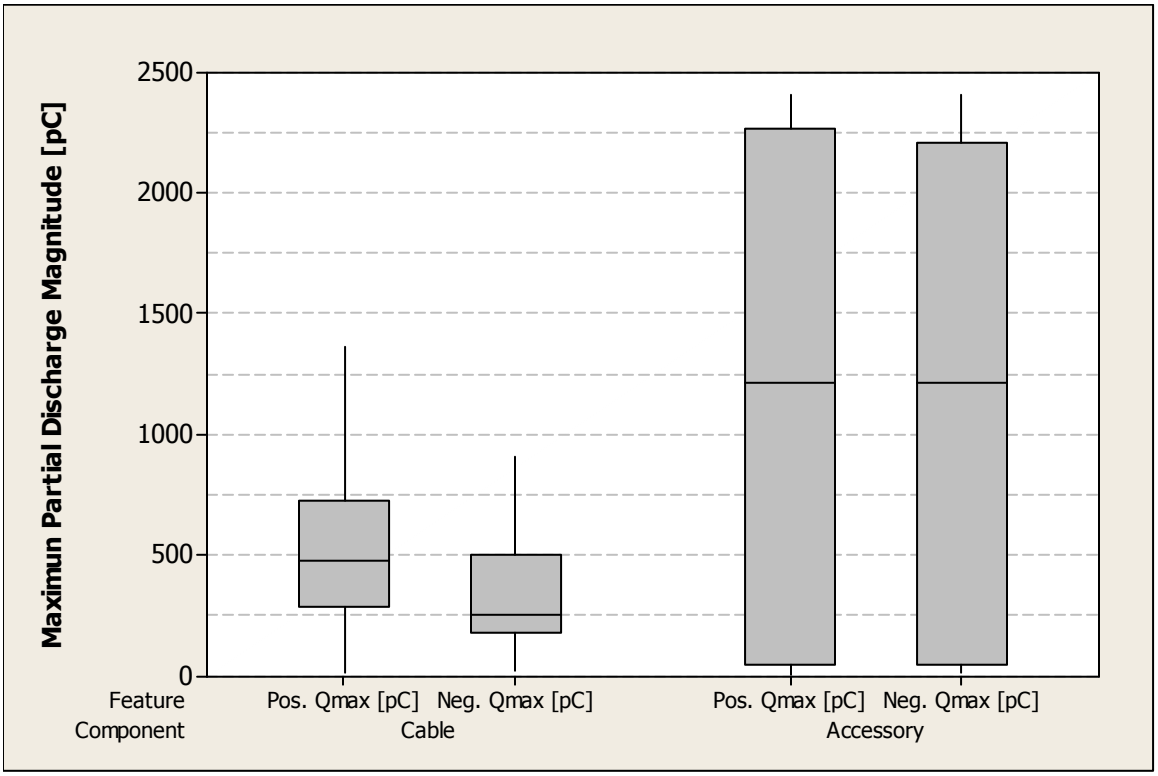

Figure 6.10. Box plot of laboratory measurements maximum discharge magnitude by component and test voltage polarity.

Figure 6.10 shows the box plot for the maximum partial discharge magnitude by component and test voltage polarity including all test voltage levels. In particular, the features Pos. Qmax and Neg. Qmax are shown in the figure. A similar behavior is observed for the maximum discharge magnitude features as compared to the mean

discharge magnitude features (*i.e.* Pos. Qmean and Neg. Qmean of Figure 6.9) in the sense that the spread in the maximum partial discharge magnitude is the smallest in cable for the negative polarity of the test voltage and that considerable difference is observed between the maximum partial discharge magnitude for cables by test voltage polarity while no major difference is observed between the maximum discharge magnitudes for accessory by test voltage and polarity.

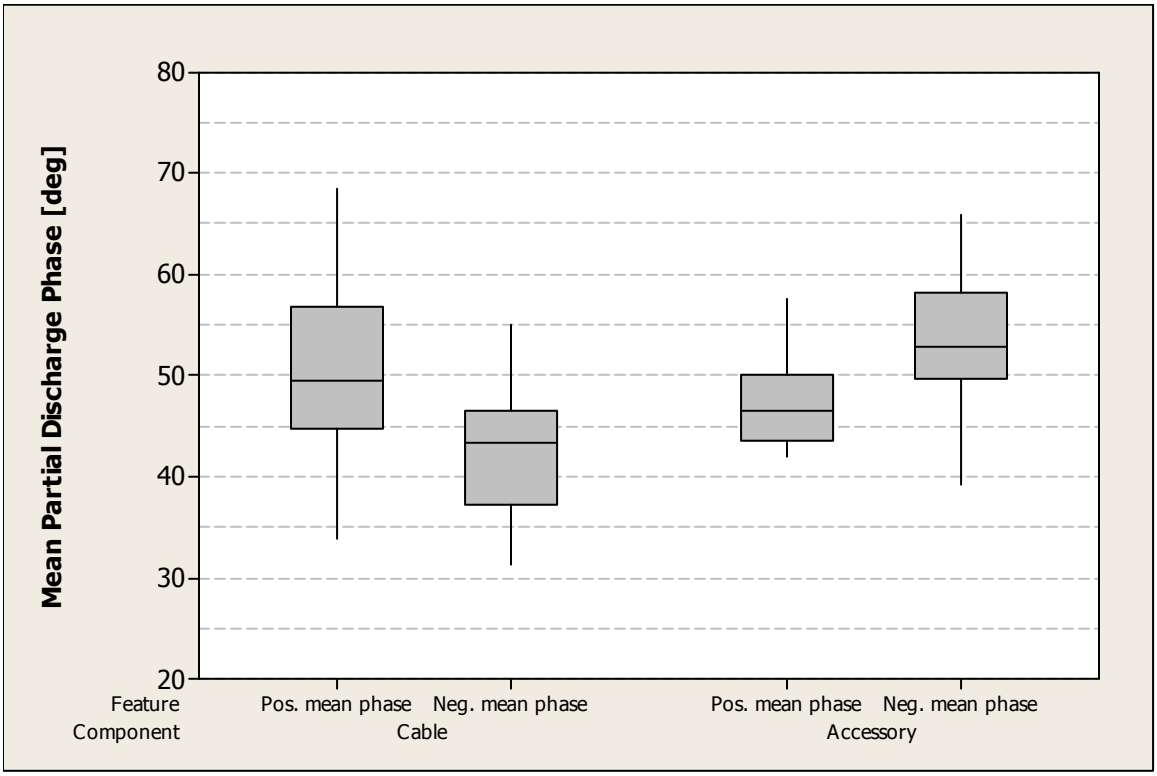

Figure 6.11. Box plot of laboratory measurements mean discharge phase by component and test voltage polarity.

In addition, Figure 6.11 shows the box plot for the mean discharge phase by component and test voltage polarity. The features Pos. mean phase and Neg. mean phase are shown in the figure. In this case, it is observed that the biggest spread in the mean phase is for cables in the positive polarity of the test voltage. Note also that generally, the

mean phase is lower for the negative polarity of the test voltage for the cable group while the contrary is observed for the accessory group, *i.e.* the mean phase is generally lower for the positive polarity compared to the negative polarity of the test voltage.

6.9.2 Field Partial Discharge Data

This section describes and presents a basic analysis of the partial discharge field data. The data have been provided to the author by one of the utilities participant of the CDFI project. The data are based on 25 partial discharge locations of an XLPE-15 kV cable system installed in the early 1970s. The tests have been performed from 1.3 to 2.5 U_0, were U_0 is the system operating voltage (7.2 kV). The data are balanced between cable system components, *i.e.* 51 % of the data correspond to partial discharge located in cable while 49 % correspond to partial discharge located in accessories; specifically, 35 % located in terminations and 14 % located in joints.

Figure 6.12 shows the phase-resolved patterns for the field partial discharge data considering the 25 partial discharge locations, each color and marker in the figure represent a different partial discharge location. In Figure 6.12, the absolute magnitude of the partial discharge is plotted for both polarities and all levels of the test voltage are considered.

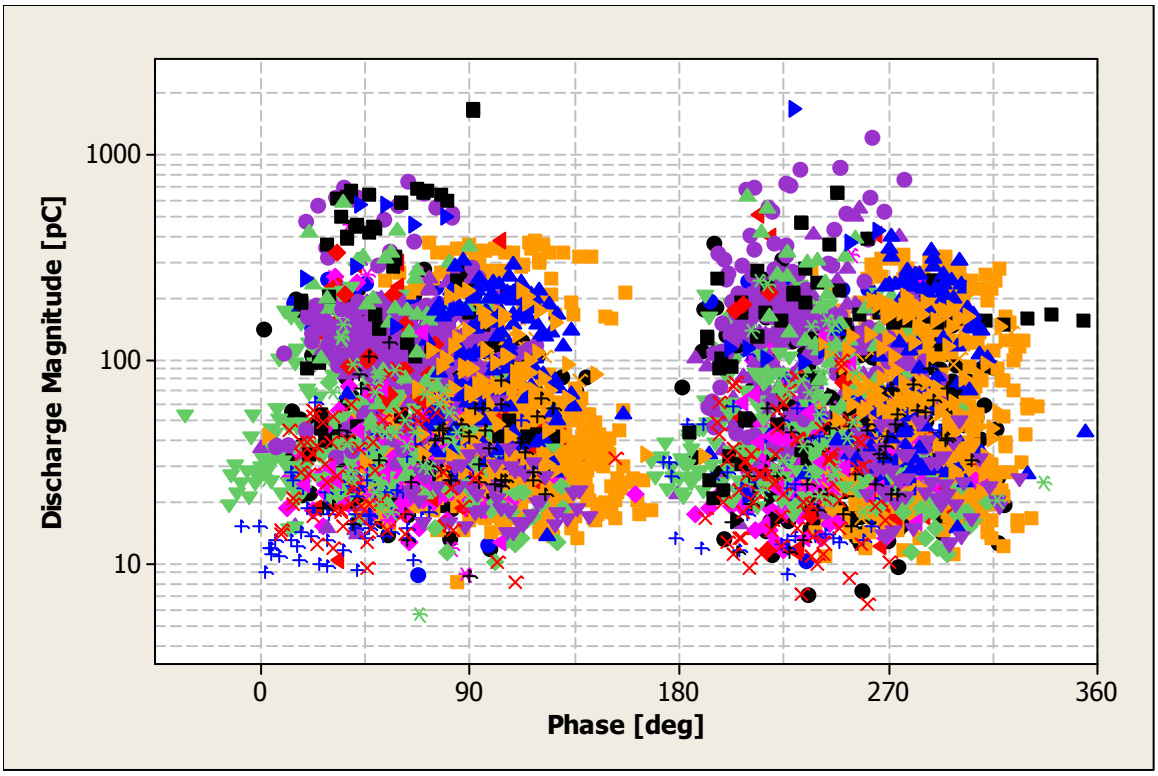

Figure 6.12. Phase-resolved patterns for the field partial discharge data.

The cumulative density functions of the partial discharge magnitude from the phase-resolved patterns by system component are presented in Figure 6.13. Similar to the laboratory data, the field data are classified by component and test voltage polarity. As seen in the figure, in general partial discharge in cables is the lowest, partial discharge in joints is the highest, and partial discharge in terminations is in between cable and joint. In addition, a similar behavior is observed between the partial discharge magnitudes for the different components for the positive and negative polarities of the test voltage.

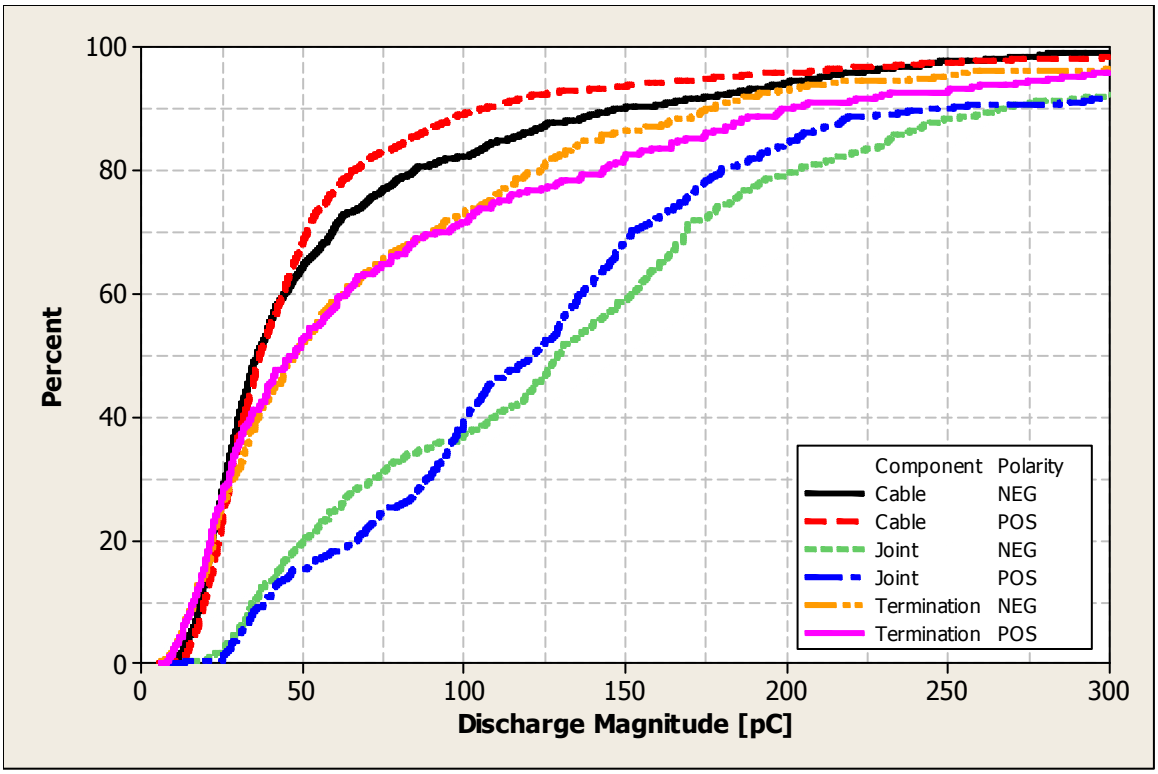

Figure 6.13. Discharge magnitude cumulative density functions by component and test voltage polarity.

The partial discharge field data can also be visualized by using a box plot. Figure 6.14 shows the box plot for the partial discharge magnitude for the field data by cable system component. It can be observed in Figure 6.14 that the lowest spread is for cable while the highest spread is observed for joints for both polarities of the test voltage. It can also be observed in Figure 6.14 (similarly to the results from Figure 6.13) that in general, the partial discharge in cables is the lowest while the partial discharge in joints is the highest and partial discharge in terminations is in between cable and joint.

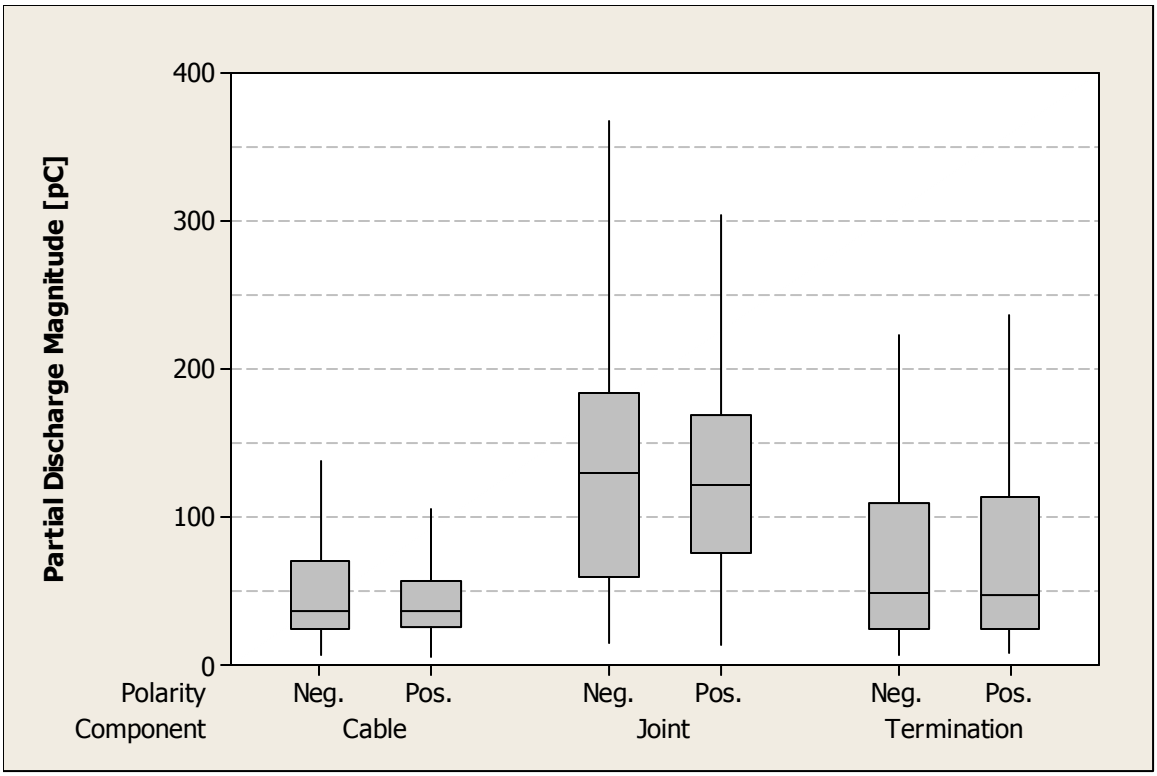

Figure 6.14. Box plot of discharge magnitude of field partial discharge data by component and polarity.

6.10 Summary and Conclusions

The Chapter has introduced the basic concepts, means of diagnosis, and limitations of partial discharge measurements. Brief descriptions of the available partial discharge data, feature extraction, and classification tools, have also been introduced. A comprehensive literature review on the "state of the art" on characterization of defects by partial discharge measurements has been presented.

Moreover, the Chapter has described and briefly analyze laboratory and field partial discharge data that are the basis for the evaluation and analysis of partial discharge diagnostic features presented in Chapter 7. The data are based on the phase-resolved partial discharge pattern and are classified into two groups, *i.e.* partial discharge in cable and partial discharge in accessory. The laboratory partial discharge data have been

measured by the author while the data from partial discharge field tests have been provided to the author by one of the utilities participant of the CDFI project.

CHAPTER 7

ANALYSIS AND EVALUATION OF PARTIAL DISCHARGE DIAGNOSTIC FEATURES

7.1 Introduction

The partial discharge phase-resolved data pattern, the main focus of this Chapter, can provide a wide range of diagnostic features that could correlate well with the nature of the partial discharge defects. The set of features form a feature vector or fingerprint that can be used to classify the partial discharge data into groups. In this work, the set of partial discharge diagnostic features is used to identify whether the partial discharge is from cable or accessory, this is a classification problem in which the goal is to use the set of partial discharge diagnostic features for the classification.

Once the set of diagnostic features has been established, there is the issue of the relevance of the features. In other words, which features have the most discriminating properties for the classification. The determination of the feature relevance is an analysis and evaluation process. Such an analysis and evaluation could lead to a reduced number of features with clearer physical meaning and effectiveness; thus, resulting in a better understanding of the partial discharge.

Therefore, this Chapter presents a process for finding a robust set of partial discharge diagnostic features, disregarding the unnecessary features, and considering partial discharge data into groups of cable and accessory. The process is divided into two portions, *i.e.* an initial analysis and a final evaluation of the partial discharge diagnostic features. The main goal of the Chapter is to show a methodology which is able to determine a suitable set of partial discharge diagnostic features that could enhance the classification. The features are analyzed using data, which have been described in Chapter 6, obtained from laboratory experiments and field tests.

The initial analysis portion of the process takes advantage of the hierarchical structure and taxonomy of the partial discharge diagnostic features by performing the cluster variable analysis of the diagnostic features. The cluster variable analysis provides a feature selection by disregarding unnecessary features that carry similar information.

The evaluation portion of the process is accomplished by performing the recursive feature elimination (RFE) of the partial discharge diagnostic features that are the result of the initial cluster variable analysis. The RFE provides a tool for ranking the partial discharge diagnostic features by taking into account the classification potential of each diagnostic feature compared to others.

Results reveal that different types of diagnostic features have to be used in order to achieve an appropriate level of dissimilarity between diagnostic features and good classification performance.

7.2 Motivation

Earlier research work conducted in the CDFI project [89] has shown that the two "traditional" partial discharge diagnostic features, *i.e.* partial discharge magnitude and inception voltage, are not sufficient to characterize partial discharge sites that eventually fail after a number of years after testing. There is no question that, this finding raises a number of questions, which are as follows:

1. If the two "traditional" partial discharge diagnostic features are not sufficient; approximately how many diagnostic features are needed?
2. What are the sorts of partial discharge diagnostic features that would be required?
3. If additional partial discharge diagnostic features are considered for classification of partial discharge data; how good might the classification be?
4. Which partial discharge diagnostic features are the most significant?

The work reported in this Chapter addresses questions 1 to 4 above. To address these questions partial discharge diagnostic features from laboratory and field partial discharge data are analyzed and evaluated. The analysis and evaluation process allows for the determination of a suitable set of partial discharge diagnostic features giving answer to the previous questions. The analysis and evaluation process is explained and results are shown in the following subsections.

7.3 Analysis and Evaluation Process of Partial Discharge Diagnostic Features

The analysis and evaluation process of partial discharge diagnostic features is shown in the flowchart of Figure 7.1. As shown in Figure 7.1, the analysis and evaluation process starts by considering an initial set of partial discharge diagnostic features derived from the phase-resolved partial discharge data pattern.

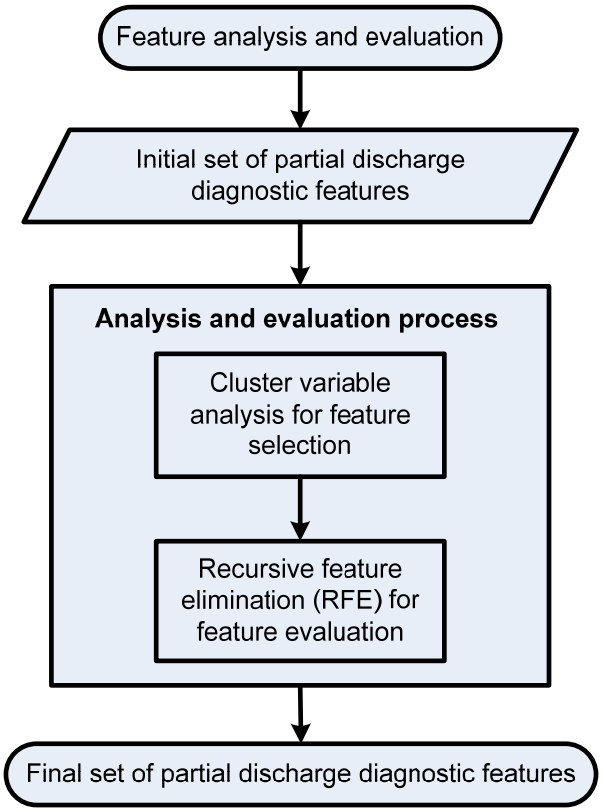

Figure 7.1. Analysis and Evaluation procedure of partial discharge diagnostic features.

Particularly, the analysis portion of the process is accomplished by performing a cluster variable analysis of the partial discharge diagnostic features while the evaluation portion of the process is accomplished by performing an innovative feature evaluation method named recursive feature elimination (RFE).

The cluster variable analysis is used to reduce the number of the initial set of available partial discharge diagnostic features; thus, the cluster variable analysis can be seen as an initial filter method that is used to select a subset of diagnostic features in terms of criterion functions that take into account the taxonomy between the diagnostic features and are independent of classification groups or type of classifier if an eventual classification problem is to be performed.

Once the initial set of partial discharge diagnostic features has been reduced by the cluster variable analysis, the RFE provides a tool to rank the diagnostic features by taking into account the classification potential of each diagnostic feature compared to others for groups in the data as cable or accessory. Descriptions of the cluster variable analysis and RFE are shown in the next subsections.

7.3.1 Cluster Variable Analysis

One of the problems present when considering a large number of partial discharge diagnostic features is how to organize them into meaningful structures, *i.e.* to develop taxonomies. For example, before a meaningful description of differences between animals is possible, biologists have to organize the different animal species into groups or clusters. In the case of the partial discharge diagnostic features the organization can be accomplished by performing a cluster variable analysis of the features.

Researchers have typically used cluster variable analysis to process the individual partial discharge measurements [76, 90-92]. In this research a different and novel approach is used, whereby the features, not the measurements, are clustered. As mentioned in the previous section, the cluster variable analysis of the partial discharge

diagnostic features is the first part of the analysis and evaluation procedure.

Cluster variable analysis [93] is useful because it identifies key variables that explain the principal dimensionality of the data. It is used to classify the data into groups when the groups are initially unknown. One important reason to cluster variables may be to reduce their number; but more importantly, clustering variables is used in this research to understand their taxonomy and meaning of the partial discharge diagnostic features. This technique may identify new variables that are more intuitively understood than those found using principal components analysis since no mathematical transformations are applied to the data.

The analysis is an agglomerative hierarchical method that begins with a separate treatment of all features, each forming its own cluster. In the initial step, the two features closest together are joined. In the next step, either a third feature joins the first two (now considered as a stand-alone cluster), or to another feature is joined with a different cluster. This process continues until all clusters are joined into one. The complete procedure, from the initial cluster variable analysis to the final feature selection, is explained in steps later in the section.

The agglomerative hierarchical method uses the distances between variables when forming the clusters. These distances are based on a single dimension that uses the absolute Pearson correlation coefficient between features [93]. The correlation coefficient can be translated to a level of similarity between clusters. The level of similarity can be used as a tool to compare the relationship between features or clusters.

The similarity level between two features or clusters, *e.g.* features or clusters *i* and *j*, is given by equation (7.1),

$$S_{ij} = \frac{100(1 - d_{ij})}{d_{\max}}, \tag{7.1}$$

where,

S_{ij}: Similarity level between features or clusters i and j,

d_{ij}: distance measure between features or clusters i and j, based on the absolute Pearson correlation coefficient,

$d_{\max}$: Maximum distance between the initial set of features before starting the clustering procedure.

The interpretation of the level of similarity is quite straight forward. The level of similarity is a number that ranges from 0 to 100 %. A similarity level around 100 % indicates that the features or clusters under investigation are redundant, *i.e.* they carry essentially the same information. In other words, the features or clusters are highly correlated; thus, they can be seen as not adding much to solving an eventual classification problem. In contrast, a level of similarity around 0 % indicates that the features or clusters under investigation are complimentary or uncorrelated. Thus, the likelihood of using these features or clusters in an eventual classification problem with good classification results is higher than using redundant features or clusters.

There are several algorithms available for the clustering of the partial discharge diagnostic features and each of them may yield to different results [75, 93]. However, in this research, the group average and the furthest neighbor methods are used in the cluster variable analysis of the partial discharge diagnostic features. Specifically, the group average method is used in the agglomerative procedure during clustering while the furthest neighbor method is used in the feature selection. The final clusters and partial discharge features are determined as follows:

1. Initially each feature is declared as a cluster and all distances between clusters are calculated.
2. Two clusters with the smallest distance between them are fused together and declared to be a new cluster. This is the beginning of the agglomerative process.

3. All distances between clusters are again calculated and the agglomerative process continues until the number of clusters is one. The group average method is used to calculate the average distance between clusters.
4. Once one cluster is left, the number of clusters to be considered for the final feature selection is determined by choosing a similarity level.
5. For each final cluster, the feature that has the furthest distance to other clusters is selected to represent its cluster in the RFE process. This is the application of the furthest neighbor method that yields to the feature selection as the result of the cluster variable analysis.

The results of the clustering procedure can be represented graphically in a tree-like plot, also known as a dendrogram plot. The dendrogram plot for the cluster variable analysis represents the features under analysis on the *x*-axis and the level of similarity between features and clusters on the *y*-axis. The clusters are represented by vertical and horizontal lines between the features.

Determining the number of clusters for the final feature selection can be termed as "cutting the dendrogram". Cutting the dendrogram is akin to drawing a line across the dendrogram to specify the final grouping at a particular similarity level. There is no pre-established procedure on choosing the similarity level for cutting the dendrogram; however, the pattern of how similarity or distance values change from step to step in the agglomerative procedure can help in choosing the final grouping. Therefore, the step where the number of cluster changes abruptly may be a good starting point for cutting the dendrogram. The final point for cutting the dendrogram is usually given by the physical sense of the taxonomy of the data, *i.e.* the final point is determined by the lowest similarity level at which the features can be clustered keeping their taxonomy. Results of the cluster variable analysis for both, laboratory and field partial discharge data, are presented in next subsections.

7.3.2 Recursive Feature Elimination (RFE)

Once the initial set partial discharge diagnostic features is reduced by performing the cluster variable analysis, there is the question of which of the features are more relevant if there are used in a classification problem. The answer to the question can be provided by an evaluation process of the partial discharge diagnostic features. The evaluation process is accomplished here by the use of the RFE algorithm based on support vector machines (SVM) classifier [94]. The basis of the partial discharge diagnostic feature evaluation procedure can be seen in Figure 7.2.

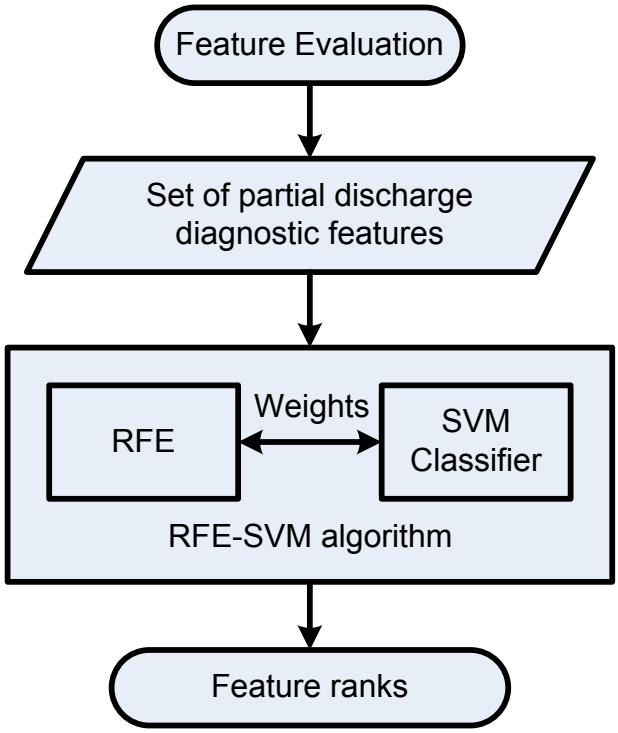

Figure 7.2. Basis of the partial discharge diagnostic features evaluation procedure.

In Figure 7.2, the evaluation procedure of the partial discharge diagnostic features begins by considering the set of partial discharge diagnostic features resulting from the cluster variable analysis. The procedure is performed by a RFE algorithm based on a

SVM classifier with a linear kernel. The results from the evaluation procedure are ranks for each partial discharge diagnostic feature. The rank is based on the potential of each diagnostic feature to classify the data between the groups of cable or accessory when all the features are considered together in the classification problem. A description of the RFE algorithm based on a SVM classifier with a linear kernel is shown in the next paragraphs.

The RFE algorithm based on SVM for feature evaluation has been proposed in [94] to conduct gene selection for cancer classification. In the algorithm, nested subsets of features are selected in a sequential backward elimination manner, which starts with all the features and removes one feature at a time. At each step, the coefficients of the weight vector **w** of a SVM with a linear kernel are used to compute the feature ranking score. The diagnostic feature, *e.g.* feature *i*, with the smallest ranking score $c_i=w_i^2$ is eliminated, where w_i represents the corresponding component in the weight vector **w** to the feature *i*. Using $c_i=w_i^2$ as the feature ranking score corresponds to removing the feature whose removal changes the performance of the SVM classifier the least [95]. In other words, the RFE algorithm seeks to improve generalization performance in the classification problem by removing the least important feature at the time whose deletion will have the least effect on training errors of the SVM.

The RFE algorithm based on SVM with linear kernel for feature evaluation is implemented as follows:

1. Start with the set of ranked features as $\boldsymbol{R}$:{Φ} and the set of partial discharge diagnostic features (from the cluster variable analysis) as $\boldsymbol{S}$:{*1, ..., i, ..., n*}.
2. Repeat steps a to e until all features are ranked:
    a. Train a SVM with linear kernel using the features in current set $\boldsymbol{S}$ as input variables.
    b. Determine the weight vector.

c. Based on the weights, compute the ranking scores for all the features in set $\boldsymbol{S}$ as $c_i=w_i^2$.

d. Find the feature with the smallest ranking score, *e.g.* feature *i*.

e. Update the set of ranked features as $\boldsymbol{R}$:{Φ,*i*} (*i.e.* adding feature *i* in the last position in the set $\boldsymbol{R}$) and the current set of partial discharge diagnostic features as $\boldsymbol{S}$:{*1, ..., i, ..., n*} – {*i*} (*i.e.* eliminating feature *i* from the set $\boldsymbol{S}$).

3. Output the ranked feature set $\boldsymbol{R}$.

Additional description of the RFE algorithm based on SVM considering overfitting to higher dimensional spaces with non-linear kernels and more than two classification groups can be found in [96].

7.4 Analysis and Evaluation of Partial Discharge Features from Laboratory Data

The laboratory data used here have been described in Section 6.9.1 of Chapter 6. Initial inspection of the partial discharge data provided by the measuring equipment shows that approximately 50 partial discharge diagnostic features are available for analysis and evaluation. They include features based on the phase-resolved data, time-resolved data, data without the phase or time information, inception and extinction voltages before and after preconditioning, fuzzy logic membership functions values, and test voltage as explained in detail in [28].

However, only a subset of the initially available features is selected for the analysis and evaluation process. The subset is selected on the basis of common diagnostic features obtained from the partial discharge phase-resolved data pattern, inception and extinction voltages and test voltage. A brief description of the initial set of features is presented in Table 7.1.

Table 7.1. Laboratory data partial discharge diagnostic features description.

No.	Name†	Description
1	Pos. Qmean [V]	Mean discharge magnitude
2	Pos. Qmax [V]	Maximum discharge magnitude
3	Pos. Qmean [pC]	Mean discharge magnitude
4	Pos. Qmax [pC]	Maximum discharge magnitude
5	Pos. Mean Phase [deg]	Mean phase
6	Pos. Phase Range [deg]	Phase range
7	Pos. Mean Energy [pC*V]	Mean energy
8	Pos. Max Energy [pC*V]	Max energy
9	Pos. Alpha Amp. Dist.	Amplitude shape parameter (Weibull)
10	Pos. Beta Amp. Dist.	Amplitude scale parameter (Weibull)
11	Pos. Skewness Amp. Dist.	Skewness of the magnitude distribution
12	Pos. Skewness Ph. Dist.	Skewness of the phase distribution
13	Neg. Qmean [V]	Mean discharge magnitude
14	Neg. Qmax [V]	Maximum discharge magnitude
15	Neg. Qmean [pC]	Mean discharge magnitude
16	Neg. Qmax [pC]	Maximum discharge magnitude
17	Neg. Mean Phase [deg]	Mean phase
18	Neg. Phase Range [deg]	Phase range
19	Neg. Mean Energy [pC*V]	Mean energy
20	Neg. Max Energy [pC*V]	Max energy
21	Neg. Alpha Amp. Dist.	Amplitude shape parameter (Weibull)
22	Neg. Beta Amp. Dist.	Amplitude scale parameter (Weibull)
23	Neg. Skewness Amp. Dist.	Skewness of the magnitude distribution
24	Neg. Skewness Ph. Dist.	Skewness of the phase distribution
25	D	Symmetry factor, positive over negative number of pulses
26	Nw [pulses/cycle]	Average number of pulse per period
27	Mean Energy Ratio	Ratio of the positive mean energy and the negative mean energy
28	IV Before[kV]	Inception voltage before preconditioning
29	IV After [kV]	Inception voltage after preconditioning
30	EV Before [kV]	Extinction voltage before preconditioning
31	EV After [kV]	Extinction voltage after preconditioning
32	Voltage [kV]	Test voltage
†: Pos. and Neg. refer to the positive and negative polarities of the test voltage respectively		

As seen in Table 7.1, a significant number of types of partial discharge diagnostic features are considered for the analysis and evaluation process. The features include typical partial discharge diagnostic features such as discharge magnitude and inception and extinction voltages in addition to other features that are available due to the capabilities of modern partial discharge acquisition equipment.

The dendrogram for the cluster variable analysis of the 32 partial discharge diagnostic features of Table 7.1 is shown in Figure 7.3. In this case, all the partial discharge data is considered together for the two test voltages levels of 1.25 and 1.50 times the inception voltage after preconditioning as mentioned previously in Chapter 6.

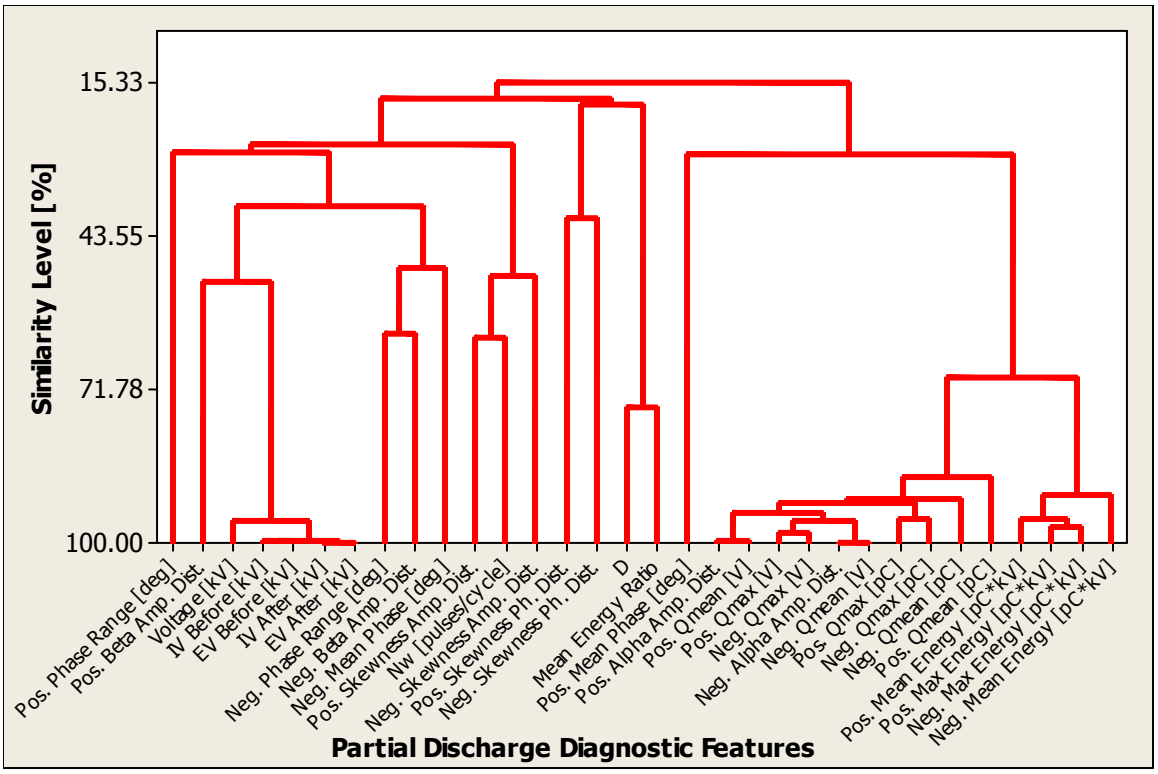

Figure 7.3. Dendrogram for the 32 partial discharge diagnostic features of laboratory data.

The dendrogram of Figure 7.3 displays the results of the tree clustering procedure and suggests features which might be combined. The features can be combined by averaging or totaling. In other words, it identifies groups whose features share common characteristics. In this case, the inception and extinction voltages before and after preconditioning are similar. High levels of similarity are also observed between the discharge magnitudes in pC and V as well the level between the mean and maximum levels of energy. On the other hand, low levels of similarity are observed between the positive phase range and the positive mean phase and the other clusters of features.

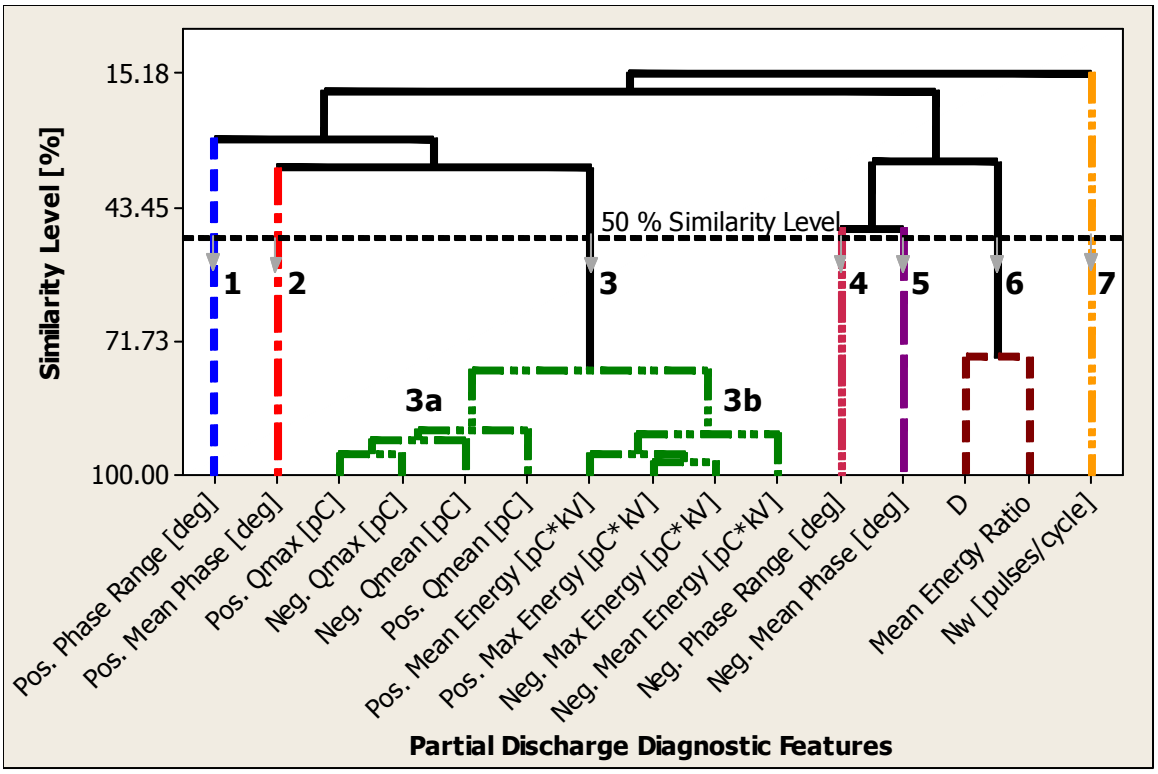

Figure 7.4. Dendrogram for the reduced set of 15 partial discharge diagnostic features.

Because of the large number of diagnostic features in Figure 7.3, the analysis of the dendrogram is quite complicated. Thus, for further analysis, the number of features is reduced to a more manageable number. For example, features such as testing voltage, and inception and extinction voltages before and after preconditioning are removed from further analysis since they depend on the geometry of the defect. The dendrogram for the reduced set of 15 features is shown in Figure 7.4.

As seen in Figure 7.4, the mean and maximum charge magnitudes contain very similar information (cluster 3a) and they can constitute a separate cluster. The same situation is also observed for the energies (cluster 3b) as well as the symmetry factor (D) and mean energy ratio (cluster 6). Note that the clusters formed by the charge magnitudes and energy levels can be also combined into one cluster (cluster 3) when comparing their similarity level with the other diagnostic features. The remaining question is how to

determine the final reduced clusters of variables.

The final grouping of variable clusters can be termed “cutting the dendrogram”. Cutting the dendrogram is akin to drawing a line across the dendrogram to specify the final grouping at a particular similarity level. As mentioned before, the similarity level at which the number of variables changes abruptly may be a good point for cutting the dendrogram. In Figure 7.4, the similarity level chosen for the final partition or feature selection is 50 %. The result of cutting the dendrogram at the 50% similarity level is shown in Table 7.2. As seen in Table 7.2, the initial set of 32 variables from Table 7.1 can be reduced to 7 clusters. Clusters 1, 2, 4, 5, and 7 have only one component as feature. In contrast, cluster 3 is formed by the features regarding the discharge magnitudes and energies and cluster 6 is formed by the symmetry factor (D) and mean energy ratio.

Table 7.2. Cluster variable analysis results of laboratory data.

Cluster No.	Feature No. (Table 7.1)	Feature Name
1	6	Pos. Phase Range [deg]
2	5	Pos. Mean Phase [deg]
3	4	Pos. Qmax [pC]
	16	Neg. Qmax [pC]
	15	Neg. Qmean [pC]
	3	Pos. Qmean [pC]
	7	Pos. Mean Energy [pC*V]
	8	Pos. Max Energy [pC*V]
	20	Neg. Max Energy [pC*V]
	19	Neg. Mean Energy [pC*V]
4	18	Neg. Phase Range [deg]
5	17	Neg. Mean Phase [deg]
6	25	D
	27	Mean Energy Ratio
7	26	Nw [pulses/cycle]

The most important conclusion from the cluster variable analysis shown in Table

7.2 is that the analysis gives an indication of the type and number of partial discharge diagnostic features that should be used for partial discharge classification. For instance, the analysis indicates that the discharge magnitude and energy level, phase information, symmetry factor, mean energy ratio, and the average number of pulses per period should be considered separately when using them as partial discharge diagnostic features.

As mentioned before in Section 7.3.1, for each cluster in Table 7.2, the diagnostic feature that has the furthest distance to the other clusters is selected to represent its cluster in the subsequent evaluation process. In Table 7.2, the selected features in each cluster are highlighted in gray; the seven clusters provide seven different features for evaluation.

Once each cluster is represented by one feature, the evaluation portion of the process is performed. Specifically, Table 7.3 shows the results for the ranking of the partial discharge diagnostic features. The ranks are the results of the feature evaluation process using RFE. As seen in Table 7.3, the Pos. mean phase is the most important feature followed by the Neg. Phase Range, D (Symmetry Factor), Pos. Qmean, Neg. Mean Phase, Pos. Phase Range, and Nw (average number of partial discharge pulses per cycle) respectively.

Table 7.3. Results for the ranking of the partial discharge diagnostic features from laboratory data using RFE.

Feature Name	**Cluster No (Table 7.2)**	**Feature No (Table 7.2)**	**Feature Rank**
Pos. Phase Range [deg]	1	6	6th
Pos. Mean Phase [deg]	2	5	1st
Pos. Qmean [pC]	3	3	4th
Neg. Phase Range [deg]	4	18	2nd
Neg. Mean Phase [deg]	5	17	5th
D	6	25	3rd
Nw [pulses/cycle]	7	26	7th

To grasp the significance of the ranked partial discharge features in an easy to understand visual manner, Figure 7.5 shows the matrix image plot of the ranked partial discharge diagnostic features and component groups. In Figure 7.5, the columns 1 to 7 on the left represent the ranked partial discharge diagnostic features with 1 corresponding to the feature ranked as the first (Pos. mean phase) and 7 corresponding to the features ranked as the last (Nw) as shown in Table 7.3. The last column in Figure 7.5 represents the grouping by component. In the component column the accessory group is represented by the black color while the cable group is represented by the white color. The lines (rows) in the figure represent the different data points. The first 64 lines, starting from the top-down, are the data points that belong to the accessory group and the remaining 96 lines represent the data points that belong to the cable group.

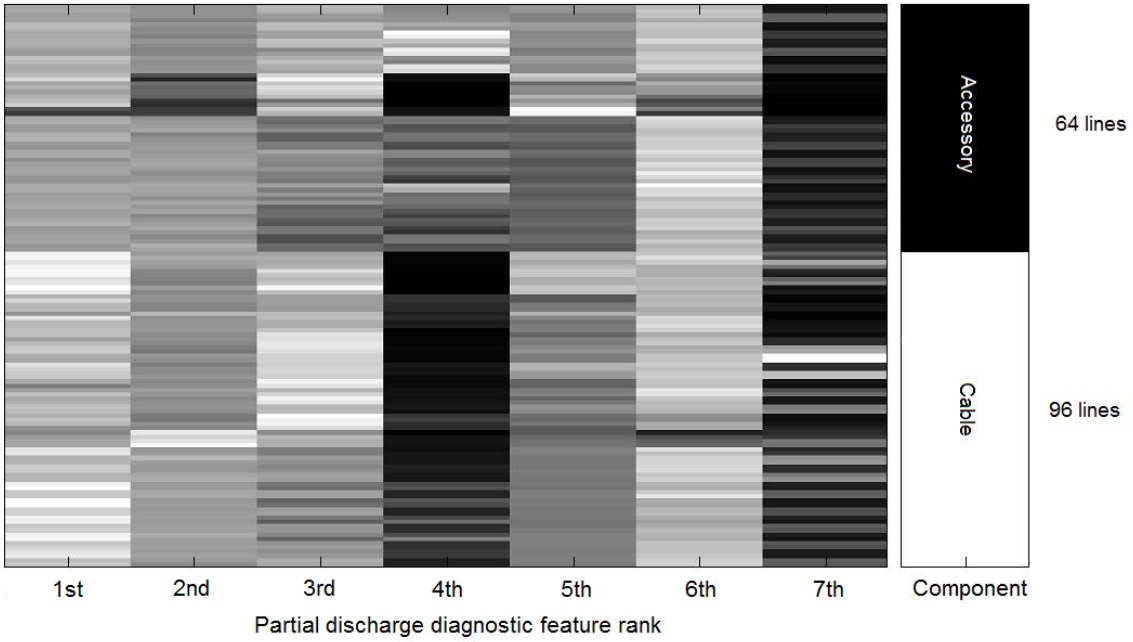

Figure 7.5. Matrix image plot of ranked partial discharge diagnostic features.

The two dimensional matrix image of Figure 7.5 is useful because it provides a

visual way of relating the ranked partial discharge diagnostic features to the grouping or component column. As seen in the figure, the features are ranked from the left to the right. The most relevant feature is at the extreme left column while the least relevant feature is at the right column just before the column representing the components grouping. The image is built using the features values as color reference for expression in a gray scale. The gray shading indicates the feature expression related to the classification groups. Specifically, the lighter the stronger the feature is correlated to the cable group and the darker the stronger the feature is correlated to the accessory group.

It can be seen in Figure 7.5 that the most relevant feature (Pos. mean phase) is also the most visually correlated with the component column in the sense that the feature expression is generally darker for the first 64 lines and generally lighter for the remaining 96 lines. In addition, it can also be observed in the figure that the least relevant feature (Nw) is also the least visually correlated with the component column in the sense that the feature expression generally alternates between dark and light for both component. These results are in accordance with the RFE results in the sense that the most visually relevant feature is ranked the first and the least visually relevant feature is ranked the last.

Another way to grasp the significance of the diagnostic feature relevance is by looking at the SVM classifier performance. The classifier performance, using the ranked features shown in Table 7.3, is presented in Table 7.4 and Figure 7.6. The classifier performance is assessed by the class loss in percent. The class loss is the total number of incorrectly classified data points for the cable and accessory groups over the total number of data points. Remember from Chapter 6 that 32 data points are considered for each cable sample (N-1, C-1, C-2, and A-1) and 16 data points are considered for each joint sample (J-1 and J-2). Therefore, a total of 160 data points (64 for the accessory group and 96 for the cable group) are considered in the evaluation process. A data point can be thought as one set of the seven diagnostic features used in the evaluation process each of which represents a phase-resolved pattern for each partial discharge data acquisition.

Table 7.4. Laboratory data SVM classifier performance using ranked features.

Ranked Feature Name	Class Loss (cable and accessory groups) [%]						
	19.70	15.50	9.80	0.00	0.00	0.00	0.00
1st - Pos. mean phase [deg]	×	×	×	×	×	×	×
2nd - Neg. Phase Range [deg]	-	×	×	×	×	×	×
3rd - D	-	-	×	×	×	×	×
4th - Pos. Qmean [pC]	-	-	-	×	×	×	×
5th - Neg. Mean Phase [deg]	-	-	-	-	×	×	×
6th - Pos. phase range [deg]	-	-	-	-	-	×	×
7th - Nw [pulses/cycle]	-	-	-	-	-	-	×

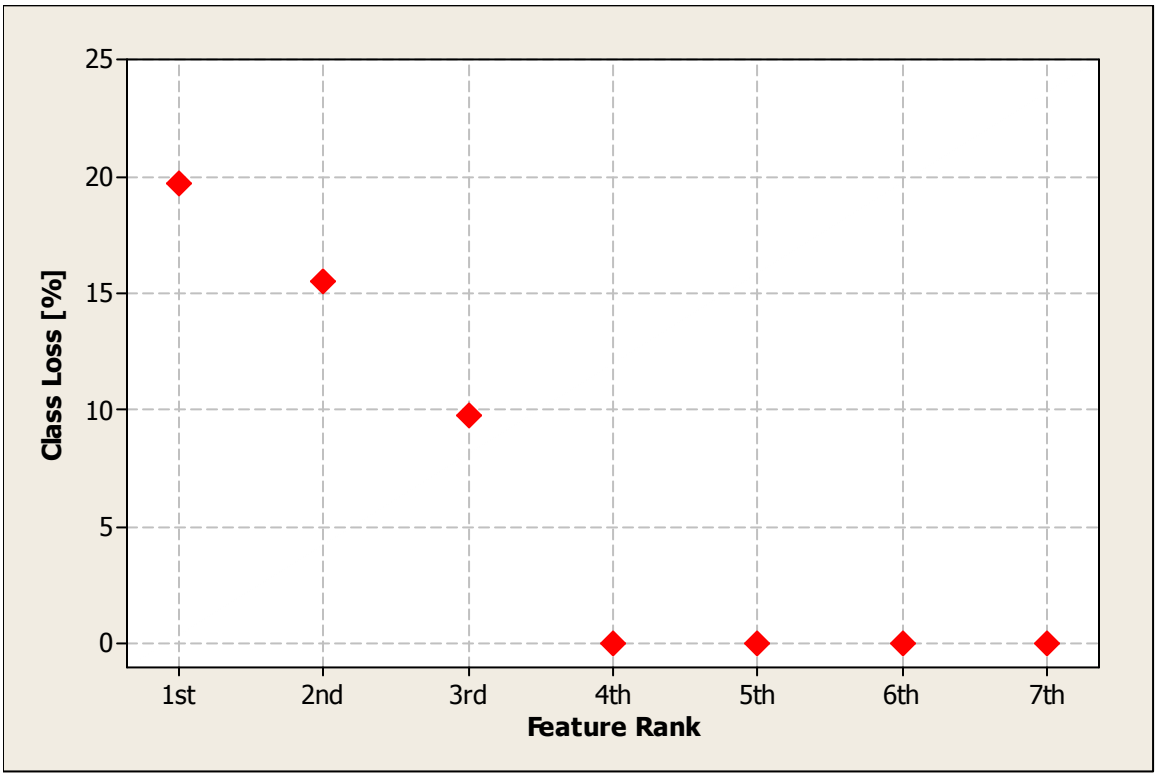

Figure 7.6. Class loss as function of feature rank for laboratory data.

As seen in Table 7.4 and Figure 7.6, the class loss for the SVM classifier when using the first ranked partial discharge diagnostic feature is 19.70 %. If the first and the second ranked features are used in the classification, the class loss improves to a value of

15.50 %. Similarly, if the first three ranked partial discharge features are used in the classification, the class loss also improves to a value of 9.80 %. Finally, if four or more of the ranked partial discharge features are used in the classification, the class loss becomes zero. In other words, the SVM with linear kernel is able to completely group the partial discharge data between the cable and the accessory groups with at least four of the seven ranked partial discharge diagnostic features. These results are significant in the sense that the analysis and evaluation process has allowed a reduction in the number of partial discharge diagnostic features from the initial set of 32 to 4 and having a complete separation between the component groups.

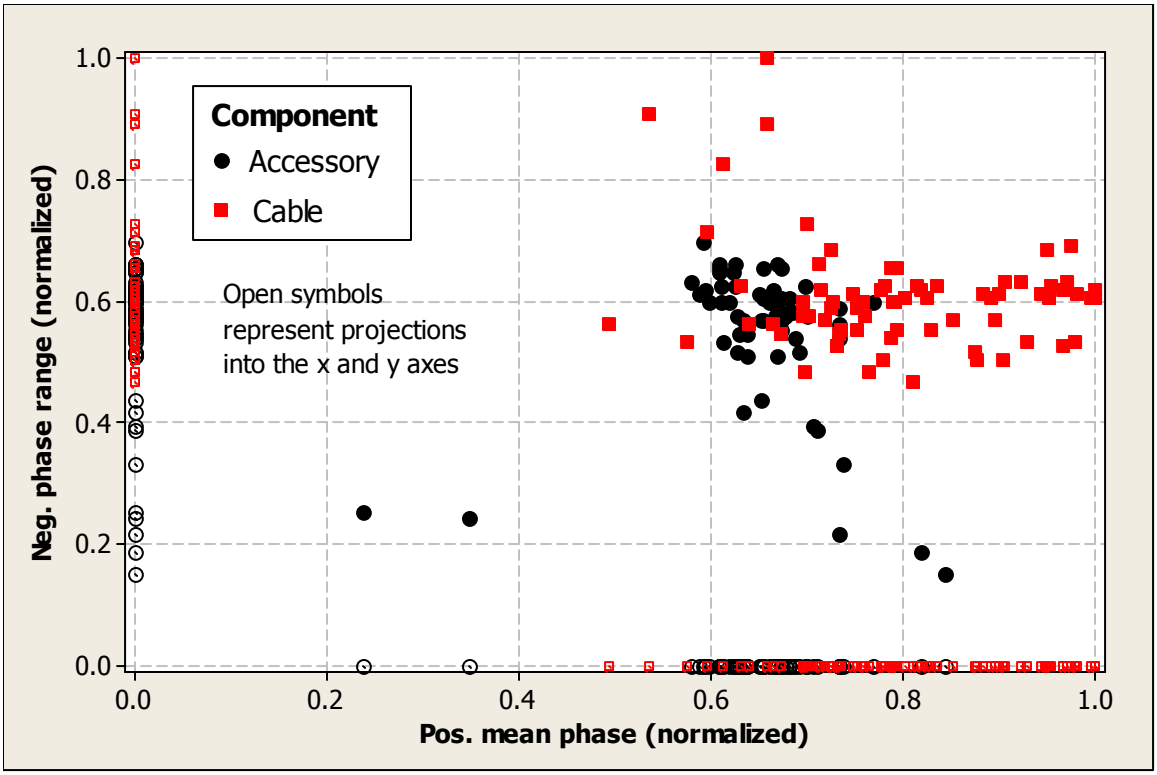

Figure 7.7. Two dimensional scatter plot by component considering the first two ranked partial discharge diagnostic features from the laboratory data.

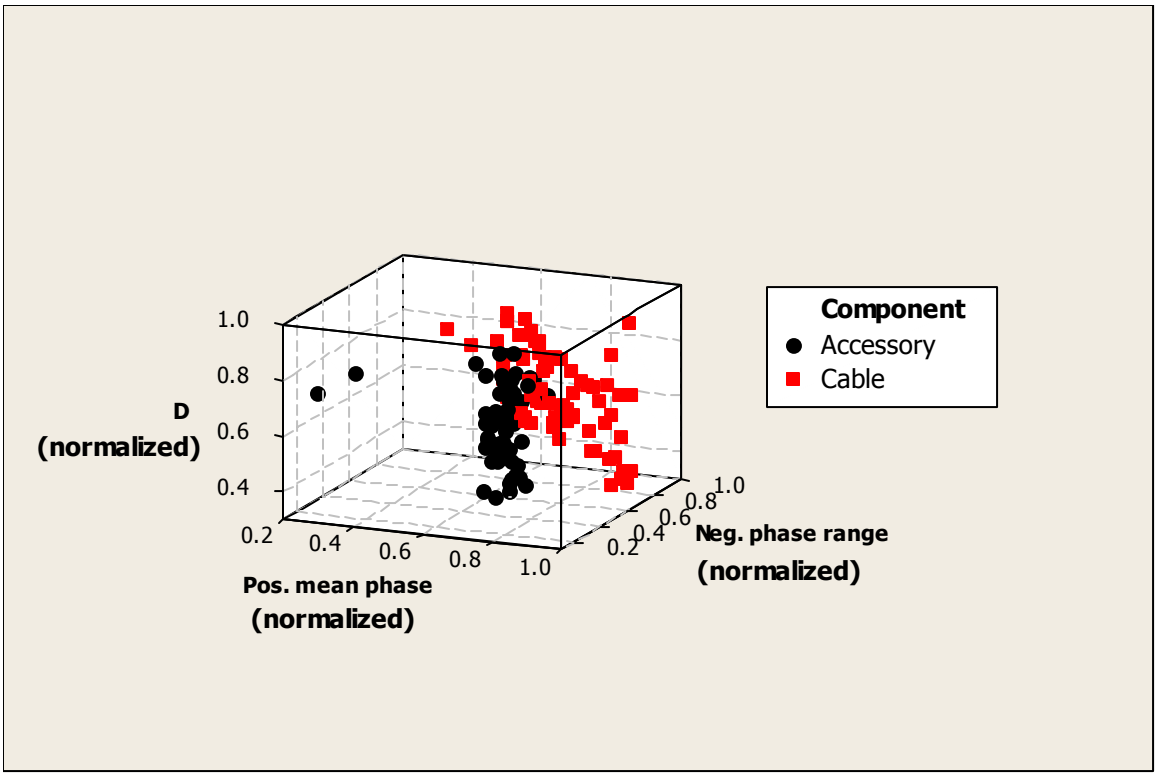

Figure 7.8. Three dimensional scatter plot by component considering the first three ranked partial discharge diagnostic features from the laboratory data.

To gain a better appreciation of the separation between the groups, Figure 7.7 shows a two-dimensional scatter plot by component considering the first two ranked partial discharge diagnostic features and Figure 7.8 shows a three-dimensional scatter plot by component considering the first three ranked partial discharge diagnostic features. In the plots, each feature has been normalized by its maximum value such that its values are in the range between zero and one.

If the group separation between Figure 7.7 and Figure 7.8 are visually compared, it is evident that a better separation is observed in Figure 7.8 in which three of the first ranked partial discharge features are used instead of the two partial discharge features of Figure 7.7. This result is expected since the class loss for the SVM classifier is 15.50 % corresponding to Figure 7.7 compared to 9.80 % corresponding to Figure 7.8.

7.5 Analysis and Evaluation of Partial Discharge Features from Field Data

The analysis and evaluation process of the partial discharge diagnostic features has also been applied to the partial discharge data obtained from field tests. The main goal in this section is to apply the analysis and evaluation process of partial discharge diagnostic features to a different set of features and compare its results with the results of the analysis and evaluation process shown in the previous section.

Particularly, the field partial discharge data used here has been described in Section 6.9.2 of Chapter 6. In this case, the initial inspection of the provided partial discharge data shows that a total of 57 partial discharge diagnostic features are available for the analysis and evaluation. The features are composed by test voltage, statistical descriptors of the partial discharge magnitude by test voltage polarity, statistical descriptors of the partial discharge phase by test voltage polarity, statistical descriptors of the partial discharge energy by test voltage polarity, symmetry factor, and partial discharge energy ratio. The description for each of the 57 partial discharge diagnostic features is shown in Table 7.5.

Table 7.5. Field data partial discharge diagnostic features description.

No.	Name†	Description
1	Voltage [U_0]	Test voltage
2	Neg. Mean Q [pC]	Mean discharge magnitude
3	Neg. Mean Phase [deg]	Mean phase
4	Neg. Mean Energy [pC*kV]	Mean energy
5	Neg. Stdv. Q [pC]	Discharge magnitude standard deviation
6	Neg. Stdv. Phase [deg]	Phase standard deviation
7	Neg. Stdv. Energy [pC*kV]	Energy standard deviation
8	Neg. Q1 Q [pC]	Discharge magnitude first quartile
9	Neg. Q1 Phase [deg]	Phase first quartile
10	Neg. Q1 Energy [pC*kV]	Energy first quartile
11	Neg. Median Q [pC]	Discharge magnitude median
12	Neg. Median Phase [deg]	Phase median
13	Neg. Median Energy [pC*kV]	Energy median
14	Neg. Q3 Q [pC]	Discharge magnitude third quartile
15	Neg. Q3 Phase [deg]	Phase third quartile
16	Neg. Q3 Energy [pC*kV]	Energy third quartile
17	Neg. IQR Q [pC]	Discharge magnitude interquartile range
18	Neg. IQR Phase [deg]	Phase interquartile range
19	Neg. IQR Energy [pC*kV]	Energy interquartile range
20	Neg. Min. Q [pC]	Minimum discharge magnitude
21	Neg. Min. Phase [deg]	Minimum phase
22	Neg. Min. Energy [pC*kV]	Minimum energy
23	Neg. Max. Q [pC]	Maximum discharge magnitude
24	Neg. Max. Phase [deg]	Maximum phase
25	Neg. Max. Energy [pC*kV]	Maximum energy
26	Neg. Range Q [pC]	Discharge magnitude range
27	Neg. Range Phase [deg]	Phase range
28	Neg. Range Energy [pC*kV]	Energy range
29	Pos. Mean Q [pC]	Mean discharge magnitude
30	Pos. Mean Phase [deg]	Mean phase
31	Pos. Mean Energy [pC*kV]	Mean energy
32	Pos. Stdv. Q [pC]	Discharge magnitude standard deviation
33	Pos. Stdv. Phase [deg]	Phase standard deviation
34	Pos. Stdv. Energy [pC*kV]	Energy standard deviation
35	Pos. Q1 Q [pC]	Discharge magnitude first quartile
36	Pos. Q1 Phase [deg]	Phase first quartile
37	Pos. Q1 Energy [pC*kV]	Energy first quartile
38	Pos. Median Q [pC]	Discharge magnitude median
39	Pos. Median Phase [deg]	Phase median
40	Pos. Median Energy [pC*kV]	Energy median
41	Pos. Q3 Q [pC]	Discharge magnitude third quartile
42	Pos. Q3 Phase [deg]	Phase third quartile
43	Pos. Q3 Energy [pC*kV]	Energy third quartile
44	Pos. IQR Q [pC]	Discharge magnitude interquartile range
45	Pos. IQR Phase [deg]	Phase interquartile range
46	Pos. IQR Energy [pC*kV]	Energy interquartile range
47	Pos. Min. Q [pC]	Minimum discharge magnitude
48	Pos. Min. Phase [deg]	Minimum phase
49	Pos. Min. Energy [pC*kV]	Minimum energy
50	Pos. Max. Q [pC]	Maximum discharge magnitude
51	Pos. Max. Phase [deg]	Maximum phase
52	Pos. Max. Energy [pC*kV]	Maximum energy
53	Pos. Range Q [pC]	Discharge magnitude range
54	Pos. Range Phase [deg]	Phase range
55	Pos. Range Energy [pC*kV]	Energy range
56	D	Symmetry factor, positive over negative number of pulses
57	Energy Ratio	Ratio of the positive mean energy and the negative mean energy
†: Pos. and Neg. refer to the positive and negative polarities of the test voltage respectively		

The partial discharge diagnostic features obtained from the field tests data (Table 7.5) are not the same as the partial discharge diagnostic features obtained from the laboratory experiments data (Table 7.1). This is due to the nature of the data sets, *e.g.* the test voltage has been excluded in the analysis and evaluation process of partial discharge diagnostic features from laboratory experiments data because it depends on the geometry of the defect; while for the partial discharge diagnostic features from field tests data, the test voltage can be considered in the analysis and evaluation process because all the partial discharge sites belong to the same cable system and therefore it can be assumed that the geometry of the defects between partial discharge sites is somewhat similar. Even though the considered partial discharge diagnostic features are not exactly the same for the laboratory experiments and field tests data, they do carry similar information regarding partial discharge magnitude, phase, and symmetries.

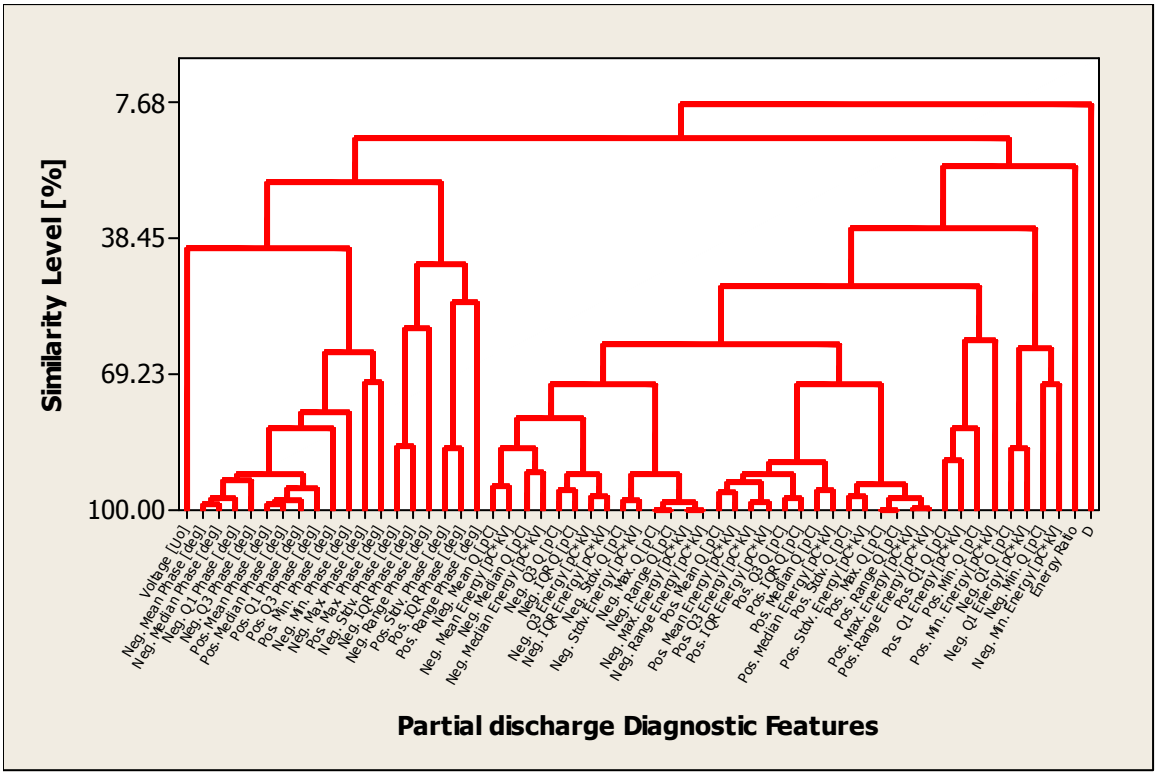

Figure 7.9. Dendrogram for the 57 partial discharge diagnostic features of field data.

The dendogram, for the 57 diagnostic features as shown in Table 7.5, is shown in Figure 7.9. As mentioned before, the dendrogram identifies groups or cluster whose features share common characteristics forming a cluster. The number of clusters can be determined by choosing the similarity level. In this case, a similarity level of 50 % is selected to cut the dendrogram determining the final cluster of features. Remember from previous sections that the similarity level, at which there is an abrupt change in the number of clustered features, is a good point for cutting the dendrogram if the final features partition makes physical sense to the data. The result of cutting the dendrogram of Figure 7.9 at the 50% similarity level is shown in Figure 7.10 and Table 7.6.

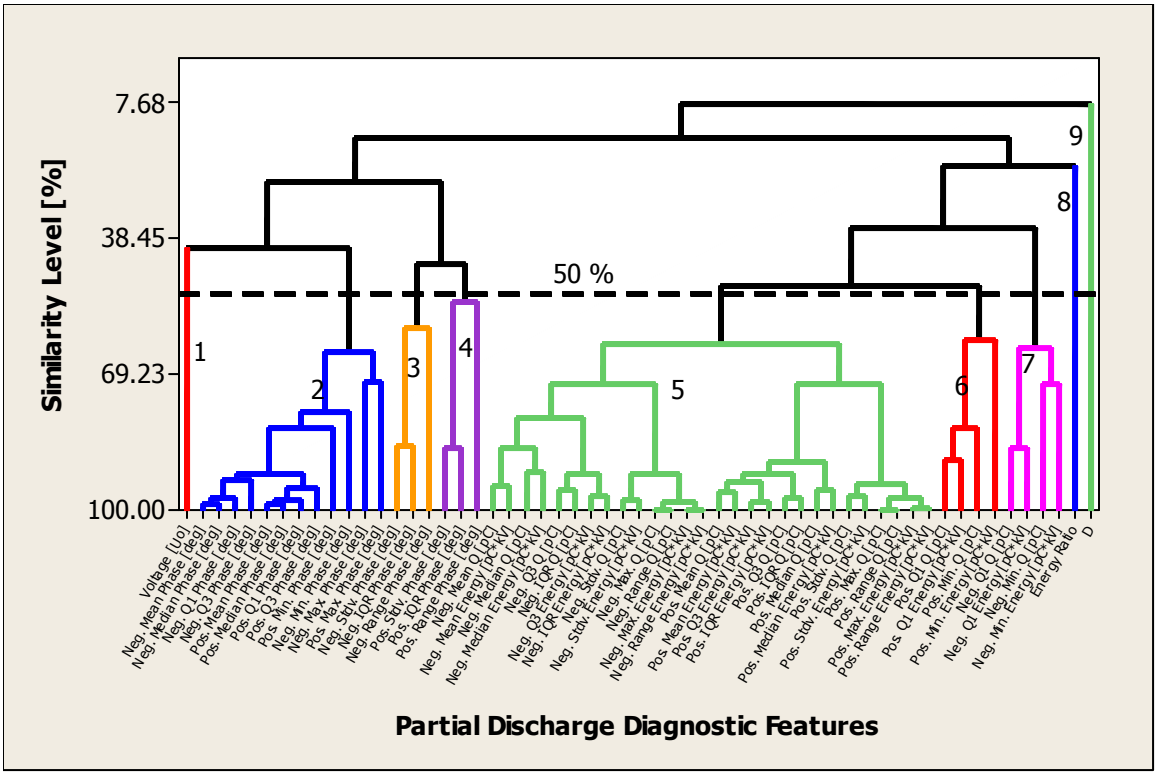

Figure 7.10. Dendrogram for the 57 partial discharge diagnostic features of field data cut at the 50 % similarity level.

Table 7.6. Cluster variable analysis results of field data.

Cluster No.	No.	Name
1	1	Voltage [U_0]
2	3	Neg. Mean Phase [deg]
	9	Neg. Q1 Phase [deg]
	12	Neg. Median Phase [deg]
	15	Neg. Q3 Phase [deg]
	21	Neg. Min. Phase [deg]
	24	Neg. Max. Phase [deg]
	30	Pos. Mean Phase [deg]
	36	Pos. Q1 Phase [deg]
	39	Pos. Median Phase [deg]
	42	Pos. Q3 Phase [deg]
	48	Pos. Min. Phase [deg]
	51	Pos. Max. Phase [deg]
3	6	Neg. Stdv. Phase [deg]
	18	Neg. IQR Phase [deg]
	27	Neg. Range Phase [deg]
4	33	Pos. Stdv. Phase [deg]
	45	Pos. IQR Phase [deg]
	54	Pos. Range Phase [deg]
5	2	Neg. Mean Q [pC]
	4	Neg. Mean Energy [pC*kV]
	5	Neg. Stdv. Q [pC]
	7	Neg. Stdv. Energy [pC*kV]
	11	Neg. Median Q [pC]
	13	Neg. Median Energy [pC*kV]
	14	Neg. Q3 Q [pC]
	16	Neg. Q3 Energy [pC*kV]
	17	Neg. IQR Q [pC]
	19	Neg. IQR Energy [pC*kV]
	23	Neg. Max. Q [pC]
	25	Neg. Max. Energy [pC*kV]
	26	Neg. Range Q [pC]
	28	Neg. Range Energy [pC*kV]
	29	Pos. Mean Q [pC]
	31	Pos. Mean Energy [pC*kV]
	32	Pos. Stdv. Q [pC]
	34	Pos. Stdv. Energy [pC*kV]
	38	Pos. Median Q [pC]
	40	Pos. Median Energy [pC*kV]
	41	Pos. Q3 Q [pC]
	43	Pos. Q3 Energy [pC*kV]
	44	Pos. IQR Q [pC]
	46	Pos. IQR Energy [pC*kV]
	50	Pos. Max. Q [pC]
	52	Pos. Max. Energy [pC*kV]
	53	Pos. Range Q [pC]
	55	Pos. Range Energy [pC*kV]
6	35	Pos. Q1 Q [pC]
	37	Pos. Q1 Energy [pC*kV]
	47	Pos. Min. Q [pC]
	49	Pos. Min. Energy [pC*kV]
7	8	Neg. Q1 Q [pC]
	10	Neg. Q1 Energy [pC*kV]
	20	Neg. Min. Q [pC]
	22	Neg. Min. Energy [pC*kV]
8	57	Energy Ratio
9	56	D

As seen in Figure 7.10 and Table 7.6, cutting the dendrogram of Figure 7.9, at a similarity level of 50 %, yields to nine clusters as the final partial discharge diagnostic features partition. In particular, four major types of partial discharge diagnostic features are observed in the taxonomy of the features. They are the test voltage (cluster 1), partial discharge phase (clusters 2, 3, and 4), partial discharge magnitude and energy (clusters 5, 6, and 7), and symmetry (clusters 8 and 9). These results are in accordance with the types of partial discharge diagnostic features resulting from the analysis portion of the process of partial discharge diagnostic features from laboratory experiments data.

Table 7.7. Results for the ranking of the partial discharge diagnostic features from field data using RFE.

Feature Name	**Cluster No (Table 7.6)**	**Feature No (Table 7.5)**	**Feature Rank**
Voltage [U_0]	1	1	6th
Pos. Mean Phase [deg]	2	30	4th
Neg. Stdv. Phase [deg]	3	6	2nd
Pos. Stdv. Phase [deg]	4	33	7th
Pos. Max. Energy [pC*kV]	5	52	1st
Pos. Q1 Q [pC]	6	35	3rd
Neg. Q1 Q [pC]	7	8	8th
Energy Ratio	8	57	9th
D	9	56	5th

In Table 7.6, each cluster can be represented by choosing one diagnostic feature from each cluster. In this case, the feature that is chosen from each cluster is the feature that has the furthest distance to the other clusters. The selected features are highlighted in grey in Table 7.6 and are used in the subsequent evaluation process using RFE.

Thus, Table 7.7 shows the results for the ranking of the partial discharge diagnostic features resulting from the cluster variable analysis. As seen in Table 7.7, the Pos. Max. Energy is the most relevant feature followed by the Neg. Stdv. Phase, Pos. Q1

Q, Pos. Mean Phase, D (symmetry factor), Voltage, Pos. Stdv. Phase, Neg. Q1 Q, and energy ratio respectively.

Table 7.8. Field data SVM classifier performance using ranked features.

Ranked Feature Name	**Class Loss (cable and accessory groups) [%]**								
	51.16	51.16	30.23	24.41	25.58	24.41	20.93	20.93	39.59
1st - Pos. Max. Energy [pC*kV]	×	×	×	×	×	×	×	×	×
2nd - Neg. Stdv. Phase [deg]	-	×	×	×	×	×	×	×	×
3rd - Pos. Q1 Q [pC]	-	-	×	×	×	×	×	×	×
4th - Pos. Mean Phase [deg]	-	-	-	×	×	×	×	×	×
5th - D	-	-	-	-	×	×	×	×	×
6th - Voltage [U_0]	-	-	-	-	-	×	×	×	×
7th - Pos. Stdv. Phase [deg]	-	-	-	-	-	-	×	×	×
8th - Neg. Q1 Q [pC]	-	-	-	-	-	-	-	×	×
9th - Energy Ratio	-	-	-	-	-	-	-	-	×

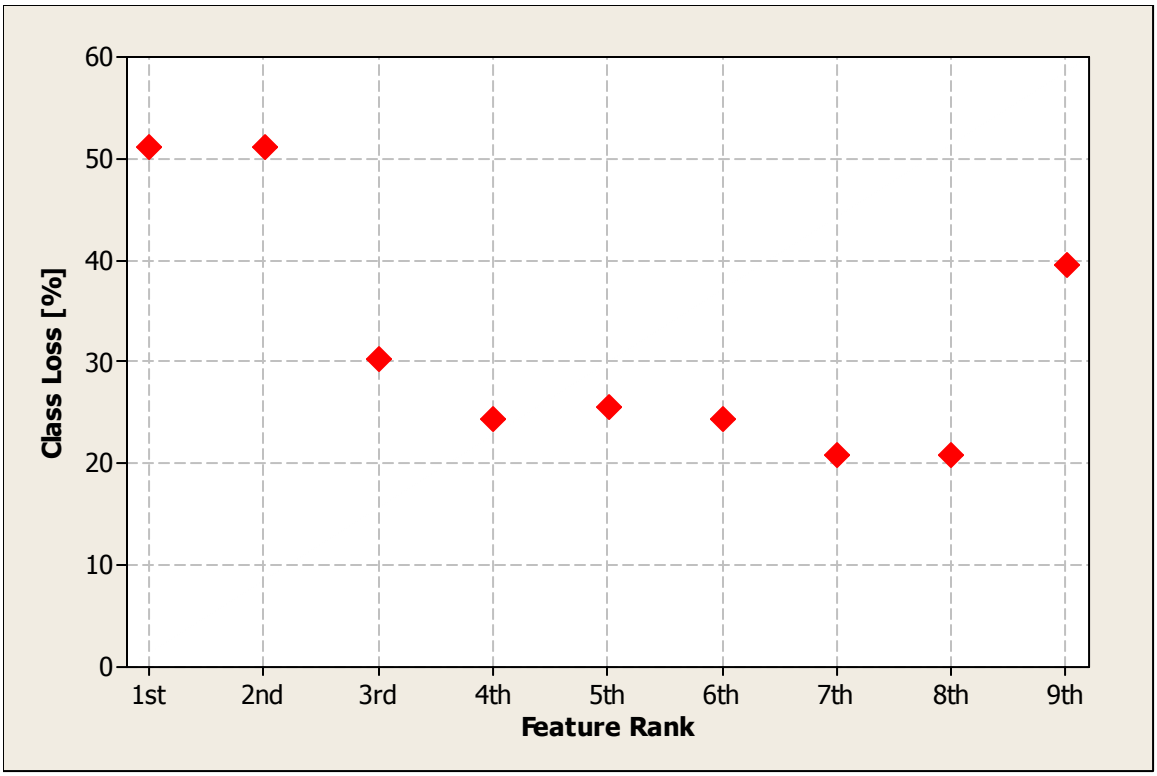

Figure 7.11. Class loss as function of feature rank for field data.

To grasp the significance of the partial discharge diagnostic features relevance, the SVM classifier performance is again considered. The classifier performance using the ranked features is shown in Table 7.8 and Figure 7.11. In this case, the classifier performance is also assessed by the class loss in percent. Remember that the class loss is the total number of incorrectly classified data points for the cable and accessory groups over the total number of data points. A data point is a set of the nine diagnostic features used in the evaluation process each of which represents a phase-resolved data pattern for each partial discharge location. The 25 partial discharge locations provide a total of 86 data points for all test voltages; particularly, 42 data points belong to the accessory group and 44 data points belong to the cable group.

As seen in Table 7.8 and Figure 7.11, the class loss for the SVM classifier when using the most relevant partial discharge diagnostic feature is 51.16 %. This means that

more than half of the data points are incorrectly classified. No improvement in the classifier performance is observed if the first two ranked partial discharge diagnostic features are used in the classification as the class loss remains 51.16 %. However, if the first three ranked partial discharge diagnostic features are used in the classification, the classifier performance improves to a value of 30.23 %. In addition, the best classifier performance is observed when seven or eight of the first ranked partial discharge features are used in the classification. Even though seven or eight features gives the best classifier performance, the SVM is not able to completely classify the data as the class loss is not zero. Only four features were required in the analysis and evaluation process of partial discharge diagnostic features from laboratory experiment partial discharge data. The differences between the classifier performances could be due to the fact that the acquisition of partial discharge data obtained from laboratory experiments is in a much more controlled conditions as compared to the field, since issues as noise coupling and attenuation of the partial discharge signal are minimal.

Another important observation in Table 7.8 is the fact that considering the last ranked partial discharge diagnostic feature degrades the performance of the SVM classifier from 20.93 % to 39.50 %. Therefore, not in all cases adding additional features aid in the classification. This is the main reason why the features have to be analyzed and evaluated in detailed.

To gain a better appreciation of the separation between the cable and accessory groups, Figure 7.12 shows a two-dimensional scatter plot by component considering the first two ranked partial discharge diagnostic features and Figure 7.13 shows a three-dimensional scatter plot by component considering the first three ranked partial discharge diagnostic features. In the plots, each feature has been normalized by its maximum values such that its values are in the range between zero and one.

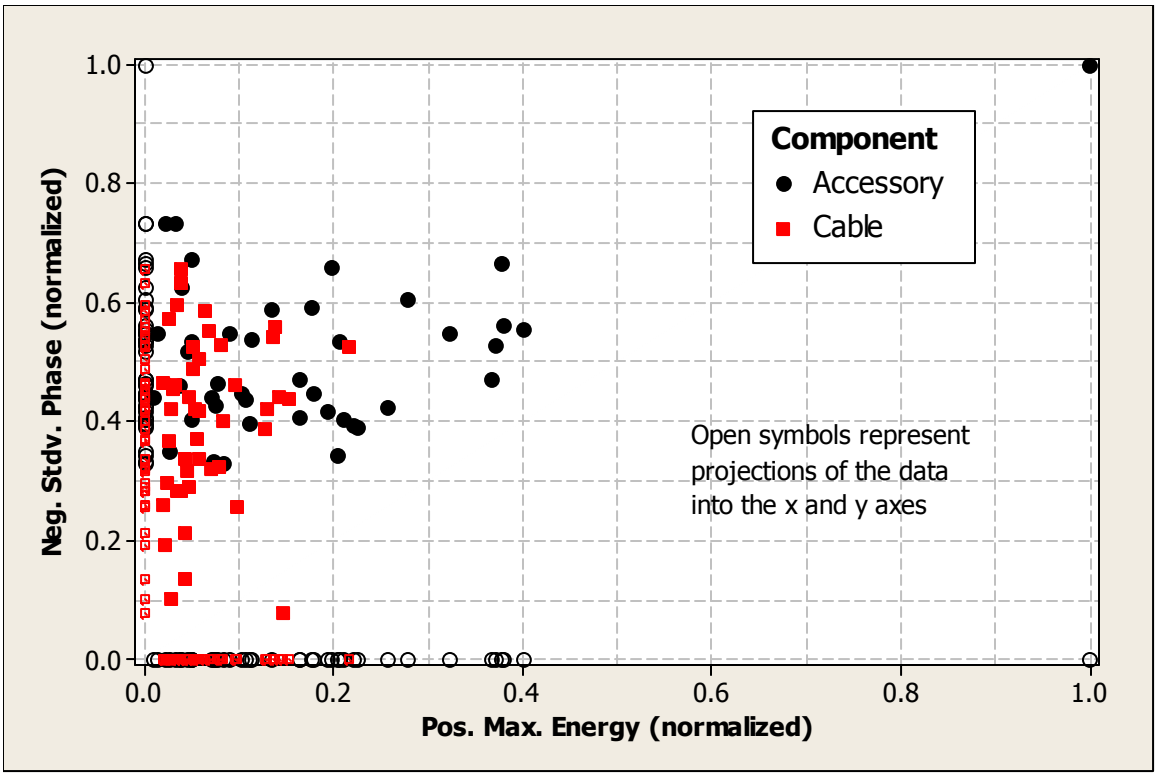

Figure 7.12. Two dimensional scatter plot by component considering the first two ranked partial discharge diagnostic features from the field data.

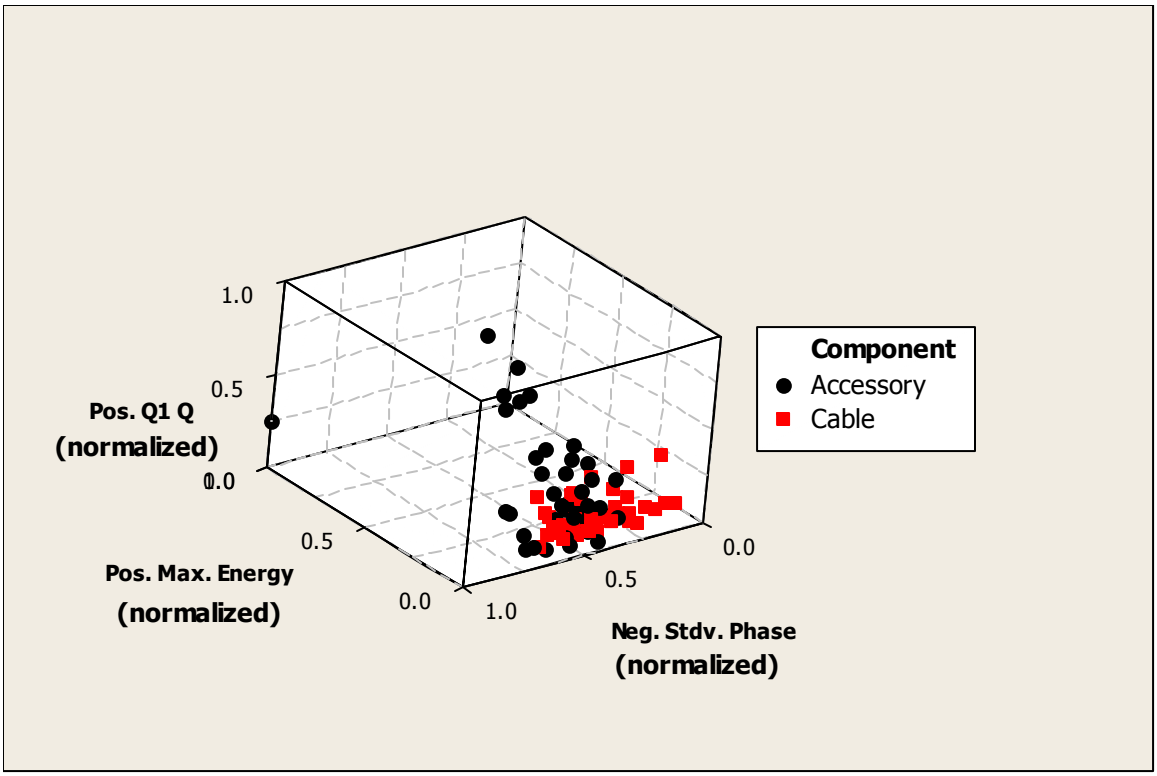

Figure 7.13. Three dimensional scatter plot by component considering the first three ranked partial discharge diagnostic features from the field data.

If the group separation between Figure 7.12 and Figure 7.13 is visually compared, a better separation between the groups of cable and accessory is observed in Figure 7.13. This result is expected since the class loss for the SVM classifier is 51.15 % corresponding to Figure 7.12 compared to 30.23 % corresponding to Figure 7.13.

7.6 Summary and Conclusions

The Chapter has presented a process for finding a robust set of partial discharge diagnostic features, disregarding the unnecessary features, and considering partial discharge data into groups of cable and accessory. The process is divided into two portions, *i.e.* an initial analysis and a final evaluation of the partial discharge diagnostic features. The features have been identified using partial discharge data, which have been described in Chapter 6, obtained from laboratory experiments and field tests.

The initial analysis portion of the process takes advantage of the hierarchical structure and taxonomy of the partial discharge diagnostic features by performing the cluster variable analysis of the diagnostic features. The cluster variable analysis has provided a feature selection by disregarding unnecessary features that carry similar information.

The final evaluation portion of the process has been accomplished by performing the recursive feature elimination (RFE) of the partial discharge diagnostic features that are the result of the initial cluster variable analysis. The RFE has provided a tool for ranking the partial discharge diagnostic features by taking into account the classification potential of each diagnostic feature compared to others.

Results from the analysis and evaluation process of both partial discharge diagnostic features from laboratory and field data reveal that different types of diagnostic features have to be used in order to achieve an appropriate level of dissimilarity between features and good classification performance between the cable and accessory groups. The types of partial discharge diagnostic features include test voltage, test voltage polarity, discharge magnitude, discharge energy, discharge phase, discharge repetition rates, and discharge symmetries.

CHAPTER 8

CONCLUSIONS, CONTRIBUTIONS, AND RECOMMENDATIONS FOR FUTURE WORK

8.1 Summary and Conclusions

In the United States, electric power distribution relies on a vast network of underground medium voltage power cable systems. The systems have a finite life span, and at some point utility engineers must decide when to replace parts of a cable system in order to avoid unexpected failures and the associated costumer outages as much as possible. In the past, corrective maintenance was typically used, *i.e.* components were replaced after failure. However, the present era of de-regularization of the electrical energy market has forced utilities to refocus their attention on the reliability of the power systems and thus the aging distribution power cable system infrastructure, while at the same time reducing maintenance costs as much as possible. Matters are further complicated by the ever increasing need for electrical energy, pushing the cable systems to their design limits.

Consequently, utilities are interested in accurately determining the condition of the power cable systems, and ultimately their expected remaining life span, before initiating permanent maintenance and replacement test programs. The correct application of condition based maintenance strategies can avoid unexpected outages and ultimately result in substantial savings for utilities. This requires the use of dependable cable diagnostic technologies. Nevertheless, while several cable diagnostic technologies are available, they have not yet been fully employed across the United States because utilities do not completely trust their assessments. This is not a simple problem to overcome since it requires a complete understanding of the diagnostic technologies as well as how to best use them.

The purpose of this research is therefore to advance the field of characterization of power cable defects by addressing a number of theoretical and practical diagnostic measurements, their interpretation, and deployment issues. The most widely used diagnostic measurements in the United States are dissipation factor (Tan δ) and partial discharge measurements; this is the main reason why they are the main focus of the research. This thesis has two major parts, the first part (Chapters 3 to 5) has been devoted to the work on Tan δ measurements (mainly at very low frequency of 0.1 Hz) and the second part (Chapters 6 and 7) has been devoted to the work on partial discharge measurements at power frequency of 60 Hz. The discussion and conclusions in both parts have been based on data from laboratory experiments and field tests of medium voltage (MV) underground distribution power cable systems and their components.

Chapter 1 has presented the background, problem statement, objective, and structure of the thesis.

Chapter 2 has introduced the basic concepts of power cable systems and their diagnostics required for understanding of this theses. The basic structure and accessories of power cable systems have been explained. In addition, aging, degradation, and breakdown mechanisms have also been presented. Finally, the Chapter has briefly presented an overview of power cable diagnostics technologies.

Chapter 3 has presented the basic concepts, means of diagnosis, limitations of Tan δ measurements, and a comprehensive literature review. Chapter 3 has also discussed a number of issues that arise when using Tan δ measurements at very low frequency (VLF) to characterize the insulation of non-aged and field-aged MV cables. The discussion has been based on data from laboratory experiments that consider time dependence, voltage dependence, and discharge time dependence tests for different test protocols. Results have indicated that there are a number of useful diagnostic features that can be used to characterize each sample. The features include Tan δ values, Tip-Ups (changes in the Tan

δ magnitude with the increasing test voltage), hysteresis, and most importantly, the scatter in the measurements for a particular test voltage level. The test protocols have enable a study of the correlation between Tan δ values at different frequencies of 0.1 Hz and 60 Hz. In this case, results have shown that there is not a perfect correlation; however, there is some correlation that could be useful in translating diagnostic criteria from one frequency to the other.

The Chapter has also presented results of Tan δ measurements from field tests. Results have provided for a reevaluation of Tan δ diagnostic criteria in two ways. First, results have indicated that existing values for diagnostic criteria are probably too conservative for American cable designs. Secondly, results have also shown that it is possible to map diagnostics criteria to lower test voltages, thereby reducing the risk of failure under test while maintaining criteria assessment.

In conclusion, Chapter 3 has shown that higher insulation losses, nonlinearities with voltage, hysteresis, and variation in voltage and time of Tan δ diagnostic measurements at VLF, are indicators that could be used to properly characterize the insulation and enhance the diagnosis. However most importantly, Tan δ can be considered a feature rich diagnostic tool when testing is performed in an appropriate way and data are analyzed correctly.

Chapter 4 has presented a laboratory test program conducted to investigate the correlation between Tan δ diagnostic features and the VLF breakdown performance for MV XLPE cables. The Tan δ diagnostic features have included the mean Tan δ magnitude, the Tip-Up, and the scatter in the Tan δ measurements for a particular test voltage level. The test program has included Tan δ measurements at different voltage levels and subsequent VLF extended-step withstand test to breakdown. It has been found that there is a correlation between the Tan δ diagnostics features and the VLF breakdown performance. This is important in the sense that the correlation between the Tan δ

diagnostic features and the breakdown performance has only been previously established for impulse and AC breakdown voltages and mainly considering the Tan δ magnitude as diagnostic feature. Results have shown that in general the VLF breakdown performance is the lowest when compared to impulse and AC.

More importantly, Chapter 4 has introduced the use of a new diagnostic feature that takes into account the scatter in the Tan δ measurements for a particular test voltage level. More scatter in the measurements implies a lower VLF breakdown voltage. The Chapter has also introduced the application of a new method called performance ranking. This method has been able to quantitatively evaluate the correlation between each diagnostic feature and the breakdown performance. Results indicate that the scatter in the measurements is the feature most correlated with the breakdown performance for the cable population under study.

Further investigations such as Weibull breakdown performance and time-voltage analysis have also been presented in Chapter 4. The Weibull breakdown performance results have allowed for evaluation of the risk of failure during testing. This is the first time in which this risk has been evaluated. It has been observed that; a considerable reduction of one order of magnitude in the risk of failure occurs when the test voltage is reduced from twice to once the rated phase-to-ground voltage.

Failure site and hot-oil examinations have also been performed. The failure site examination test has not revealed the cause of failure for any of the samples. Nevertheless, the hot-oil examination has shown that most of the samples have water-tree sites and other irregularities. Therefore, the possible cause of failure has been more likely to be a water-tree related failure mechanism.

Chapter 5 has presented the basics of low voltage time domain reflectometry (TDR) test on power cables. Because of its ease of use, cost, and simplicity in indentifying power cable systems configuration and basic problems with neutral wires,

the TDR test has been proposed and used as one of the initial steps for any cable condition assessment in the field. The Chapter has also presented the Tan δ versus length models. The most common situations of non-uniform degradation and neutral issues have been modeled and demonstrated through both theory and experiments. It has been shown that both situations, rather than limitations, provide useful diagnostic indicators that aid an enhanced condition assessment.

More importantly, Chapter 5 has introduced a new approach for condition assessment of MV polyethylene (PE) based power cable systems. The approach considers the use of combined diagnostics, which include time domain reflectometry (TDR), VLF-Tan δ, and VLF-Tan δ monitored withstand. The approach is executed by an evaluation procedure that uses diagnostic features management with feature categorization and decision organization. The evaluation process constitutes a step forward to the currently condition assessment approach presented in the American standards.

Chapter 6 has introduced the basic concepts, means of diagnosis, and limitations of partial discharge measurements. Brief descriptions of the available partial discharge data, feature extraction, and classification tools, have also been introduced. A comprehensive literature review on the "state of the art" on characterization of defects by partial discharge measurements has been presented.

Moreover, Chapter 6 has described and briefly analyzed laboratory and field partial discharge data that are the basis for the analysis and evaluation process of partial discharge diagnostic features presented in Chapter 7. The data are based on the phase-resolved partial discharge pattern and are classified into two groups, *i.e.* partial discharge in cable and partial discharge in accessory. The laboratory partial discharge data have been measured by the author while the data from partial discharge field tests have been provided to the author by one of the utility participants of the CDFI project.

Chapter 7 has presented a process for analysis and evaluation of partial discharge

diagnostic features. The process has enabled the selection of the most relevant diagnostic features when the partial discharge data is considered into groups of cable and accessory. The process is divided into two portions, *i.e.* an initial analysis and a final evaluation.

The initial analysis portion of the process has taken advantage of the hierarchical structure and taxonomy of the partial discharge diagnostic features by performing a cluster variable analysis of the diagnostic features. The cluster variable analysis has provided a feature selection by disregarding unnecessary features that carry similar information. The second evaluation portion of the process has been accomplished by performing the recursive feature elimination (RFE) of the partial discharge diagnostic features that are the result of the first cluster variable analysis. The RFE has provided a tool for ranking the partial discharge diagnostic features by taking into account the classification potential of each diagnostic feature compared to others.

Results from the analysis and evaluation process, of both partial discharge diagnostic features from laboratory and field data, have revealed that different types of diagnostic features have to be used in order to achieve an appropriate level of dissimilarity between features and good classification performance between the cable and accessory groups. The types of partial discharge diagnostic features include test voltage, test voltage polarity, discharge magnitude, discharge energy, discharge phase, discharge repetition rates, and discharge symmetries.

8.2 Contributions

The main contributions of this research in the field of power cable diagnostics are summarized as follows:

- **Deployment of Tan δ diagnostic features:** An elaborate step-by-step approach is presented (Chapter 5) for condition assessment of MV PE-based power cable systems. The approach considers the use of combined diagnostics; the combination includes TDR, VLF-Tan δ, and VLF-Tan δ

monitored withstand. The approach is executed by an evaluation procedure that uses diagnostic features management with feature categorization and decision organization. The evaluation process constitutes a step forward to the currently condition assessment approach presented in the American standards.

- **Analysis and evaluation of partial discharge diagnostic features**: A process which is able to determine a suitable set of partial discharge diagnostic features (Chapter 7) that could enhance the classification and diagnostics of power cable systems. The process takes advantage of the hierarchical structure and taxonomy of the partial discharge diagnostic features as well as their classification potential. The process is divided into two portions, an initial analysis and a final evaluation. The analysis is accomplished by performing the cluster variable analysis and the evaluation is accomplished by performing the recursive feature elimination (RFE) of the partial discharge diagnostic features that are based on the phase-resolved data pattern.
- **Tan δ feature richness:** It has been shown (Chapter 3) that higher insulation losses, nonlinearities with voltage, hysteresis, and variation in voltage and time of Tan δ diagnostic measurements at VLF, are indicators that could be used to properly characterize the insulation and enhance the condition assessment of MV power cable systems. More importantly, Tan δ can be considered a feature rich diagnostic tool when testing is performed in an appropriate way and data are analyzed correctly.
- **Tan δ and VLF breakdown**: The correlation (Chapter 4) between Tan δ diagnostic features such as Tan δ magnitude, Tip-Up, and scatter in the measurements with the breakdown performance at VLF, has been established.
- **Effect of length on Tan δ**: Development, simulation, experimentation,

verification, and identification of diagnostic indicators of Tan δ versus cable system length models (Chapter 5) considering the most common situations such as non-uniform degradation and neutral issues, have been presented.

- **Tan δ diagnostic criteria**: The reevaluation (Chapter 3) of Tan δ diagnostic criteria in two ways has been introduced. First, existing values for diagnostic criteria are too conservative for the American cable designs. Second, it is possible to map diagnostic criteria to lower test voltages, thereby reducing the risk of failure under test while maintaining the accuracy of the condition assessment.
- **Literature review**: A comprehensive literature survey (Chapter 2) on power cables systems including components, aging, degradation, and breakdown mechanisms as well as the fundamentals for diagnostic testing technologies, has been presented.

Moreover, other contributions of the research work reported in this thesis have been classified as contributions to papers, industry, standards, and patents. They are as follows:

8.2.1 Contributions to Papers

A poster titled "*Classification and Identification of Real Cable Insulation Defects by Partial Discharge Measurements*" has been presented at the IEEE Power Engineering Society (PES) General Meeting in June 2006 in Montreal, Canada. This poster was awarded second place in the IEEE-PES Student Poster Contest.

In addition, as a result of the research presented in Chapter 3, a paper titled "*Practical Issues Regarding the Use of Dielectric Measurements to Diagnose the Service Health of MV Cables*" was accepted and presented at the 7th International Conference on Insulated Power Cables 2007 (JICABLE'07) in June 2007, Paris, France [97].

The research presented in Chapter 3 has also been published as a conference and a journal papers. The conference paper titled "*Validation of the Accuracy of Practical Diagnostic Tests for Power Equipment*" has been presented at the Conseil International des Grands Reseaux Électriques (CIGRÉ) in August 2008 in Paris, France [59]. This paper was selected between the top 10 United States papers allowed to be present at the conference. The transaction paper titled "*Characterization of Ageing for MV Power Cables Using Low Frequency Tan δ Diagnostic Measurements*" is under review for publication in the IEEE Transactions on Dielectrics and Electrical Insulation [98].

Based on the research on Chapter 4, a paper titled "*Correlation between Tan δ Diagnostic Measurements and Breakdown Performance at VLF for MV XLPE Cables*" is also under review for publication in the IEEE Transactions on Dielectrics and Electrical Insulation [52].

Part of the research presented in Chapters 6 and 7 is contained in a paper titled "*Determining Routes for the Analysis of Partial Discharge Signals Derived from the Field*" has been accepted for journal publication in the IEEE Transactions on Dielectrics and Electrical Insulation Special Issue on Partial Discharge Measurements [89].

8.2.2 Contributions to Industry

A presentation titled "*Defect Classification by Partial Discharge Measurements*" has been presented at the NEETRAC Cable Diagnostics Focus Initiative Project (CDFI) Update Meeting in May 2006, Atlanta, Georgia.

The literature review of Chapter 2 contributed to the development of a handbook on cable diagnosis titled "*Overview of Cable System Diagnostic Technologies and Applications.*" The handbook was published by NEETRAC in December 2006, Atlanta, Georgia.

Three presentations titled "*Laboratory Studies using VLF Tanδ Techniques*,"

"*Tanδ evaluations in the Field*," and "*Partial Discharge (PD) Evaluations in the Field*," have been presented at the NEETRAC Cable Diagnostics Focus Initiative Project (CDFI) Update Meeting in February 2007, Atlanta, Georgia.

Three presentations titled "*Analysis of Tan δ*," "*Laboratory Studies of Partial Discharge in Cables and Joints*," and "*CDFI Field Tests 2007-2008*," have been presented at the NEETRAC Cable Diagnostics Focus Initiative Project (CDFI) Update Meeting in February 2008, Atlanta, Georgia.

8.2.3 Contributions to Standards

A paper titled "*Reflections on 'First Experiences' with IEEE 400*," has been presented at the IEEE Insulated Conductors Committee (ICC) Fall – 2006 Meeting, WG C – 18, in October 2006, St. Petersburg, Florida.

At the present, the author is participating in the review and rewriting process of the IEEE Std. 400.2, which is titled "*IEEE Guide for Field Testing of Shielded Power Cable Systems Using Very Low Frequency (VLF).*"

8.2.4 Contribution to Patents

A provisional patent application titled "*Methods to Determine Alternate Success Criteria for Field Testing of Underground Cable Systems Using Dielectric Measurements*" has been filed with the Georgia Tech Research Corporation in February 2007, Atlanta, Georgia.

8.3 Recommendations for Future Work

The ultimate goals of using power cable diagnostic technologies are to improve the overall reliability of the power distribution network system, reduce maintenance cost, and avoid undesirable service failures that inevitably lead to costumer outages. Although this thesis has presented contributions to various areas that are important to reach these

goals, there are still several interesting future research directions, which could build on the findings of this thesis. The more important of these directions are as follows:

- **Other insulation materials:** The work presented in this thesis regarding the characterization using Tan δ measurements has only considered field-aged cross-linked (XLPE) cable samples. Thus, the characterization could be expanded by considering field-aged cable samples with other type of insulation materials, *i.e.* ethylene propylene rubber (EPR) and paper insulations. Particularly, the correlation between the Tan δ diagnostic features and some kind of breakdown performance could also be considered as a valuable future work for these insulation materials.
- **Other very low frequencies:** The characterization and correlation between the Tan δ diagnostic features and the VLF breakdown performance has only been performed for 0.1 Hz, which is the most typical value used in field testing applications. However, frequencies as low as 0.01 Hz could also be used. In this case, the characterization and correlation at those lower frequencies could also be useful for improving the condition assessment of MV power cable systems using Tan δ measurements.
- **Dielectric response:** Different Tan δ characteristic responses for different field-aged cable samples have been observed during the course of this work. However, even though models are proposed [12], the origin of the dielectric response is not yet fully understood. More understanding of what physical processes cause the responses will provide valuable information for improving condition assessment criteria.
- **Additional partial discharge diagnostic features:** In the analysis and evaluation of partial discharge diagnostic features, the analysis has been based in features obtained from the phase-resolved data pattern. Partial discharge

diagnostic features from partial discharge time-resolved data and data without phase or time information may also be considered in the analysis and evaluation process. Another important observation is that this work has only considered diagnostic features for which a physical basis can be described. Work in other areas has shown that more abstract and potentially useful features can be derived from techniques such as principal component analysis. Therefore, the analysis and evaluation of these more abstract features may aid the classification.

- **Partial discharge classification groups:** The partial discharge diagnostic features analysis and evaluation process presented here has divided all the partial discharge data into groups of either cables or accessories. The next step will be to extend the study by using classifications in terms of test voltage, physical process, or service performance (fail and no fail groups). This next step may also include the recursive feature elimination evaluation process using a support vector machine (SVM) classifier with a non-linear kernel.
- **Optimization of partial discharge diagnostic features:** Once the features ranks have been established, with linear or non-linear kernel for the SVM, an optimization problem can be formulated. The objective of the optimization problem would be to find from a final set of partial discharge diagnostic features which combination of them provides the largest potential for the classification.
- **Tan δ and partial discharge interaction:** the Tan δ magnitude can be affected by the presence of partial discharges. The mechanisms of how partial discharges affect either the true Tan δ magnitude or its measurement are still not completely understood especially for extruded insulation power cable systems. If there is any interaction between Tan δ and partial discharge, it

would be valuable to have a method or model to separate these two mechanisms since a correct diagnosis will require the information regarding the relative magnitudes of the respective insulation losses.

APPENDIX A

MODELING OF EQUIVALENT TAN δ AS A FUNCTION OF LENGTH FOR NON-UNIFORM DEGRADATION

To model the equivalent Tan δ as a function of length for a cable segment with non-uniform degradation, the healthy and aged portions of the cable segment are considered separately. Specifically, the approach is to model each portion by itself considering the proper set of parameters, *i.e.* insulation resistance and capacitance, that result in the corresponding Tan δ magnitude and connecting the separate models in parallel as shown in Figure A.1.

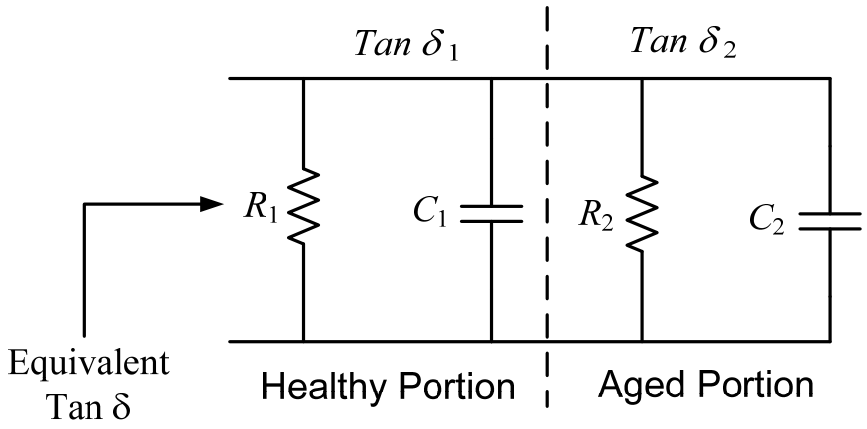

Figure A.1. Model for non-uniform degradation.

In Figure A.1, the parameters R_1 and C_1 represent the healthy portion and the parameters R_2 and C_2 represent the aged portion of the cable segment respectively. The healthy and aged portions are connected in parallel. The main goal is to find a mathematical model that relates the equivalent Tan δ, as it would be seen by the measurement equipment, with the Tan δ magnitudes of the healthy and aged portions and cable segment length.

As mentioned in Chapter 5, the assumption here is that the aged portion of the cable segment has a higher Tan δ magnitude as compared to the healthy portion of the cable segment. No neutral issues are considered in the model; *i.e.* if the cable segment under evaluation is unjacketed; then, the insulation shield has low volume resistivity, there is a good contact between the insulation shield and neutral wires, and the neutral wires are not corroded to any extent. The followed procedure in finding the model is shown in the next paragraphs.

Tan δ_1 and *Tan* δ_2 are defined as the Tan δ magnitudes of the healthy and aged portions of the cable segment respectively. In Figure A.1, *Tan* δ_1 and *Tan* δ_2 as a function of the model parameters are as follows,

$$Tan\,\delta_1 = \frac{1}{\omega R_1 C_1} \quad \text{(a)},$$
$$Tan\,\delta_2 = \frac{1}{\omega R_2 C_2} \quad \text{(b)}, \tag{A.1}$$

where,

Tan δ_1: Tan δ of the healthy portion of the cable segment,

ω: Angular frequency in rad/s,

R_1: Insulation resistance of the healthy portion of the cable segment in Ω,

C_1: Insulation capacitance of the healthy portion of the cable segment in F,

Tan δ_2: Tan δ of the aged portion of the cable segment,

R_2: Insulation resistance of the aged portion of the cable segment in Ω,

C_2: Insulation capacitance of the aged portion of the cable segment in F,

Tan δ: Equivalent Tan δ for both healthy and aged portions of the cable segment.

The equivalent Tan δ can be written as,

$$Tan\,\delta = \frac{1}{\omega R_e C_e}, \tag{A.2}$$

where,

R_e: Insulation equivalent resistance of the healthy and aged portions of the cable segment in Ω,

C_e: Insulation equivalent capacitance of the healthy and aged portions of the cable segment in F.

R_e and C_e are as follows,

$$\begin{aligned} R_e &= \frac{R_1 R_2}{R_1 + R_2} \quad \text{(a)}, \\ C_e &= C_1 + C_2 \quad \text{(b)}. \end{aligned} \tag{A.3}$$

Substituting equations (A.3)(a) and (A.3)(b) into equation (A.2), the equivalent Tan δ as a function of the healthy and aged model parameters is as follows,

$$Tan\ \delta = \frac{R_1 + R_2}{\omega R_1 R_2 (C_1 + C_2)}. \tag{A.4}$$

Equation (A.4) can be rewritten as,

$$\frac{1}{Tan\ \delta} = \frac{\omega R_1 R_2 C_1}{R_1 + R_2} + \frac{\omega R_1 R_2 C_2}{R_1 + R_2}. \tag{A.5}$$

Then, considering $Tan\ \delta_1$ and $Tan\ \delta_2$ from equation (A.1), equation (A.5) becomes,

$$\frac{1}{Tan\ \delta} = \frac{1}{Tan\ \delta_1}\frac{R_2}{R_1 + R_2} + \frac{1}{Tan\ \delta_2}\frac{R_1}{R_1 + R_2}. \tag{A.6}$$

Therefore, from equation (A.6), the equivalent Tan δ is as follows,

$$Tan\ \delta = \frac{(1 + R_2 / R_1)\,Tan\ \delta_1\, Tan\ \delta_2}{Tan\ \delta_1 + (R_2 / R_1) Tan\ \delta_2}. \tag{A.7}$$

Subsequently, if R_1, R_2, C_1, C_2, Γ, and L are defined as,

$$R_1 = \frac{r_1}{L_1} \text{ (a)}, \quad R_2 = \frac{r_2}{L_2} \text{ (b)}, \quad C_1 = c_1 L_1 \text{ (c)},$$
$$C_2 = c_2 L_2 \text{ (d)}, \quad \Gamma = \frac{L_1}{L_2} \text{ (e)}, \quad L = L_1 + L_2 \text{ (f)}, \tag{A.8}$$

where,

r_1: Insulation resistance per-unit length of the healthy portion of the cable segment in Ω-ft,

L_1: Length of the healthy portion of the cable segment in ft,

r_2 : Insulation resistance per-unit length of the aged portion of the cable segment in Ω-ft,

L_2: Length of the aged portion of the cable segment in ft,

c_1: Insulation capacitance per-unit length of the healthy portion of the cable segment in F/m,

c_2: Insulation capacitance per-unit length of the aged portion of the cable segment in F/m,

Γ: Ratio between L_1 and L_2,

L: Total cable segment length in ft.

Then, equation (A.7) can be rewritten as follows,

$$Tan\ \delta = \frac{1 + (r_2 / r_1)\Gamma}{(Tan\ \delta_1 / Tan\ \delta_2) + (r_2 / r_1)\Gamma} Tan\ \delta_1 \text{, in terms of } Tan\ \delta_1 \quad \text{(a)},$$
$$Tan\ \delta = \frac{1 + (r_2 / r_1)\Gamma}{1 + (r_2 / r_1)(Tan\ \delta_2 / Tan\ \delta_1)\Gamma} Tan\ \delta_2 \text{, in terms of } Tan\ \delta_2 \quad \text{(b)}. \tag{A.9}$$

$Tan\ \delta_1$ and $Tan\ \delta_2$ as a function of the per-unit length parameters are as follows,

$$Tan\ \delta_1 = \frac{1}{\omega r_1 c_1} \quad \text{(a)},$$
$$Tan\ \delta_2 = \frac{1}{\omega r_2 c_2} \quad \text{(b)}. \tag{A.10}$$

If the cable geometry and electrical permittivity between the healthy and aged portions of the cable system are assumed equal; then, the insulation capacitance per-unit length of the healthy portion of the cable segment (c_1) is identical to the insulation capacitance per-unit length of the aged portion of the cable segment (c_2). The electrical permittivity between the healthy and aged portions of the cable segment can be assumed to be equal since it has been shown for water-tree degradation [13] that this intrinsic parameter of insulation material only changes marginally between the healthy and the aged portions of the cable segment. Therefore, the ratio between $Tan\ \delta_1$ and $Tan\ \delta_2$ is as follows,

$$\frac{Tan\ \delta_1}{Tan\ \delta_2} = \frac{\cancel{\omega} r_2 \cancel{c_2}}{\cancel{\omega} r_1 \cancel{c_1}} = \frac{r_2}{r_1}. \tag{A.11}$$

Substituting equation (A.11) into equation (A.9)(a) or (A.9)(b), the equivalent Tan δ as a function of the length ratio is as follows,

$$Tan\ \delta = \frac{Tan\ \delta_2 + Tan\ \delta_1 \Gamma}{1 + \Gamma}. \tag{A.12}$$

The equivalent Tan δ as a function of length can be obtained by substituting equations (A.8)(e) and (A.8)(f) into equation (A.12). In this case, the equivalent Tan δ is as follows,

$$Tan\ \delta = \frac{L_2}{L} \Delta Tan\ \delta + Tan\ \delta_1 \quad \text{(a)},$$
$$\Delta Tan\ \delta = Tan\ \delta_2 - Tan\ \delta_1 \quad \text{(b)}. \tag{A.13}$$

If the equivalent Tan δ is much larger than the Tan δ of the healthy portion of the

cable segment ($Tan\ \delta_1$), *i.e.* if $Tan\ \delta >> Tan\ \delta_1$, then equation (A.13) becomes,

$$Tan\ \delta = \frac{L_2}{L}\Delta Tan\ \delta \quad \text{(a)}, \qquad \Delta Tan\ \delta = Tan\ \delta_2 \quad \text{(b)}. \tag{A.14}$$

The equivalent Tan δ as a function of length in a log-log scale is shown in equation (A.15),

$$\log(Tan\ \delta) = \log(L_2\ Tan\ \delta_2) - \log(L)\,. \tag{A.15}$$

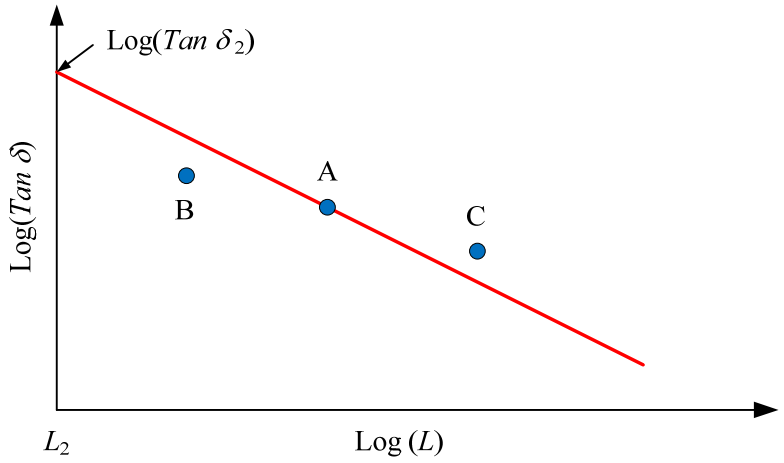

Figure A.2. Illustration of equivalent Tan δ as a function of length on a log-log scale.

Figure A.2 shows the equivalent Tan δ as a function of length as an illustration of equation (A.15). As seen in Figure A.2, when the equivalent Tan δ as a function of length is plotted in a log-log scale, then the equivalent Tan δ follows a linear model in length. The initial value of the equivalent Tan δ, *i.e.* when $L=L_2$, is $Tan\ \delta_2$. As the length increases the equivalent Tan δ decreases. The point A in Figure A.2, represents the case of a match between the model and the actual cable system configuration. A point below the line, point B, represents the case of a shorter portion of aged cable or a lower actual

Tan δ_2 value than the value used in the model. Finally, a point above the line, point C, represents a longer portion of aged cable or a higher actual *Tan* δ_2 value than the value used in the model.

APPENDIX B

MODELING OF NEUTRAL ISSUES

To model the neutral issues, a quadruple model, or two-port network, per-unit length is used. The model in time domain is shown in Figure B.1.

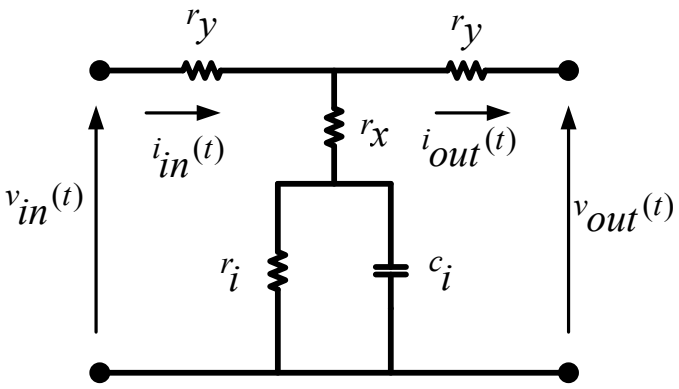

Figure B.1. Neutral issues quadrupole model per-unit length.

In Figure B.1, the model variables and parameters are described as follows,

$v_{in}(t)$: Input quadrupole voltage in V,

$i_{in}(t)$: Input quadrupole current in A,

$v_{out}(t)$: Output quadrupole voltage in V,

$i_{out}(t)$: Output quadrupole current in A,

r_i: Insulation resistance per-unit length in Ω-ft,

c_i: Insulation capacitance per-unit length in F/ft,

r_x: Contact resistance between the insulation shield and neutral wires in Ω-ft,

r_y: Neutral wires resistance in Ω/ft.

If neutral issues are not present, then the parameters r_x and r_y in Figure B.1 would be zero. To establish the relationship between the input and output variables, the quadrupole model in Figure B.1 is transformed to the frequency domain using the

Laplace transformation. The quadrupole model in frequency domain is shown in Figure B.2. In this case, all the elements in the model are represented as impedances and *s* is the Laplace parameter.

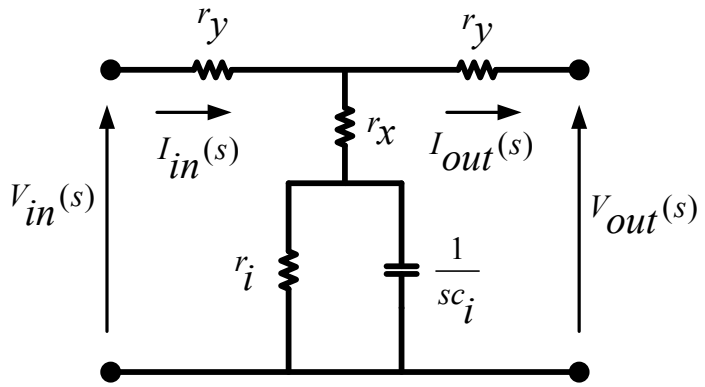

Figure B.2. Neutral issues quadrupole model per-unit length in frequency domain.

The quadrupole in Figure B.2 can be represented as a generalized quadrupole model as seen in Figure B.3. In Figure B.3, X_{in} is defined as the input variable vector, X_{out} is defined as the output variable vector and M is defined as the forward transfer function matrix.

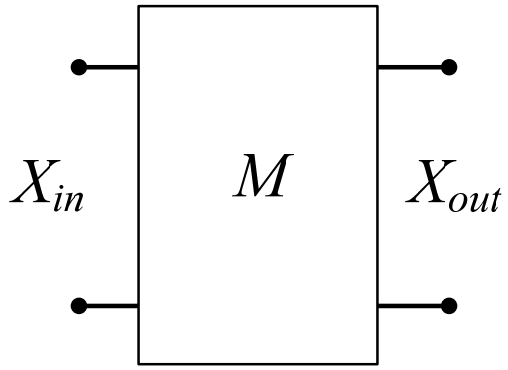

Figure B.3. Generalized quadrupole model.

The relationship between X_{in}, X_{out}, and M is given by equation (B.1) as follows,

$$X_{out} = M X_{in}. \tag{B.1}$$

As seen in equation (B.1), the forward transfer function matrix M expresses the relationship between the input and output variable vectors. In particular, to obtain the output variable vector, the input variable vector is multiplied by the forward transfer function matrix.

In Figure B.2, the input and output variable vectors are defined as follows,

$$X_{in} = \begin{bmatrix} V_{in}(s) \\ I_{in}(s) \end{bmatrix} \quad \text{(a)},$$

$$X_{out} = \begin{bmatrix} V_{out}(s) \\ I_{out}(s) \end{bmatrix} \quad \text{(b)}. \tag{B.2}$$

And the forward transfer function matrix is given by,

$$M = \frac{1}{r_i + r_x + sc_i r_i r_x} \begin{bmatrix} r_y + r_i + r_x + (r_y + r_x) sc_i r_i & -(2r_i + 2r_x + r_y) r_y - (r_x r_y + r_y^2) sc_i r_i \\ -1 - sc_i r_i & r_y + r_i + r_x + (r_y + r_x) sc_i r_i \end{bmatrix}. \tag{B.3}$$

In addition, Figure B.4 shows the case of two generalized quadrupole models connected in cascade with different transfer function matrices.

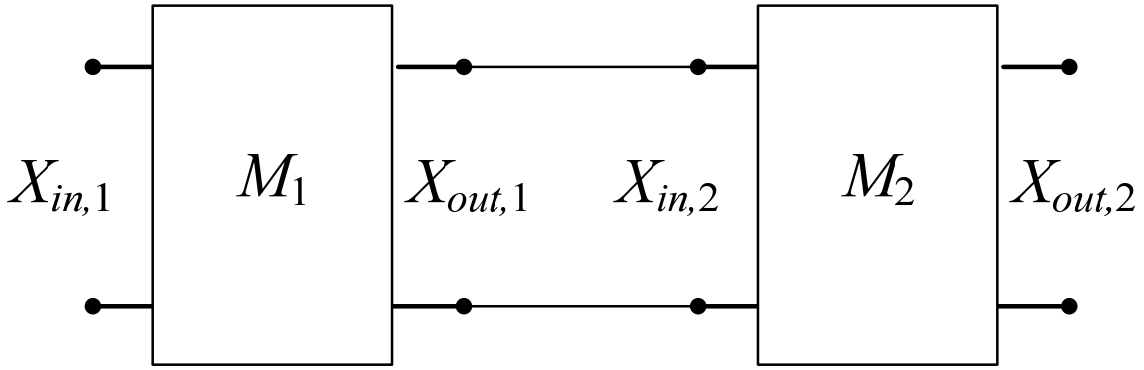

Figure B.4. Two generalized quadrupole models connected in cascade.

The relationship between the input and output variable vectors for quadrupoles 1 and 2 is as follows,

$$X_{out,1} = M_1 X_{in,1} \quad \text{(a)},$$
$$X_{out,2} = M_2 X_{in,2} \quad \text{(b)}. \tag{B.4}$$

But, because of the cascade connection, $X_{in,2}$ is equal to $X_{out,1}$; therefore, the relationship between $X_{in,1}$ and $X_{out,2}$ is as follows,

$$X_{out,2} = M_2 M_1 X_{in,1}. \tag{B.5}$$

In the most general case, if n quadrupole models are cascade connected, as shown in Figure B.5; then, the overall input variable vector is defined as the input vector of the first quadrupole model ($X_{in,1}$) and the overall output variable vector is defined as the output vector of the last quadrupole model ($X_{out,n}$). By following the same procedure, starting from the last quadrupole model and back to the first quadrupole model, as the procedure used to find equation (B.5), the relationship between the overall input and output variable vectors for the equivalent system, *i.e.* considering all quadrupole models connected in cascade, is as follows,

$$X_{out,n} = M_n M_{n-1} \cdots M_2 M_1 X_{in,1}. \tag{B.6}$$

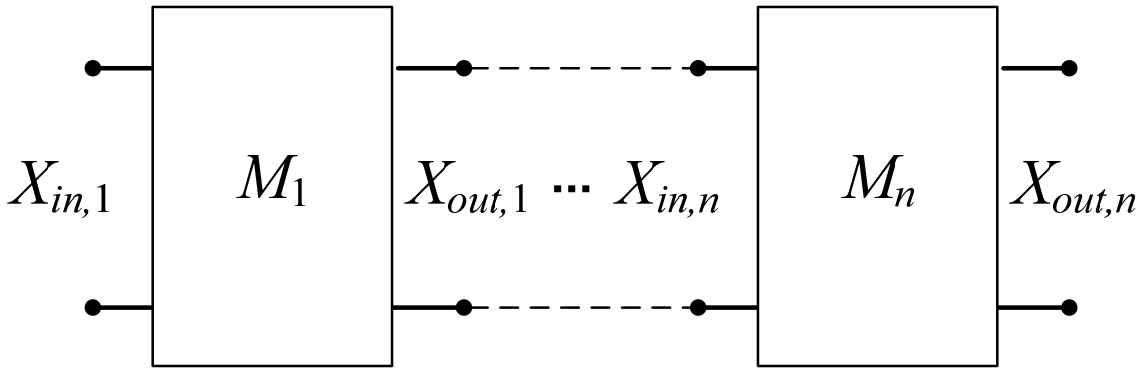

Figure B.5. A number of *n* quadrupole models connected in cascade.

If the *n* quadropole models have the same circuit configuration, then all the forward transfer function matrices are equal; thus, equation (B.6) becomes,

$$X_{out,n} = M^n X_{in,1}. \tag{B.7}$$

In equation (B.7), M^n represents the equivalent forward transfer function of the equivalent system. The equivalent system is defined here as a generalized quadrupole model with forward transfer function M^n that represents all the individual quadrupole models connected in cascade.

From equation (B.7), the overall input variable vector can be expressed in terms of the overall output variable vector as follows,

$$X_{in,1} = M^{-n} X_{out,n}. \tag{B.8}$$

If the inverse of the overall equivalent forward transfer function matrix is defined as shown in equation (B.9),

$$M^{-n} = \begin{bmatrix} A & B \\ C & D \end{bmatrix}. \tag{B.9}$$

Then, equation (B.8) becomes,

$$X_{in,1} = \begin{bmatrix} A & B \\ C & D \end{bmatrix} X_{out,n} \rightarrow \begin{bmatrix} V_{in,1} \\ I_{in,1} \end{bmatrix} = \begin{bmatrix} A & B \\ C & D \end{bmatrix} \begin{bmatrix} V_{out,n} \\ I_{out,n} \end{bmatrix}. \tag{B.10}$$

Therefore, if the output current is zero ($I_{out,n} = 0$), the input variables are,

$$\begin{aligned} V_{in,1} &= AV_{out,n} \quad \text{(a)}, \\ I_{in,1} &= CV_{out,n} \quad \text{(b)}. \end{aligned} \tag{B.11}$$

Thus, the equivalent input impedance is,

$$Z_{in} = \frac{V_{in,1}}{I_{in,1}} = \frac{A}{C}. \tag{B.12}$$

Using the equivalent input impedance (Z_{in}), the equivalent Tan δ for the system quadrupoles connected in cascade can be computed as shown in equation (B.13),

$$Tan\ \delta = \tan(\pi/2 - \angle Z_{in}). \tag{B.13}$$

A similar procedure can be followed for any system configuration, *i.e.* once the overall equivalent forward transfer function matrix is determined and the total output current is assumed to be zero, the equivalent Tan δ can be determined by equation (B.13) using the *A* and *C* elements of the new inverse equivalent forward transfer function matrix.

REFERENCES

[1] IEEE, "IEEE standard dictionary of electrical and electronics terms," IEEE Std. 100-1977, ISBN 77-92333.

[2] TOSHIKATSU, T. and GREENWOOD, A. "Advanced power cable technology: present and future," CRC Press Inc., Vol. I and II, Boca Raton, FL, 1983, ISBN 0-8493-5165-0 (Vol. I) and 0-8493-5166-9 (Vol. II).

[3] ORTON, H. and R. HARTLEIN, R. "Long-life XLPE-insulated power cables," Internal Publication by Dow Wire and Cable and Borealis, Somerset, NJ, 2006.

[4] ELECTRIC POWER RESEARCH INSTITUTE (EPRI), "Power cable materials selection guide," EPRI, No. 1001894, Palo Alto, CA, 2001.

[5] BARTNIKAS, R. and SRIVASTAVA, K. "Power and communication cables: theory and applications," IEEE Series on Power Engineering, New York, NY, 1999, ISBN 0-7803-1196-5.

[6] RAMACHANDRAN, S., HARTLEIN, R., and CHANDAK, P., "A comparative economic analysis for underground distribution cables insulated with TR-XLPE and EPR," IEEE Transmission and Distribution Conference, T&D-1999, 1999, Vol. 1, pp. 112-119.

[7] HARTLEIN, R. "Where do AEIC cable specifications come from?," IEEE Electrical Insulation Magazine, Vol.8, No.5, pp. 25-33, Sep./Oct. 1992.

[8] HARTLEIN, R., HAMPTON, N., HERNÁNDEZ, J.C., and PERKEL, J., "Overview of cable system diagnostic technologies and application," The National Electric Energy Testing Research and Applications Center (NEETRAC), Cable Diagnostic Focus Initiative Project (CDFI), No. 04-211 and 04-212, 2006.

[9] DYBA, J. "The rise and decline in the United States of impregnated paper insulated metallic sheathed cable," IEEE Electrical Insulation Magazine, Vol. 15. No. 4, pp. 13-16, July/Aug. 1999.

[10] HAMPTON, N. and HARTLEIN, R. "Survey of installed cable network, component failure and experience of diagnostic test," The National Electric Energy Testing Research and Applications Center (NEETRAC), Cable Diagnostic Focus Initiative Project (CDFI), No. 04-211 and 04-212, 2006.

[11] FRUTH, B. and NIEMEYER, L. "The importance of statistical characteristics of partial discharge data," IEEE Transactions on Dielectrics and Electrical Insulation, Vol. 27, No. 1, pp. 60-69, Feb. 1992.

[12] DISSADO, L. and FOTHERGILL, J. “Electrical degradation and breakdown in polymers,” IEE Materials and Devices Series 9, Peter Peregrinus Ltd., London, 1992, ISBN 0-86341-196-7.

[13] WERELIUS, P. “Development and application of high voltage dielectric spectroscopy for diagnosis of medium voltage XLPE cables,” Doctoral Thesis, Royal Institute of Technology (KTH), Stockholm, Sweden 2001.

[14] NUNES, S. and SHAW, M. “Water treeing in polyethylene – a review of mechanisms,” IEEE Transactions on Electrical Insulation, Vol. EI-15, No. 6, pp. 437-449, Dec. 1980.

[15] HARTLEIN, R., HAMPTON, N., WARE, N., TAYLOR B., and DENSLEY, J., “Introduction to cable design, failure mechanisms and diagnostics,” The National Electric Energy Testing Research and Applications Center (NEETRAC), Cable Class Presentation Cable Diagnostic Focus Initiative Project (CDFI) Update Meeting, Atlanta, GA, Feb. 2007.

[16] ILDSTAD, E. “Application of dielectric response measurements for condition assessment of service aged XLPE cables,” Proceedings of the IEEE Conference on Electrical Insulation and Dielectric Phenomena, CEIDP-1999, 1999, pp. 122-127.

[17] HVIDSTEN, S., ILDSTAD, E., and FAREMO, H., “Mechanisms causing nonlinear dielectric response of water treed XLPE cables,” Proceedings of the IEEE International Conference on Conduction and Breakdown in Solid Dielectrics, 1997, pp. 73-78.

[18] BULINSKI, A., BAMJI, S., and DENSLEY, J., “Factors affecting the transition from a water tree to an electrical tree,” Proceedings of the IEEE International Symposium on Electrical Insulation, ISEI-1988, 1988, pp. 327-330.

[19] DISSADO, L. “Characterization of the growth of water trees,” IEEE Transactions on Electrical Insulation, Vol. EI-17, No. 5, pp. 392-398, Oct. 1982.

[20] MASHIKIAN, M. and SZATKOWSKI, A. “Medium voltage cable defects revealed by off-line partial discharge testing at power frequency,” IEEE Electrical Insulation Magazine, Vol. 22, No. 4, July/Aug. 2006, pp. 24-32.

[21] ROSS, R. “Inception and propagation mechanisms of water treeing,” IEEE Transactions on Dielectrics and Electrical Insulation, Vol. 5, No. 5, pp. 660-680, Oct. 1998.

[22] NOTINGHER, P., RADU, I., and FILIPPINI, J., “Electric field calculations in polymers in the presence of water trees,” Proceedings of the IEEE 5th International Conference on Conduction and Breakdown in Solid Dielectrics, ICSD-1995, 1995, pp. 666-670.

[23] PATSCH, R. “Electrical and water treeing: a chairman’s view,” IEEE Transaction on Electrical Insulation, Vol. 27, No. 3, pp. 532-542, June 1992.

[24] DENSLEY, J. “Aging mechanisms and diagnostics for power cables-an overview,” IEEE Electrical Insulation Magazine, Vol. 17, No. 1, pp. 14-22, Jan./Feb. 2001.

[25] SHIMIZU, N. and LAURENT, C. “Electrical tree initiation,” IEEE Transactions on Dielectrics and Electrical Insulation, Vol. 5, No.5, pp. 651-659, Oct. 1998.

[26] GULSKI, E., SMIT, J., and WESTER, F., “PD knowledge rules for insulation condition assessment of distribution power cables,” IEEE Transactions on Dielectrics and Electrical Insulation, Vol. 12, No. 2, pp. 223-239, Apr. 2005.

[27] BARTNIKAS, R. “Editorial - partial discharge measurements,” IEEE Transactions on Dielectrics and Electrical Insulation, Vol. 12, No. 2, pp. 195, Apr. 2005.

[28] SAHOO, N., SALAMA, M., and BARTNIKAS, R., “Trends in partial discharge pattern classification: a survey,” IEEE Transactions on Dielectrics and Electrical Insulation, Vol. 12, No. 2, pp. 248-264, Apr. 2005.

[29] CONTIN, A., CAVALLINI, A., MONTANARI, G., PASINI, G., and PULETTI, F., “Artificial intelligence methodology for separation and classification of partial discharge signals,” Proceedings of the IEEE Conference on Electrical Insulation and Dielectric Phenomena, CEIDP-2000, 2000, pp. 522-526.

[30] TIAN, Y., LEWIN, P., DAVIES, A., and RICHARDSON, Z., “Acoustic emission detection of partial discharges in polymeric insulation,” Proceedings of the IEE High Voltage Engineering Symposium, Vol. 1, 1999, pp. 82-85.

[31] LUNDGAARD, L. “Partial discharge part XIV: acoustic partial discharge detection - practical application,” IEEE Electrical Insulation Magazine, Vol. 8, No. 5, pp. 34-43, Sep./Oct. 1992.

[32] AHMED, N. and SRINIVAS, N. “On-line partial discharge detection in cables,” IEEE Transactions on Dielectrics and Electrical Insulation, Vol. 5, No. 2, pp. 181-188, Apr. 1998.

[33] KREUGER, F., WEZELENBURG, M., WIEMER, A., and SONNEVELD, W., “Partial discharge part XVIII: errors in the location of partial discharges in high voltage solid dielectric cables,” IEEE Electrical Insulation Magazine, Vol. 9, No. 6, pp. 15-22, Nov./Dec. 1993.

[34] IEEE, “IEEE Guide for Field Testing of Shielded Power Cable Systems Using Very Low Frequency (VLF),” IEEE Std. 400.2-2004, Feb. 2005.

[35] MOHAUPT, P., BAUR, M., and SCHLICK, T., "VLF testing and diagnosis on medium voltage power cables," Proceedings of the IEEE 10th International Conference on Transmission and Distribution Construction, Operation, and Live Line Maintenance, 2003, pp.202-209.

[36] WERELIUS, P., THARNING, P., ERIKSSON, R., HOLMGREN, B., and GAFVERT, U., "Dielectric spectroscopy for diagnosis of water tree deterioration in XLPE cables," IEEE Transactions on Dielectrics and Electrical Insulation, Vol. 8, No. 1, pp. 27-42, Mar. 2001.

[37] IEEE, "IEEE Guide for Field Testing and Evaluation of the Insulation of Shielded Power Cable Systems," IEEE Std. 400-2001, Apr. 2002.

[38] IEEE, "Draft: IEEE Guide for Field-Testing of Laminated Dielectric, Shielded Power Cable Systems Rated 5kV and above with High Direct Current Voltage," IEEE Std. 400.1, Draft 5 D5, Oct. 2004.

[39] ILDSTAD, E. and GUBANSKI, S. "Dielectric properties of water-treed XLPE insulation," Proceedings of the IEEE Conference on Electrical Insulation and Dielectric Phenomena, CEIDP-1994, 1994, pp. 497-505.

[40] BIRKNER, P. "Field experience with a condition-based maintenance program of 20 kV XLPE distribution systems using IRC-analysis," IEEE Transactions on Power Delivery, Vol.19, No. 1, pp. 3-8, Jan. 2004.

[41] PEDERSEN, K., SEDDING, H., FENGER, M., HOLBOELL, J., and HENRIKSEN, M., "Laboratory results from dielectric spectroscopy of field aged XLPE cables with respect to water tress," Proceedings of the IEEE International Symposium on Electrical Insulation, ISEI-2006, 2006, pp. 509-514.

[42] ANDREWS, T., BEGOVIC, M., HAMPTON, N., HARTLEIN, R., HARLEY, R., HERNÁNDEZ, J.C., PARKER, T., and PERKEL, J., "Reflections on 'first experiences' with IEEE Std. 400," Presentation at the IEEE Insulated Conductors Committee (ICC), Fall 2006 Meeting, WG C-18, Oct. 2006.

[43] JONSCHER, A. "Dielectric relaxation in solids," Chelsea Dielectrics Press, London, 1983, ISBN 0-9508711-0-9.

[44] SKJOLBERG, J., HVIDSTEN, S., and FARMEO, H., "Experience from on-site condition assessment of XLPE MV cables," Proceedings of the IEEE International Symposium on Electrical Insulation, ISEI-2006, 2006, pp. 432-435.

[45] YAMAGUCHI, S., SODA, S., and TAKADA, N., "Development of a new type insulation diagnostic method for hot-line XLPE cables," IEEE Transactions on Power Delivery, Vol. 4, No. 3, pp. 1513-1520, July 1989.

[46] HVIDSTEN, S., ILDSTAD, E., HOLMGREN, B., and WERELIUS, P., "Correlation between AC breakdown strength and low frequency dielectric loss of water tree aged XLPE cables," IEEE Transactions on Power Delivery, Vol. 13, No. 1, pp. 40-45, Jan. 1998.

[47] BAUR, M. and BLANK, R. "On site assessment of the insulating condition in high voltage electrical equipments using high voltage at very low frequency," On Site Assessment of the Insulation in HV Electrical Equipment BAUR® Pruf-und Messtechnik GmbH Technical Report, 2000, pp. 1-7.

[48] KUSCHEL, M., PLATH, R., STEPPUTAT, I., and KALKNER, W., "Diagnostic techniques for service-aged XLPE-insulated medium voltage cables," Proceedings of the 4th International Conference on Insulated Power Cables, JICABLE-1995, 1995, pp. 504-508.

[49] AVELLAN, A., WERELIUS, P., and ERIKSSON, R., "Frequency domain response of medium voltage XLPE cable terminations and its influence on cable diagnostics," Proceedings of the IEEE International Symposium on Electrical Insulation, ISEI-2000, 2000, pp. 105-108.

[50] AMYOT, N., DAVID, E., FOURNIER, D., JEAN, D., and LALANCETTE, D., "Dielectric response of cable accessories and its influence on cable diagnostics," Proceedings of the IEEE Conference on Electrical Insulation and Dielectric Phenomena, CEIDP-2002, 2002, pp. 434-437.

[51] HVIDSTEN, S., HOLMGREN, B., ADEEN, L., and WETTERSTROM, J., "Condition assessment of 12 and 24 kV XLPE cables installed during the 80s-results from a joint Norwegian/Swedish research project", IEEE Electrical Insulation Magazine, Vol. 21, No. 6, pp. 17-23, Nov./Dec. 2007.

[52] HERNÁNDEZ-MEJÍA, J.C., PERKEL, J., HARLEY, R., HAMPTON, N., and HARTLEIN, R., "Correlation between Tan δ diagnostic measurements and breakdown performance at VLF for MV XLPE cables," under review to be published in the IEEE Transactions on Dielectrics and Electrical Insulation.

[53] OHATA, K., FURUHATA, H., NAKAGAWA, S., SAKAMOTO, T., EBINUMA, Y., and YOSHIDA, T., "Characteristics of long term deterioration of XLPE cable and its diagnostics techniques in Japan," International Conference on Insulated Power Cables, JICABLE-1999, 1999, paper No. B-5.3.

[54] EAGER, G., KATZ, C., FRYSZCZYN, B., DENSLEY, J., and BERNSTEIN, B., "High voltage VLF testing of power cables," IEEE Transactions on Power Delivery, Vol. 12, No. 2, pp. 565-570, Apr. 1997.

[55] KUSCHEL, M. and KALNER, W. "Relevance of the charging period to the dielectric response based diagnosis of PE/XLPE cables," IEE High Voltage Engineering Symposium, 1999, paper No. 467.

[56] HVIDSTEN, S. and ILDSTAD, E. "Criteria for diagnostic evaluation of water treed XLPE cables," IEEE 7th Conference Solid Dielectrics 2001, 2001, pp. 385-389.

[57] HVIDSTEN, S. and BENJAMINSEN, J. "Diagnostic testing of MV XLPE cables with low density of water trees," IEEE International Symposium Electrical Insulation, ISEI-2002, 2002, pp. 108-111.

[58] MOH, S. "Very low frequency testing – its effectiveness in detecting hidden defects in cables," Cogrès International des Réseaux Electriques de Distribution (CIRED), 2003, Session 1, paper No. 84.

[59] PERKEL, J., HAMPTON, N., BEGOVIC, M., HERNÁNDEZ, J.C., and HARTLEIN, R., "Validation of the accuracy of practical diagnostic tests for power equipment," Accepted for publication in the Conférence Internationale des Grandes Reseaux Électriques (CIGRE'08), 2008.

[60] PERKEL, J., HAMPTON, N., BEGOVIC, M., and HARTLEIN, R., "Validating diagnostic tests for cables in service," International Conference on Insulated Power Cables, JICABLE-2007, 2007, pp. 449-454.

[61] ABDOLALL, K., HALLDORSON, G., and GREEN, D., "Condition assessment and failure modes of solid dielectric cables in perspective," IEEE Transactions on Power Delivery, Vol. 17, No.1, pp. 18-24, Jan. 2002.

[62] BOGGS, S. "Failure mechanisms of shielded power cable related to high ground shield resistance and/or insulation of neutral wires from the ground shield," IEEE Transactions on Power Delivery, Vol. 17, No. 2, pp. 295-301, Apr. 2002.

[63] HANCK, J. and NEKOKSA, G. "Research to develop guidelines for cathodic protection of concentric neutral cables," IEEE Transactions on Power Apparatus and Systems, Vol. PAS-101, No.7, pp. 1878-1887, July 1982.

[64] NATIONAL ELECTRIC ENERGY TESTING RESEARCH AND APPLICATIONS CENTER (NEETRAC), Cable Diagnostic Focus Initiative (CDFI) Project, "12th project report to the U.S. Department of Energy and CDFI participants," Project No. 04-211, October 2007.

[65] BOGGS, S. "Partial discharge: overview and signal generation," IEEE Electrical Insulation Magazine, Vol.6, No.4, pp. 33-39, July/Aug. 1990.

[66] BOGGS, S. "Partial discharge-part II: detection sensitivity," IEEE Electrical Insulation Magazine, Vol.6, No.5, pp. 35-44, Sep./Oct. 1990.

[67] MASHIKIAN, M. “Preventive maintenance testing of shielded power cable systems,” IEEE Transactions on Industry Applications, Vol. 38, No. 3, pp. 736-743, May/June 2002.

[68] BOGGS, S., PATHAK, A., and WALKER, P., “Partial discharge XXII: high frequency attenuation in shielded solid dielectric power cable and implications thereof for PD location,” IEEE Electrical Insulation Magazine, Vol. 12, No. 1, pp. 9-16, Jan./Feb. 1996.

[69] BROSCHE, T., HILLER, W., and FAUSER, E., “Novel characterization of PD signals by real-time measurement of pulse parameters,” IEEE Transactions on Dielectrics and Electrical Insulation, Vol. 6, No. 1, pp. 51-59, Feb. 1999.

[70] SRIRAM, S., NITIN, S., PRABHU, K., and BASTIAANS, M., “Signal denoising techniques for partial discharge measurements,” IEEE Transactions on Dielectrics and Electrical Insulation, Vol. 12, No. 6, pp. 1182-1191, Dec. 2005.

[71] LAURENT, C. and MAYOUX, C. “Partial discharge-part XI: limitations to PD as a diagnostic for deterioration and remaining life,” IEEE Electrical Insulation Magazine, Vol. 8, No. 2, pp. 14-17, Mar./Apr. 1992.

[72] NATTRASS, D. “Partial discharge XVII: the early history of partial discharge research,” IEEE Electrical Insulation Magazine, Vol.9, No.4, pp. 27-31, July/Aug. 1993.

[73] IEEE, “IEEE Guide for Partial Discharge Testing of Shielded Power Cable Systems in a Field Environment,” IEEE Std. 400.3, Feb. 2007.

[74] VAN BRUNT, R. “Stochastic properties of partial-discharge phenomena,” IEEE Transactions on Electrical Insulation, Vol. 26, No. 5, pp. 902-948, Oct. 1991.

[75] KRIVDA, A. “Recognition of discharges: discrimination and classification,” Doctoral Thesis Delft University of Technology, Delft University Press, Delft, Netherlands, 1995, ISBN 90-407-1156-9.

[76] KREUGER, F., GULSKI, E., and KRIVDA, A., “Classification of partial discharges,” IEEE Transactions on Dielectrics and Electrical Insulation, Vol. 28, No.6, pp. 917-931, Dec. 1993.

[77] GULSKI, E. and KRIVDA, A. “Neural networks as a tool for recognition of partial discharges,” IEEE Transactions on Dielectrics and Electrical Insulation, Vol. 28, No. 6, pp. 984-1001, Dec.1993.

[78] JAMES, R. and PHUNG, B. “Development of computer-based measurements and their application to PD pattern analysis,” IEEE Transaction on Dielectrics and Electrical Insulation, Vol. 2, No. 5, pp. 838-856, Oct. 1995.

[79] GULSKI, E. and KREUGER, F. "Computer-aided recognition of discharge sources," IEEE Transaction on Dielectrics and Electrical Insulation, Vol. 27, No. 1, pp. 82-92, Feb. 1992.

[80] HOOF, M., FREISLEBEN, B., and PATSCH, R., "PD source identification with novel discharge parameters using counter propagation neural networks," IEEE Transactions on Dielectrics and Electrical Insulation, Vol. 4, No. 1, pp. 17-32, Jan./Feb. 1997.

[81] CACCIARI, M., CONTIN, A., RABACH, G., and MONTANARI, G., "An approach to partial discharge investigation by height distribution analysis," IEE Proceedings on Science, Measurement and Technology, Vol. 142, No. 1, pp. 102-108, Jan. 1995.

[82] CACCIARI, M., CONTIN, A., and MONTANARI, G., "Use of a mixed weibull distribution for the identification of PD phenomena," IEEE Transaction on Dielectrics and Electrical Insulation, Vol. 2, No. 6, pp. 1166-1179, Dec. 1995.

[83] HUCKER, T. and KRANZ, H. "Requirements of automated PD diagnosis systems for fault identification in noisy conditions," IEEE Transaction on Dielectrics and Electrical Insulation, Vol. 2, No. 4, pp. 544-556, Aug. 1995.

[84] CONTIN, A., CAVALLINI, A., MONTANARI, G., and PASINI, G., "Digital detection and fuzzy classification of partial discharge signals,'' IEEE Transaction on Dielectrics and Electrical Insulation, Vol. 9, No. 3, pp. 335-348, June 2002.

[85] SALAMA, M. and BARTNIKAS, R. "Fuzzy logic applied to PD pattern classification," IEEE Transaction on Dielectrics and Electrical Insulation, Vol. 7, No. 2, pp. 118-123, Feb. 2000.

[86] MAZROUA, A., BARTNIKAS, R., and SALAMA, M., "Discrimination between PD pulse shapes using different neural network paradigms," IEEE Transaction on Dielectrics and Electrical Insulation, Vol. 1, No. 6, pp. 1119-1131, Nov./Dec. 1994.

[87] MA, X., ZHOU, C., and KEMP, I., "Interpretation of wavelet analysis and its application in partial discharge detection," IEEE Transactions on Dielectrics and Electrical Insulation, Vol. 9, No. 3, pp. 446-457, June 2002.

[88] FRIGGE, M., HOAGLIN, D., and IGLEWICZ, B., "Some Implementations of the Box Plot," American Statistical Association, The American Statistician, Vol. 43, No. 1, pp. 50-54, Feb. 1989.

[89] HERNÁNDEZ-MEJÍA, J.C., PERKEL, J., HARLEY, R., BEGOVIC, M., HAMPTON, N., and HARTLEIN, R., "Determining Routes for the Analysis of Partial Discharge Signals Derived from the Field," Accepted for publication in the IEEE Transactions on Dielectrics and Electrical Insulation.

[90] ASCHENBRENNER, D., KRANZ, H., RUTGERS, W., and VAN DEN AARDWEG, P., "Online PD measurements and diagnostics on power transformers," IEEE Transactions on Dielectrics and Electrical Insulation, Vol. 12, No. 2, pp. 216-222, Apr. 2005.

[91] KRANZ, H. "PD pulse sequence analysis and its relevance for on-site PD defect identification and evaluation," IEEE Transactions on Dielectrics and Electrical Insulation, Vol. 12, No. 2, pp. 276-284, Apr. 2005.

[92] MEIJER, S. and SMIT, J. "UHF defect evaluation in gas insulated equipment," IEEE Transactions on Dielectrics and Electrical Insulation, Vol. 12, No. 2, pp. 285-296, Apr. 2005.

[93] DUDA, R., HART, P., and STORK, D., "Pattern Classification," Second Edition, John Wiley & Sons, Inc., New York, 2000, ISBN 0-471-05669-3.

[94] GUYON, I., WESTON, J., BARNHILL, S., and VAPNIK, V., "Gene selection for cancer classification using support vector machines," Machine Learning, Vol. 46, No. 1–3, pp. 389–422, 2002.

[95] DUAN, K., RAJAPAKSE, J., WANG, H., and AZUAJE, F., "Multiple SVM-RFE for gene selection in cancer classification with expression data," IEEE Transactions on Nanobioscience, Vol. 4, No. 3, pp. 228-234, Sept. 2005.

[96] GUYON, I. and WESTON, J. "Methods of identifying patterns in biological systems and uses thereof," Health Discovery Corporation, Savannah, GA, U.S. Patent No. 7,117,188 B2, Oct. 2006, pp. 1-70.

[97] HERNÁNDEZ-MEJÍA, J.C., HAMPTON, N., HARLEY, R., and HARTLEIN, R., "Practical issues regarding the use of dielectric measurements to diagnose the service health of MV cables," International Conference on Insulated Power Cables, JICABLE-2007, 2007, pp. 203-208.

[98] HERNÁNDEZ-MEJÍA, J.C., HARLEY, R., HAMPTON, N., and HARTLEIN, R., "Characterization of Ageing for MV Power Cables Using Low Frequency Tan δ Diagnostic Measurements," under review to be published in the IEEE Transactions on Dielectrics and Electrical Insulation.

VITA

JEAN CARLOS HERNÁNDEZ MEJÍA

Jean Carlos Hernández Mejía was born on June 24, 1977 in Boconó – Estado Trujillo, Venezuela. He attended the Universidad de Los Andes (ULA – University of the Andes) in Mérida, Venezuela, and received his *summa cum laude* Bachelor of Engineering degree in Electric Power in July, 2000. After graduation, he joined the Power Engineering Department of the School of Electrical Engineering of the Universidad de Los Andes as an instructor in December, 2000. After three year, he was awarded the Organization of American States (OAS) scholarship to get his M.Sc. degree. He received the M.Sc. degree in Electrical and Computer Engineering from The Georgia Institute of Technology Atlanta, Georgia in December, 2005. In January 2006, Jean Carlos began his studies towards the Ph.D. degree at The Georgia Institute of Technology Atlanta, Georgia. He was awarded the Ph.D. degree in Electrical and Computer Engineering in December 2008. While at The Georgia Institute of Technology, Jean Carlos was employed as teaching assistant during 2004 and research assistant from 2005 until the end of his Ph.D. studies. His Ph.D. research work was oriented on defect characterization and diagnosis of power cable systems. At the present, Jean has rejoined the Universidad de Los Andes and now holds the position of assistant professor.